Cooperative Research in Coal Liquefaction

Technical Progress Report on DOE Contract No. DE-FC22-93PC93053 Period: May 1, 1993 to April 30, 1994

Submitted to the
U.S. Department of Energy

Edited by

Gerald P. Huffman, Director
Consortium for Fossil Fuel Liquefaction Science
341 Bowman Hall
University of Kentucky
Lexington, KY 40506-0059
Phone: (606) 257-4027
FAX: (606) 257-7215

Submitted by the University of Kentucky
On Behalf of the

Consortium for Fossil Fuel Liquefaction Science

University of Kentucky
University of Utah
University of Pittsburgh
West Virginia University
Auburn University

TABLE OF CONTENTS

SUMMARY

Coliquefaction of Waste Material with Coal

During the past two years, the CFFLS has been investigating methods to convert waste materials into oil using direct coal liquefaction technology. Although the program is still young, CFFLS scientists have obtained some very promising results from the liquefaction of plastics, rubber tires, paper, and other wastes, and the coliquefaction of wastes with coal. A brief summary of the principal results is given below.

Waste plastics: Currently, over 44 billion lbs. of plastic waste material are disposed of in the U.S. each year.[1] The dominant components of plastic waste (polyethylene, polyethylene terephthalate(PET), polypropylene, polystyrene) have the high hydrogen to carbon ratio and molecular chain structure that are well suited for liquefaction. Experiments conducted by Consortium scientists have yielded a number of promising results.[2-4] Under typical direct liquefaction conditions (~400-450 °C, 1500-2000 psi of hydrogen, 30-60 minutes reaction time), in the presence of an HZSM-5 zeolite catalyst, plastics exhibit oil yields of 80-98% and total liquefaction conversions of 90-100%. When coliquefied with coal of several different ranks, oil yields as high as 60-80% were observed, while the total liquefaction conversions reached levels of over 90%. Simulated distillation analysis of the oil products[5] from such experiments indicates that they are high in quality and could readily be upgraded to transportation fuel(gasoline, jet fuel, diesel fuel) or used as the feedstock to produce new plastics or rubber. Future work will focus on optimizing liquefaction conditions, using lower pressures and cheaper catalysts, and liquefying more representative commingled waste plastics.

Rubber tires: Over 280 million automotive tires are discarded in the U.S. each year[6]. Major problems have been encountered with old tire fires, which are very difficult to extinguish. Retreading, combustion, and conversion to rubberized asphalt have all been considered as disposal solutions. Liquefaction is an attractive alternative option. Liquefaction of tires alone yields approximately 65% of high quality oil, and 35% of a solid residue which is primarily carbon black.[7,8] Since tire manufacturers typically add 30-35% of carbon black to aromatic oils to make up the feedstock from which tire rubber is prepared, this indicates that essentially all of the oil in tires can be recovered by direct liquefaction. Furthermore, high hydrogen pressures do not appear to be required to convert tires to oil by hydrotreatment.[8] Coliquefaction of tires with coal gives higher liquid product yields than expected on the basis of the results obtained from the liquefaction of rubber and coal separately, possibly because of catalytic activity by the carbon black.[7]

ASPEN plus has been used to simulate a plant coliquefying 10,000 scrap tires and 75 tons of coal per day. It was found that coliquefaction is more profitable than combustion in power plants or cement kilns. Initial work has been conducted to examine the economics of a commercial-scale process for coliquefying coal and waste plastics.

Waste oils: Almost 1.2 billion barrels of waste oil are generated in the U.S. each year, posing an environmental hazard due to metal-bearing compounds, possible halogenated hydrocarbons, and other toxic materials. Investigation of the coliquefaction of coal with waste oil by CFFLS scientists[9] indicates that this process provides many benefits including increased conversion of coal to oil, removal of metals from the oil,[10] and reduction of the amount of recycle solvent required.
Surfactants in the oil appear to disperse the coal and catalyst during liquefaction. Coal to liquid conversions of over 90% and oil yields of 70-80% are achieved.

Waste cellulosic materials: Cellulosic wastes(paper, yard wastes, food wastes, agricultural wastes) constitute more than half of the material in landfills, both by volume and by weight. Earlier research[10] demonstrated that such materials could be converted to oils, and a small pilot plant was operated for some time at Albany, Oregon. Recently, CFFLS scientists have investigated two different methods of coliquefying paper with coal.[11] In one approach, standard direct liquefaction technology was used and a molybdenum catalyst was employed. In the second approach, an alkali catalyst was used, and the reaction took place under a CO-H_2O atmosphere. Hydrogen is produced under these conditions by a catalytic reaction. In both approaches, nearly 100% of the paper alone was converted to hydrocarbon products, with oil yields of 20-25% and gas yields of 50 to 70%. When paper was mixed with coal(Wyodak subbituminous coal), the total conversion of the coal was 80-90%, with oil yields of 20-30%, and gas yields of 20-30%. Although the gas yield is higher than desired, the gas is rich in hydrogen that could be used in the upgrading of coal-waste coliquefaction products.

To summarize, the goal of the CFFLS research program is to develop economical processes to liquefy waste materials with coal and transform a major environmental disposal problem into a valuable transportation fuel resource. The size of this potential resource is substantial. By coliquefaction of petroleum-based wastes(plastics, rubber, and waste oil) with coal, 280 million barrels of oil per year could be produced. This is about the amount of oil currently imported into the U.S. each month. If we were to utilize just 25% of this currently wasted resource, it would be sufficient to provide 2% of our transportation fuel needs. Preliminary economic analysis[12] of the coliquefaction of plastic wastes with coal indicates that oil could be produced from this process at about $18 per barrel with tipping fees for waste disposal of $25 per ton.

Catalysis for Coal Liquefaction to Clean Transportation Fuels

A number of water soluble coal liquefaction catalysts have been comparatively tested. Conditions were 500-3,000 psig H_2, 380-450 °C, 15-60 min. Iron, cobalt, nickel, and molybdenum were tested. Ammonium tetrathiomolybdate was the most active catalyst, yielding 75% liquids and 40% oil at a concentration of 0.05 wt.%. Iron sulfate dodecahydrate, cobalt nitrate hexahydrate, and nickel nitrate hexahydrate were all effective at concentrations of approximately 0.5 wt.%, producing oil yields of approximately 40%. Analysis of the oils using GC and TG/MS indicated that the quality of the oils was in the order: Fe > Ni > Co.

Model compounds studies have been conducted using anion-modified metal oxide catalysts at mild conditions(200 °C, 500 psi). These studies demonstrate that catalysts such as $Mo/Fe_2O_3/SO_4$ are bifunctional; that is, they possess both an acidic component and a hydrogenation function.

Fe-S catalysts have been prepared using an aerosol reactor. Preparation conditions have been correlated with the size and structure of the particles and their activity for coal liquefaction. Preliminary experiments have been conducted with mixed-metal aerosol catalysts.

The hydrogenation of naphthalene was investigated in a trickle bed reactor using a $NiMo/Al_2O_{32}$ catalyst and a nanoscale iron oxide catalyst at 250-300 °C. The aromatic hydrogenation activity of the iron catalyst decreases in the order Fe > FeS_x > Fe_2O_3. On a per unit surface area basis, the reduced iron is more active than the $Ni\text{-}Mo/Al_2O_3$ catalyst. The hydrogenation activity of Pt-promoted $NiMo/Al_2O_3$ is much superior to that of $NiMo/Al_2O_3$. Studies have been initiated on alumina-aluminum phosphate supports for upgrading catalysts.

Laser pyrolysis has been used to prepare a variety of Mo-, Co-, Fe-, and W- ultrafine particle(UFP) catalysts in the form of sulfides, nitrides, carbides, and oxides. Most of the catalysts were binary catalysts(e.g., MoS_2), but ternary catalysts(e.g., $Fe_xMo_yS_z$) and supported catalysts(Mo_2N/SiO_2) were also prepared. The catalytic activities of UFP Mo_2N, Mo_2C, and MoS_2 for various model compound reactions were determined and found to be more active, on a per surface area basis, that those of a Mo-promoted sulfated hematite catalyst.

A variety of ultrafine binary ferrihydrite(FYHD) catalysts containing such secondary elements as Si, Al, Mo, P, and Zn, and organic acid treated FHYD have been prepared. It has been demonstrated that the secondary element and acid groups reside principally on the surfaces of the FHYD particles and act to prevent agglomeration and growth of the particles during liquefaction. The binary FHYD catalysts are more active than 30 Å FHYD from Mach I and resist agglomeration significantly better.

A high pressure, high temperature, FTIR system is being used to investigate the interaction of dihydrogen with Fe_2O_3 and Fe_3O_4 films. Initial experiments were unsuccessful due

to the fact that the attainable temperature was not high enough. A new cell is being built that will allow in situ FTIR studies up to 600 °C.

Fundamental Research in Coal Liquefaction

Mossbauer spectroscopy, XAFS spectroscopy, TEM, and XPS have been used to characterize a variety of catalysts and other samples from numerous Consortium and DOE liquefaction projects. XAFS was used to characterize the structure of Mo in coal liquefaction residues that utilized a molybdenum naphthenate catalyst precursor, in $Mo/Fe_2O_3/SO_4$ catalysts, and in FHYD/Mo binary catalysts. XAFS was also used to characterized Mo and W in laser pyrolysis catalysts, and to examine the Zn in waste oils and residues from waste oil-coal coprocessing experiments. Mossbauer spectroscopy was used to examine the structure of the iron in a variety of catalysts, before and after liquefaction. These included binary FHYD catalysts, aerosol catalysts, "red mud", and Fe_2O_3/SO_4 after liquefaction in tests at Sandia. TEM and XPS were utilized particularly in the characterization of binary FHYD catalysts containing secondary elements such as Si, Mo, P, and Al. HZSM-5 zeolite and aerosol catalysts were also characterized by TEM.

^{13}C NMR magic angle turning (MAT) experiments have a number of advantages over other 2D experiments. Research in the current year has improved the MAT experiment by employing a rotor synchronization device to trigger the pulse train at the appropriate rotor position. This improves the quality of the spectral information obtained. Two additional techniques, using short contact times and dipolar dephasing, further separate the powder patterns of protonated and nonprotonated carbons in complex compounds.

An HPLC technique has been developed for rapid analysis of coal liquids. Compound class separation is obtained with polars resolved by functional groups and aromatics separated by ring size. Work on better quantification is in progress.

The effect of bacterial concentration and H_2 pressure on the biological hydrogenation of fumaric acid to succinic acid has been investigated. The time required for reprecipation of iron released by pyrite in the presence of *Adidanus brierleyi* has been reduced. The ultrafine iron(FeOOH) acts as a catalyst for liquefaction. A literature survey had been done on the possibility of biodegradation of polymers.

Catalytic dehydrogenation of model compounds has been carried out to gain information on the nature of donor hydrogen in coal, coal liquefaction resids, and heavy oils from petroleum. Most of the work was carried out with polycyclic hydroaromatic compounds. Dehydrogenation experiments were also carried out on recycle oils from a continuous coal liquefaction facility. Evidence of their hydrogen donor abilities was obtained and related to the coal liquefaction process. Results demonstrate that catalytic dehydrogenation is useful for assessing the amount and nature of transferable hydrogen in coals, resids and heavy petroleum residues.

In Situ Analytical Techniques for Coal Liquefaction

In situ ESR measurements of the free radical density have conducted at temperatures from 100 to 600 °C and H_2 pressures up to 600 psi. Significant results include the observation that the free radical density, N_s, at ~400 °C increases in approximately a linear fashion with activity of different iron-based catalysts. A device for adding catalyst or other material during an in situ ESR measurement has been developed. Using this apparatus, it has been possible to observe increases in N_s as a result of adding a catalyst during the hydrotreatment of coal, and decreases in N_s resulting from the addition of rubber tread.

Experiments were performed on the decomposition of waste rubber tire, commingled waste plastic, polystyrene, polyethylene and coal in a high pressure TG/GC/MS system under a hydrogen pressure of 900 psig. The different shapes of the TG profiles have implications for co-processing. Various molecular component were monitored as a function of time and temperature at 900 psig. TG/GC/MS studies were also conducted on wood components.

An in situ XAFS cell capable of H_2 pressures up to 2,000 psig and temperatures up to 600 °C has been built and successfully tested. In the initial runs, iron-ion exchanged Black Thunder coal and Blind Canyon coal(DECS 6) with added binary ferrihydrite catalysts were examined. High quality Fe K-edge XAFS data were obtained which can be used to investigate the kinetics of the transformation of the initial iron forms to pyrrhotite.

REFERENCES

1. Franklin Associates, Ltd., Characterization of Plastic Products in Municipal Solid Waste, Feb., 1990; final report to the Council for Solid Waste Solutions.

2. L.L. Anderson and W. Tuntawiroon, **1993**, Amer. Chem. Soc., Div. of Fuel Chem. Preprints, 38(3), 816-822.

3. M. Mehdi Taghiei, F.E. Huggins, and G.P. Huffman, **1993**, Amer. Chem. Soc., Div. of Fuel Chem. Preprints, 38(3), 810-815.

4. M. Mehdi Taghiei, F.E. Huggins, and G.P. Huffman, "Coliquefaction of Waste Plastics with Coal," Energy & Fuels, in press.

5. J.S. Shabtai and W. Zmierczak, "Depolymerization - Liquefaction Reactions of Plastics and Rubber", presented at the Eighth Annual CFFLS Technical Meeting, July 6-8, 1994, Snowbird, Utah.

6. Hearing before the Subcommittee on Environment and Labor and Subcommittee on Regulation, Business Opportunities and Energy of the Committee on Small Business:

House of Representatives, April 18, 1990. Scrap Tire Management and Recycling Opportunities, Serial No.101-52.

7. M. Farcasiu and C.M. Smith; **1992**, Prepr. Div. Fuel Chem. 37(1), 472.

8. Z. Liu; J.W. Zondlo; D.B. Dadyburjor; **1994**, Energy & Fuels, *8*, 607-612.

9. H.G. Sanjay, A.R. Tarrer, and C. Marks, **1994**, Energy & Fuels, *8*, 99-104.

10. F.E. Huggins, M. Mehdi Taghiei, and G.P. Huffman, "XAFS Spectroscopic Investigation of Element Speciation in Carbonaceous Materials from Coliquefaction of Coals and Waste Materials", to be presented at the I&EC Special Symposium, Atlanta, GA, September 19-21, 1994.

11. H.R. Appell, I. Wender, and R.D. Miller, **1963**, Chem.Ind.(London), *47*, 1703.

12. H. Jung, J.W. Tierney and I. Wender, **1993**, Amer. Chem. Soc., Div. of Fuel Chem. Preprints, *38(3)*, 880-885.

13. Malvina Farcasiu, "Recent Initiatives in Coal-Waste Coprocessing," presented at the Eighth Annual CFFLS Technical Meeting, July 6-8, 1994, Snowbird, Utah.

TASK I

COLIQUEFACTION OF COAL WITH WASTE MATERIALS

Coordinators: Irving Wender and Gerald Huffman

TASK I

Project I.1

FUNDAMENTAL REACTION STUDIES IN CO-PROCESSING OF COAL AND WASTE POLYMERS

Joseph S. Shabtai, W. Zmierczak and X. Xiao
University of Utah

The main research activities during the May 1, 1993 - April 30, 1994, period of this project were in the following directions:

1. Fundamental studies on the catalytic depolymerization-liquefaction reactions of polystyrenes and styrene-butadiene rubbers (SBR).
2. Fundamental studies on the catalytic depolymerization-liquefaction of selected polyolefins, i.e., polyethylene, polypropylene and polybutadiene.
3. Initiation of systematic coprocessing studies of coal and commercial polymers of the above types, based on results from 1 and 2.

Following is a description of research performed and results obtained:

I.1.1. Studies on the Catalytic Depolymerization-Liquefaction of Polystyrenes and Styrene-Butadiene Rubbers (SBR)

Although it is known that commercial polymers undergo thermal breakdown at high temperature (≥ 450°C), no precise information on the direction and rates of catalytic depolymerization reactions of such polymers at moderate temperatures (300-450°C) was available. Such basic information could be considered as prerequisite for designing efficient, high-yield procedures for coliquefaction of coal and waste polymers.

During the reporting period, a detailed study on the depolymerization-liquefaction behavior of commercial polymers was performed. Some of these studies were carried out in collaboration with Prof. H.L.C. Meuzelaar and his group. The commercial polymers used as feeds in Sections 1-3 of this report are listed in Table I.1.1. Runs with these feeds in the solid state (powders or small particle size materials) were performed using either 50 cc Microclave reactors or 300cc autoclaves (Autoclave Engineers). The effects of reaction temperature and of

catalyst type (including acids, solid superacids and solid bases) upon the yield and distribution of liquid products were examined.

In all runs, the feed was mixed with the solid catalyst (without any solvent) and the mixture introduced in the autoclave reactor. The latter was sequentially purged with nitrogen and hydrogen, and then pressurized with H_2 to an initial pressure of 1200-1500 psig. The reactor was heated with mixing (100-500 rpm) to the desired temperature (heatup time, 15-45 min, depending on the reactor type). Typical reaction times were in the range of 1-3 h. At the end of the run, the product was removed from the reactor and, in the case of incomplete conversion, separated into liquid product and unreacted polymer. Products were identified mainly by GC/MS and FTIR, and quantitatively analyzed by gas chromatography.

A. Depolymerization-Liquefaction Reactions of Polystyrenes

An example of GC/MS analysis of the depolymerization product obtained from a polystyrene feed (M.W. 280,000) at 425°C, using Fe_2O_3/SO_4^{2-} as catalyst, is given in Figure I.1.1. As seen, the following types of depolymerized (and partially depolymerized) products are found.

(a) benzene and alkylbenzenes, in particular, ethylbenzene (with traces of styrene) and toluene, accompanied by C_3-alkylbenzenes (mostly cumene) and C_4-alkylbenzenes.

(b) diphenylalkanes, predominantly 1,3-diphenylalkanes, in which the phenyl groups are separated by 3 aliphatic carbons, as in the polymeric feed.

(c) some cyclization products, e.g., diphenylcyclopentane.

(d) some polyphenyls and triphenylalkanes

The composition of the depolymerization-liquefaction product changes markedly with processing variables, e.g., temperature, reaction time, type and concentration of catalyst, etc. An example is provided in Table I.1.2 which shows the change in product composition as a function of temperature. The main trend observed is that the intermediate depolymerization products, e.g., diphenyl- and triphenylalkanes, decrease in concentration from a total of about 45 wt% at 350°C to about 3 wt% at 450°C, whereas benzene and alkylbenzenes correspondingly increase from a total of ~44 wt% at 350°C to ~88 wt% at 450°C. This clearly demonstrates the gradual, stepwise conversion of polystyrene into monocyclic arenes with increase in temperature.

B. Depolymerization-Liquefaction Reactions of (Non-Vulcanized) Styrene-Butadiene Rubber (SBR)

The feed used was a sample of non-vulcanized styrene-butadiene rubber (30 wt% styrene, 70 wt% butadiene, corresponding to a butadiene/styrene molar ratio = 4.2). The GC/MS analyses of the lower and higher M.W. ranges of a product obtained at 400°C, with Fe_2O_3/SO_4^{2-} as catalyst, are given in Figures I.1.2 and I.1.3, respectively. The following compositional features are found:

(A) In addition to benzene, toluene and ethylbenzene, there are significant amounts of C_5-C_{10} paraffins in the product. Those are obviously derived from the aliphatic (ex-butadiene) blocks of the polymer.

(B) Alkylbenzenes with longer alkyl and alkenyl chains (C_5-C_8) are found. No such compounds were detected in the product from polystyrene.

(C) Significant amounts of side-chain cyclization products, i.e., cyclopentylbenzene, (methyl)cyclopentylbenzene, indanes, and tetrahydronaphthalenes are found. Those are apparently derived by catalytic cyclization reactions of C_5-C_8 alkyl- and alkenylbenzenes.

The product composition changes with change in processing conditions. Table I.1.3 provides an example of composition changes as a function of reaction temperature. The following trends are observed:

(a) C_5-C_9 paraffins and cycloparaffins (derived from the aliphatic blocks) increase to some extent with increase in temperature. In agreement with this, the gaseous low paraffins (C_1-C_4) also increase with temperature.

(b) Benzene, toluene and ethylbenzene increase but only slightly with increase in temperature

(c) The total concentration of higher, C_5-C_8 alkyl- and alkenylbenzenes decreases only slightly to moderately with temperature up to 450°C. This may depend on the partial cyclization of such compounds to cycloalkylbenzenes, indanes, etc., which are somewhat more resistant to dealkylation.

(d) Diphenylalkanes decrease markedly with temperature, as expected for these intermediate compounds.

The change in composition of products from polystyrenes and SBR as a function of temperature and reaction time, allows for conclusions regarding the probable mechanism of the depolymerization-liquefaction process.

Figure I.1.4 outlines some probable mechanistic pathways for the acid-catalyzed depolymerization-liquefaction of polystyrenes, as follows:

Carbonium ions along the polymeric chain can be formed either by hydride abstraction at benzylic positions or by protonation of aromatic rings. β-cleavage (of benzylic carbonium ions) at end positions or adjacent to the end position can produce either ethylbenzene (plus styrene) or toluene, which are found to be predominant monocyclic arene products. Cumene, which is next in importance, can be produced likewise by β-cleavage of a corresponding end group (having two substituents at the benzylic carbon).

On the other hand, carbonium ions produced by protonation of aromatic rings in the polymer will undergo α-cleavage leading to benzene plus a product in which some sites have a longer aliphatic chain between two aromatic rings (A). Further cleavage of such intermediates will yield longer-chain alkyl- and alkenylbenzenes, which undergo to a limited extent intramolecular cyclization reactions leading to cycloalkylbenzenes, indanes and some tetrahydronaphthalenes. The above-indicated protonation of benzene rings as a source for formation of benzene was confirmed by the sharp increase in benzene when a stronger protonic acid, e.g., ZrO_2/SO_4^{2-}, was used as catalyst.

Figure I.1.5 indicates a series of plausible mechanistic pathways for depolymerization-liquefaction of non-vulcanized styrene-butadiene rubber (SBR). As known, SBR has quite different structural features as compared with polystyrene. With a 4.2 to 1 molar ratio of butadiene to styrene, there are many sties in the polymeric chain where aromatic rings are separated by relatively long aliphatic-olefinic blocks (ex-butadiene blocks), which contain double bonds. The latter can undergo partial hydrogenation (due to the moderate hydrogenation activity of the Fe_2O_3/SO_4^{2-} catalyst) and double bond migrations. Benzylic carbonium ions in this case will undergo β-cleavage reactions leading not only to (C_1-C_3 alkyl)benzenes but also to alkyl and alkenylbenzenes with longer, e.g. C_4-C_8 alkyl groups. The latter could then undergo in part intramolecular cyclization reactions leading to cycloalkylbenzenes, indanes, and small amounts of tetrahydronaphthalenes. β-cleavage at both ends of the ex-butadiene chains will produce C_5-C_{12} paraffins and olefins, and by secondary cyclization reactions-cycloparaffins. The latter, of course, can be produced also by dealkylation of cycloalkylbenzenes.

I.1.2 Depolymerization-Liquefaction Reactions of Polyolefins.

In this part of the project, fundamental studies on the depolymerization-liquefaction reactions of selected polyolefins were performed. The feeds included isotactic polypropylene, polyethylene, and polybutadiene. Following is a short description of work performed and results obtained:

A. Depolymerization-Liquefaction of Polypropylene and Polyethylene

Processing conditions were developed and catalysts identified for high-yield depolymerization-liquefaction of isotactic polypropylene (see Table I.1.1) into a light, gasoline-like product. For example, at 390-420°C and an initial H_2 pressure of 1200 psig, with 1 wt% of Fe_2O_3/SO_4^{2-} as catalyst, the polypropylene is converted in very high yield (>90 wt%) into a low-boiling liquid. An example of the b.p. distribution of a product (obtained at 400°C), as derived by simulated distillation, is given in Figure I.1.6. The GC/MS profile of another liquid product (85.7% wt% boiling <200°C;96.1 wt% boiling <275°C) is given in Figure I.1.7. As seen, branched C_5-C_{10} paraffins (and some olefins) are predominant components of the product. An example of the change in product composition as a function of reaction temperature is given in Table I.1.4.

Depolymerization-liquefaction of polyethylene with Fe_2O_3/SO_4^{2-} as catalyst required somewhat higher processing temperature (425-450°C). Liquid yields in the range of 75-85 wt% were found, and the product consisted of a mixture of C_2-C_{30} (mostly C_5-C_{12}) normal and branched paraffins. An example of the b.p. distribution of the product obtained at 425°C is given in Figure I.1.8. Work is presently underway with the markedly more acidic ZrO_2/SO_4^{2-} catalyst for the purpose of (a) decreasing the reaction temperature, and (b) increasing the isoparaffin/n-paraffin ratio in the product.

B. Depolymerization-Liquefaction of Polybutadiene

Polybutadiene (98 wt% cis) is smoothly depolymerized-liquefied at 400°C and 1200 psig initial H_2 pressure, with 1 wt% of Fe_2O_3/SO_4^{2-} as catalyst. The liquid yield under these conditions is about 85 wt%. Figure I.1.9 provides the GC/MS profile of the liquid product. As seen, the product consists of a mixture of paraffins and cyclic compounds. Among the latter are alkylcyclohexanes, alkylcyclopentanes, and alkylbenzenes with C_1-C_3 alkyl groups (C_1-C_3 indicating either single or two alkyl substituents).

The formation of cyclic hydrocarbons from polybutadiene can be rationalized as follows. Butadiene obtained by depolymerization of polybutadiene, can undergo fast cyclic dimerization

to form 4-vinylcyclohexene (see Gil-Av, Shabtai and Steckel, Ind. Eng. Chem., 1960, 52,31; Shabtai and Gil-Av, Tetrathedron, 1962, 18, 87), which undergoes a sequence of rearrangement and aromatization (or ring hydrogenation) reactions to yield a full range of alkylsubstituted naphthenes and benzenes.

C. Depolymerization Kinetics and Mechanisms

Kinetic studies of polyolefin depolymerization reactions are being undertaken with the purpose of deriving rate constants for these reactions and clarifying their mechanism. Based on the change in product composition as a function of reaction temperature, a probable mechanism for depolymerization of polypropylene into branched paraffins and olefins is proposed in Figure I.1.10. Results from the kinetic studies will be provided in subsequent progress reports.

Table I.1.1.
Commercial Polymers Used as Feeds in Catalytic Depolymerization-Liquefaction Studies

Polymer type	Average, M.W.	Tm,° C[a]	Density, g/cm^3	Form	Supplier
Polystyrene (A)	800	Liquid	N/A	Liquid	Aldrich
Polystyrene (B)	45,000	60-90	1.060	Powder	Aldrich
Polystyrene (C)	280,000	237.5	1.047	Powder	Aldrich
SBR co-polymer (30% styrene)	144,000	~410	0.940	20-80 mesh[c]	Scientific Polymer Products, Inc.
SBR co-polymer (45% styrene)	~100,000[b]	N/A	0.965	20-80 mesh[d]	Scientific Polymer Products, Inc.
Polypropylene (isotactic)	250,000	189	0.900	Powder	Aldrich
Polyethylene (high density)	125,000	130	0.959	Pulverized beads	Aldrich
Polyethylene (low density)	N/A	115	0.915	Powder	Aldrich
Polybutadiene (98% cis)	197,000	140-170	0.910	20-80 mesh[d]	Scientific Polymer Products, Inc.
Polybutadiene (36% cis,55% trans 9% 1,2-add)	191,000	170-200	>0.900	20-80 mesh[d]	Scientific Polymer Products, Inc.

[a] Melting point/range or softening range
[b] Approximate value
[c] Crushed crumbs
[d] Crushed slab

Table I.1.2
Composition of Products from Depolymerization-Liquefaction of Polystyrene as a Function of Processing Temperature[a]

Temperature, °C	350	375	400	425	450
Conversion, wt%	87	~100	~100	~100	~100
Product Distribution, wt%[b]:					
Benzene	0.1	0.2	0.6	1.2	2.3
Toluene	5.2	11.9	19.7	22.4	29.2
Ethylbenzene	22.1	22.7	24.5	25.4	35.0
C_3-alkylbenzenes	15.9	16.1	16.7	17.8	19.7
C_4-alkylbenzenes	0.5	1.2	1.3	1.6	0.6
C_5-alkylbenzenes	0.1	0.2	0.3	0.5	0.3
Diphenylethanes	1.0	1.5	2.8	3.7	1.6
Diphenylpropanes	16.7	12.5	6.1	2.4	0.4
Diphenylbutanes	14.6	9.9	5.3	2.3	0.0
Diphenylpentanes	3.1	2.7	2.3	1.9	0.6
Diphenylhexanes	1.8	1.7	1.4	1.3	0.8
Triphenylalkanes	7.2	6.1	2.4	1.0	0.0
Terphenyls	0.1	0.5	1.6	2.9	3.1
Quaterphenyls	4.5	4.6	5.2	4.9	1.2
Other compounds	7.3	8.1	9.8	10.7	5.2

[a] In each run was used 15 g of polystyrene (M.W. 280,000) and 0.15 g of Fe_2O_3/SO_4^{2-} catalyst; reaction time, 2 hr; H_2 pressure, 1500 psig.

[b] All alkylbenzenes include minor amounts of corresponding alkenylbenzenes.

Table I.1.3
Composition of Products from Depolymerization-Liquefaction of (Non-Vulcanized) Styrene-Butadiene Rubber (SBR) as a Function of Processing Temperature[a]

Temperature, °C	375	400	425	450
Conversion, wt%	94	~100	~100	~100
Product Distribution, wt%[b]:				
Gas (C_1-C_4)	3.9	5.9	10.1	12.0
Liquid	95.5	93.0	88.2	85.7
Coke	0.6	1.1	1.7	2.3
Liquid Distribution, wt%:				
C_5-C_9 paraffins and cycloparaffins	10.3	11.5	13.6	16.1
Benzene	2.8	2.9	4.3	4.5
Toluene	18.1	18.2	18.5	21.0
Ethylbenzene	26.0	26.3	28.0	29.5
Styrene	0.7	1.0	1.0	1.1
C_3-alkylbenzenes[c]	10.5	11.2	11.3	8.7
C_4-alkylbenzenes[c]	2.6	2.9	2.7	2.3
C_5-C_8-alkyl and cycloalkylbenzenes[d]	15.1	14.7	14.0	11.8
Diphenylalkanes	11.3	9.2	5.1	4.5
Other compounds	2.6	2.1	1.5	0.5

[a] In each run was used 15 g of polymer and 0.15 g of Fe_2O_3/SO_4^{2-} catalyst; H_2 pressure, 1500 psig; reaction time, 2 h.

[b] Wt % of converted product.

[c] Includes some amounts of corresponding alkenylbenzene.

[d] Includes corresponding alkenylbenzenes and small amounts of indanes and tetralins.

TABLE I.1.4
Product Composition from Depolymerization-Liquefaction of Isotatic Polypropylene as a Function of Reaction temperature[a,b]

Temperature, °C	380	390	400	410	420	450
Conversion, wt%	79.8	97.0	99.8	100	100	100
Product Distribution, wt%[c]:						
Gas (C_1-C_4)	3.74	5.75	5.88	9.90	19.42	40.59
Liquid	71.27	83.04	82.18	81.29	70.05	53.27
Solid	20.19	3.05	0.21	0.00	0.00	0.00
Coke	0.11	0.13	0.10	0.09	0.07	----
Weight Loss	4.69	8.03	11.63	8.72	10.46	6.14
Gas Product Distribution, wt%[d,e]:						
C_1	0.02	0.02	0.09	0.44	0.52	0.43
C_2	0.27	0.33	0.45	1.51	4.18	4.91
C_3	1.63	2.79	2.92	4.00	9.28	20.87
C_4	1.82	2.61	2.42	3.95	5.44	14.38
Liquid Product Distribution, wt%[d,e]:						
C_5H_{12}	3.58	6.25	5.46	7.51	6.45	9.30
C_6H_{14}	4.58	8.11	7.16	8.03	8.37	9.57
C_7H_{16}	4.17	6.54	6.02	6.05	6.88	6.62
C_8H_{18}	5.01	7.72	7.39	7.37	7.63	6.56
C_9H_{20}	8.73	11.96	12.23	11.61	10.96	8.23
$C_{10}H_{22}$	4.86	6.13	6.35	6.36	6.76	3.74
$C_{11}H_{24}$	6.18	6.13	7.12	6.89	5.74	2.84
$C_{12}H_{26}$	4.89	4.86	4.98	5.05	4.56	2.22
C_{13+}	49.49	28.40	25.70	22.42	12.70	4.20
Gasoline Range, wt%:						
C_5-C_{12}	42.00	57.70	56.71	58.87	57.45	49.09

[a] In each run was used 10.0 g of polymer and 0.10 g of ZrO_2/SO_4^{2-} catalyst; reaction time, 2 hr; H_2 initial pressure, 1500 psig.
[b] Data are given by weight percentage based on the feed polymer.
[c] Liquid and solids were separated by decantation and filtration in which the solid was rinsed with little hexane.
[d] All products of a given C number consist of mixtures of isomeric branched paraffins with the exception only of the C_4H_{10} and C_5H_{12} fractions which contain some normal paraffins.
[e] All paraffin fractions contain small amounts (< 10 wt%) of corresponding olefins.

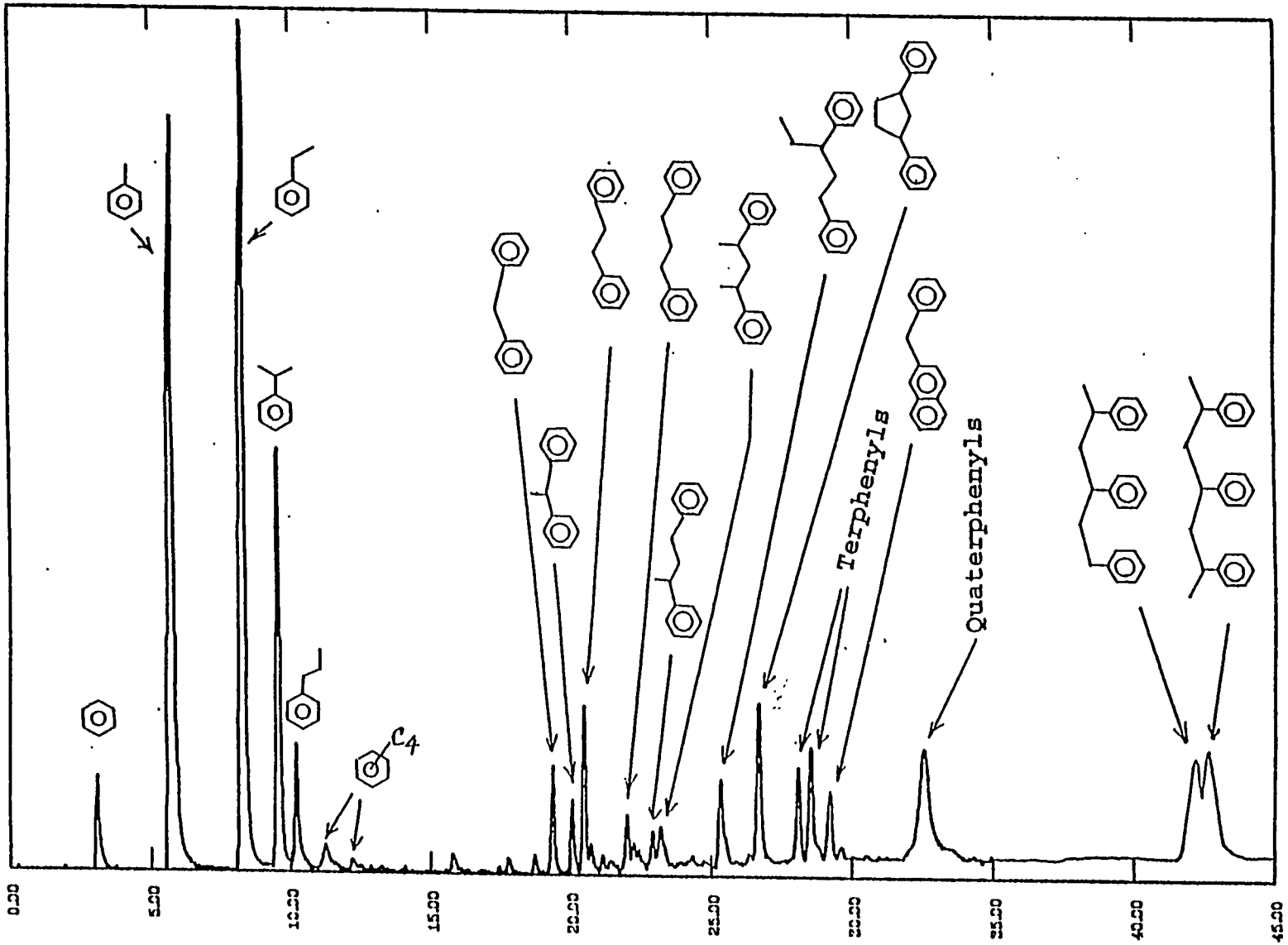

Fig. I.1.1
GC/MS Analysis of Polystyrene (M.W. 280,000) Depolymerization Product
(425 °C; Fe_2O_3/SO_4^{2-})

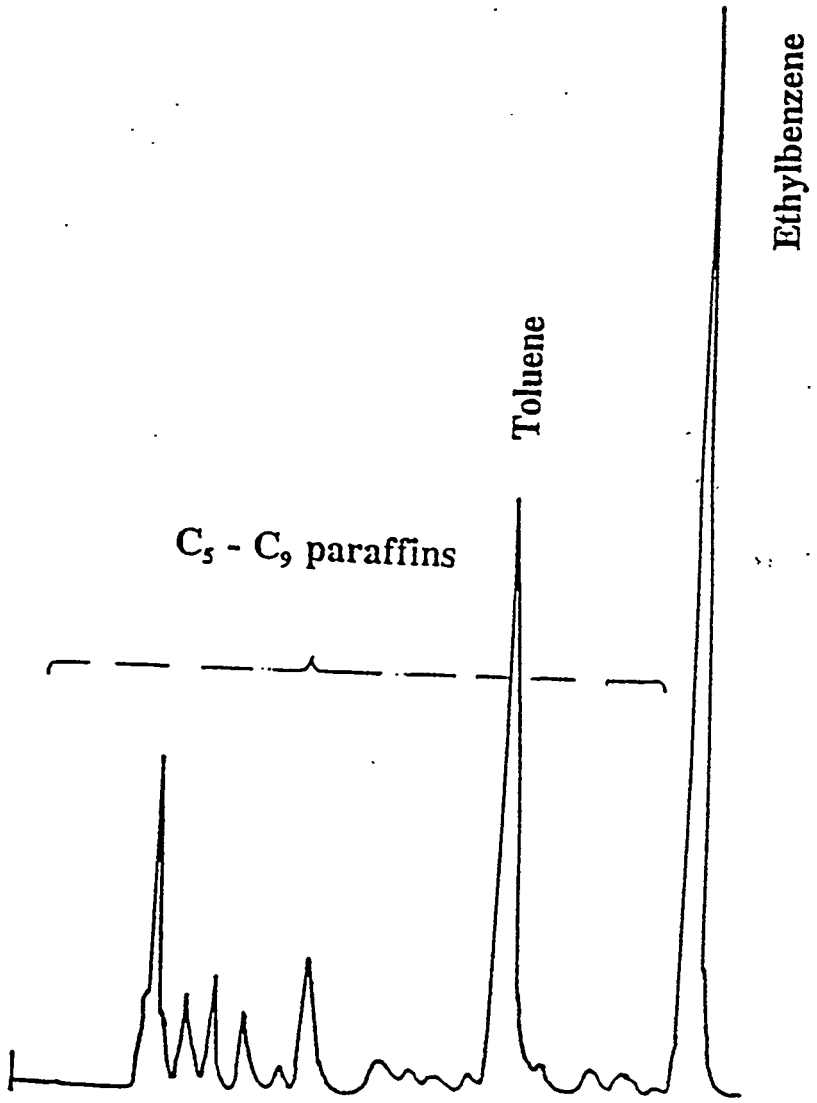

Fig. I.1.2
GC/MS Analysis of SBR Depolymerization-Liquefaction Product
(Low M.W. fraction; 400 °C; Fe_2O_3/SO_4^{2-} catalyst)

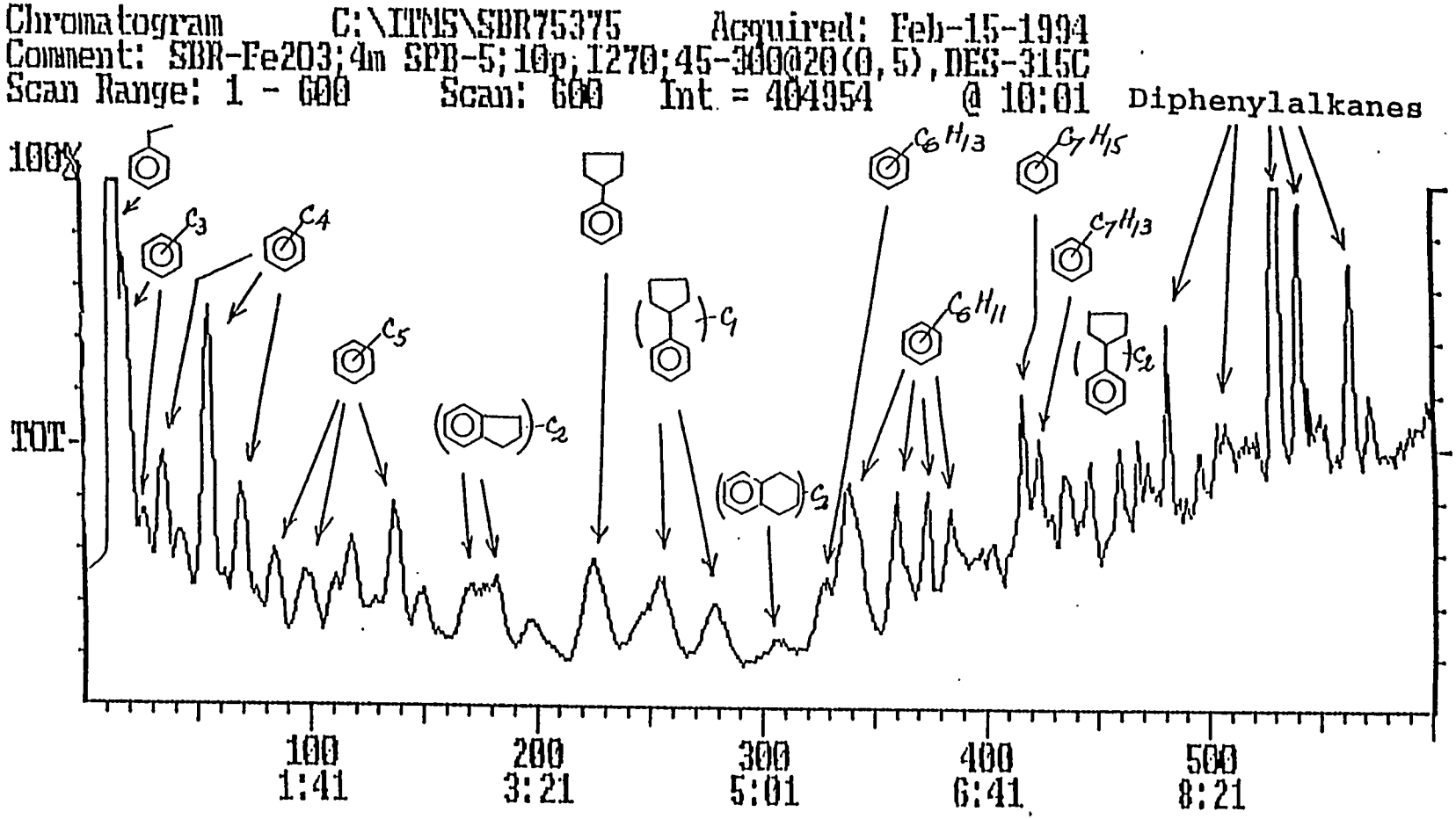

Fig. I.1.3
GC/MS Analysis of SBR Depolymerization-Liquefaction Product
(400 °C; Fe_2O_3/SO_4^{2-} catalyst)

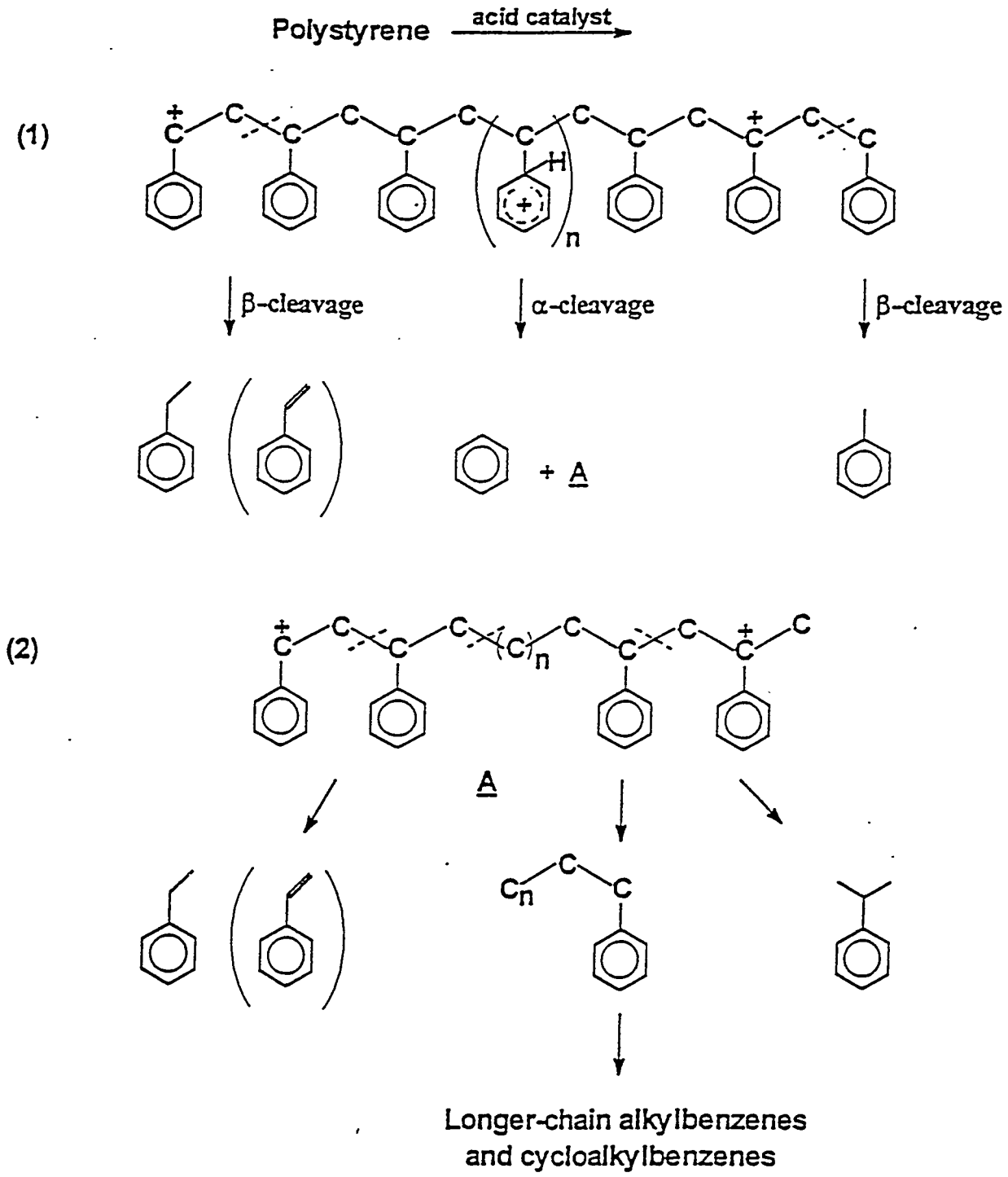

Fig. I.1.4
Probable Mechanistic Pathways
in the Depolymerization-Liquefaction of Polystyrenes

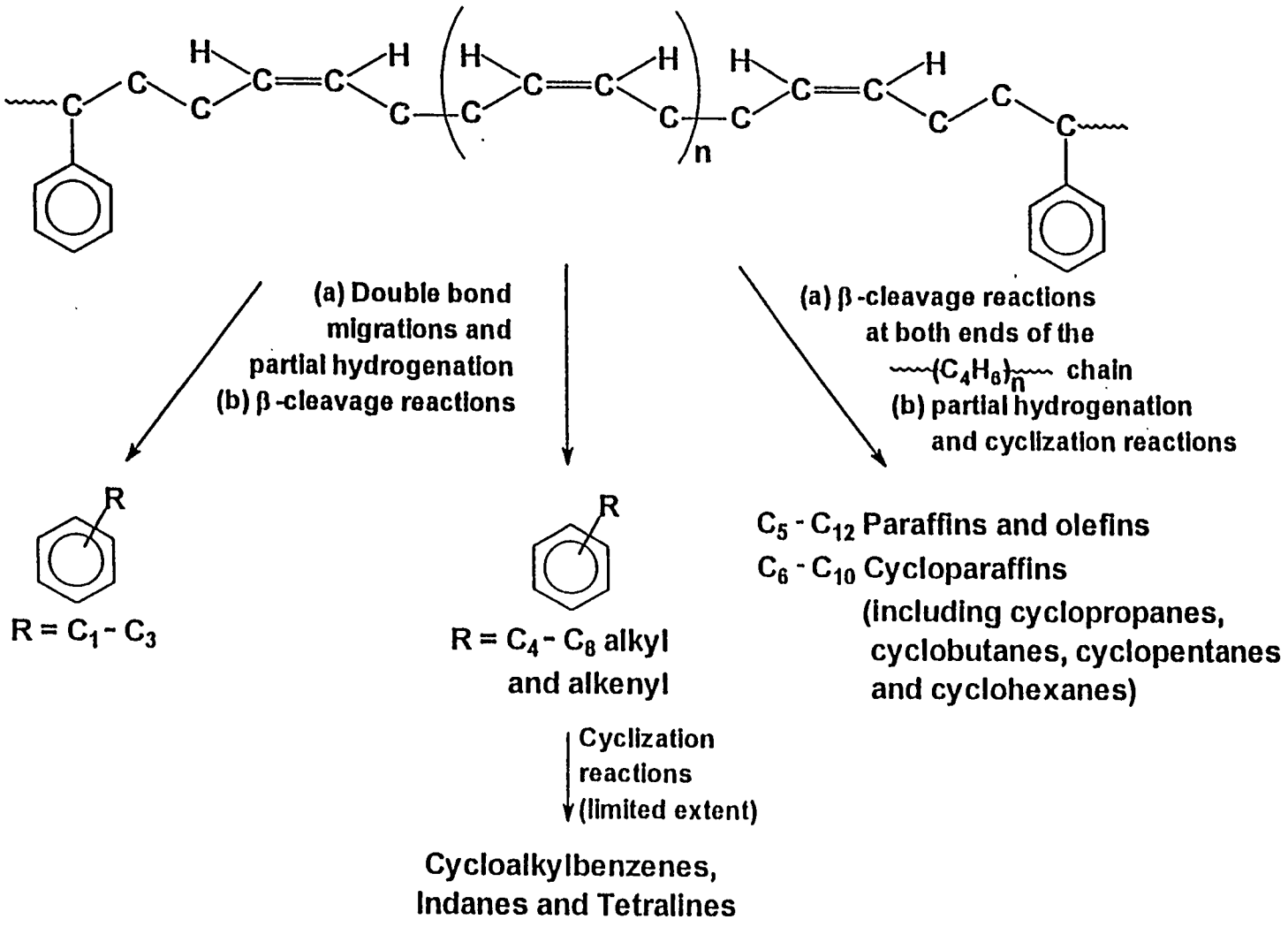

Fig. I.1.5
Probable Mechanistic Pathways
in the Depolymerization-Liquefaction of Styrene-Butadiene Rubber (Non-Vulcanized SBR)

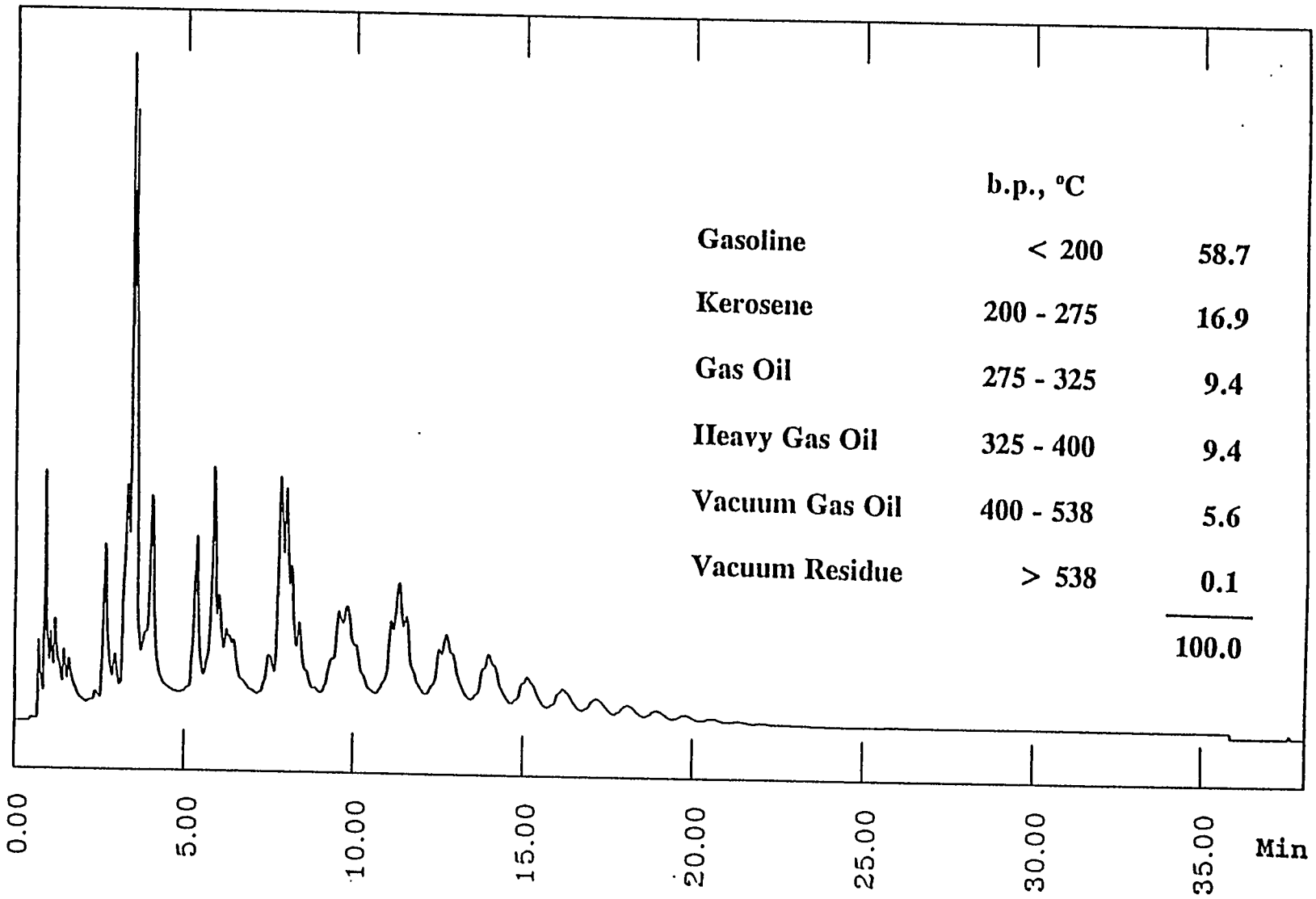

Fig. I.1.6
Boiling Point Distribution of the Liquid Product from Polypropylene by Simulated Distillation (SIMD)

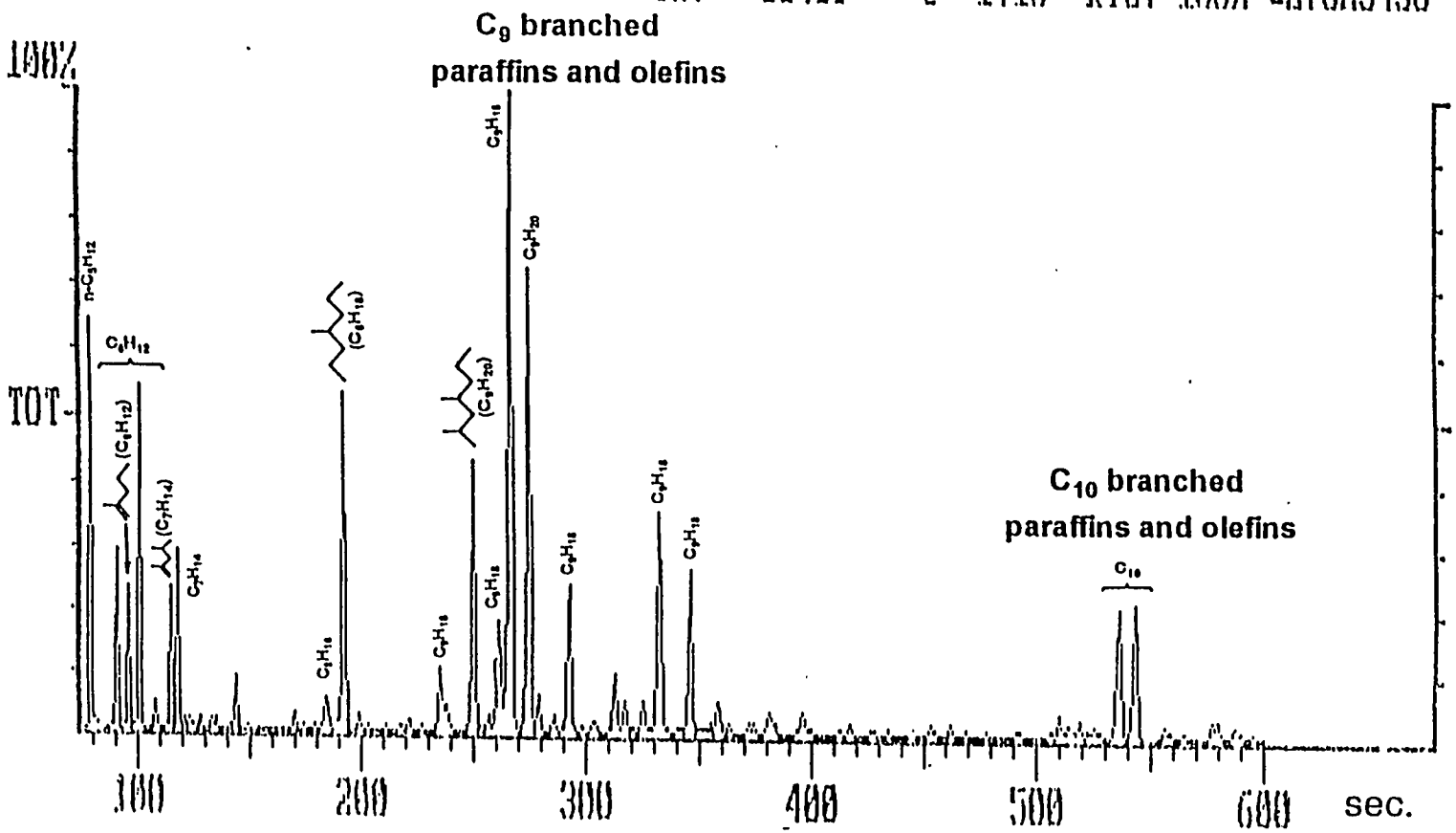

Fig. I.1.7
GC/MS of Liquid Product (Gasoline-Range Fraction) from Depolymerization-Liquefaction of Isotactic Polypropylene (Temp. 410 °C; Fe_2O_3/SO_4^{2-} Catalyst)

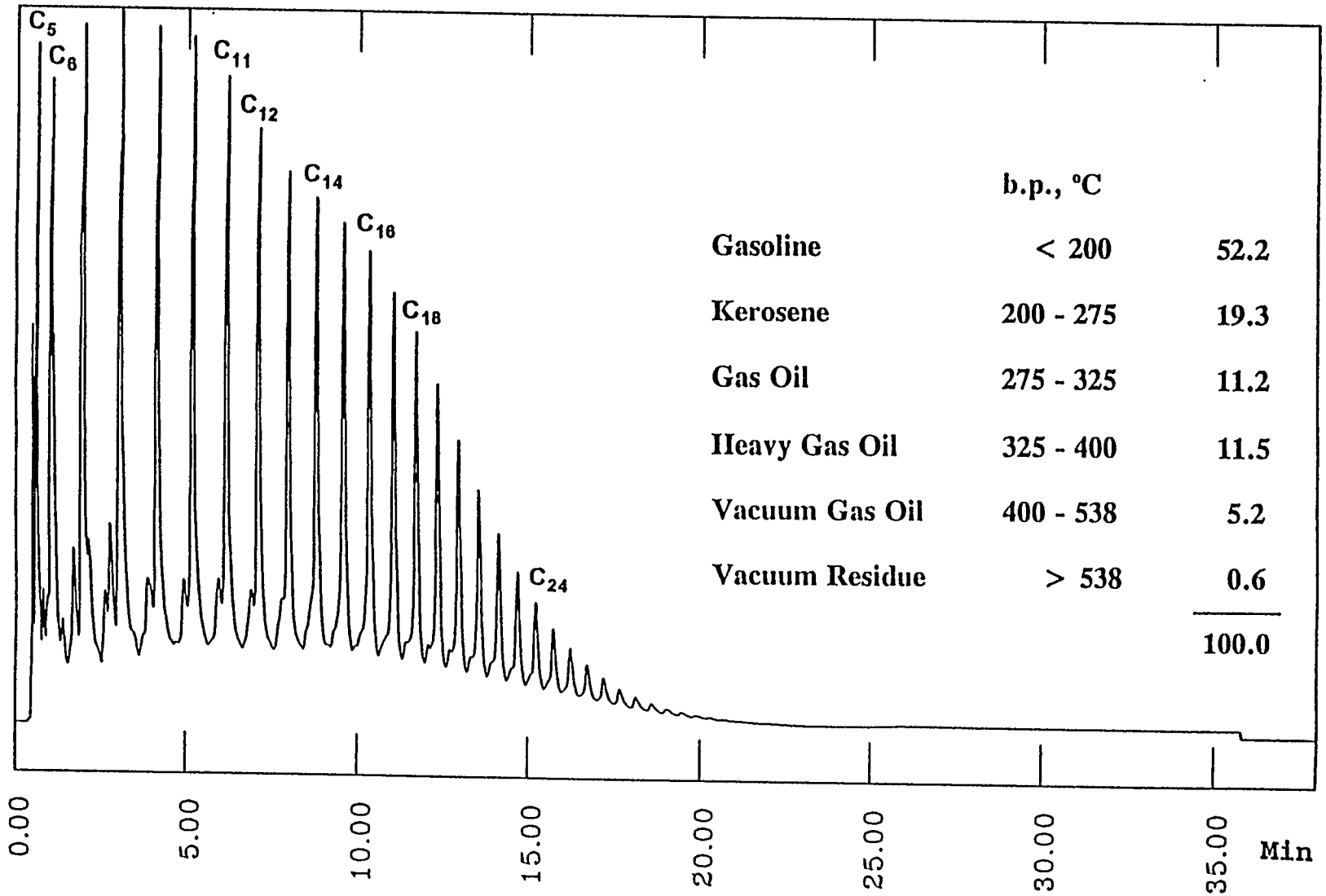

Fig. I.1.8
Boiling Point Distribution of the Liquid Product from Polyethylene by Simulated Distillation (SIMD). wt%

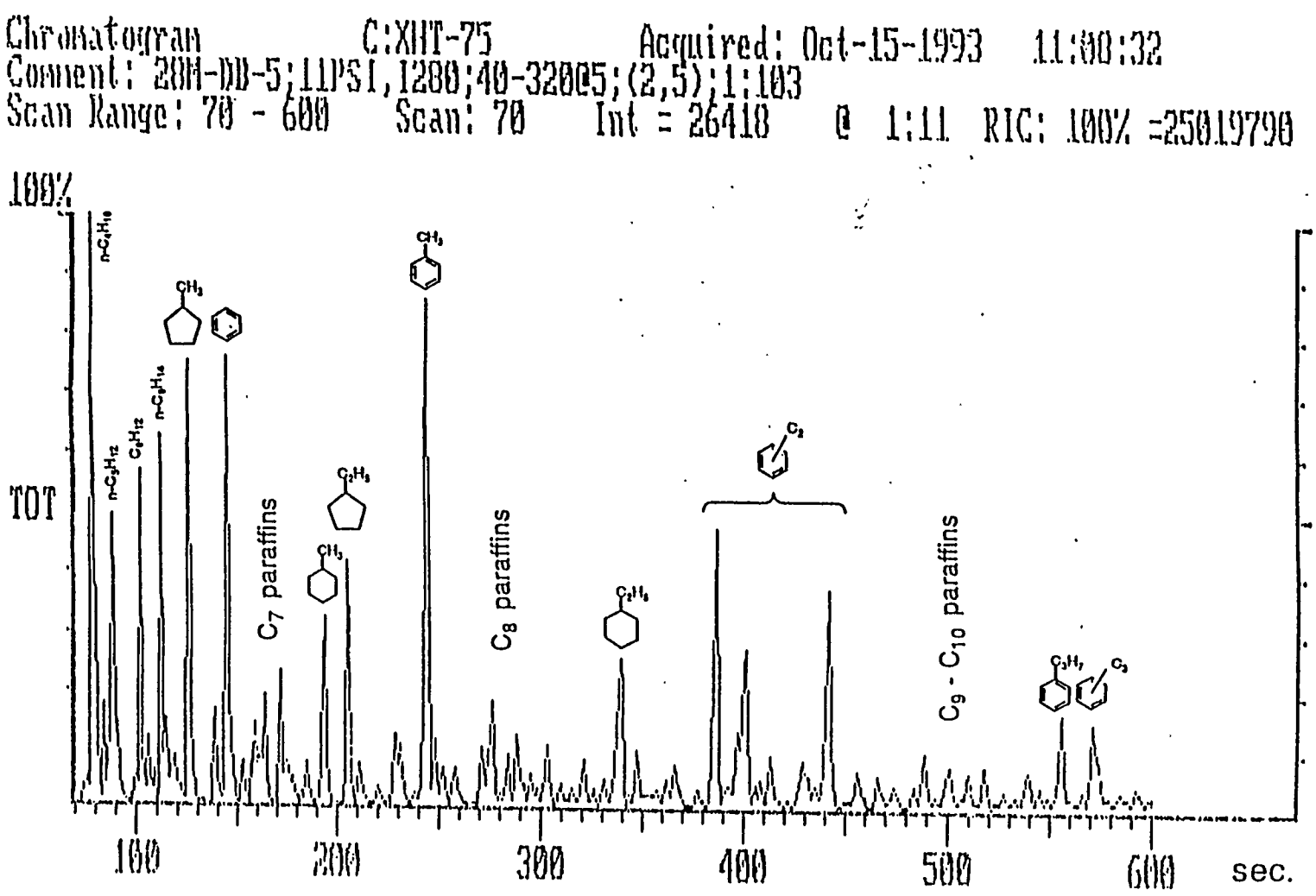

GC/MS of liquid product (gasoline-range fraction) from depolymerization-liquefaction of polybutadiene, 98% cis (temp., 400 °C; catalyst, Fe_2O_3/SO_4^{2-})

Fig. I.1.9
GC/MS of Liquid Product (Gasoline-Range Fraction) from Depolymerization-Liquefaction of Polybutadiene, 98 % cis (Temp.,400 °C; Fe_2O_3/SO_4^{2-})

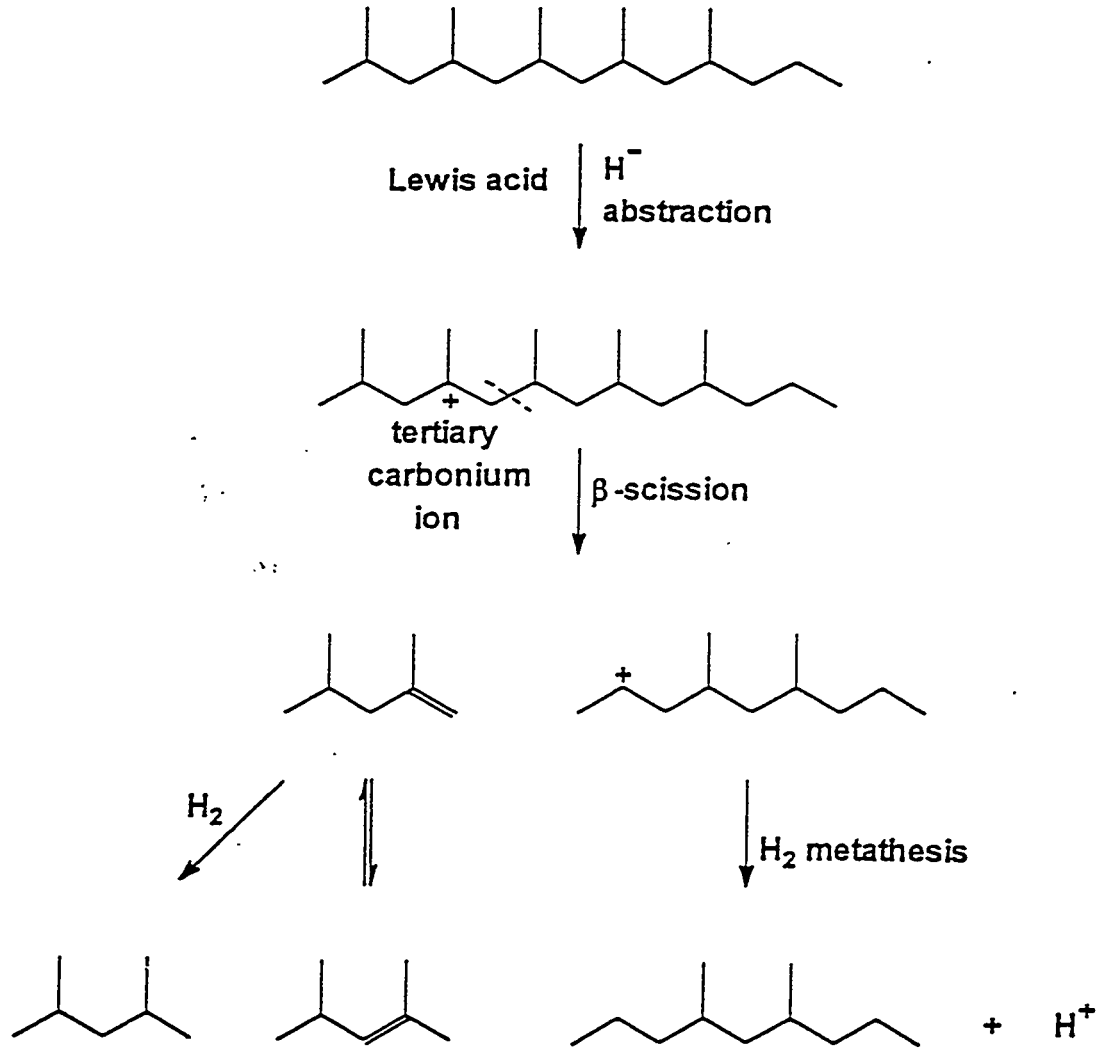

Fig. I.1.10
Proposed Mechanism for Polypropylene Depolymerization into Branched Paraffins and Olefins

TASK I

Project I.2

COLIQUEFACTION OF COAL AND WASTE POLYMERS

Edward M. Eyring and Edward C. Orr
University of Utah

In the past year we have investigated several interesting coal topics: The possibility that Blind Canyon DECS-6 coal scavenges heavy metals during liquefaction, the construction of a home made sandbath, the feasibility of using nitroxide spin probes to characterize coal pores that have been affected by supercritical CO_2, the optimum composition of a waste rubber tire /coal mixture for maximum coliquefaction yields, and the impregnation of coal with $Mo(CO)_6$ from supercritical CO_2.

Scavenging of Heavy Metals With Coal

Waste materials contain many heavy metals which may be transferred from the waste materials to liquid fuels produced by coliquefaction of the waste materials with coal. This is one possible drawback to the use of waste materials as hydrogen donors in coal liquefaction. Our earlier electron probe microanalysis studies indicated that some metal catalysts used in coal liquefaction enter the coal particles.[1,2] This scavenging effect by coal may be beneficial in the coliquefaction of waste materials with coal.

To explore this metal scavenging effect, the following experiment was carried out: Blind Canyon (Utah) coal (DECS-6, -60 mesh) was obtained from the Penn State Coal Sample Bank and ground under nitrogen to -100 mesh. Waste rubber tire samples were obtained (from the University of Utah waste material bank) that had been ground to -25 mesh. The catalyst, ammonium tetrathiomolybdate (Aldrich) was used to make an aqueous solution of molybdenum. The ground waste rubber tire and coal were mixed dry (40 % tire and 60 % coal, by weight) with different heavy metals (1 % by weight) (nickel acetylacetonate, vanadium oxide, manganese acetylacetonate, chromium acetylacetonate, and zinc oxide obtained from Strem and Aldrich) and then impregnated with (1 % by weight) molybdenum catalyst solution using the incipient wetness technique. The mixture was vacuum dried for 2 hours at 100° C. The dried mixture was placed in glass tubes and stoppered with glass wool. The glass tubes were placed in 27 cc tubing

bombs, purged with nitrogen, and pressurized to 1000 psig H_2 (cold). Tubing bombs were placed in a fluidized sandbath held at 350 ° C. The tubing bombs were shaken at 160 rpm for one hour and removed. The tubing bombs were allowed to cool overnight while under pressure. Samples were removed and extracted with tetrahydrofuran (THF) using a soxhlet extractor. Products soluble in THF were isolated using a rotary evaporator and then dried two hours under vacuum at 100 ° C. The insoluble sample (char/ash) was vacuum dried under similar conditions and then mixed with Petropoxy 154 (Pullman, Washington) and polished with a Syntron diamond paste polisher for eight hours. Electron probe microanalysis (EPMA) micrographs were obtained using a CAMECA Model SX-50 electron microprobe (Courbevoie, France).

No penetration of the coal particles by heavy metals was noted in the EPMA micrographs except for chromium in tire particles. The experiment was repeated because many of the heavy metals used are somewhat soluble in THF. THF solubility may have caused the strange dispersion patterns of chromium that we observed in the EPMA micrographs of tire and coal samples spiked with chromium acetylacetonate. Further work showed that the THF solubles did contain chromium. Therefore, any dispersion in the coal and tire particles could be attributable to the THF solvent and not to the scavenging effect of the coal particles.

The experiment was repeated and samples were extracted with cyclohexane instead of THF. The results are as follows:

Figure I.2.1 shows a variety of tire particles and coal particles from a sample that was doped with zinc oxide. Tire particles contain both sulfur and zinc which allows them to be easily distinguished from coal particles by comparison of the sulfur and zinc micrographs. The particle in the upper right hand corner is a tire particle. Moving from the tire particle towards the lower left hand corner, a roughly circular coal particle can be observed in the sulfur micrograph. The coal particle contains less sulfur than the tire particles. In the zinc micrograph, the coal particle shows that some zinc has accumulated at the edges of the coal particle. It appears as if the coal has scavenged some of the artificially added zinc during liquefaction.

Figure I.2.2 shows a tire particle and a coal particle from a sample that had been doped with nickel acetylacetonate. The coal particle appears in the left hand side of the sulfur micrograph and the tire particle in the right hand side of the sulfur micrograph. The nickel micrograph show an outline of nickel around the left hand side of the coal particle indicating the presence of nickel in the borders of the coal particle. The presence of zinc in the coal particle

even though zinc was not added to this sample is also noteworthy. The only source of zinc in this system is the tire. This further suggests that coal may be acting as a scavenger for heavy metals.

Figure I.2.3 shows a tire particle and a coal particle from a sample that had been doped with vanadium pentoxide. The coal particle makes up over half of the field of view on the right hand side of the micrograph. The tire particle, observed in the left hand side of the micrograph, shows a greater sulfur density and is easily distinguished by the zinc abundance shown in the zinc micrograph. The vanadium micrograph shows that there is no evidence of vanadium in the coal particle.

Figure I.2.4 presents a combination of tire particles and coal particles taken from a sample that was spiked with chromium acetylacetonate. The sulfur micrograph shows a coal particle at the center of the micrograph and three other coal particles surrounding the center particle at the 2, 3, and 6 o'clock positions. There are three tire particles. One tire particle is found in the upper right hand corner and the other two are found on the left hand side of the sulfur micrograph. The tire particles are easily distinguished from the coal particles by the presence of zinc noted in the zinc micrograph. The chromium micrograph shows an enhanced density of chromium in all four coal particles.

From the above it is clear that there is evidence that Blind canyon coal may act as scavenger for heavy metals. This scavenging effect will be further investigated by analyzing the coliquefaction liquids and the char/ash for the presence of heavy
metals.

Construction of a Sandbath

We built our own sandbath at a minimal cost to facilitate running more samples to finish our initial projects. The sandbath was constructed in our own machine shop. The design of this in-house sandbath was based on that of Techne's model which would cost approximately $5,500 to purchase. Our cost was only $1,500 to build, and it operates in a similar fashion. Having the sandbath in one of our labs has considerably increased the number of experiments that can be completed in a work week.

Use of EPR Active Nitroxide Spin Probes in Supercritical CO_2

Kispert, Cooray, and Spears have demonstrated that EPR active spin probes (nitroxide molecules) can be used to characterize the size, and shape, of coal pores for coals of differing rank.[3,4,5] This technique may be used to elucidate the effect that the solvent supercritical CO_2 (T_c=31.5° C, P_c=1074 psi) has on coal pores.

We have successfully impregnated Beulah DECS-11 coal with 2,2,6,6-tetramethylpiperidine-1-oxyl (TEMPO) from supercritical CO_2. We intend to use other coals and nitroxide spin probes (4-hydroxy-2,2,6,6-tetramethylpiperidine-1-oxyl and 4-amino-2,2,6,6-tetramethylpiperidine-1-oxyl) introduced with supercritical CO_2 to compare solvent effects of supercritical CO_2 to the corresponding effects of organic solvents on coal pores.

We have constructed a high pressure EPR cell to monitor diffusion of nitroxide spin probes into coal under supercritical CO_2 conditions.

Impregnation of Coal with $Mo(CO)_6$ from Supercritical CO_2

In the past year we have investigated the effect of using supercritical CO_2 as an impregnation solvent for $Mo(CO)_6$. EPMA data for the impregnated coal before liquefaction were examined to determine whether the catalyst was dispersed in the coal. No catalyst was detected by EPMA in the coal. However, liquefaction yields were much greater than without catalyst indicating the presence of $Mo(CO)_6$ in the coal below the threshold for EPMA detection.

We intend to use the above mentioned high pressure EPR cell to measure diffusion of $V(CO)_6$ from supercritical CO_2 into the coal. We will use $V(CO)_6$ instead of $Mo(CO)_6$ because the vanadium species is EPR active whereas the molybdenum species is not.

Optimum Mix of Waste Rubber Tires and Coal

In our 1993 Summer quarterly report, we indicated that a mixture of 40 % waste rubber tire and 60 % Blind Canyon DECS-17 coal produces the optimum THF soluble yields. We have recently switched our tire sample source. We are now using ground rubber tires from the University of Utah waste material bank. We will carry out experiments to determine whether this new tire sample with DECS-6 coal still provides an optimum yield in a 40 % tire and 60 % coal mix. We have upgraded our gas chromatograph to allow us to perform simulated distillations. This will permit us to characterize more accurately the liquids derived from waste materials.

References

1. Sommerfeld, D.; Jaturapitpornsakul, J.; Anderson, L.; Eyring, E. Fuel Proc. Tech., 1993, **34**, 187.

2. Sommerfeld, D.; Tuntawiroon, W.; Anderson, L.; Eyring, E. ACS Prepr. Pap. Am. Chem. Soc. Div. Fuel Chem., 1993, **38**, 211.

3. Kispert, L.; Wuu, S. Fuel, 1985, **64**, 1681.

4. Cooray, L. Thesis, University of Alabama, Tuscaloosa, 1988, 27.

5. Spears, D. Thesis, University of Alabama, Tuscaloosa, 1991, 97.

Figure I.2.1.

EPMA Micrograph

40 % waste rubber tire mixed with 60 % Blind Canyon DECS-6 by weight
Catalyst: 1 % ammonium tetrathiomolybdate
Doped with: 1 % zinc oxide
Hydrotreated for 1 hour at 350° C under 1000 psig hydrogen (cold)

Secondary Electron Image

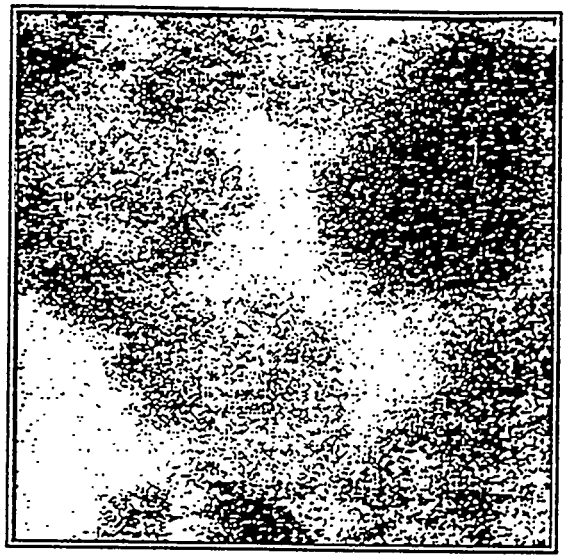

Sulfur K_α

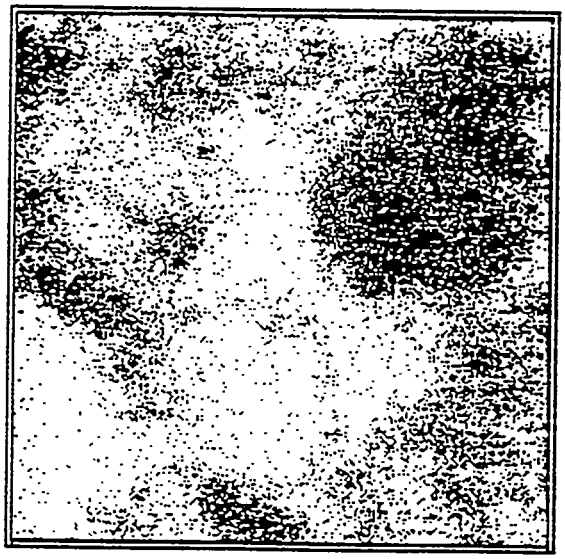

Zinc L_α

Figure I.2.2.

EPMA Micrograph

40 % waste rubber tire mixed with 60 % Blind Canyon DECS-6 by weight
Catalyst: 1 % ammonium tetrathiomolybdate
Doped with: 1 % nickel acetylacetonate
Hydrotreated for 1 hour at 350° C under 1000 psig hydrogen (cold)

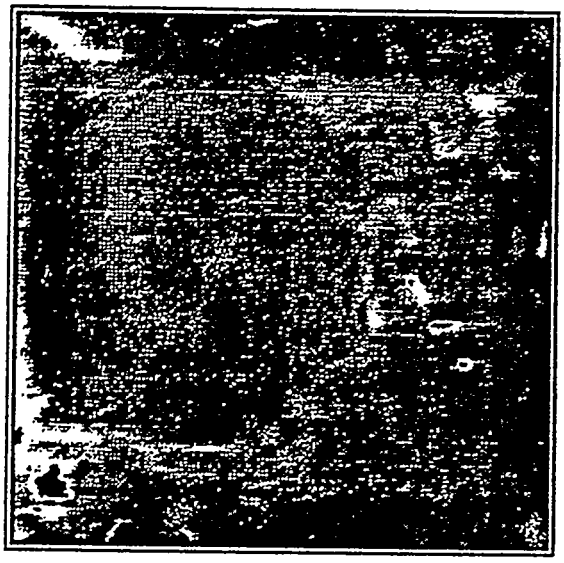

Secondary Electron Image

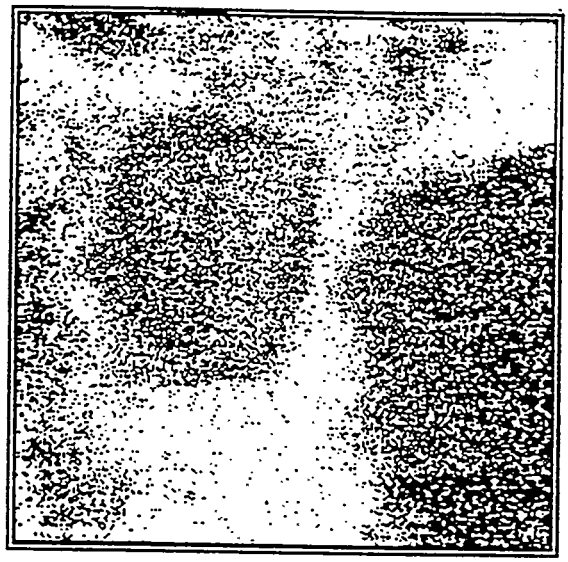

Sulfur K_α

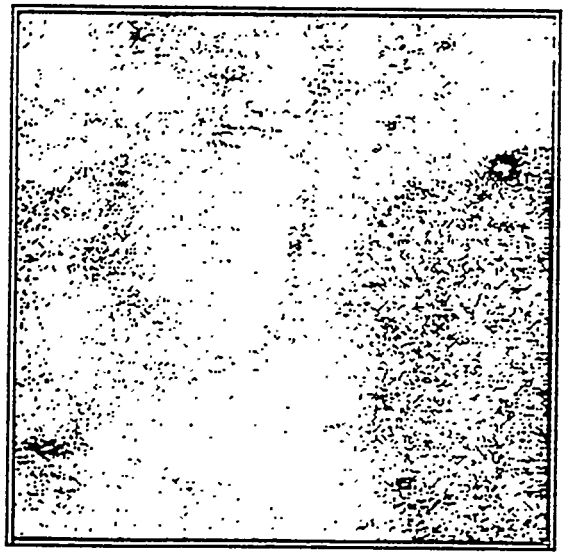

Zinc L_α

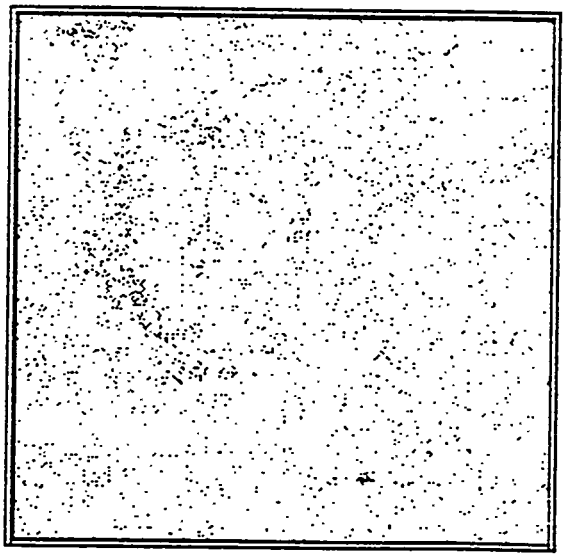

Nickel K_α

Figure I.2.3.

EPMA Micrograph

40 % waste rubber tire mixed with 60 % Blind Canyon DECS-6 by weight
Catalyst: 1 % ammonium tetrathiomolybdate
Doped with: 1 % vanadium pentoxide
Hydrotreated for 1 hour at 350° C under 1000 psig hydrogen (cold)

Secondary Electron Image

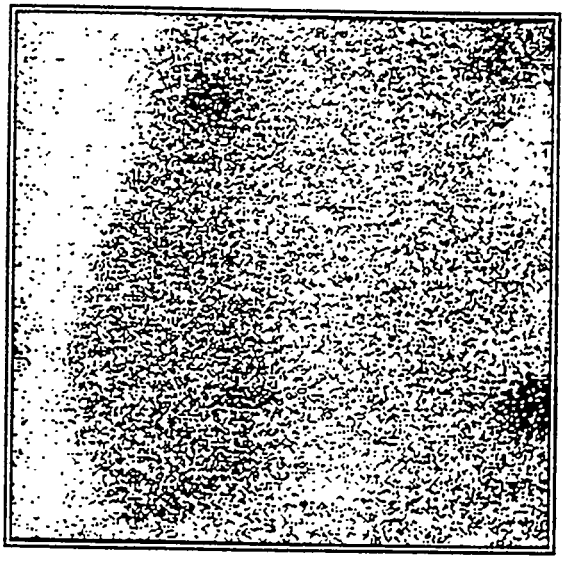

Sulfur K_α

Zinc L_α

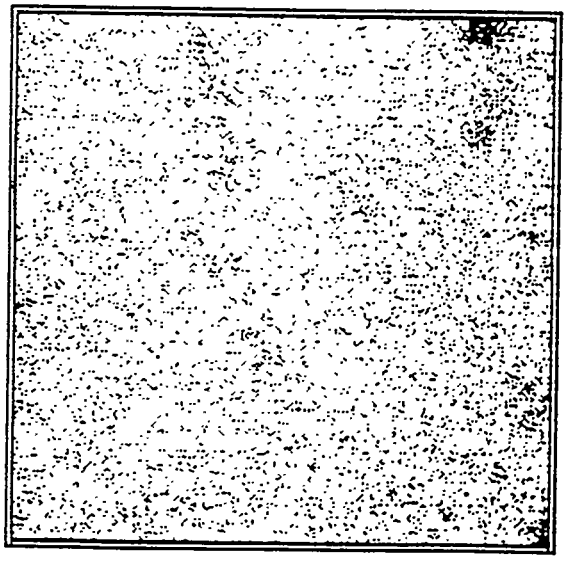

Vanadium K_α

Figure I.2.4

EPMA Micrograph

40 % waste rubber tire mixed with 60 % Blind Canyon DECS-6 by weight
Catalyst: 1 % ammonium tetrathiomolybdate
Doped with: 1 % chromium acetylacetonate
Hydrotreated for 1 hour at 350° C under 1000 psig hydrogen (cold)

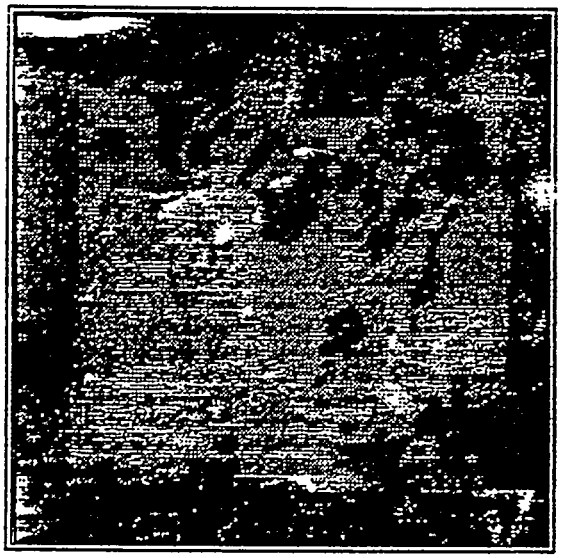

Secondary Electron Image

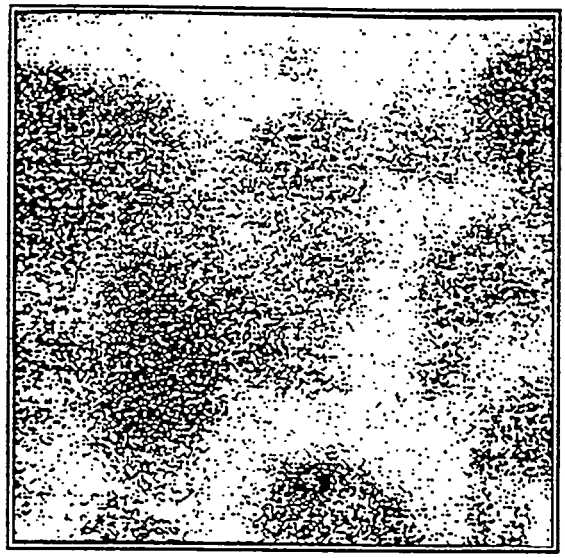

Sulfur K_α

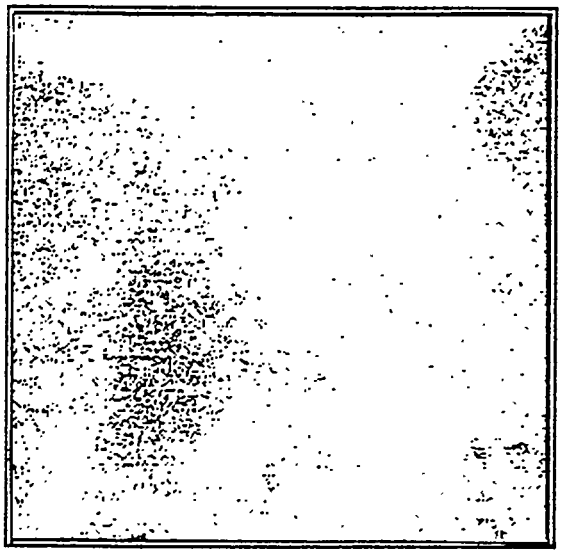

Zinc L_α

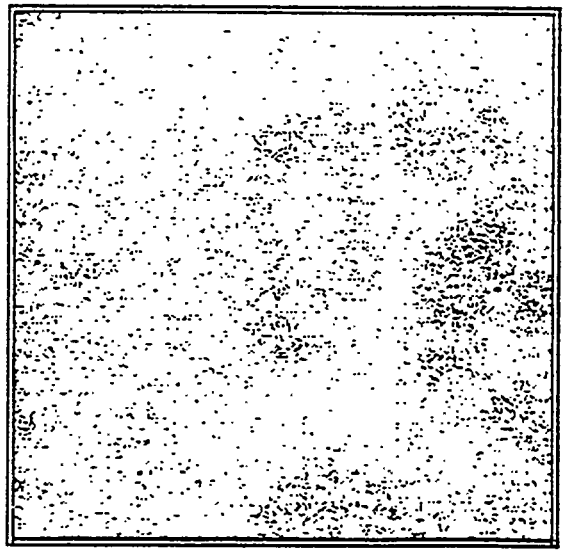

Chromium K_α

TASK I

Project I.3

USE OF MIXED PYRRHOTITE/PYRITE CATALYSTS FOR CO-LIQUEFACTION OF COAL AND WASTE RUBBER TIRES

D.B. Dadyburjor, J.W. Zondlo,
Z. Liu and R.K. Sharma
Department of Chemical Engineering
West Virginia University

OBJECTIVES

The overall objective of this research program is to determine the optimum processing conditions for the co-liquefaction of coal with tires and other similar organic waste in the first stage of liquefaction. Thermal processes as well as catalytic ones are to be investigated. The catalysts considered are our pyrrhotite/pyrite mixtures, obtained from disproportionation of ferric sulfide, as well as promising catalysts from other consortium laboratories. The intent here is to achieve the maximum waste/coal conversion at the mildest conditions of temperature and pressure. Specific objectives include an investigation of the effects of time, temperature, pressure, waste constituents, catalyst and co-solvent on the conversion and product slate of the co-liquefaction.

RESULTS

In this report, we present the results of co-liquefaction of coal and tire. The coal used was DECS-6 which is a high-volatile A bituminous coal from the Blind Canyon seam in Utah. The coal was received from the Pennsylvania State University Coal Bank (PSCB) and ground to -60 mesh under nitrogen. Three different tire materials were available for this study. The first sample was prepared from a Goodyear Invicta tire, recycled in-house at WVU (Tire-1). A portion of the tire (from both front and side walls) was ground to less than 1 mm, washed, and magnetically treated to remove the steel particles from the belts. Another sample, obtained from the University of Utah, was a recycled tire ground to -30 mesh (Tire-2). The third sample consists of tire buffings, also obtained from the University of Utah. Only the first two samples have been used during the time period of this report. Table I shows proximate and ultimate analyses of the tire

materials (obtained from Galbraith Laboratories) and DECS-6 coal (from PSCB). As seen in the table, the amounts of volatile matter in all the tire samples are very high. The 26-31% fixed carbon mainly represents the amount of carbon black present in the sample. The tire samples also have fairly high levels of sulfur, more than double that of the coal.

For all the data reported below, total conversion was based on the measurement of tetrahydrofuran (THF)-insoluble matter. The asphaltene yield was found from the measurement of hexane-insoluble matter. The oil+gas yield was found by difference. For some runs, the gas fraction was measured separately, using gas chromatography as described in earlier reports.

1. Uncatalyzed Liquefaction

Tire-1 Runs

Preliminary liquefaction results are currently in press [1] and will only be briefly referred to here. The Tire-1 sample and DECS-6 coal were used for these.

Runs were first performed on both coal and tire separately, with and without tetralin, at 350-400°C and 1000 psi H_2 (cold) for 30 min. The conversion of coal (alone) at 400°C increases in the presence of tetralin from 37% (no tetralin) to 81%. The yield of asphaltenes also increases similarly, while the increase in oil+gas yield is relatively small, from 22% to 26%. The increased yield of asphaltene (relative to oil+gas) when tetralin is added implies that radicals formed during coal liquefaction are mainly in the asphaltene size range. The gas yield is 5.7%. Analysis, on a hydrogen-free basis, yields: CO, 2.5%; CH_4, 9%; CO_2, 15%; C_2, 40%; C_3, 14%; C_4, 6%; and C_5, 12%.

In the case of tire (alone), the addition of tetralin has virtually no effect on the conversion, which remains at about 66%. The conversion corresponds to the amount of volatile matter in the tire, indicating that the carbon black is essentially unreactive under the conditions used in these runs.

Liquefaction runs at temperatures below 400°C indicate a stronger effect of tetralin on the conversion of Tire-1. The conversion increases from 43% (no tetralin) to 63% in the presence of tetralin at 350°C, and from 60% to 64% at 375°C. One explanation of the temperature-dependence of the solvent effect may be as follows. It may be that tire liquefaction follows a thermal cracking mechanism and/or a hydrogenation mechanism, depending upon the reaction temperature. At 350°C, hydrogenation should be a necessary step for bond breakage, therefore the tetralin helps the conversion. At the higher temperatures, thermal cracking may be

predominant, so the presence of tetralin or even hydrogen should have little effect. Free radicals would be expected to be generated at these higher temperatures, and these would then combine to form aliphatic products. The existence of aliphatic free radicals containing a few carbon atoms is consistent with results of other investigators [2]. In addition, the aromatization of the styrene component into multiple-ring aromatics may generate hydrogen free radicals. Hence these radicals are smaller than coal-generated radicals, which are in the asphaltene size range.

Analysis of the gas-phase products of tire liquefaction at the highest temperature in hydrogen results in the following, on a hydrogen-free basis: CO, 2.5%; CH_4, 7.2%; CO_2, 8.2%; C_2 hydrocarbons, 34%; C_3 hydrocarbons, 14%; C_4 hydrocarbons, 22%; and C_5 hydrocarbons, 12%. Compared to the coal-alone analysis, the gas from tire contains more C_4 at the expense of CO_2 and C_2 hydrocarbons. Compared to the results after tire pyrolysis [2], there is a significant contribution from the C_5 hydrocarbons. Furthermore, the total gas yield is approximately 6.2%, significantly smaller than the value of 10% during pyrolysis (and approximately equal to that from the tire). Hence the presence of hydrogen in the gas phase influences the gas products formed during the reaction of the tire material at the higher temperatures, and may influence the fate of the free radicals formed under these conditions.

Preliminary FTIR spectra for the unreacted (THF-insoluble) material from tire liquefaction at 400°C show no detectable amount of aromatic or aliphatic hydrogen. Therefore, it is reasonable to assume that all organic matter, except carbon black, in the tire can be liquefied when the maximum conversion is reached.

Since tire rubber can be fully liquefied at 400°C without a solvent, it is of interest to determine the effect of H_2 pressure at this condition. When the hydrogen partial pressure is increased from 0 psi to 1000 psig (cold), the conversion and the oil+gas yield are practically unchanged. The results of 0 psi hydrogen were obtained under 15 psi (cold) nitrogen. The nitrogen results are consistent with those of others [2,3]. All these results imply that, with the possible (and minor) exception of the gas yield, the tire liquefaction is actually tire pyrolysis, at least at temperatures of 400°C or higher.

The co-liquefaction of coal and Tire-1 was performed at 400°C and 1000 psig (cold) of H_2. No tetralin was present in these experiments. In analyzing these and all of the subsequent co-liquefaction runs, we assume that the organic matter of the tire is completely converted to oil+gas at 400°C, even in the presence of coal. Hence, the weighted contribution of the tire can be

subtracted from the co-liquefaction results to calculate the conversion and product distribution based on the coal alone in the coal/tire mixture.

Addition of an equal mass of Tire-1 to coal results in an increase in conversion at the standard conditions from 37% (in the absence of the tire) to 50%, and relatively little change in the oil+gas yield from the coal. The gas yield from the coal, again subtracting the tire contribution, is approximately 1.6%, much less than that from the coal alone. The individual analyses (again subtracting the tire contribution) are: CO, 2%; CH_4, 33%; CO_2, 52%; C_2, 6%; C_3 9%; C_4, 1% and C_5, -3%. Compared to the gas from the coal-alone liquefaction, the gas here contains approximately the same amount of CO, CH_4 and CO_2, but much smaller amounts of C_{2+} hydrocarbons.

The tire-to-coal ratio was varied from 0 to 4 (weight basis). For co-liquefaction of coal and Tire-1, the conversion of coal increases from 37% (for coal alone) to a value of 68%, at a tire-to-coal ratio of 2. At higher ratios, the value is more-or-less level, reaching 66% at a ratio of 4. The oil+gas yield remains more-or-less constant at all ratios from 0 to 4, around 22%. This suggests that the major result of co-liquefaction is to enhance the asphaltene yield, although the enhancement is less than that achieved when tetralin is added to the coal.

It is difficult to cite explicitly the role of the tire as a solvent since a solvent can improve liquefaction in many ways. Our results with tire alone, as well as tire pyrolysis results, catalyzed and uncatalyzed, in the literature indicate that the formation of free radicals by the tire plays at least some part in the role of the tire as solvent. Recent ESR results from consortium laboratories [3] indicate that even stable coal radicals disappear (i.e., are capped) in the presence of the tire at liquefaction temperatures. Radicals from the tire are probably in the oil range, whereas those from tetralin are small hydrogen radicals. Radicals from coal probably have a wide size distribution centered in the asphaltenic range. Since the tire-based radicals are bigger than the tetralin-based radicals, any increase in conversion using tire should result in mainly increased yields of asphaltenes, while using tetralin should result in an appreciable increase in oils. The hypothesis is consistent with the observed yields and also with the observed loss of C_{2+} hydrocarbons from the gas phase during the co-liquefaction.

The effect of hydrogen on co-liquefaction is somewhat different than that on tire liquefaction. As before, the partial pressure of hydrogen was increased from 0 to 1000 psig (cold), and the tire-to-coal ratio was unity. Both the conversion and the oil+gas yield increase

with an increase of H_2 pressure, up to around 500 psig (cold). At higher H_2 pressures, the conversion and oil + gas yield are relatively insensitive to the pressure. The same behavior can be found qualitatively for coal liquefaction in the absence of the tire but in the presence of tetralin, at the same reaction conditions. Clearly, coal liquefaction needs some hydrogen from the gas phase, whether the solvent is tetralin or liquefied tire. In either case, a H_2 pressure of greater than 500 psig is not necessary with this particular coal under these reaction conditions.

Further, the asymptotic values of conversion at H_2 pressures greater than 500 psig are different for co-liquefaction (coal plus Tire-1) than for liquefaction with tetralin. This suggests a difference between the actions of tetralin and liquefied tire. The tire-based radical is larger than the tetralin-based hydrogen radical. Hence, it is reasonable to believe that the capping process involving the former is less efficient than that involving the latter. This could account for the higher total conversion using tetralin relative to that using tire.

The effects of tetralin on coal liquefaction and coal-tire co-liquefaction were also investigated. For the co-liquefaction, the tire/coal ratio was maintained at unity. Addition of tetralin increases the conversion of coal, with or without tire. In other words, the relationship between tetralin and coal conversion is not affected by the presence of tire. Consistent with the arguments made above, this may be because tetralin is a better radical donor than the (liquefied) tire for coal liquefaction, and the effect of tetralin overwhelms the effect of the tire. This result also seems to indicate that the solids in the tire (carbon black, zinc oxide, sulfur, etc.) apparently do not have significant catalytic activity. Otherwise, the presence of the tire would have increased the conversion and oil+gas yield of the coal.

To investigate further the effect of the tire solids on the co-liquefaction, oils obtained from the liquefaction of Tire-1 (alone) were used as the solvent in coal liquefaction, instead of raw tire material. The tire-oil/coal ratio was 2/3, equivalent to a tire/coal ratio of 3/3. The values of conversion and oil+gas yield were found to be no different from the corresponding values during the co-liquefaction of (equal parts of) tire and coal. Hence, it would appear that the tire solids play no catalytic role during tire-coal co-liquefaction. This would seem to contradict the results of Farcasiu and Smith [4], who compared conversions and yields of coal plus the individual tire components without carbon black with coal plus components including 138 m^2/g carbon black. However, there is a large variety of carbon blacks with different particle sizes, shapes and surface areas. Perhaps the characteristics of the carbon black used by Farcasiu and Smith are different

from those of the carbon black which was present in our tire sample.

Tire-2 Runs

In the last quarter, a more systematic series of experiments has been started with the Tire-2 sample, which is expected to be a common sample for all consortium members. Figure 1 shows the results from co-liquefaction runs at 400°C as a function of the tire-to-coal ratio. Again, the results are calculated on a coal-alone basis, i.e., the contribution of the tire has been subtracted out. The values for simple coal liquefaction correspond to a ratio of 0, and the values for the tire alone are shown as dashed horizontal lines. Since the Tire-1 results [1] may have shown a maximum in conversion around a tire-to-coal ratio of 2, additional data were obtained around that point, and also at a much larger value of the ratio. Gas yields were measured separately and the oil yield was obtained by difference.

Figure 1 does indeed show a slight maximum in conversion between ratios of 2 and 3, and then a very high value at a ratio of 15. Oil yields are greatest at a ratio around 2, and at higher ratios, the gas yield increases. The oil+gas yield (not shown) appears to pass through a minimum as the ratio is increased. However, the reliability of calculations at high tire-to-coal ratios is rather low, since the large amount of tire present results in the subtraction of two relatively large numbers of approximately equal value.

Hence, runs at this value of the ratio were not repeated in Figure 2, which shows the results of co-liquefaction at 350° and 375° C. The oil and gas yields are combined here. At these two lower temperatures, the oil+gas yield follows the same trend as at 400°C. However, the conversion appears to increase steadily with tire-to-coal ratio, at least for the range of values used in Figure 2.

The effect of carbon black (in the tire) on the liquefaction of coal was also investigated. In order to do this, individual components of the tire, including carbon black, were obtained from Dr. Farcasiu of USDOE/PETC. The components, without carbon black, were first mixed in approximately the same proportion as in the tire sample. The mixture was then liquefied at 400°C and 1000 psi (cold) for 30 min, both in the presence and the absence of coal corresponding to a tire/coal ratio of unity. The experiments were then repeated, this time with the appropriate amount of carbon black present. In addition, the appropriate amount of carbon black was added to the coal alone, i.e., without the rest of the tire components, and the experiment was repeated again. In all cases, the results were calculated on a carbon-black-free basis in order to make a

direct comparison; for the case of coal plus tire components (with or without carbon black), the results were calculated on a carbon-black-free and coal-alone basis, i.e., with the weighted effect of the components (with or without carbon black) subtracted.

The results are presented in Figure 3. They indicate that the conversion and product distribution from the separate liquefaction of tire components (alone) and coal (alone) are not significantly affected by the presence of carbon black. Similarly, the conversion of coal in the co-liquefaction of coal plus tire components (without carbon black) is not significantly affected by the presence of carbon black; neither is the oil+gas yield of the coal alone in the co-liquefaction. However, the presence of the tire components (without carbon black) increases the conversion of coal in the tire-component/coal mixture, just as the presence of the tire does in the tire/coal mixtures of Figures 1 and 2.

Figure 4 shows the effect of run time on the co-liquefaction of coal plus tire components, with and without carbon black. At the smallest value of run time, the effect of the carbon black can actually be considered to be negative. However, the negative effect diminishes with run time, and at 38 min., there is a slight positive effect of the carbon black. This is lost again at the largest value of the run time.

2. Catalytic Liquefaction

The catalytic runs were carried out with catalysts based on iron sulfide, Fe_2S_3. The results have been submitted for publication, and a patent application is expected to be filed.

Three different methods of catalyst preparation have been used: premixed (PMS), impregnated (IS), and in-situ impregnated (IIS). In the first method (PMS), the catalyst is prepared by mixing aqueous solutions of ferric chloride and sodium sulfide. The Fe_2S_3 suspension is filtered, dried and later mixed with the coal sample. The second method (IS) is similar to the first except that, in this case, the coal is directly added to the aqueous Fe_2S_3 suspension. The coal/catalyst mixture is then filtered, washed and dried. In the third method (IIS), the coal is first mixed with a dilute aqueous solution of Na_2S and agitated vigorously before adding $FeCl_3$ solution. The suspension containing coal and the catalyst is then treated as for the IS catalyst.

The above methods of catalyst preparation were compared by performing catalytic co-liquefaction at 400°C for 30 min. using the Tire-1 sample and DECS-6 coal. The catalyst loading in these runs was 1.67 wt% of coal. The results, presented in Table II, indicate that the conversion of coal and oil+gas yield (again on a tire-free basis) in all the catalytic runs are

considerably higher compared to those in the thermal run. The method of catalyst preparation also influences the results significantly. The highest conversion is achieved for the IIS catalyst. The high activity of this catalyst may be due to uniform distribution of fine catalyst particles over the coal surface.

The effect of varying the temperature at which the catalyst and coal mixture was dried was also investigated. The liquefaction conditions in these runs were similar to those in the above runs and the IIS catalyst was used. The catalyst loading was 1.67 wt% and the tire/coal ratio was 1. The results, presented in Table III, indicate that the optimum drying temperature may be around 75°C. This is much lower than the preferred temperature previously obtained for hydrothermal disproportionation, 200°C [5], corresponding to a pyrrhotite-to-pyrite ratio of unity for the catalyst. The difference may be due to the smaller size of the catalyst particles in this study. Alternatively, the optimum ratio of pyrrhotite/pyrite for coal liquefaction in the presence of tire may not be unity as in the absence of tire.

It is of interest to study the effect of catalyst loading on the liquefaction. Based on the above results, loadings of 0.21, 0.42, 0.84 and 1.67 wt% of the IIS catalyst were used. As before, the tire/coal ratio was kept constant at unity and the results were calculated on a tire-free basis. Table IV shows that the conversion of coal increases continuously with catalyst loading. However, the greatest increase on a catalyst-loading basis is at the lowest catalyst loading (0.21 wt%). The oil+gas yield also increases with catalyst loading from 10% (thermal) to 19% at 1.67 wt% loading. The greatest increase on a catalyst-loading-basis in this case is again at a low loading, 0.42 wt%. These results are contrary to those found earlier [6] for hydrothermally disproportionated catalyst using coal alone, for which the oil+gas yield actually decreases at low catalyst loadings. The present results suggest that, in order to have a maximum effect on the product slate (based on catalyst loading), the optimum catalyst loading may be around 0.5 wt% or less.

FUTURE PLANS

The systematic study of co-liquefaction using the Tire-2 sample and DECS-6 coal will be continued. Other coals will also be used, to ensure that results obtained are sufficiently general. A matrix of experiments involving the parameters of temperature, pressure, coal type, and tire/coal ratio has been developed for this purpose. Longer-term work includes the use of

other waste materials (such as motor oil) for co-liquefaction, and the use of catalysts for co-liquefaction.

REFERENCES

1. Liu, Z., Zondlo, J.W., and Dadyburjor, D.B., Energy & Fuels, in press (1994).
2. Larsen, J.W., and Chang, B., Rubber Sci. Technol. **49**, 1120 (1976); Williams, P.T., Bester, S., Taylor, D.T., Fuel **69**, 1474 (1990).
3. Ibrahim, M.M., and Seehra, M.S., Prepr. Pap.- Am. Chem. Soc., Div. Fuel Chem. **38**, 841 (1993).
4. Farcasiu, M., and Smith, C., Prepr. Pap.- Am. Chem. Soc., Div. Fuel Chem. **37**, 4 7 2 (1992).
5. Stansberry, P.G., Wann, J.-P., Stewart, W.R., Yang, J., Zondlo, J.W., Stiller, A.H., and Dadyburjor, D.B., Fuel **72**, 793 (1993).
6. Dadyburjor, D.B., Stewart, W.R., Stiller, A.H., Stinespring, C.D., Wann, J.-P., and Zondlo, J.W., Energy & Fuels **8**, 19 (1994).

TABLE I

Proximate and Ultimate Analyses of Coal and Tires Used
Tire-1: Ground Goodyear Invicta tire from WVU sample
Tire-2: 30 mesh recycled tire from Utah sample bank
Tire-3: 80 mesh tire buffings from Utah sample bank

SAMPLE	H_2O %	ASH %dry	VOLATILE MATTER, %daf	FIXED CARBON, %daf	C %	H %	N %	S %daf
Tire-1	0.3	4.7	67.1	32.9	84.29	7.39	<0.5	1.6
Tire-2	0.4	8.1	71.0	29.0	79.65	7.45	<0.5	1.7
Tire-3	0.5	7.3	67.1	32.9	81.82	7.32	<0.5	1.4
DECS-6	1.8	6.3	49	51	81.9	6.3	1.5	0.9

TABLE II

Comparison of Catalytic Activity of Catalyst Samples
Co-Liquefaction of Tire-1 and DECS-6

	NON-CATALYTIC	PMS	CATALYTIC[1] IS	IIS
Conversion, %	44	60	79	84
Oil+Gas Yield, %	10	21	16	19

[1]PMS - Physically Mixed Sample; IS - Impregnated Sample;
IIS - In-situ Impregnated Sample.

Table III

Effect of Catalyst Drying Temperature on Catalytic Activity
Tire-1/DECS-6 = 1, IIS catalyst, loading = 1.67 wt%,
400°C, 1000 psi H_2 (cold), 30 min.

TEMPERATURE, °C	25	75	110
CONVERSION, %	78	84	78
OIL+GAS YIELD, %	19	19	18

Table IV

Effect of Catalyst Loading on the Co-Liquefaction of Coal and Tire
Tire-1/DECS-6 = 1, IIS Catalyst, 400°C, 1000 psi H_2 (cold), 30 min.

CATALYST LOADING, WT%	0.0	0.21	0.42	0.84	1.67
CONVERSION, %	44.3	60.0	67.0	73.0	82.4
ASPHALTENE YIELD, %	34.0	46.6	49.3	54.5	63.6
OIL+GAS YIELD, %	10.3	13.4	17.7	18.5	18.8

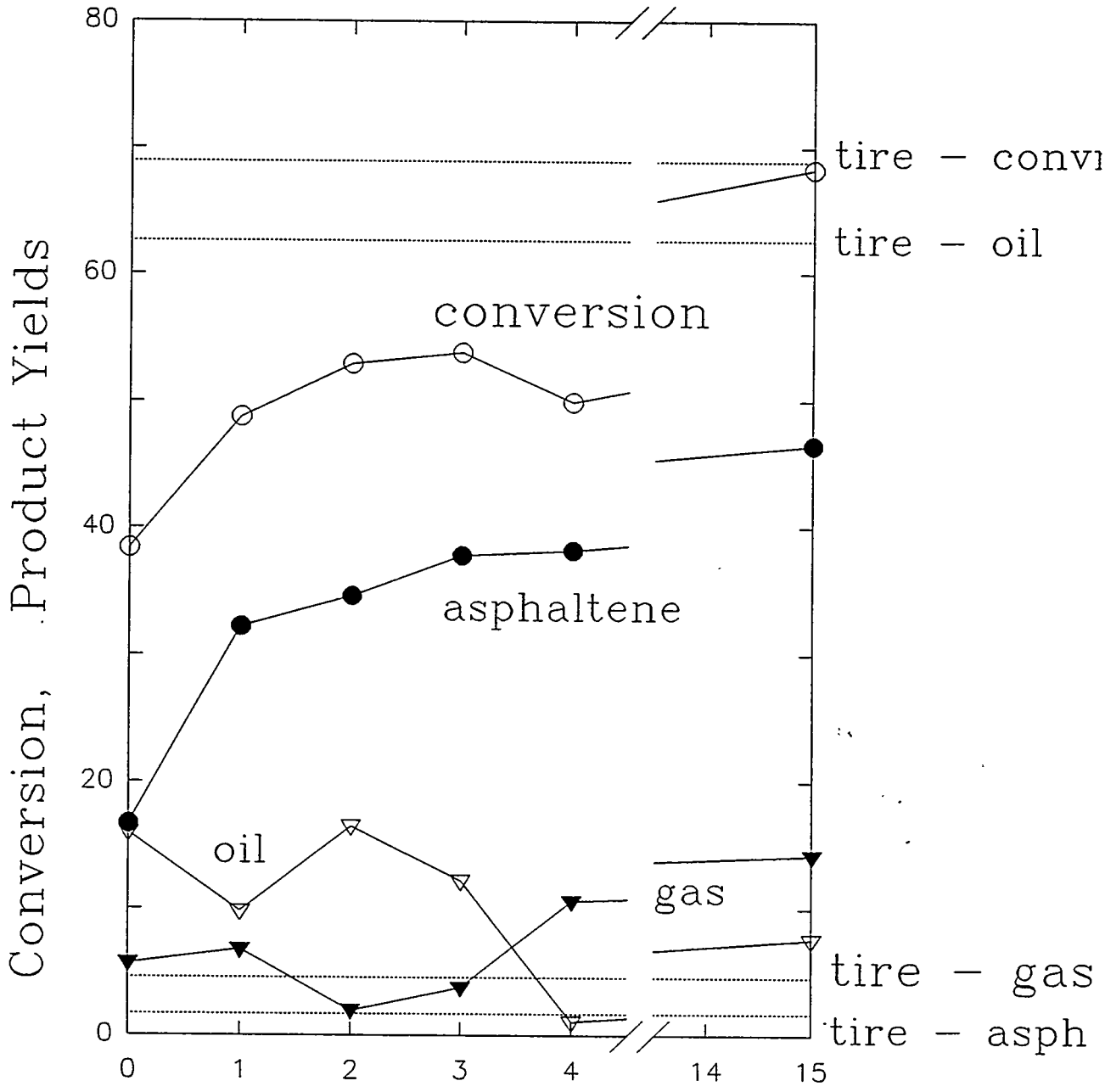

Figure 1. Conversion and product yields of coal in a coal/tire mixture, as functions of tire/coal ratio. Parameters for tire alone are shown as dashed lines. Conditions: 400°C, 1000 psi H_2(cold), 30 min., 500 cpm. Tire-2 and DECS-6 were used.

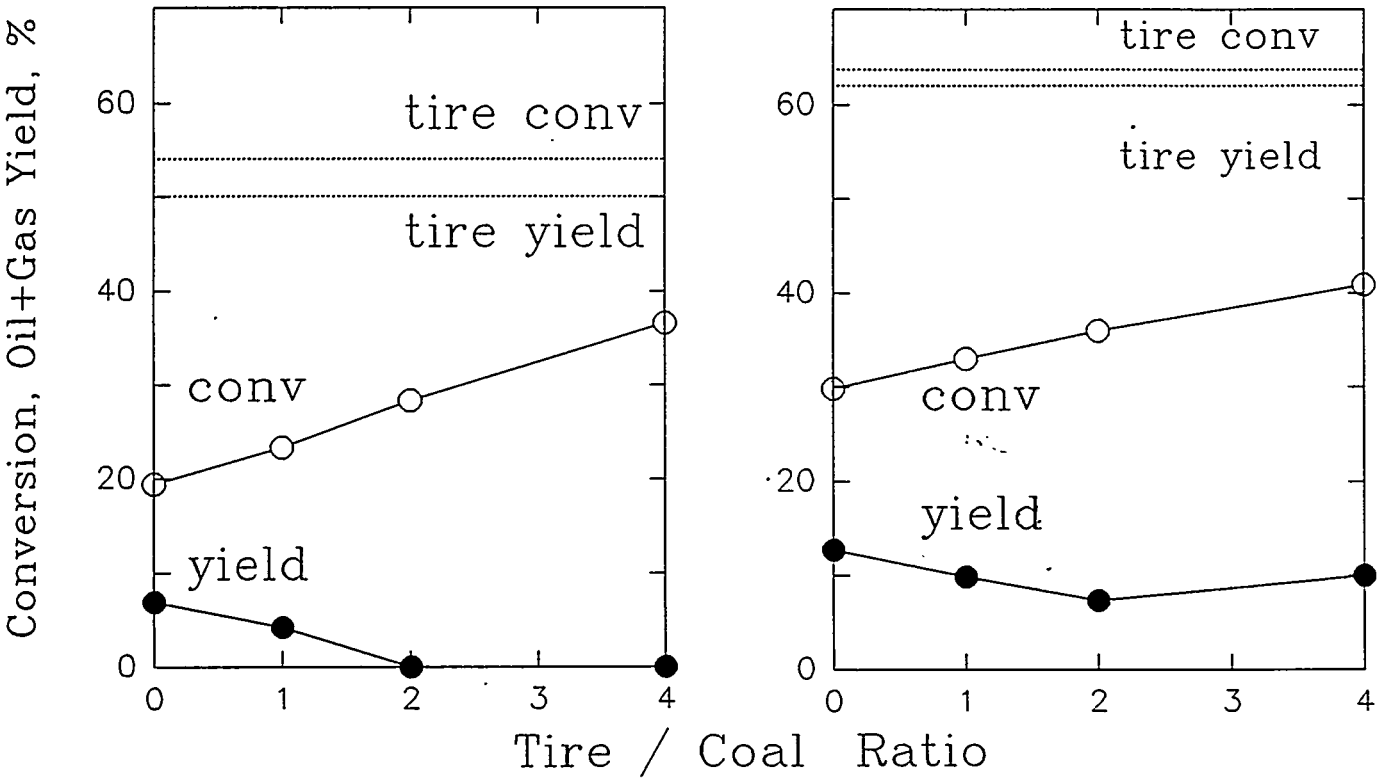

Figure 2. Conversion and oil+gas yield of coal in a coal/tire mixture, as functions of tire/coal ratio. Conditions of Figure 1, except that T = 350°C (left), T = 375°C (right).

Task I.3 Figure 3

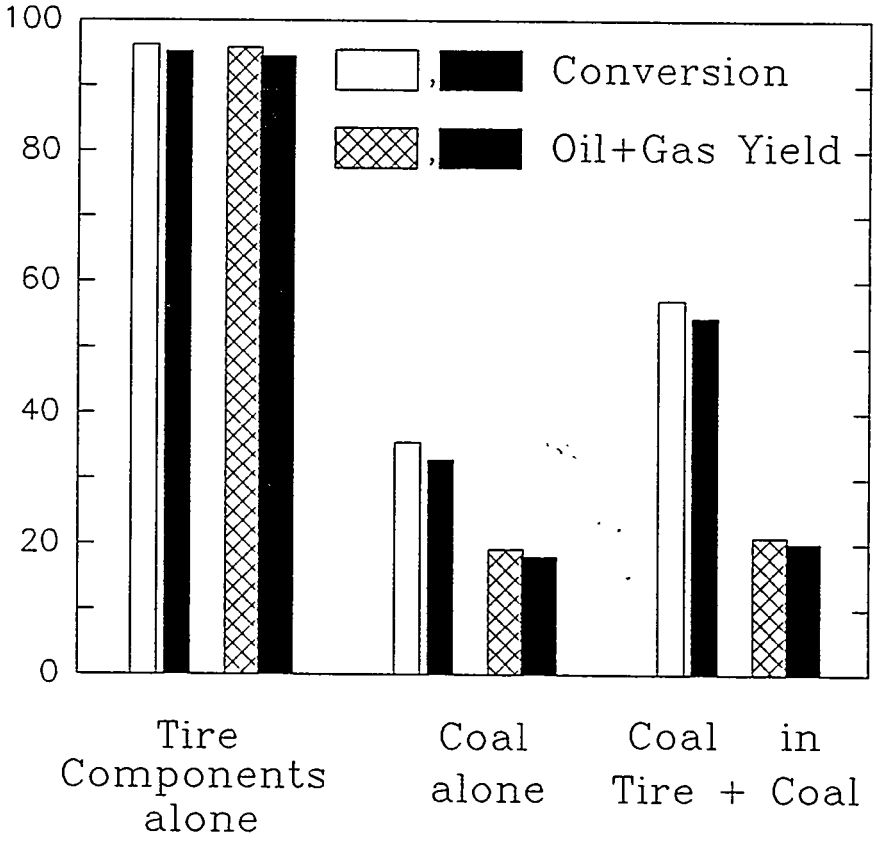

Figure 3. Conversion and oil+gas yield for mixtures of tire components (except carbon black), carbon black, and DECS-6 coal. Conditions: 400°C, 1000 psi H_2(cold). All calculations are on a carbon-black-free basis; for coal plus tire components, a coal-alone basis as well. (Solid bars indicate runs with carbon black; white bars and crosshatched bars indicate runs without carbon black.)

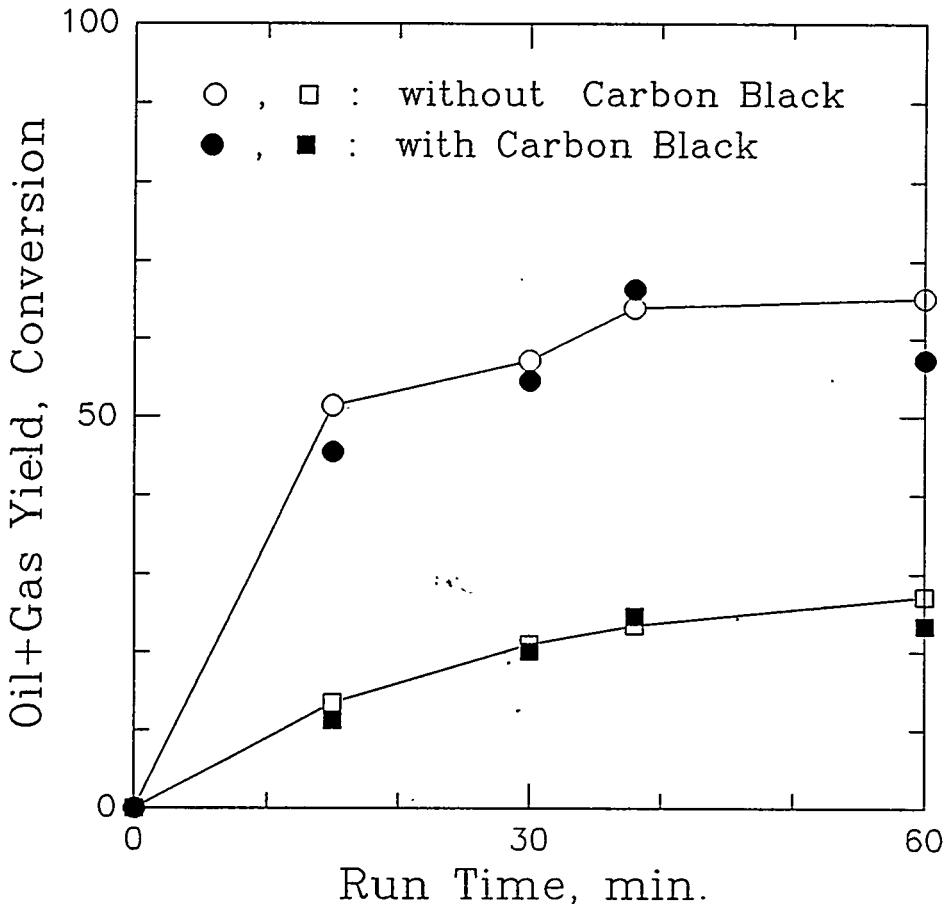

Figure 4. Effect of liquefaction run time on conversion and oil+gas yield for mixtures of tire components (with and without carbon black) and coal. Conditions as in Figure 3. (Circles indicate conversion; squares indicate oil + gas yield.)

TASK I

Project I.4

COPROCESSING COAL WITH WASTE PETROLEUM PRODUCTS

A. R. Tarrer
Chemical Engineering Department
Auburn University

I. Introduction

The work for the past year focused on coal/waste oil/waste grease/waste plastic coprocessing, characterization of waste oils and products, and thermocracking effects. The effects of temperature, pressure, and reaction time on coal/waste oil/waste grease mixtures were studied. Conversion and selectivity increased with temperature, pressure, and reaction time in both systems. However, coprocessing coal with waste grease resulted in consistently higher conversions than coprocessing coal with a mixture of waste oil and waste grease. The difference in coal conversions between the two systems may be due to higher metal contents and aromatic compounds in the waste grease than in the waste oil.

To increase the aromaticity of waste oil, preliminary tests were performed to determine if polystyrene and waste rubber from tires can be dissolved in waste oil. Under coprocessing conditions, the polystyrene dissolves almost completely, suggesting that polystyrene (or plastic) may be a suitable material for use in a coal/waste oil coprocessing system. Further studies are needed.

A significant reduction of viscosity was observed after coprocessing coal with both waste oil and waste grease. The viscosity reduction correlates with our TGA results, and can be explained in terms of thermocracking and hydrocracking processes occurring during coprocessing.

Efforts were made to develop analytical techniques for characterizing waste oils and products. A viscometer and a TGA (ThermoGravometric Analyzer) have been applied to characterize waste oils. A gas chromatography simulated-distillation method (ASTM method D-2887), based on the unit at West Virginia University, has been set up. A microdistillation unit is being tested. Aniline point measurements and an NMR technique are being used to characterize the aromaticity of waste oil.

II. ACTIVITIES

Coal/Waste Oil/Waste Grease

The effects of temperature and pressure on oil-free coal conversion and selectivity in a coal/waste oil system are shown in Tables 1 and 2, respectively. Conversion and selectivity increased with temperature and pressure. Waste grease consists of about 70-95% oil and contains more heavy metals than waste oil, which might act as catalysts to enhance coal conversion. Tables 3 and 4 show that conversion and selectivity of coal increases with temperature in both coal/waste grease and coal/waste grease/waste oil systems. Table 5 shows the effect of pressure on a coal/grease system. At 1475 psig and 400°C, the system reaches 97% coal conversion and 99% selectivity. Tables 6 and 7 show the effect of reaction time on conversion and selectivity in a coal/waste oil/waste grease system. Coprocessing coal with waste grease alone results in higher conversions but generally lower selectivity than in a coal/waste oil/waste grease system.

The coal conversion to THF solubles during coprocessing was defined as:

Conversion (Y) = 100 * (1-X) where,

$$X=\frac{W_R-W_C-W_{ash}}{W_{moisture,ash-freecoal}}$$

and conversion to hexane solubles (H) was defined in a similar manner. The selectivity was defined as the ratio of conversion to hexane solubles and conversion to THF solubles, i.e.,

Selectivity = 100 * S where,

$$S=\frac{H}{Y}$$

W_R = weight of residue remaining after THF wash,

W_C = weight of catalyst (It was assumed that all the iron oxide was converted to FeS.)

W_{ash} = weight of ash in the coal

Table 1
EFFECT OF TEMPERATURE ON CONVERSION AND SELECTIVITY
COAL + WASTE OIL

Reaction Temp (°C)	Coal Conversion[1] (%)	Selectivity (%)
375	38.1	38.7
385	52	43
400	61	54
410	69	65
425	83	68
445	92	81

Reaction Conditions: 1250 psig H_2, 0.6g DECS 6 coal, 6g waste oil, 0.15g Fe_2O_3, 780 rpm agitation rate, 1 hour.
[1]moisture-free, oil-free, ash-free basis

Table 2
EFFECT OF PRESSURE ON CONVERSION AND SELECTIVITY
COAL + WASTE OIL

H_2 Pressure (psig)	Total Conversion[1] (%)	Selectivity (%)
825	50	56
1025	59	57
1250	61	54

Reaction conditions: 400 °C, 0.6g DECS 6 coal, 6.0g waste oil, 0.15g Fe_2O_3, 780 rpm agitation rate, 1 hour.
[1]moisture-free, oil-free, ash-free basis

Table 3
TEMPERATURE EFFECTS IN COAL/WASTE OIL/GREASE COPROCESSING

Temperature (°C)	Conversion[1] (%)	Selectivity (%)
385	37.22	72.86
400	52.17	65.63
425	75.13	63.81
440	82.40	74.58

Conditions: 0.6 grams DECS 6, 6 grams waste oil, 0.6 g grease, 1200 psig H_2 pressure, 1 hr reaction time
[1]moisture-free, oil-free, ash-free basis

Table 4
TEMPERATURE EFFECTS IN COAL/WASTE GREASE COPROCESSING

Temperature (°C)	Conversion[1] (%)	Selectivity (%)
390	66.0	8.3
405	76.76	40.72
445	97.09	70.15

Conditions: 0.6 grams DECS 6 coal, 5.4 g grease, 1200 psig H_2 pressure, 1 hr reaction time
[1]moisture-free, oil-free, ash-free basis

Table 5
EFFECTS OF PRESSURE IN COAL/WASTE GREASE COPROCESSING

Pressure (psig)	Conversion[1] (%)	Selectivity (%)
1365	90.0	88.88
1380	95.0	92.23
1475	97.31	99.11

Conditions: 0.6 grams DECS 6 coal, 5.4 g grease, 405°C, 1 hr reaction time
[1]moisture-free, oil-free, ash-free basis

Table 6
EFFECTS OF REACTION TIME IN COAL/OIL/GREASE COPROCESSING

Time (min)	Conversion[1] (%)	Selectivity (%)
30	43	88
45	45	87
60	58	72

Conditions: 0.6 grams DECS 6 coal, 6 grams waste oil, 0.6g grease, 400°C, 1250 psig H_2 pressure
[1]moisture-free, oil-free, ash-free basis

Table 7 EFFECTS OF REACTION TIME IN COAL/WASTE GREASE COPROCESSING		
Time (min)	Conversion[1] (%)	Selectivity (%)
30	72	15
45	83	28
60	86	37

Conditions: 0.6 grams DECS 6 coal, 5.4 g grease, 400°C, 1250 psig H_2 pressure
[1]moisture-free, oil-free, ash-free basis

Effect Of Surfactants

Literature reviews have turned up some significant effects of surfactants on coal liquefaction. Surfactants are believed to disperse coal species and prevent asphaltene and preasphaltene agglomerations. Both total conversions and conversions to oil can thus be improved. It was reported in U.S. patent 4,121,995 that a surfactant, polyflo-100, increases total yield of coal from about 40-50% to about 70-80%, and enhances the yield of liquid oil fractions two-fold (reaction conditions: 325°C, 1000 psig H_2, 4 hrs.). Similar results were obtained at the Jet Propulsion Laboratory (DOE/PC/89882-T1) in which a 40% increase in light soluble solids was observed with the addition of sodium lignin sulfonate (conditions: 350°C, 1000 psig H_2). These reports are consistent with the results found in our laboratory.

In general, the effectiveness of surfactants depends on the type of surfactant, concentrations, and reaction conditions. Preliminary tests show that some surfactants did not improve coal conversions. Further studies are being undertaken to identify types of surfactants that would enhance coal coprocessing.

Waste Oil Sample Bank and Characterization of Waste Oil

A waste oil sample bank has been set up at the Auburn Waste Oil Reprocessing Laboratory (AWORL) for coal coprocessing research. The oil has been characterized for its water, sulfur, PCB's, metals, and ash contents, and samples have been distributed to other universities (the University of Utah, West Virginia University, and the University of Pittsburgh) for their coal research. Table 8 shows typical specifications of the waste oil in our sample bank.

Table 8	
Water	<1%
Sulfur	0.4-0.7%
Viscosity	3.3 cst
Ash	0.4-0.6%
PCB's	<1 ppm

The aromaticity of waste oil is a key parameter for higher conversions in coal coprocessing. The aniline point is an indicator of aromatic hydrocarbons in a waste oil, and a test for determining it has been set up according to ASTM D 611-82. This test method measures the temperature at which two phases, aniline and oil, become miscible. Aromatic hydrocarbons exhibit lower aniline values while paraffins exhibit higher ones. The aniline point of some waste oils processed by AWORL ranges from 60-120°C. The waste grease used in our coprocessing work was found to be very aromatic, partially explaining the high yields (>90%) obtained. Some waste oils from AWORL are dark black in color; consequently, it is not possible to observe the point at which the phases are miscible. An alternative technique, NMR (Nuclear Magnetic Resonance), is therefore being investigated for monitoring the aromaticity of waste oil.

A gas chromatography simulated-distillation method (ASTM method D-2887), based on the unit at West Virginia University, has been set up for characterizing oil and coal coprocessing products. A TGA analyzer has also been employed to characterize oil and grease, and a microdistillation unit is being set up.

Viscosity Reduction

An important factor observed during coal coprocessing was a significant reduction of viscosity in the waste oil. Table 9 shows that the oil kinematic viscosity dropped from 275 cst to about 1.5 cst after coprocessing. Tables 10 and 11 also show similar kinematic viscosity reductions in both coal/grease and coal/grease/waste oil systems. This effect is caused by thermocracking and hydrocracking processes occurring during coprocessing.

Viscosity reductions are also observed using the TGA technique. Figures 1 and 2 show the changes in the TGA diagrams of waste oil and grease after coal coprocessing. The gain in light fractions after coprocessing the waste oil and the grease is consistent with the reduction in viscosity.

Thermocracking and hydrocracking are important processes to convert heavy oils into

Figure 1: TGA Analysis Of Oil

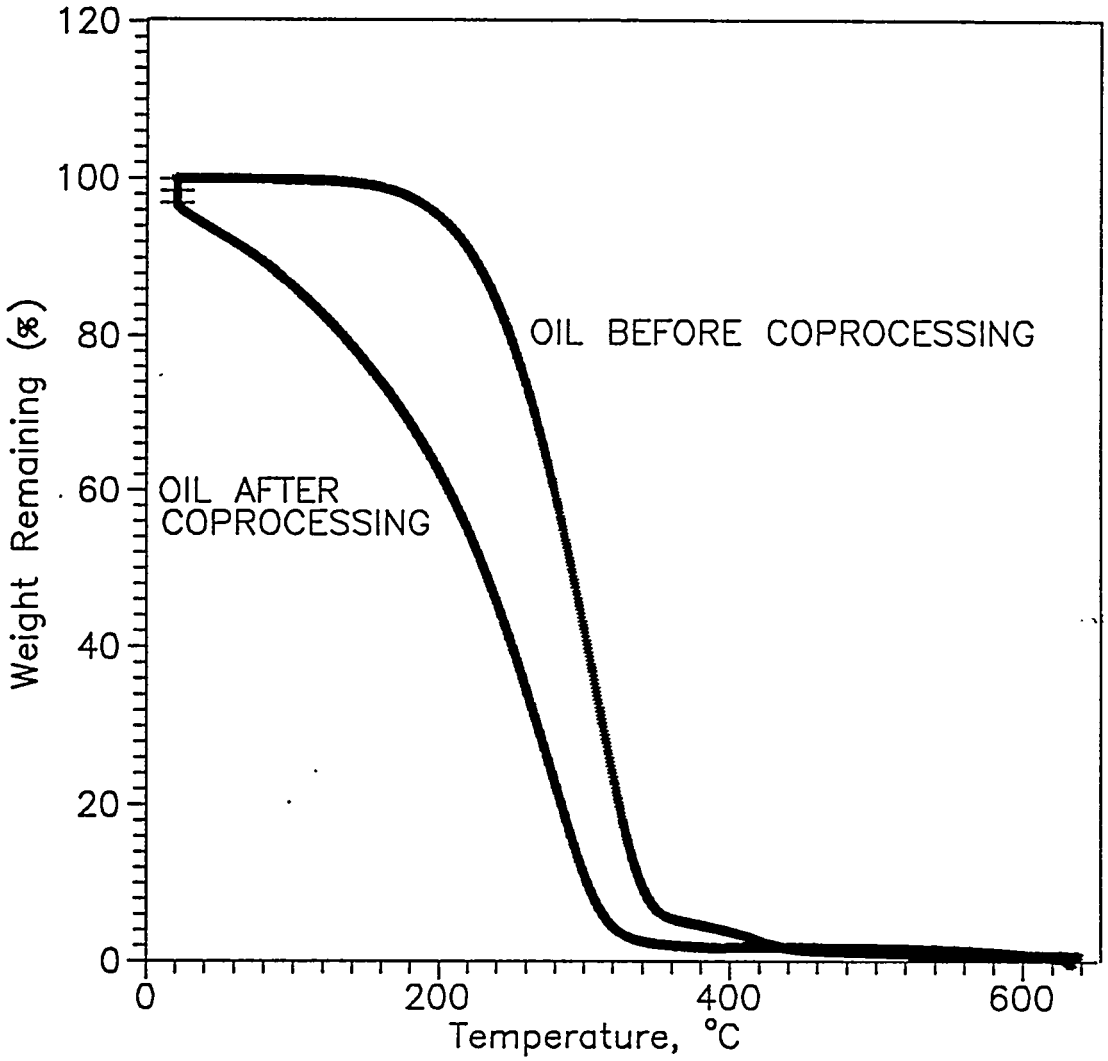

Figure 2: TGA ANALYSIS OF COAL/GREASE/OIL

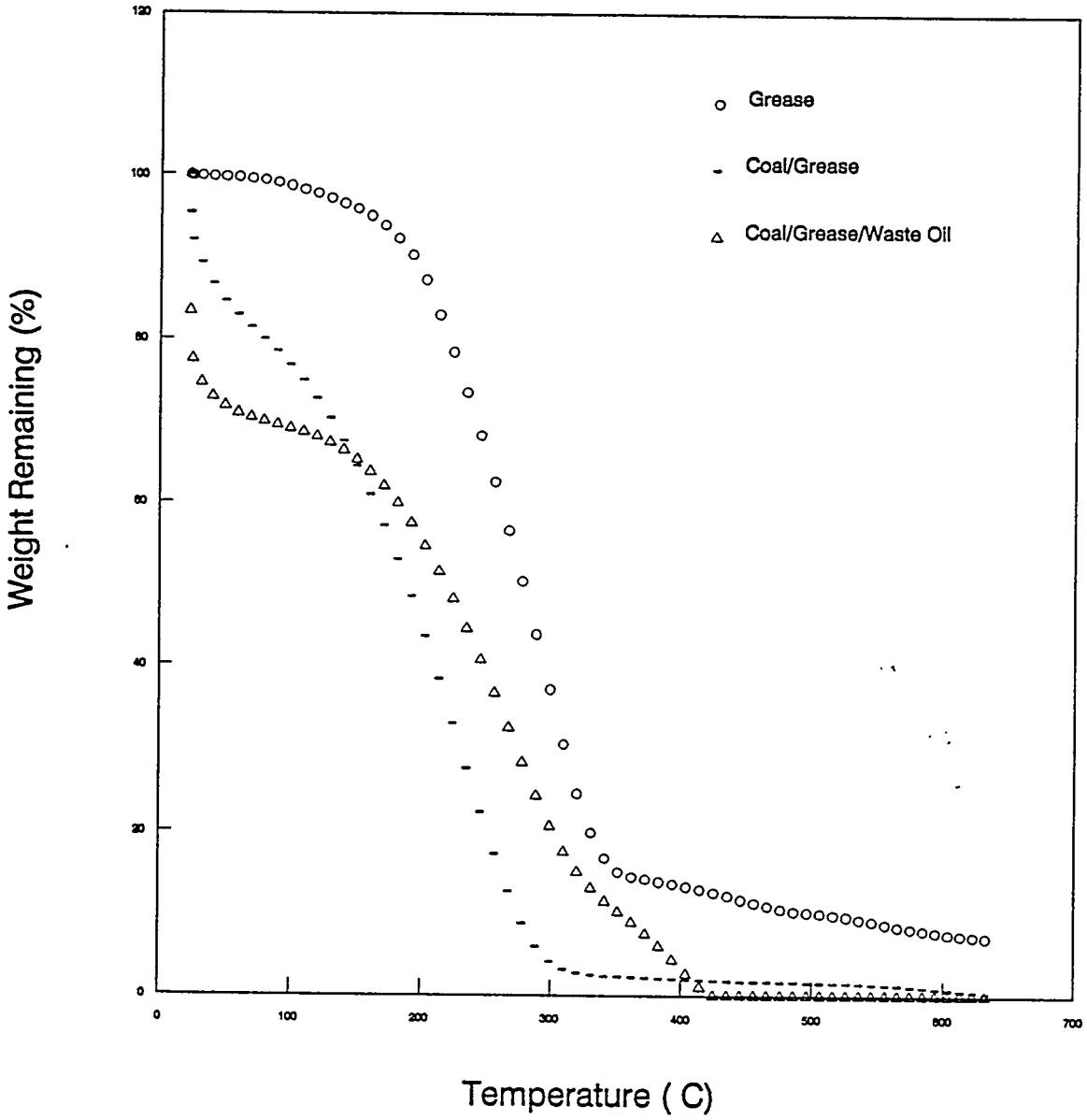

lighter fractions for use as fuels. In addition, most plastics can be pyrolyzed or cracked at the temperatures used in coal coprocessing. Figure 3 shows the effect of temperature on polystyrene and HDPE. Thus, visbreaking observed in coal coprocessing augments the benefits of coprocessing waste materials.

Table 9
EFFECT OF COPROCESSING ON OIL VISCOSITY[1]

Oil Type	Pressure (psig)	Temperature (°C)	Kinematic Viscosity (cst)
Used Oil	Atm	25	275
Oil	250 (N_2)	410	17
Coal+Oil	1250 (H_2)	410	1.34
Coal+Oil	1250 (H_2)	425	1.65
Coal+Oil	1250 (H_2)	445	1.42
Coal+Oil	1500 (H_2)	425	1.09

[1]Viscosity measured at 25 °C.

Table 10
EFFECT OF COPROCESSING ON OIL VISCOSITY[1]
COAL+GREASE

Type	Temperature °C	Kinematic Viscosity cst
Used Oil	25	275.0
Grease	400	1.2
Coal+Grease	385	1.5
Coal+Grease	405	1.4
Coal+Grease	445	2.6

Reaction conditions: 0.6g DECS 6 coal, 5.0g grease, 1200 psig H_2, 780 rpm agitation rate, 1 hour reaction time
[1]Viscosity measured at 25 °C.

Figure 3: TGA ANALYSIS OF WASTE OIL AND PLASTICS

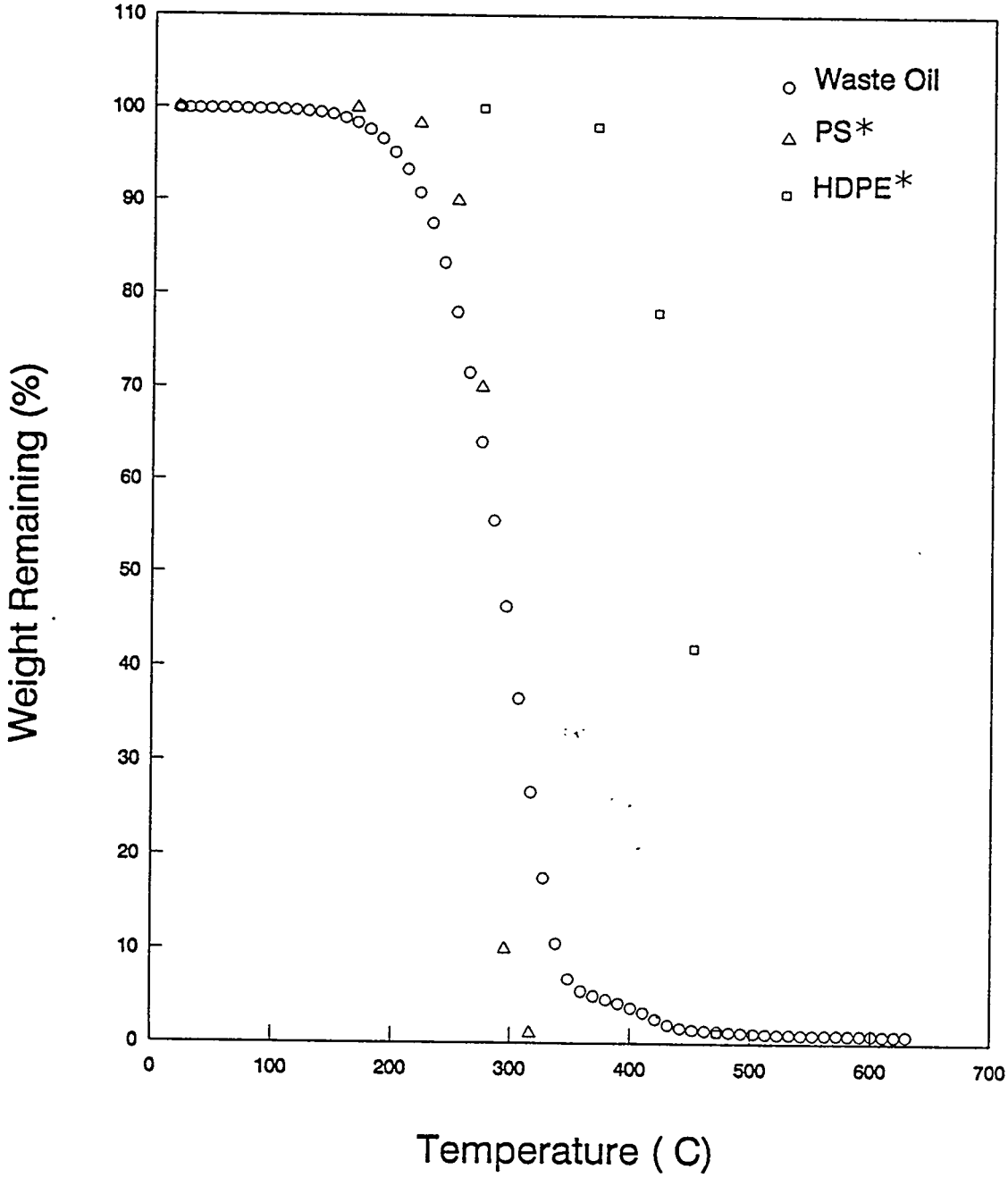

* data obtained from C.Y. Chang et. (1992)

Table 11
EFFECT OF COPROCESSING ON OIL VISCOSITY[1]
COAL+OIL+GREASE

Type	Temperature (°C)	Kinematic Viscosity (cst)
Used Oil	25	275.0
Grease	400	1.2
Coal+Oil+Grease	400	3.6
Coal+Oil+Grease	425	2.5
Coal+Oil+Grease	440	1.0

Reaction conditions: 0.6g DECS 6 coal, 5.0g grease, 6.0g waste oil, 1200 psig H_2, 780 rpm agitation rate, 1 hour
[1]Viscosity measured at 25 °C.

Regulatory Considerations

To coprocess coal with waste oil, certain environmental regulations must be taken into consideration. Under current federal regulations, any facility that processes waste oil, including re-refiners, must comply with waste oil processor standards (40.CFR 279 subpart F).

Waste oil containing more than 1000 ppm in halogens is considered to be a hazardous waste unless the oil does not contain halogenated solvents.

Although processors of hazardous waste oil are generally required to obtain a hazardous waste treatment, storage and disposal (TSD) permit from EPA, coal coprocessing would be exempt if it can be shown to be a legitimate recycling process.

The questions that regulatory agencies will probably consider when determining whether coprocessing is a legitimate recycling process include: What raw material is the hazardous waste oil replacing? Is the hazardous waste oil as economical and as good a feed material as the raw material it replaced? Does the addition of the hazardous waste oil complicate the process? Will the hazardous constituents of the hazardous waste oil contribute to the process or will they simply move passively through the process?

Coal coprocessing could prove to be a sound method of disposal for hazardous waste oils. Also, PCB-contaminated oils containing less than 50 ppm PCB's could be coprocessed, as long as the resulting products contained less than 25 ppm PCB's on an average daily basis, with a maximum content of 50 ppm PCB's.

TASK I

Project I.5

COLIQUEFACTION OF COAL AND WASTE MATERIALS: LIQUID FUELS FROM COAL WHILE CLEANING THE ENVIRONMENT

Irving Wender, John W. Tierney and Gerald D. Holder
University of Pittsburgh

Introduction

Paper and other lignocellulosic wastes constitute more than half of landfill volumes. These materials could be a significant energy source[1]. The objective of this work is to find ways of converting these huge volumes of waste, especially paper, to liquid transportation fuels.

In this work, we studied the direct liquefaction of paper and other lignocellulosic wastes and waste-coal coprocessing in two different routes; liquefaction in the presence of hydrogen or hydrogen donor solvents with molybdenum catalysts (Route A), and the so-called COSTEAM process which involves treatment of coal with carbon monoxide or synthesis gas ($CO + H_2$) in the presence of water and an alkali compound as catalyst (Route B). Most of the coprocessing experiments were carried out with paper and a variety of lignocellulosic wastes and Wyodak subbituminous coal with emphasis on determining any synergistic effects of coliquefaction.

Results and Discussion

Route A (H_2-tetralin system)

The detailed experimental and the product analysis procedures have been reported previously[2]. Here we refer to ordinary copy paper as paper. Table 1 lists the results at 400°C using two different molybdenum catalysts with added sulfur. The conversion of paper is almost complete with paper yielding only about 10% of high molecular weight asphaltenes, with a high yield of oil and gas when $Mo(CO)_6$ was used as a catalyst. Wyodak coal was also converted in high yield but with significant amounts of asphaltenes. Since conversions and yields of oil and gas are very high for paper, the conversion and yield of coal in the coprocessing runs were calculated with the assumption that addition of coal has no influence on paper conversion. As shown in Table 1, the conversion of coal was increased to 91.7% when 50 wt% of paper was

coprocessed, up from 86% conversion when coal was reacted alone with $Mo(CO)_6$ as catalyst. The yield of oil and gas, however, remained unchanged. Addition of paper evidently increased the conversion of coal. The coprocessing results with a molybdenum naphthenate catalyst showed the same trend as that obtained with a $Mo(CO)_6$ catalyst; that is, coal conversion and asphaltene yields increased due to addition of paper during coliquefaction at 400°C.

Reactions were carried out at a lower temperature (325°C) and the results showed that both the coal conversion and the yield of oil and gas from the coprocessing run are almost the same as those from coal alone at 325°C, suggesting that the possible synergistic effect of paper is small at 325°C.

Route B (CO-H_2O system)

Paper and various lignocellulosic wastes with different lignin contents were studied in this route. The lignin contents were determined by the ASTM D-1105 procedure; results are listed in Table 2. Liquefaction of the individual wastes resulted in almost complete conversion at 400°C (>96%), with larger amount of asphaltenes and oils and less gases from wastes containing larger amounts of lignin (this is due to the fact that lignin contains less oxygen than cellulose). The results of coprocessing runs when 50% of Wyodak coal was replaced with various lignocellulosic wastes in COSTEAM experiments at 400°C are listed in Table 2. Again, the values listed in Table 2 are those for coal calculated assuming that coal has no effect on waste conversion. Addition of lignocellulosic wastes to coal gave little change in coal conversion except for coprocessing with cotton which is composed of glucose molecules, as is cellulose. However, coprocessing paper and other lignocellulosic wastes with coal decreased the amount of asphaltenes produced from coal while almost doubling the amount of oils from coal. These results clearly indicate that coprocessing of lignocellulosic wastes and coal via COSTEAM yields higher quality products from coal. In other words, the addition of paper and other lignocellulosic wastes to coal liquefaction results in formation of lighter products from coal, which could be a reduced burden to the product upgrading stage in a liquefaction process.

The amount of lignin in the lignocellulosic material is shown to be an important factor in the extent of the synergistic effect in COSTEAM coprocessing. Increased lignin in the lignocellulosic material reduced the yield of asphaltenes from coal, while increasing gas yields. However, the oil yield from coal was about the same (~30%) regardless of the type of added lignocellulosic wastes (Table 2). This synergistic effect was greater when the amount of added

lignocellulosic waste to coal was increased. When 75% of coal was replaced with paper, the conversion of coal was more than 100% (102.7%) and the yield of asphaltenes from coal was negative (-5.8%) with a high oil yield from coal (62.5%). These results strongly suggest that in addition to the product quality enhancing effect of paper, coal also increased paper conversion and decreased asphaltenes resulting from paper. The effect of lignocellulosic waste-coal coliquefaction appears to be synergistic.

It has been proposed that phenoxy radicals generated from lignin aid in lignin-coal coliquefaction via Route A[3]. They may also play an important role in improving the product quality of coal during coliquefaction in a CO-H_2O environment. Oils from the newsprint via COSTEAM were analyzed by GC-MS and found to contain many phenolic compounds. During lignocellulosic waste-coal coprocessing, the liquid product generated from lignocellulosic waste may also act as a hydrogen donor solvent to stabilize coal radicals, thus reducing high molecular weight asphaltenes from coal to form more oil. In order to test this hypothesis, 4 g of tetralin were added to 8 g of Wyodak coal in a COSTEAM reaction run at 400°C. The conversion of coal with small amount of tetralin was almost same as the conversion without tetralin (84%). But the addition of tetralin reduced the asphaltene yield of coal from 42.8% to 33.6%, which is the same effect obtained by addition of lignocellulosic wastes during coprocessing.

Coprocessing via the COSTEAM route was also studied at 370°C with Wyodak coal and North Dakota lignite coal and copy paper. However, the synergistic effect of paper was not observed at 370°C for either coal.

A significant amount of valuable hydrogen is produced as the byproduct from COSTEAM runs. Hydrogen production is the result of the water gas shift reaction ($CO + H_2O \rightleftharpoons CO_2 + H_2$) catalyzed by an alkali catalyst. This hydrogen could be separated and then could be used in the second stage of product upgrading. It could also be utilized during the reaction (*in situ*) to be incorporated in the coal products. Since most alkali catalysts are known to poison hydrogenation catalysts, the combination of a less poisonous $NaAlO_2$ and the hydrogenation catalyst (Mo) was studied in the liquefaction of Wyodak coal alone at 400°C to achieve this goal and the results are shown in Table 3. The addition of a molybdenum catalyst increased the yield of asphaltenes and oils from coal significantly. Moreover, the molybdenum catalyst increased the conversion of gaseous CO, indicating its water gas shift activity. The higher hydrogen consumption with the combined catalyst system suggests that a portion of the byproduct hydrogen is utilized in forming

more oils by the hydrogenation activity of the molybdenum catalyst.

Summary

A possible desirable effect of paper and other lignocellulosic wastes in coprocessing with coal was observed in both the H_2/tetralin/Mo system and the CO/H_2O/alkali system at 400°C. More specifically, the conversion of coal was increased due to the addition of paper in the H_2/tetralin/Mo system, and the increase in coal conversion resulted in an increase in asphaltenes. Little increase in coal conversion was observed in lignocellulosic waste-coal coprocessing in the CO/H_2O/alkali system, while the quality of products from coal was significantly improved (more oil and less asphaltenes). This desirable effect is greater when lignocellulosic wastes contain larger amounts of lignin and when larger amounts of lignocellulosic wastes were coprocessed. At 370°C, added copy paper did not improve the product quality of Wyodak coal or North Dakota lignite coal in CO/H_2O/alkali environment. No synergistic effect of paper was observed at 325°C in the H_2/tetralin/Mo system.

Future Work

A detailed study of the products will be made, including simulated distillation for product quality analysis, NMR, and GC-MS studies. By using an active hydrogenation catalyst as well as the alkali catalysts, *in situ* utilization of byproduct hydrogen in the COSTEAM process will be investigated further. Several other types of coal, such as the higher rank Illinois #6 coal and a lower rank North Dakota lignite will also be studied for coprocessing, especially with newsprint. Coprocessing of plastic wastes with coal using the COSTEAM scheme will be investigated.

Literature Cited

1. Anderson, L. L. and Tillman, D.A., "Fuels from Waste," p 10, Academic Press, New York, (1977).

2. Jung, H., Tierney, J.W. and Wender, I., Div. Fuel Chem. Preprints, Amer. Chem. Soc. 38(3), 880 (1993).

3. Coughlin, R. W. and Davoudzadeh, F., Nature, 303, 789 (1983).

Table 1. Liquefaction results in the H_2/tetralin/Mo system at 400°C for 1 hour ($Mo(CO)_6$ runs; 3 g of reactant and 12 g of tetralin with 5000 ppm of Mo and 10000 ppm of S in 45 cc microautoclave. Initial pressure of H_2 was 1000 psi and at 400°C about 2100 psi. Molybdenum naphthenate runs; 8 g of reactant and 32 g of tetralin with 5000 ppm of Mo and 10000 ppm of S in 300 cc autoclave. Initial pressure of H_2 was 1000 psi and at 400°C about 2300 psi).

Catalyst	Reactant	Conversion (%)	Asphaltenes (%)	Oil and Gas (%)
$Mo(CO)_6$	copy paper	98.6	10.2	88.4
	coal	86.0	39.9	46.1
	coal + paper	91.7[a]	44.0[a]	47.7[a]
molybdenum naphthenate	copy paper	98.8	1.9	96.9
	coal	87.5	38.8	48.7
	coal + paper	89.5[a]	40.6[a]	48.8[a]

a: conversion and yield with respect to coal.

Table 2. Lignocellulosic waste-Wyodak coal coliquefaction results in the $CO/H_2O/Na_2CO_3$ system at 400°C for 1 hour (8 g of reactant, 24 gm H_2O and 1.02 g of Na_2CO_3 in 300 cc autoclave. Initial pressure of CO was 580 psi and at 400°C total pressure was about 4200 psi).

Coprocessed Material	Lignin (%)	Conversion[a] (%)	Asphaltenes[a] (%)	Oil[a] (%)	Gas[a] (%)
cotton[b]	0	93.1	30.7	30.1	32.3
copy paper[b]	0	81.7	24	27.3	30.4
newsprint[b]	23.6	84.1	20.2	29.7	34.2
corncobs[b]	29.7	85.3	13.7	29.2	42.4
coal	-	84.2	42.8	15.1	26.3

a: conversion and yield are for coal, assuming that conversion and yield of waste remains unchanged.

b. reactant mixture contains 50% Wyodak coal and 50% waste.

Table 3. Effect of molybdenum catalyst in the liquefaction of Wyodak coal in the $CO/H_2O/NaAlO_2$ system at 400°C for 1 hour (8 g of reactant, 24 g of H_2O and 1.02 g of Na_2CO_3 in 300 cc autoclave. Initial CO pressure was 580 psi; at 400°C total pressure was about 4000 psi).

Catalyst	Conversion (%)	Asphaltenes (%)	Oil (%)	Gas (%)	CO conversion (%)	H_2 consumption (mmole)
$NaAlO_2$	75.0	24.9	8.6	41.5	73.1	111.4
$NaAlO_2$/Mo	73.7	28.3	22.3	23.1	82.9	119.8

TASK 1

Project I.6

COPROCESSING OF COAL WITH WASTE POLYMERS USING FINELY DISPERSED IRON CATALYST

Christine W. Curtis, Principal Investigator
Mingsheng Luo
Ying Tang
Auburn University

The overall objective of this research is to determine the feasibility of coprocessing coal with waste polymers in the presence of finely dispersed catalysts in order to produce high quality product slates. To fulfill the overall objective, the following specific objectives are being undertaken this year. The first specific objective is to evaluate the liquefaction of waste polymers and tires thermally and catalytically with finely divided catalysts to determine their behavior and achievable products at liquefaction conditions. The second objective is to coprocess individual waste polymers and tires with coal in the presence and absence of finely dispersed catalysts in order to determine the type and quality of products produced. Other types of catalysts may be needed to liquefy some of the waste materials.

Coprocessing Coal with Polymers

Coprocessing reactions with waste polymers and coal were performed to elucidate the individual and mutual liquefaction behavior of each material. The polymers used in this study were polyisoprene, polystyrene, high density polyethylene (HDPE) and low density polyethylene (LDPE). These polymers were reacted individually and with coal using the following reaction sequence: (1) thermal reactions without solvent; (2) thermal reaction with solvent; (3) catalyzed reaction using Fe naphthenate (FeNaph) plus sulfur but without solvent; (4) catalyzed reaction using FeNaph plus sulfur with solvent; (5) catalyzed reaction using Mo naphthenate (MoNaph) plus sulfur but without solvent; and (6) catalyzed reaction using MoNaph with solvent.

Experimental

The coprocessing reactions with polymers were performed using Illinois No. 6 coal obtained from the Argonne Premium Coal Sample Bank. The Illinois No. 6 coal was reacted with the model polymers, polyisoprene, polystyrene, HDPE and LDPE, which were obtained from Aldrich Chemical Company. The coprocessing reactions were performed thermally and catalytically using either FeNaph or MoNaph reacted with sulfur. When coal or polymer was liquefied alone, 2 g of polymer or coal were charged; when these materials were coliquefied, 1 g of each material was charged. In the catalytic reactions, each catalyst was charged at 1,000 ppm of active metal and 6,000 ppm of elemental sulfur was also added on a total gram basis. In some reactions, a solvent was not used; however, in other reactions a mixture of 70% hexadecane and 30% tetralin was used as solvent. A total solvent charge of 2 g was introduced.

The coprocessing reactions were performed in ~20 cm^3 stainless steel tubular microreactors at 400 °C for 30 min which were agitated horizontally at 450 rpm. The liquefied products were obtained by first extracting with hexane to yield the oil product and with THF to yield the THF soluble and hexane insoluble products. The organic matter that was not soluble in THF was defined as insoluble organic matter (IOM).

Results of Coprocessing with Polymers Reactions.

A series of reactions was performed in which Illinois No. 6 coal was reacted with four different polymers: polyisoprene, polystyrene, HDPE and LDPE. Each material was also reacted individually as well. Each material and the combination of coal with polymer were reacted under the reaction sequence presented earlier. The coal conversions achieved are presented in Table 1.

Under the coprocessing temperature and pressure conditions, both polyisoprene and polystyrene converted substantially yielding more than 95% conversion regardless of the presence of a solvent or a catalysts. By contrast, under the coprocessing conditions, neither HDPE nor LDPE dissolved readily. The conversions were very low for both of these materials. In fact, the conversions were sometimes negative indicating an absorption of the solvent into the PE polymer during reaction.

At each reaction condition, coal was also reacted individually. The coal conversion achieved was largely dependent upon whether a catalyst or a solvent was used. For example, without either a solvent or catalyst present, 38% coal conversion was achieved. When a solvent composed of 30% tetralin and 70% hexadecane was used with coal, the coal conversion increased to 74%. However, when a FeNaph + S catalyst was added without a solvent, only a small improvement in coal conversion over the thermal case was achieved. When both catalyst and solvent were added, the coal conversion remained the same as the solvent alone case. The addition of MoNaph + S without solvent or with solvent increased coal conversion to 50.6% and 76.3%, respectively, which was only slightly more than the corresponding FeNaph reactions. Therefore, on the basis of the coal conversion, the presence of the tetralin solvent was crucial for the upgrading of liquefied coal since coal conversion was strongly affected by the presence of a hydrogen donor solvent and much less by the presence of a catalyst.

Coprocessing reactions performed with coal and polymer resulted in a product in which both coal and polymer were converted and in which both materials contributed to the IOM formed. The coal and polymers conversions achieved in the individual reactions were compared to a hypothetical mean value. The hypothetical mean is defined as the arithmetic mean of the coal conversion and polymer conversion when both were reacted alone. When coal was coprocessed with either polyisoprene, polystyrene or HDPE without solvent the amount of coal conversion achieved was greater than the hypothetical mean. The addition of solvent to the coprocessing reaction increased coal conversion substantially for polystyrene and slightly for HDPE and LDPE. However, for polyisoprene the amount of conversion decreased suggesting that polyisoprene acted as a fairly good solvent for coal liquefaction. The noncatalytic coprocessing reactions with solvent gave coal conversions below their respective hypothetical mean values.

The reactions using FeNaph + S without solvent resulted in coal conversions that were intermediate between the no solvent, no catalyst case and the solvent added, no catalyst case.

The exception was the coprocessing reaction using polyisoprene, which gave the same conversion as the no solvent, no catalyst case. The reactions using FeNaph + S and solvent produced more coal conversion for the combinations of Illinois No. 6 coal with polystyrene, HDPE and LDPE. However, the reaction with polyisoprene did not yield increased coal conversion with solvent ahead FeNaph + S as the catalyst; the same effect was observed in the thermal reaction when no improvement occurred with the addition of a solvent.

The coprocessing reactions with MoNaph + S without solvent yielded higher coal conversions than the reactions containing FeNaph + S without solvent. In fact, reactions with polyisoprene and polystyrene yielded higher coal conversions than the hypothetical mean, indicating that both polymers served a good solvating agents for coal. When tetralin was added to the systems with MoNaph + S, coal conversion increased for all four polymers systems coprocessed with coal. Polyisoprene and polystyrene yielded the highest coal conversion with MoNaph + S and tetralin while both PE polymers yielded low and similar conversions to those obtained with FeNaph + S and solvent.

Summary for the Coprocessing of Coal with Different Polymers

Under the coprocessing reaction conditions used in this study, polystyrene and polyisoprene were effective solvents for coal liquefaction. For the polyisoprene system, increases in coal conversion compared to the thermal, no solvent case required MoNaph + S. The presence of tetralin with MoNaph + S increased coal conversion even further. For polystyrene, improvements compared to the thermal case were observed both with catalyst and with solvent addition. Neither HDPE nor LDPE was effectively converted at coprocessing conditions regardless of whether solvent was used. Further experimentation with hydrotreating catalysts is required to convert PE effectively at coprocessing conditions.

Coprocessing of Coal with Waste Tires

Previous researchers have shown the feasibility of using waste rubber tires as a coliquefaction component with coal.[1-3] In this work, two different sets of experiments were performed: (1) a model compound, 4-(1-naphthylmethyl)bibenzyl (NMBB) was used as a representative model for the carbon-carbon bonds in coal and was reacted in the presence of waste tire and carbon black, a component of waste tire; and (2) coal was reacted with waste tire thermally and catalytically to evaluate the effect of waste tire on coal conversion and the product slate produced.

Experimental

Materials. The model NMBB (99% purity) was obtained from TCI America and used as received. The catalysts tested in this study were iron naphthenate (FeNaph) (6% Fe), iron stearate (FeSTR) (9.0% Fe, 98% purity) from Strem, hydrated iron oxide (FeOOH) (63.3% Fe) from Aldrich, and molybdenum naphthenate (MoNaph) (6.0% Mo) from Shepherd Chemical. Three waste rubber samples, GF30 (30 mesh), GF40 (40 mesh) and GF80 (80 mesh), were supplied by Rouse Rubber Industries, Vicksburg, MS. A waste tire sample was also obtained from Uniroyal, Opelika, AL. The coal used in the study was Illinois No. 6 bituminous coal from Amoco and carbon black, Black Pearls 2000, was supplied by Cabot Industries. All of the

additives to the NMBB reaction were used as received.

Reaction Procedures for Model Reactions. Reactions were performed in stainless steel tubular microreactors of ~20 cm^3 at 400 °C for 30 min with a H_2 pressure of 1250 psig introduced at ambient temperature. The reactor was agitated horizontally at 450 rpm. The reaction system consisted of 0.25 g of NMBB; when additives were used, waste tire, coal or carbon black was added at an equivalent gram amount of 0.25 g. When the relative amount of the additives was changed, the amount of NMBB was held constant. The additive amount was either 5 times 0.25 g or 0.2 times 0.25 g. Catalyst precursors of MoNaph, FeNaph, FeOOH and FeSTR were added at a level of 900 to 1,100 ppm active metal on a per gram of material basis. When dual catalysts of Fe-based precursors and MoNaph were used, the total level of metal was kept constant at 900 to 1100 ppm with Fe:Mo weight ratios of 1:1. When sulfur was added to the reaction, elemental sulfur was added in a 3:1 stoichiometric ratio of sulfur to metal assuming that either Fe_7S_8 or MoS_2 was formed.

The reaction products obtained from reactions of NMBB and the various additives were analyzed by gas chromatography using a Varian Model 3700 gas chromatograph equipped with a fused silica J&W capillary DB-5 30 m column and a flame ionization detector. The only products that were analyzed were those from NMBB. The products obtained from NMBB were primarily hydrocracked products; trace amounts of hydrogenated products were detected. Percent hydrocracking (%HYC) of NMBB was defined as the moles of hydrocracked liquid products as a percentage of total moles of liquid products produced.

Reaction Procedures for Coprocessing Reactions. Coprocessing reactions were performed using Beulah Zap Lignite, Wyodak subbituminous, Pittsburgh No. 8 bituminous and Illinois No. 6 bituminous coals from the Argonne Premium Coal Sample Bank. The reactions were reacted in stainless steel tubular microreactors at 400 °C for 30 min with 1000 psig (6.9 MPa) hydrogen introduced at ambient temperature. The solvents used for these reactions were the relatively inert hexadecane, and two different waste tires from Rouse Rubber and Uniroyal. The total amount charged was 4 grams with the solvent to maf coal ratio being 1:1. The catalytic reactions used either FeNaph or MoNaph at 1000 ppm; sulfur was added to these reactions on the same basis as the model reactions.

The liquefied products were obtained by extracting first with hexane to obtain the hexane soluble oils and with THF to obtain the THF soluble, hexane insoluble materials which were labeled asphaltenes and preasphaltenes. The organic material that was not soluble in THF was defined as IOM which contained the insoluble material from both coal and waste tire when waste tire was used. The IOM was calculated on an ash free basis.

Hydrocracking of 4-(1-naphthylmethyl) bibenzyl

The model hydrocracking compound 4-(1-naphthylmethyl) bibenzyl (NMBB) was reacted noncatalytically and catalytically with and without sulfur in the presence of added material of waste tires, carbon black, and coal as presented in Table 2. Different combinations were used to test the effect of the individual additives and combinations of additives on the hydrocracking activity of NMBB. The products produced from NMBB were determined and defined as the lumped parameter, percent hydrocracking. When NMBB was hydrocracked at the reaction conditions and in the presence of any additive or catalyst used, the primary products obtained were methylbibenzyl (MBB) and naphthalene (NAP). Secondary products, such as naphthyltolymethane (NTM), bibenzyl (BB), methylnaphthalene (MN) and toluene (TOL), were

obtained in small amounts as the extent of hydrocracking increased.

The cleavage of NMBB can occur at five different sites which are shown in Figure 1 and are labeled a through e. The selectivity of the bond cleavage that occurred with the different additives is given in Table 2. The primary cleavage that occurred with all of the additives and catalysts was at bond a. In most systems, the second most prevalent cleavage occurred at bond d, with a small amount of cleavage occurring at bond b. No cleavage was observed at bonds c or e in any of the reactions performed. The selectivity for hydrocracking NMBB at a given bond is given in Table 2 as SA for bond a, SB for bond b and SD for bond d. These selectivities are defined as cleavage at either bond a, b, or d which is divided by the sum of the bond cleavage a, b and d. Therefore, the parameters chosen to compare the results of the different additives and catalysts on NMBB were % HYC, which described the activity for hydrocracking under the specific reaction conditions, and SA, SB, and SD, which reflected the selectivity of the additive or catalyst for NMBB bond cleavage.

Effect of Waste Rubber, Additives and Catalysts on NMBB Hydrocracking. Table 2 presents the effect of different additives and catalysts on NMBB hydrocracking. Initial reactions employed waste tires in three mesh sizes added to NMBB. With increasing mesh size from 30 to 80 and decreasing particle size, the waste tire's effect on NMBB hydrocracking increased from 11.3 to 15.3%. The decreased particle size may have allowed more contact between the reacting NMBB and the active hydrocracking component in waste tire, carbon black. All subsequent experiments were performed with GF 30 waste tire. When the weight ratio of NMBB to waste tire decreased from 1:0.2 to 1:5, the % HYC of NMBB increased from 9.3 to 13.1%, while the selectivity for bond cleavage at bond a decreased from 91 to 62% with a corresponding increase at bond d from 9 to 38%. Although the selectivity changed rather substantially with increased waste tire, the change in the total amount of hydrocracking was small.

Since carbon black composes between 20 to 30% of waste tires, the effect of carbon black on the hydrocracking of NMBB was evaluated. Introducing carbon black at a 1:1 weight ratio yielded 79.1% HYC of NMBB. Adding waste rubber or coal at the same level resulted in much less HYC, 11.3 and 7.0%, respectively. A higher ratio, 1:0.2, of NMBB to carbon black was used to approximate the lower amount of carbon black present in waste tire; the amount of HYC achieved was 17.7% which was higher than that obtained with a 1:1 ratio of NMBB to waste tire containing at a minimum 20% carbon black. Likewise, when the ratio of NMBB to waste tire was 1:5 in which carbon black was present in an equivalent amount as in the reaction with a NMBB to carbon black ratio of 1:1, the % HYC was much less yielding 13.1% compared to 79.1%. The carbon black contained in the GF 30 waste tire was not nearly as active as carbon black introduced directly. The selectivity for cleavage at bond a was greater for carbon black than for carbon black in waste tire at equivalent carbon black loadings.

In the coprocessing of waste tire with coal, hydrogenation catalysts would be used to increase the conversion of both coal and waste tire. Two slurry phase hydrogenation catalysts, FeNaph and MoNaph, were used in conjunction with NMBB individually and with additives of waste tire and carbon black. Reactions were performed with and without sulfur. When MoNaph was combined with waste tire, 38.2% HYC of NMBB occurred which was more than double the amount obtained with FeNaph. The addition of sulfur increased the amount of % HYC with FeNaph but decreased the effectiveness of MoNaph. Combining FeNaph or MoNaph with carbon black resulted in high levels of % HYC: 86.4% for FeNaph and 97.9% for MoNaph. The selectivity for cleavage at bond a was greater for Mo than for Fe even when sulfur or carbon

black was added.

Ternary systems of NMBB with waste tire and carbon black were reacted without additional catalysts and with three different iron catalysts or MoNaph. The combination of waste tire and carbon black at a 1:0.2:0.2 ratio yielded 29% HYC of NMBB. Addition of MoNaph to this ternary system increased the % HYC to 71.3% although the selectivity for cleavage at bond a remained high and constant. Increasing the amount of waste tire in the system to a ratio of 1:1:0.2 of NMBB to waste tire to carbon black increased % HYC to an even higher value of 83.5%. Utilization of three types of Fe catalysts at that same ratio resulted in % HYC of 42.6% for FeSTR, 53.7% for FeNaph and 55.2% for FeOOH. All of these hydrocracking values were lower than that obtained for MoNaph.

Reactions with NMBB and waste tires were also performed with combined catalysts containing one of the iron precursors, FeNaph, FeOOH, or FeSTR with MoNaph and sulfur. All three of the reactions yielded % HYC between 16.5 and 20.3% so that the type of iron present made little difference in the hydrocracking behavior of NMBB. The % HYC of 18.5% achieved by the combined catalyst of MoNaph with FeNaph was only slightly higher than the 17.5% HYC yielded by the reaction with FeNaph alone. The selectivity for all of the combined catalysts was very high, ranging from 94 to 98%. The presence of the combined catalysts was not synergetic for promotion of NMBB hydrocracking.

Results of Coprocessing of Coals with Waste Tires

Coprocessing reactions were performed with two types of waste tires and coals ranging in rank from lignite to bituminous. The proximate and ultimate analysis of the materials used are given in Table 3. The two waste tire materials were both obtained from waste generated during tire processing. The Rouse waste tire contained much higher organic content than did the Uniroyal sample. The Uniroyal waste tire had much higher ash content but less fixed carbon; consequently, Uniroyal waste tire gave higher conversion to THF soluble material on an ash-free basis since the Uniroyal waste tire had less fixed carbon. Coprocessing reactions performed under noncatalytic conditions are presented in Table 4 and under catalytic conditions in Table 5. Reactions were also performed using hexadecane as a baseline solvent. The coal conversions given in Tables 4 and 5 are on a solvent free basis where the solvent is either defined as waste tire or hexadecane. Coal conversion is defined as (1-(g of IOM)) / (g of maf coal) x 100% where maf is moisture and ash-free.

Thermal reactions were performed with four coals of different rank: Beulah Zap lignite, Wyodak subbituminous coal, Pittsburgh No. 8 and Illinois No. 6 bituminous coals. Three different solvents were used: hexadecane as a baseline and Rouse and Uniroyal waste tires. For all three solvents the low rank coals gave much lower coal conversions than the higher rank bituminous coals. For both Beulah Zap and Wyodak the type of solvent did not affect the amount of conversion. By contrast, both Pittsburgh No. 8 and Illinois No. 6. coals were affected by the type of solvent. Both hexadecane and Rouse waste tire as solvents resulted in similar coal conversion from Pittsburgh No. 8 while Uniroyal waste tire was a much less effective converter of Pittsburgh No. 8 coal. A different result was obtained with Illinois No. 6 coal; hexadecane and Uniroyal waste tire both yielded similar coal conversions while Rouse waste tire was the best solvent for coal liquefaction, yielding nearly 69% coal conversion.

The two bituminous coals were analyzed in more detail. These coals were coprocessed with Rouse and Uniroyal waste tires under catalytic conditions using FeNaph + S and MoNaph

+ S as shown in Table 5. Rouse waste tire when combined with FeNaph + S yielded 43.1% coal conversion while 64.7% coal conversion was achieved with MoNaph + S. Lower conversions were obtained with hexadecane but Uniroyal waste tire yielded even less coal conversion. For Illinois No. 6, hexadecane provided the best solvent medium but Rouse waste tire with either catalyst was also effective converting in 81.7% with FeNaph + S and 84.5% with MoNaph + S. Uniroyal waste tire was ineffectual as a liquefaction solvent for Illinois No. 6 coal, yielding between 51 and 55% coal conversion for both catalysts.

Summary of Coprocessing with Waste Tires

When waste tires are used as solvents in the coprocessing of coal, the composition of the tire material is very important. This effect was demonstrated by the differences in solvating power of two different waste tires in noncatalytic and catalytic reactions of coal with waste tires. Hence, analysis of the waste tire material and reactivity experiments will be necessary to predict the activity of these materials in noncatalytic and catalytic coprocessing.

References

1. Farcasiu, M.; Smith, C. *ACS Fuel Chem Div Prepr*, 37, 1, 472-479, 1992.

2. Zondlo, J. W.; Liu, Z.; Dadyburjor, D. B.; Stiller, A. H. Presentati on, Consortium for Fossil Fuel Liquefaction Science, 7th Annual Technical Meeting, Callaway, GA. July 1993.

3. Orr, E. C.; Tuntawiroon, W.; Anderson, L. L.; Eyring, E. M. Presentation, Consortium for Fossil Fuel Liquefaction Science, 7th Annual Technical Meeting, Callaway, GA. July 1993.

Figure 1. Cleavage Sites for 4-(1-Naphthylmethyl)bibenzyl

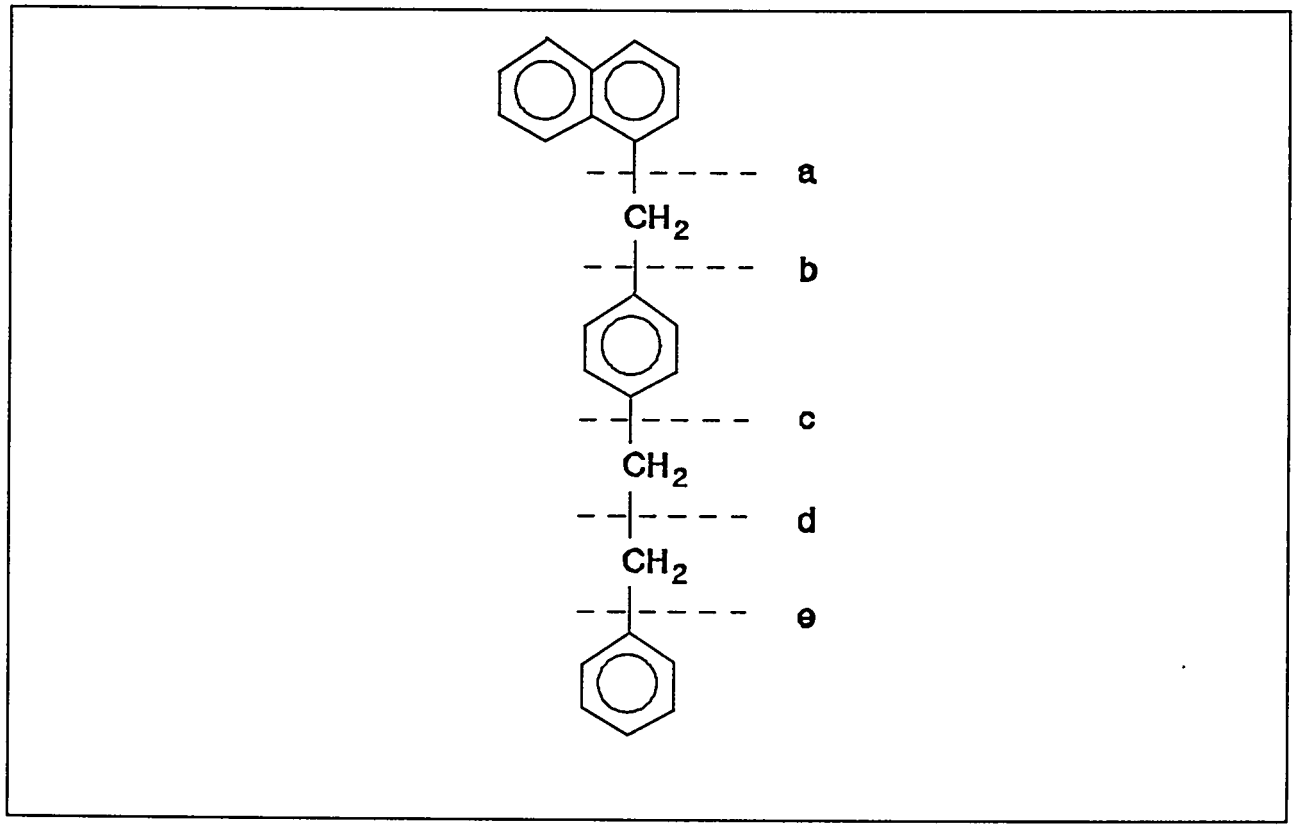

Table 1. Thermal and Catalytic Coprocessing of Coal with Different Polymers

Reactant	Catalyst	Solvent	Conversion(%)			
			Polyisoprene	Polystyrene	HDPE	LDPE
Coal	None	None	38.5±1.0	38.5±1.0	38.5±1.0	38.5±1.0
Polymer	None	None	99.1±1.2	98.2±0.0	1.9±0.8	5.8±2.0
Coal + Polymer	None	None	80.2±0.6	60.8±1.4	23.0±0.4	15.8±3.4
Hypothetical Mean	None	None	68.8	68.4	20.2	22.2
Coal	None	Tetralin	85.1±0.6	85.1±0.6	85.1±0.6	85.1±0.6
Polymer	None	Tetralin	99.8±0.0	99.4±0.4	- 11.3±3.0	1.1±1.2
Coal + Polymer	None	Tetralin	78.6±0.0	75.6±0.1	24.0±3.2	24.8±0.0
Hypothetical Mean	None	Tetralin	92.4	92.2	36.9	43.1
Coal	FeNaph+S	None	49.4±0.7	49.4±0.7	49.4±0.7	49.4±0.7
Polymer	FeNaph+S	None	99.4±0.0	99.2±0.0	0.8±0.1	2.0±0.8
Coal + Polymer	FeNaph+S	None	80.2±0.4	66.4±0.4	20.9±0.9	22.9±1.9
Hypothetical Mean	FeNaph+S	None	64.8	74.3	25.1	25.7
Coal	FeNaph+S	Tetralin	87.2±1.6	87.2±1.6	87.2±1.6	87.2±1.6
Polymer	FeNaph+S	Tetralin	98.1±1.1	98.2±0.2	- 25.5±0.8	5.0±0.6
Coal + Polymer	FeNaph+S	Tetralin	77.3±0.4	84.0±0.5	33.8±0.8	35.4±1.4
Hypothetical Mean	FeNaph+S	Tetralin	92.6	92.7	30.8	46.1
Coal	MoNaph+S	None	54.8±2.2	54.8±2.2	54.8±2.2	54.8±2.2
Polymer	MoNaph+S	None	97.8±0.1	98.4±0.6	0.4±0.1	2.6±0.0
Coal + Polymer	MoNaph+S	None	89.3±0.0	81.3±5.8	26.2±0.0	13.4±1.0
Hypothetical Mean	MoNaph+S	None	76.3	76.6	27.6	28.7
Coal	MoNaph+S	Tetralin	88.1±0.8	88.1±0.8	88.1±0.8	88.1±0.8
Polymer	MoNaph+S	Tetralin	96.8±1.3	97.7±0.9	- 21.6±1.7	- 0.6±1.1
Coal + Polymer	MoNaph+S	Tetralin	92.8±0.9	94.4±0.0	35.2±0.6	33.8±2.5
Hypothetical Mean	MoNaph+S	Tetralin	92.4	92.8	33.2	43.8

Table 2. Selectivity of the Slurry Catalysts for Hydrocracking 4-(1-Naphthylmethyl)bibenzyl

Reaction Systems	%HYC[b]	Cleavage of a+b+d[c]	Selectivity*100%		
			SA	SB	SD
NMBB (thermal)	4.9±1.3	2.5	61	0	39
NMBB+S	9.3±2.7	4.7	66	2	32
NMBB+GF30WT(1:1)	11.3±2.2	5.7	77	0	23
NMBB+GF40WT(1:1)	13.5±2.5	6.8	76	0	24
NMBB+GF80WT(1:1)	15.3±2.4	7.7	81	0	19
NMBB+WT[a](1:0.2)	9.3±2.1	4.7	91	0	9
NMBB+WT(1:5)	13.1±1.7	6.6	62	0	38
NMBB+CB(1:1)	79.1±2.7	39.6	78	6	16
NMBB+CB(1:0.2)	17.7±2.7	8.9	84	4	12
NMBB+Coal(1:1)	7.0±2.1	3.5	83	0	17
NMBB+FeNaph	5.5±1.0	2.8	79	0	21
NMBB+MoNaph	6.4±0.9	3.3	76	0	24
NMBB+FeNaph+S	15.5±1.4	7.7	86	4	10
NMBB+MoNaph+S	39.4±2.3	19.7	92	5	3
NMBB+WT+FeNaph(1:1)	15.5±2.6	7.8	73	0	27
NMBB+WT+MoNaph(1:1)	38.2±2.2	19.2	95	1	4
NMBB+CB+FeNaph(1:1)	86.4±3.8	43.3	89	4	7
NMBB+CB+MoNaph(1:1)	97.9±2.2	49.0	94	4	2
NMBB+WT+FeNaph+S(1:1)	17.5±2.6	8.8	75	0	25
NMBB+WT+MoNaph+S(1:1)	30.1±2.4	15.1	96	0	4
NMBB+CB+FeNaph+S(1:1)	87.3±3.8	43.7	88	6	6
NMBB+CB+MoNaph+S(1:1)	99.7±1.6	49.8	94	5	1
NMBB+WT+MoNaph+S(1:0.2)	29.4±3.0	14.8	98	0	2
NMBB+WT+MoNaph(1:0.2)	13.8±3.0	6.9	97	0	3
NMBB+CB+MoNaph+S(1:0.2)	79.9±3.6	40.0	95	4	1

Table 2. Selectivity of the Slurry Catalysts for Hydrocracking 4-(1-Naphthylmethyl)bibenzyl(Continued)

Reaction Systems	%HYC[b]	Cleavage of a+b+d[c]	Selectivity*100%		
			SA	SB	SD
NMBB+WT+MoNaph(1:5)	23.2±2.4	11.7	69	0	31
NMBB+WT+MoNaph+S(1:5)	18.0±2.1	9.1	67	0	33
NMBB+WT+CB(1:0.2:0.2)	29.0±1.7	14.6	92	3	5
NMBB+WT+CB+MoNaph (1:0.2:0.2, 1000 ppm)	71.3±2.5	35.7	95	4	1
NMBB+WT+CB+MoNaph (1:1:0.2, 1000 ppm)	83.5±2.4	41.8	93	5	2
NMBB+WT+CB+FeNaph (1:1:0.2, 1000 ppm)	53.7±2.5	26.9	89	5	6
NMBB+WT+CB+FeOOH (1:1:0.2, 1000 ppm)	55.2±3.0	27.7	95	2	3
NMBB+WT+CB+FeSTR (1:1:0.2, 1000 ppm)	42.6±2.8	21.4	97	0	3
NMBB+WT+FeNaph+MoNaph+S (1:1, 500 ppm each)	18.5±2.1	9.3	98		2
NMBB+WT+FeOOH+MoNaph+S (1:1, 500 ppm each)	20.3±2.2	10.2	96		4
NMBB+WT+FeSTR+MoNaph+S (1:1, 500 ppm each)	16.5±3.0	8.3	94	0	6

[a] WT=waste tire rubber GF30 unless specified; CB=carbon black; MoNaph=Mo Naphthenate; FeNaph=Fe Naphthenate; FeSTR=FeStearate

[b] % HYC is defined as the moles of hydrocracked liquid products as a percentage of the total moles of liquid products produced.

[c] Cleavage of Bonds a, b, and d is defined as bond cleavage of bond a, b, and d in NMBB.

[d] Selectivity is defined as bond cleavage at a (SA) or b (SB) or d (SD) divided by the combined bond cleavage of a, b, and d.

Table 3. Analysis of Coals and Waste Tires

Sample	Organic Elemental Analysis (wt%)				
	C	H	O	N	S
Rouse Waste Tire	85	7.4	--	---	1.6
Uniroyal Waste Tire	56	8.0	--	---	1.0
Beulah Zap	73	4.8	20	1.1	0.8
Wyodak	75	5.4	18	1.1	0.6
Illinois No. 6	78	5.0	14	1.4	0.6
Pittsburgh No. 8	83	5.3	9	1.6	2.2

Sample	Proximate Analysis (wt%)			
	Moisture	Ash	Volatile Matter	Fixed Carbon
Rouse Waste Tire	0.83	3.60	65.81	29.76
Uniroyal Waste Tire	0.15	31.04	63.29	5.52
Beulah Zap	32.24	6.59	30.45	30.72
Wyodak	28.09	6.31	32.17	33.43
Illinois No. 6	7.97	14.25	36.86	40.92
Pittsburgh No. 8	1.65	9.10	37.20	52.05

Sample	Product Distribution of Liquefied Waste Tire (%)*			
	Gas + Oil	Asphaltenes + Preasphaltenes	IOM	Waste Tire Conversion
Rouse Waste Tire	64.4±1.5	4.8±1.1	30.8±1.5	69.2±1.5
Uniroyal Waste Tire	78.0±1.2	3.6±1.2	18.4±1.0	81.6±1.0

* product yields are based on maf basis.

Table 4. Effect of Waste Tire Coal Conversion and Product Distribution for Coals of Different Rank

Coal	Solvent	Yields (%)[b]			Coal Conversion (%)
		Gas + Oil	Asphaltenes + Preasphaltenes	IOM	
Beulah Zap	Hexadecane	16.9±4.0	5.0±1.3	78.1±4.0	21.9±4.0
Beulah Zap	Rouse WT[c]	11.8±4.0	13.8±3.3	74.4±4.0	25.6±4.0
Beulah Zap	Uniroyal WT	19.9±1.3	3.0±0.2	77.1±1.3	22.9±1.3
Wyodak	Hexadecane	20.9±4.1	5.6±1.0	73.5±4.1	26.5±4.1
Wyodak	Rouse WT	8.0±3.7	23.7±0.4	68.3±3.7	31.7±3.7
Wyodak	Uniroyal WT	20.0±1.4	5.5±0.3	74.5±1.4	25.5±1.4
Pittsburgh No. 8	Hexadecane	19.5±2.9	33.1±2.4	47.4±2.9	52.6±2.9
Pittsburgh No. 8	Rouse WT	13.1±2.5	40.8±2.4	46.1±2.5	53.9±2.5
Pittsburgh No. 8	Uniroyal WT	15.1±1.0	17.7±0.8	67.2±1.0	32.8±1.0
Illinois No. 6	Hexadecane	18.9±2.1	36.4±1.9	44.7±2.1	55.3±2.1
Illinois No. 6	Rouse WT	10.1±3.1	57.8±3.0	32.1±3.1	68.9±3.1
Illinois No. 6	Uniroyal WT	10.9±2.7	40.2±1.2	48.9±2.7	51.1±2.7

[a] Reaction Conditions: 400 °C, 1000 psig H_2 introduced at ambient temperature, 30 min, 550 ppm horizontal agitation.
[b] Yields and conversions are given on a solvent-free basis.
[c] WT = Waste tire

Table 5. Effect of Catalysts and Waste Tire on Liquefaction Coal Conversion and Product Distribution[a]

Coal	Solvent	Catalyst	Yields [b] (%)			Coal Conversion (%)
			Gas + Oil	Asphaltenes + Preasphaltenes	IOM	
Wyodak	Hexadecane	FeNaph+S[d]	22.2±.3.3	12.2±2.4	65.6±3.3	34.4±3.3
Wyodak	Hexadecane	MoNaph+S	24.3±3.0	25.3±2.7	50.4±3.0	49.6±3.0
Wyodak	Rouse WT[c]	FeNaph+S	17.7±1.3	25.4±0.8	56.9±1.3	43.1±1.3
Wyodak	Rouse WT	MoNaph+S	21.5±1.1	43.2±0.9	35.3±1.1	64.7±1.1
Wyodak	Uniroyal WT	FeNaph+S	20.4±2.1	7.5±0.7	72.1±2.1	27.9±2.1
Wyodak	Uniroyal WT	MoNaph+S	23.0±2.0	9.1±1.0	67.9±2.3	32.1±2.3
Illinois No. 6	Hexadecane	FeNaph+S	23.6±2.0	66.7±2.9	9.7±2.0	90.3±2.0
Illinois No. 6	Hexadecane	MoNaph+S	20.6±1.9	70.8±0.4	8.6±1.9	91.4±1.9
Illinois No.6	Rouse WT	FeNaph+S	11.5±1.7	70.2±1.5	18.3±1.7	81.7±2.0
Illinois No. 6	Rouse WT	MoNaph+S	14.0±1.8	70.5±1.7	15.5±1.8	84.5±1.8
Illinois No. 6	Uniroyal WT	FeNaph+S	10.9±1.9	40.6±1.8	48.5±1.9	51.5±1.9
Illinois No. 6	Uniroyal WT	MoNaph+S	15.1±2.0	39.2±1.7	45.7±2.0	54.3±2.0

[a] Reaction Conditions: 400 °C, 1000 psig H_2 at ambient temperature 30 min, 550 rpm horizontal agitation.
[b] Yields and conversions are given on a solvent free basis.
[c] WT = Waste tire
[d] FeNaph = Fe naphthenate; MoNaph = Mo naphthenate

TASK I

Project I.7

COLIQUEFACTION OF WASTE PLASTICS WITH COAL

**M. Mehdi Taghiei, Zhen Feng, Frank E. Huggins,
and Gerald P. Huffman
University of Kentucky**

INTRODUCTION

Polyethylene (PE), poly(ethylene terephthalate) (PET), polypropylene (PPE), and actual plastic wastes from such items as milk jugs, soft drink bottles, plastic wraps, plastic flatware, etc., have been successfully converted to oil in direct liquefaction experiments with coal. Comparative experiments were performed with and without the presence of coal under typical direct liquefaction conditions(420-450°C, 60 minutes reaction time, 800 psig H_2 cold). Two types of catalysts were used: highly dispersed iron-based catalysts, and an HZSM-5 zeolite catalyst. Using PE, PPE, PET and a mixed waste plastic with the zeolite catalyst, oil yields of 80 to 98% and total conversions of 90 to 100% were obtained at liquefaction temperatures of 420-430 °C. A nanoscale ferrihydrite catalyst in a sulfided state was less active, but also gave similar results at somewhat higher temperatures. Coliquefaction experiments were performed on coal-plastic mixtures(usually 50:50 mixtures) using a bituminous coal, a subbituminous coal, and a lignite. The HZSM-5 zeolite catalyst and nanoscale iron catalysts were used, separately and together. The oil yields for these coliquefaction experiments were as high as 60 to 80%, while the total conversions reached levels of over 90%. Oil yields for coal-plastic mixtures were higher, typically by ~10%, than the average of the oil yields for the coal and plastic alone, implying synergistic effects.

The research summarized here has been summarized in two publications.[1,2]

EXPERIMENTAL PROCEDURE

Medium density polyethylene (MDPE), high density polyethylene (HDPE), poly(ethylene terephthalate) (PET), polypropylene (PPE) and actual plastic wastes, such as milk jugs, and soft drink bottles, and a mixed waste plastic (MWP) prepared in our laboratory from a variety of

items (milk jugs, soft drink bottles, yogurt containers, motor oil bottles, disposable plastic flatware, plastic sacks and wraps, etc.) were liquified. Coliquefaction experiments were performed on mixtures of MDPE and the MWP with Blind Canyon bituminous coal, iron ion-exchanged Beulah lignite,[3] and iron ion-exchanged Black Thunder subbituminous coal.[4] Proximate and ultimate analyses for these coals and the mixed waste plastic (MWP) prepared in our laboratory are shown in Table I. The experiments used several types of catalysts: iron ion-exchanged iron,[3,4] ultrafine ferrihydrites,[5,6] and an HZSM-5 zeolite catalyst.
The structure of the ion-exchanged iron and ferrihydrite catalysts and their activity in coal liquefaction have been discussed in detail elsewhere.[3-6]

Most of the liquefaction experiments were conducted in 50 ml tubing bombs charged with 5 g of feedstock (plastic or coal plus plastic). Tetralin was added with feedstock in most experiments in a 3:2 tetralin:feedstock ratio. Several experiments were run using a waste motor oil as a solvent (waste oil:plastic ratio = 3:2). Unless otherwise noted, the zeolite and ferrihydrite catalysts were added at a concentration level of 1 wt.% of the feedstock. In order to sulfidize the iron when iron catalysts were present, dimethyl disulfide (DMDS) was added with a sulfur to iron ratio of 2. The reactors are then pressurized to 800 psig hydrogen (cold) and heated to the desired temperature in a fluidized sand bath while being agitated at 400 cycles per min.

At the end of the reaction period, the microreactor is quenched in a room temperature sand bath. The liquefaction products are determined by Soxhlet extraction and the gaseous products are collected and analyzed by gas chromatography. The liquefaction products are separated into oil (THF and pentane soluble), asphaltene and preasphaltene (THF soluble, but pentane insoluble), and insoluble residues or IOM (THF insoluble). Total conversion is defined as {100 - %(THF insolubles)}, while oil yield is defined as {100 - %(pentane insolubles) - %(THF insolubles) - %(gas)}. Although the gas yield was not determined for some experiments, it was generally quite low(<1 to 2%). PET was the only feedstock exhibiting a significant gas yield(13-14%). The reproducibility of experiments
run by a single operator on a single system was normally ±1%, while measurements by different operators on different systems were repeatable to within ±5%.

Soxhlet extraction results for various plastic resins and the MWP prior to reaction are summarized in Table 2. It is seen that the MDPE exhibited significant solubility in THF prior to reaction, which increased with extraction time. The pentane solubility of MDPE is small, but

not negligible. The extraction percentages for all of the other resins and the MWP are seen to be quite low(<1-2%).

RESULTS AND DISCUSSION

Direct liquefaction results for individual plastic resins are presented in Table 3. The experiments were carried out with a 3:2 solvent:feedstock ratio at temperatures of 420 to 450°C, 800 psig hydrogen(cold), for a reaction time of 60 minutes. Two types of catalyst were used: an HZSM-5 zeolite catalyst and a nanoscale ferrihydrite treated with citric acid(FHYD/CA)[6] added at a concentration of 1 wt.% of the feedstock. Dimethyl disulfide(DMDS) was added to convert the FHYD/CA to pyrrhotite during the reaction.

The non-catalytic oil yields for MDPE and HDPE at 430°C with a tetralin solvent are 26 and 11%, respectively. It is seen that the HZSM-5 zeolite catalyst is highly active, increasing the oil yields for HDPE and MDPE to over 90% under the same conditions. The FHYD/CA catalyst was significantly less effective at 420 and 430°C. PPE exhibited very high thermal oil yields, which increased to nearly 100% at 420°C in tetralin with the addition of either catalyst. The oil yield of PET at 430°C in tetralin was increased only slightly by addition of either catalyst, from 62 to 64%. The gas yield of PET was also significant(13-14%); this is not surprising in view of the ester linkages (carbonyl groups) present in its structure.

Experiments conducted in a waste motor oil solvent also indicated that the zeolite was the most effective catalyst. However the FHYD/CA catalyst was nearly as active, particularly at 450°C, where both catalysts produced over 90% oil yield and nearly 100% total conversion.

The oil yields for the MDPE and HDPE are shown graphically in Figure 1. Figure 2 shows the oil yields for the mixed waste plastic(MWP)(liquefaction conditions - 430°C, tetralin:feedstock ratio = 3:2, reaction time - 60 minutes, 800 psig H_2 cold) and for milk jug and coke bottle samples. These results demonstrate that an acid cracking catalyst such as the HZSM-5 zeolite is highly effective in depolymerization of plastic under direct liquefaction conditions.

Coliquefaction results for 1:1 mixtures of a bituminous coal (Blind Canyon, DECS-6) and the MWP (430°C, 60 min., 800 psig H_2 cold, tetralin:feed = 3:2) are shown in Figure 3. The largest increase in oil yield (~ 20%) was achieved by addition of 1 wt.% of the HZSM-5 zeolite catalyst to the coal and plastics mixture. The addition of 1 wt.% of a binary Zn-ferrihydrite ($(Fe_{0.95}Zn_{0.05})OOH$ with added DMDS) to the Blind Canyon coal increases the total conversion

of the coal by 12% and the oil yield by 8%. Mixtures of Blind Canyon coal and the MWP, both with and without the presence of the FHYD/Zn catalyst (1 wt.%) exhibited higher oil yields than either the MWP or Blind Canyon coal alone under the same liquefaction conditions, implying synergistic effects (Figure 4).

A significant enhancement of the liquefaction conversion of low-rank coals was achieved in our previous studies[10,11] by incorporating iron in the coals by an ion-exchange process. The liquefaction behavior of low rank coals containing ion-exchanged iron in terms of both total yield and desirable products, is superior to that obtained by mixing an ultrafine iron oxide with the coal. In Figure 5, results for the coliquefaction of medium density polyethylene and Beulah coal containing 0.9 wt.% ion-exchanged iron with no added solvent are presented (reaction conditions - 450°C, 800 psig H_2 (cold), 60 min.). It is seen that both the total conversion and oil yield increase in a roughly linear manner as the percentage of polyethylene in the mixture increases. At a PE:coal ratio of 3:1, the total conversion exceeds 90% and the oil yield exceeds 80%. These results suggest that the PE plays the role of a hydrogen donor solvent for the coal under these conditions.

Figure 6 illustrates the results obtained for coliquefaction of Black Thunder coal containing 0.5 wt.% ion-exchanged iron and mixed waste plastics with added tetralin (coal:plastic - 1:1; tetralin:feedstock = 3:2; 430°C; 800 psig H_2 (cold); 60 min.). The liquefaction results for the MWP and iron ion-exchanged coal in the presence of HZSM-5 (1.0 wt. %) show significant enhancements of both total conversion and oil yield. Synergistic effects also occur here. If the oil yields for the ion-exchanged coal alone and the waste plastic plus HZSM-5 alone are averaged, the anticipated oil yield from the 50:50 mixture would be 59%; however, the oil yield obtained is about 68%.

Coliquefaction of waste carbonaceous materials with coal is being examined as a possible strategy to derive a useful liquid fuel that could be used as a feedstock for conventional petroleum cracking or similar processes. The use of hydrogen-rich materials, such as waste oil and plastics, in liquefaction with hydrogen-poor coal should enhance both the yield and quality of desirable liquid products. Moreover, this process also results in a solid residue, derived in large part from the ash-forming elements in coal, that may act as an effective internal filter for unwanted components from both the waste material and the coal. For example, much of the sulfur present in coal reports to the solid residue, and it is anticipated that most inorganic

elements, whether derived from the coal or from the waste material, should also migrate into the solid residue.

Of great environmental importance in coliquefaction of wastes and coal is the behavior and mobilization of specific trace and minor elements and their compounds that have been identified by the U.S. Environmental Protection Agency as potentially detrimental to the Nation's air and water quality if they were to be released to the environment in significant concentrations. Such species may derive from either the waste material or the coal or both components in the coliquefaction process. To follow the mobilization and segregation reactions of critical elements during coliquefaction, it is necessary to utilize a technique that will directly determine the speciation of the element in these complex materials. Over the last year, we have used X-ray absorption fine structure (XAFS) spectroscopy for investigation of chlorine in the coliquefaction of polyvinyl chloride (PVC) contaminated waste plastics with lignite. As is well known, PVC is a chlorinated plastic that is difficult to recycle by other methods because of its chlorine content. It was anticipated that the chlorine from PVC would end up in the solid residue, rather than the oil, by reaction of chlorine with calcium and sodium in the lignite.

Coliquefaction experiments:

Mixtures of a lignite (Beulah seam, ND) and waste plastics contaminated with PVC and of lignite with small amounts (<10 wt%) of PVC alone were subjected to liquefaction at 350°C or 400°C, 800 psi (cold), for 60 min in tubing bombs at University of Kentucky Center for Applied Energy Research (UKCAER). In all experiments, the solid residue was separated from the liquid product and both fractions were used for the XAFS experiments.

XAFS Experiments:

Chlorine and calcium XAFS spectroscopies were performed on the PVC/coal starting mixtures, oils, and residues at beam-line X-19A at the National Synchrotron Light Source (NSLS), at Brookhaven National Laboratory. Spectra were recorded in fluorescent geometry using a Lytle detector for all experiments.

Analysis of the XAFS spectra was conducted at the University of Kentucky. As is usually done, the XAFS spectra are subdivided into separate XANES (X-ray absorption near-edge structure) and EXAFS (extended X-ray absorption fine structure) regions. Whereas the XANES

region is used as it is as a spectral fingerprint, the EXAFS region is mathematically manipulated to obtain a radial structure function that describes the local structure about the absorbing element.

Discussion:

Residues and oils from three coliquefaction experiments were examined by Ca and Cl XAFS spectroscopy. These experiments were as follows: (i) Beulah lignite (50%) + waste plastics mixed with 5% PVC (50%) at 350°C, 800 psi H_2 (cold), for 60 mins; (ii) as (i), except at 400°C; and (iii) Beulah lignite (90%) + PVC (10%) at 400°C, 800 psi H_2 (cold), 1 hour. Oil and residue fractions, defined as soluble or insoluble fractions in tetrahydrofuran (THF), were prepared from the product of each coliquefaction experiment.

The chlorine K-edge spectrum of polyvinyl chloride is similar to those of other chlorinated hydrocarbons we have examined previously [7]. There is sharp peak at about -1 eV (relative to the major spectral inflection point in NaCl) that is highly characteristic of organochlorine compounds. However, such a feature is absent from the Cl XANES spectra of both the residue and oil samples, indicating that the Cl-C bonds in PVC have been more or less completely eliminated in the processing. Although there appears to be no organochlorine compounds in the products of the coliquefaction process, both the XAFS analysis and chloride ion chromatography indicate that significant chlorine is present in both the THF soluble and insoluble fractions. Comparison of the Cl XANES spectra of the residues with those of various inorganic chlorides [7] indicates that a major component in these residues is NaCl. Subtraction of the NaCl spectrum from the Cl XANES spectrum of one of the residues leaves a difference spectrum that is similar to that from a hydrated chloride species. However, it is difficult to attribute such a spectrum, particularly a difference spectrum, to a specific form of chlorine, such as $CaCl_2.2H_2O$, because all hydrated chloride forms give quite similar spectra [7].

The chlorine XANES spectra of the oil fractions are typical of a hydrated chloride anion species [7]. The most likely candidate would appear to be an adduct compound formed between HCl in the gas phase and a polar functional group in the oil, such as a quaternary amine hydrochloride. Such compounds have been identified previously in the products of coal liquefaction of high chlorine-containing coals [8]. Furthermore, the high pressures of the coliquefaction experiments, as well as the procedure of cooling the sample under pressure after reaction,

are conducive to formation of basic nitrogen organohydrochlorides. It is likely that such components are also present in the residues.

The interpretation of the Ca XANES spectra is underway, but appears less conclusive than that of the Cl XANES data. A summary of this work was given at the Consortium meeting in Snowbird, UT, in July 1994, and at the ACS IEC Meeting on Emerging Technologies in Hazardous Waste Management VI, to be held in Atlanta, GA, in September, 1994 [9].

CONCLUSIONS

The following conclusions can be made from this investigation:

1- Catalytic direct liquefaction appears to be an attractive recycling alternative for waste plastics, giving very high oil yields and total conversions.

2- An HZSM-5 catalyst is much more active at moderate temperatures (420-430°C) for the liquefaction of plastic than nanoscale, sulfided, iron-based catalysts that are effective for the liquefaction of coal. This indicates that acid cracking catalysts will be very useful for direct liquefaction of plastics. The iron-based catalysts are significantly more effective for plastics liquefaction at higher temperatures (450°C).

3- Coliquefaction of mixed waste plastics with a bituminous coal, both with and without the addition of an iron catalyst, exhibits higher oil yields than obtained by liquefaction of either the waste plastics or the coal alone implying synergistic effects. The addition of the HZSM-5 zeolite catalyst increased the total conversion to approximately 90% and the oil yield to 60% for a 50:50 mixture of waste plastic and bituminous coal.

4- Coliquefaction of a 50:50 mixture of mixed waste plastic and an iron ion-exchanged subbituminous coal with the addition of 1.0 wt.% of HZSM-5 zeolite catalyst gave a total conversion of over 90% and an oil yield of approximately 70% The oil yield of the mixture appeared to have been increased approximately 10% by synergistic effects.

5- Coliquefaction of an iron ion-exchanged Beulah lignite with medium density polyethylene with no added solvent gave very good oil yields and total conversions at 450 °C, indicating that the plastic plays the role of a hydrogen donor solvent for the coal under those conditions.

Future studies will attempt to establish optimum conditions for coliquefaction of waste plastics and coal, including the effect of temperature, pressure, reaction time, and coal/plastic

ratio. A variety of potential acid catalysts, such as different types of zeolite, clays, and highly dispersed metal oxides, will be investigated.

REFERENCES

1- Taghiei, M.M.; Huggins, F.E.; Huffman, G.P., **1993**, ACS Div. Fuel Chem. Preprints, 38(4), 810-815.

2- Taghiei, M.M.; Huggins, F.E.; Huffman, G.P. "Coliquefaction of Waste Plastic with Coal," **1994**, Energy & Fuels, in press.

3- Taghiei, M. Mehdi; Huggins, F.E.; Ganguly, B.; Huffman, G.P., *Energy & Fuels*, **1993**, 7, 399.

4- Taghiei, M. Mehdi; Huggins, F.E.; Mahajan, V.; Huffman, G.P., Energy & Fuels, **1994**, *1*, 31.

5- Zhao, J.; Feng, Z.; Huggins, F.E.; Huffman, G.P., Energy & Fuels, **1994**, 1, 38.

6- Zhao, J.; Feng, Z.; Huggins, F.E.; Huffman, G.P., Energy & Fuels, in press.

7- Huggins, F.E.; Huffman, G.P. In *Chlorine in Coal*; Stringer, J. and Banerjee, D.D., Eds.; Coal Science and Technology, Vol. 17; Elsevier: Amsterdam; 1991; pp. 43-61; also, Huggins, F.E.; Huffman, G.P. *Fuel*; 1994, to be published.

8- Davis, B.H. In *Chlorine in Coal*; Stringer, J. and Banerjee, D.D., Eds.; Coal Science and Technology, Vol. 17; Elsevier: Amsterdam; 1991; pp. 129-173.

9- F. E. Huggins, M. M. Taghiei, and G. P. Huffman, Extended Abstract for American Chemical Society (I&EC Division) Symposium, *Emerging Technologies in Hazardous Waste Management VI*, Atlanta, GA, (1994).

Table 1. Proximate and ultimate analyses of coal samples and waste plastics used in this research.

Proximate[a]	Beulah Lignite	Black Thunder Coal	Blind Canyon Coal	Mixed Waste Plastic
% Ash	9.56	6.34	6.57	0.45
% Volatile	56.08	43.62	46.75	98.80
% Fixed Carbon	34.36	49.83	46.68	0.74
Ultimate[b]				
% Carbon	73.14	73.49	81.61	84.65
% Hydrogen	4.47	3.09	6.21	13.71
% Nitrogen	1.01	1.29	1.38	0.65
% Total Sulfur	0.77	0.60	0.47	0.01
% Oxygen	20.61	19.33	10.33	0.98

a = Dry Basis, b = Dry Mineral Matter Free Basis

Table 2. THF and pentane solubility of plastics.
Soxhlet extraction time - 20 hours.

Material	THF Soluble (%)	Pentane Soluble (%)
PPE	1	1
PET	2	2
MDPE	24	5
MDPE	38*	
HDPE	1	1
MWP	0.1	0

* Extraction time - 32 hours

Table 3. Liquefaction yields for pure plastic resins: medium density and high density polyethylene (MDPE and HDPE); polyethylene terephthalate (PET); and polypropylene (PPE).

Sample	Catalyst	Solvent	T(°C)	Oil(%)	Gas(%)	Total(%)
MDPE	None	Tetralin	430	26	<1	65
MDPE	None	Tetralin	450	33[+]		100
MDPE	FHYD/CA	Tetralin	420	14	<1	74
MDPE	FHYD/CA	Tetralin	430	34	<1	68
MDPE	HZSM-5	Tetralin	420	79	<1	92
MDPE	HZSM-5	Tetralin	430	96	1	99
HDPE	None	Tetralin	430	11	<1	33
HDPE	HZSM-5	Tetralin	430	96	1	98
PET	None	Tetralin	430	62	13	91
PET	HZSM-5	Tetralin	430	64	14	96
PET	FHYD/CA	Tetralin	430	64	13	92
PPE	None	Tetralin	420	83	<1	89
PPE	HZSM-5	Tetralin	420	98	2	100
PPE	FHYD/CA	Tetralin	420	98	2	100
PPE	HZSM-5	Waste Oil	420	93	2	95
MDPE	HZSM-5	Waste Oil	420	44	1	81
MDPE	HZSM-5	Waste Oil	430	55	1	93
MDPE	HZSM-5	Waste Oil	450	93	4	97
MDPE	FHYD/CA	Waste Oil	420	50	1	82
MDPE	FHYD/CA	Waste Oil	450	91[+]		96

[+]Oil + gas; gas not determined.

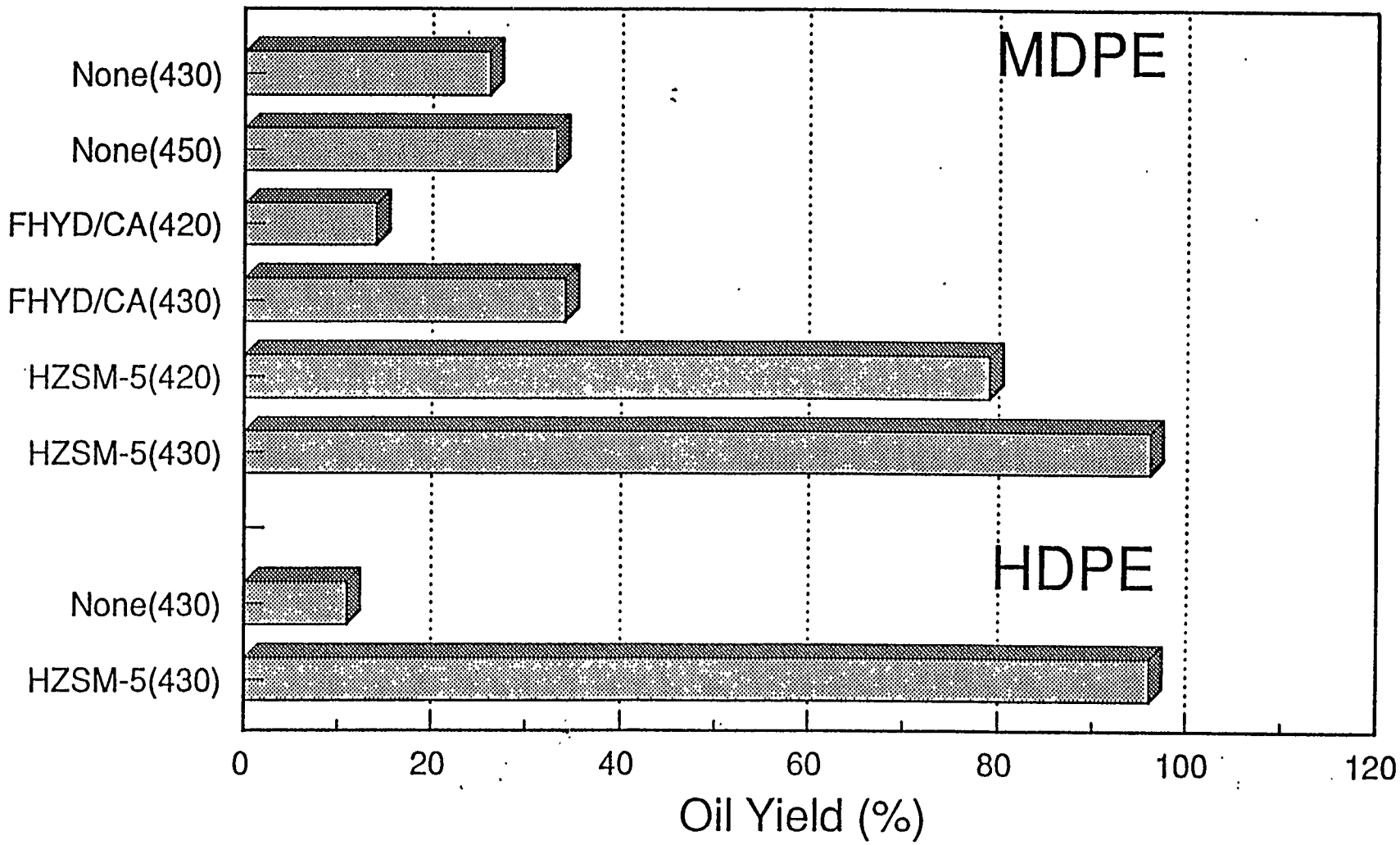

Figure 1. Oil yields for medium density and high density polyethylene (MDPE and HDPE). Catalysts and reaction temperatures (C) are indicated.

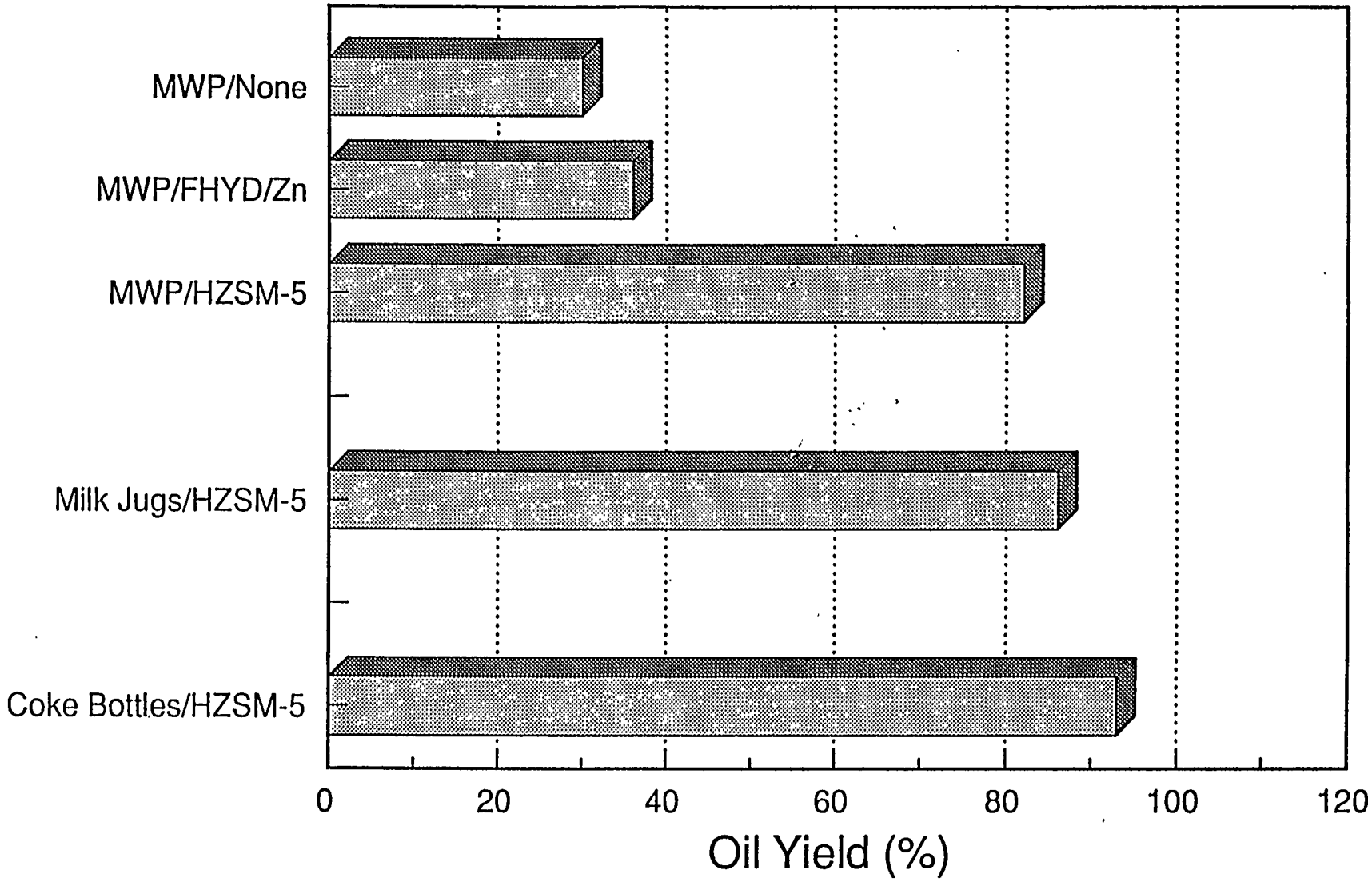

Figure 2. Oil yields for a mixed waste plastic (MWP), milk jugs, and coke bottles.

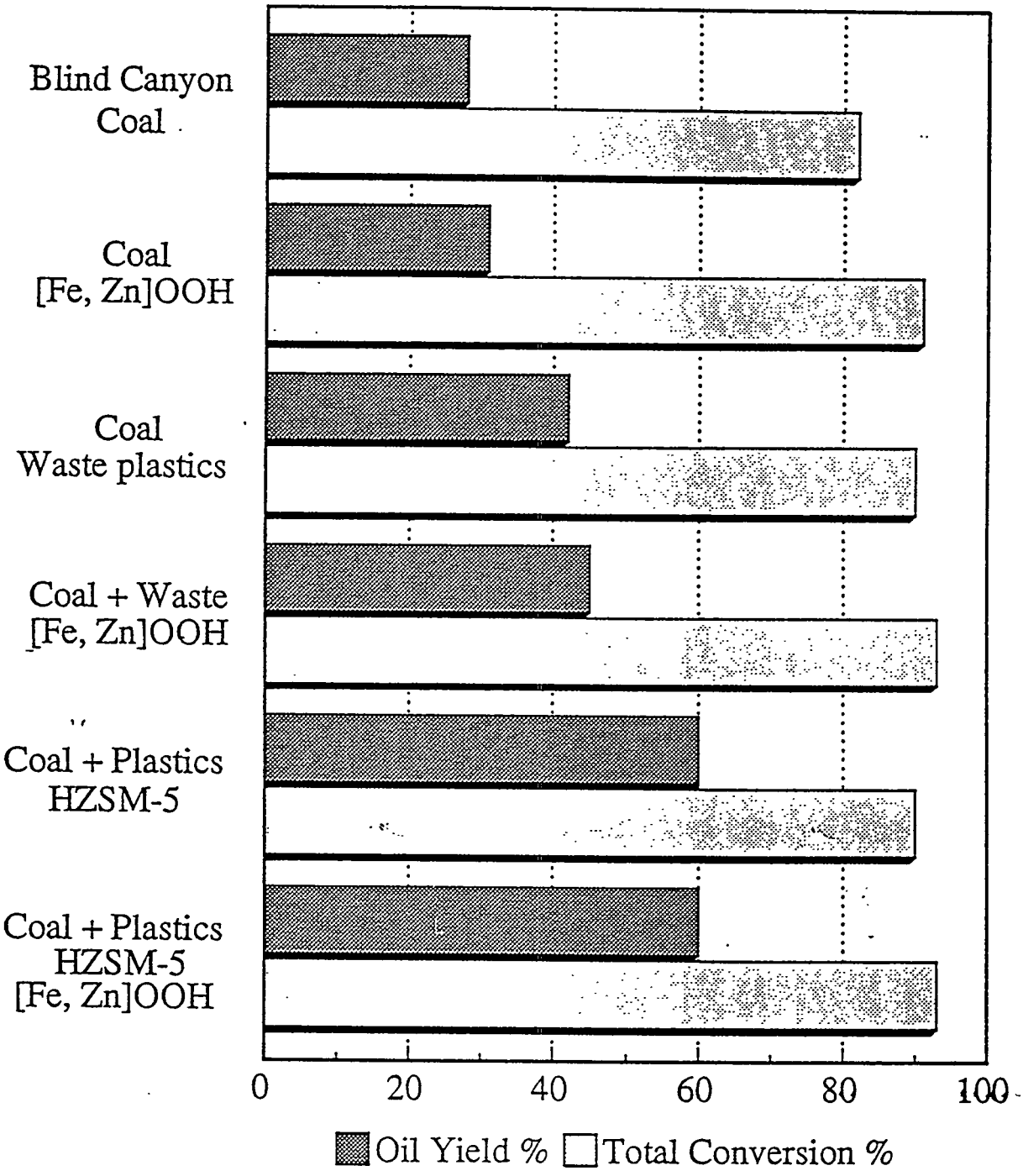

Figure 3. Coliquefaction results for a bituminous coal and a mixed waste plastic.

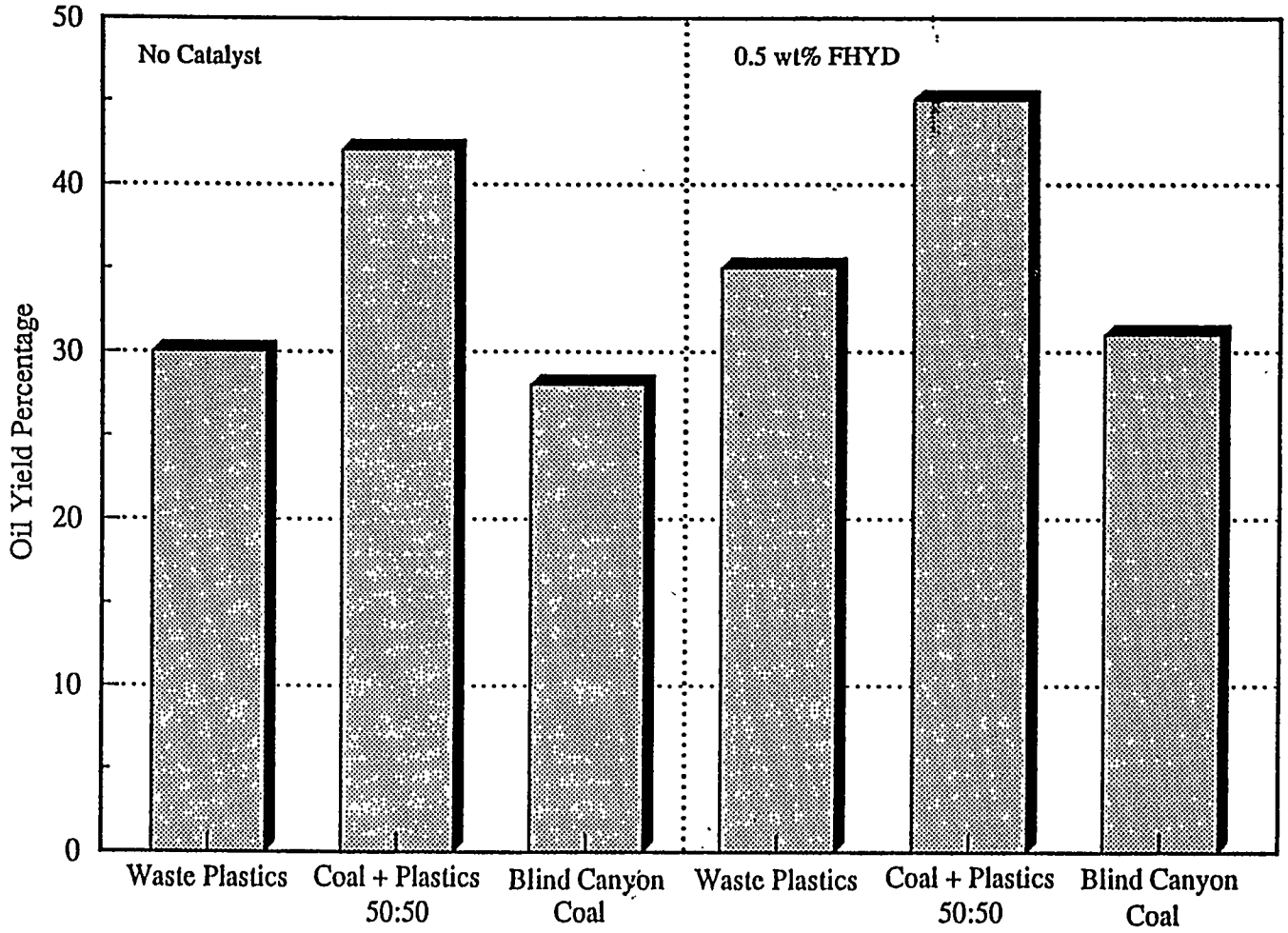

Figure 4. Synergistic effects on oil yields observed in the coliquefaction of bituminous coal and plastics.

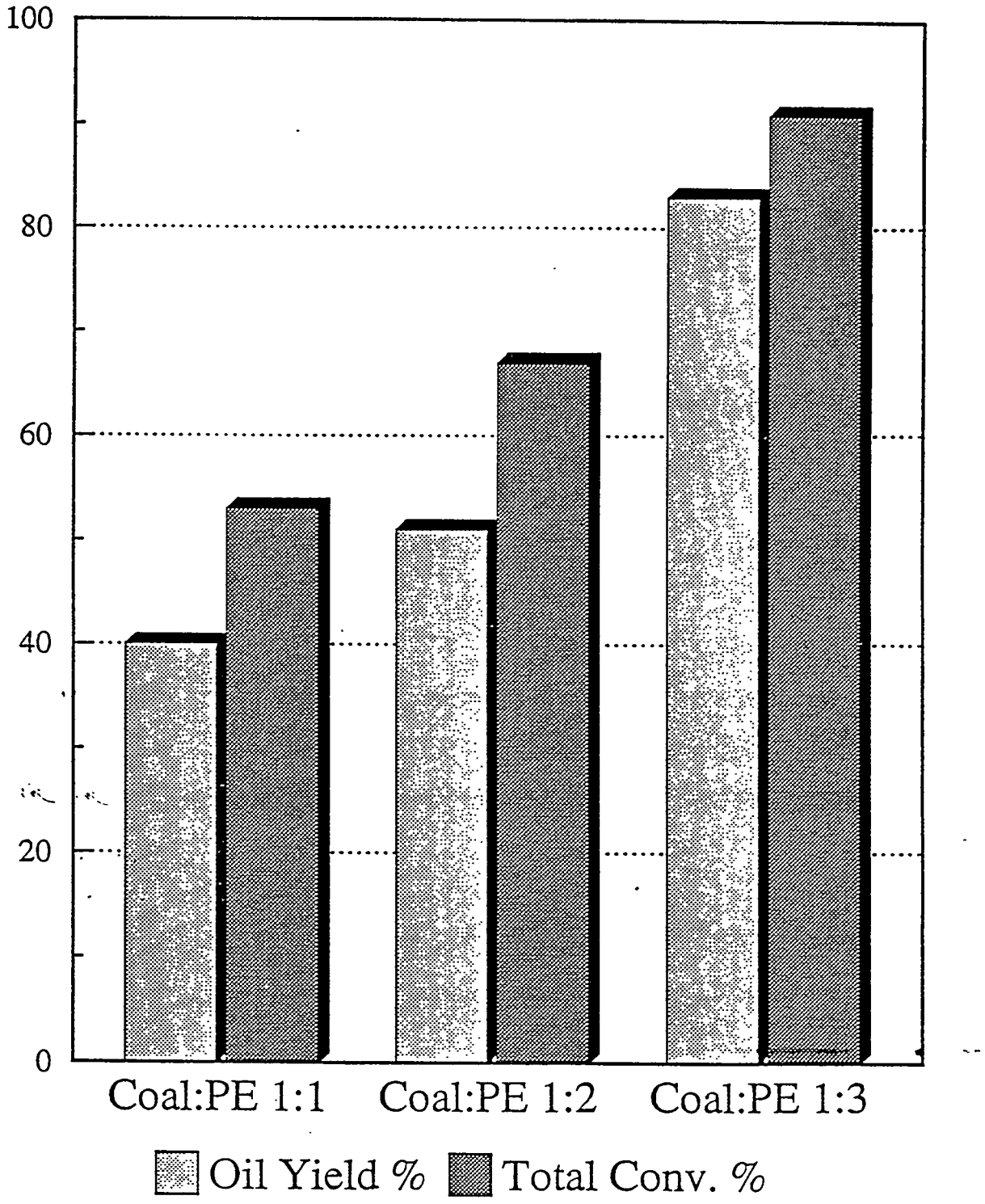

Figure 5. Coliquefaction results for PE and iron ion-exchanged Beulah lignite with no added solvent.

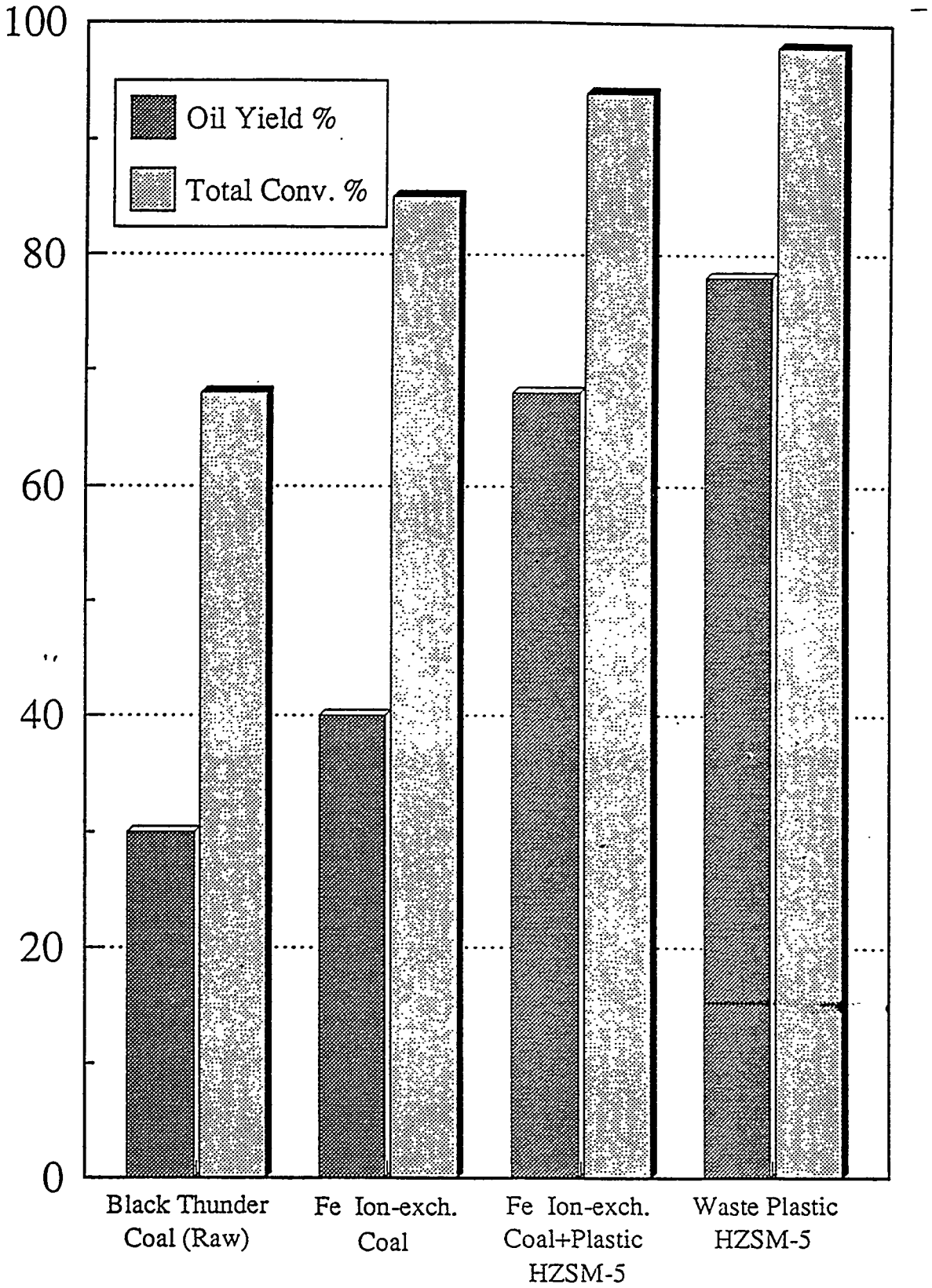

Figure 6. Coliquefaction results for an iron ion-exchanged subbituminous coal and a mixed waste plastic.

TASK I

Project I.8

TECHNICAL AND ECONOMIC EVALUATION OF CO-LIQUEFYING COAL AND WASTE MATERIALS

Mahmoud El-Halwagi
Chemical Engineering Department
Auburn University

1. SUMMARY

Efforts have been undertaken to assess the technical and economic feasibility of co-liquefying coal and waste materials. Most of the work has been dedicated to the co-liquefaction of coal and scrap tires. This assessment is based on incorporating recent experimental data on rubber/coal liquefaction within a conceptual process framework. A preliminary design was developed to co-liquefy 10,000 scrap tires per day with 75 tons per day of coal. The plant products include hydrocarbon gases, naphtha, jet fuel and diesel fuel. Material and energy balances along with plant-wide simulation were conducted for the process. These results were used to undertake a preliminary cost-estimation study. It was found that the annual sales of the process are slightly less than the annual production cost (including depreciation). However, the return on investment for the process is not high enough. The co-liquefaction process has also been compared to other technologies for utilizing scrap tires. It was found that co-liquefaction offers higher gross profit per tire than combustion in power plants and cement kilns. Nonetheless, co-liquefaction entails longer payback periods than the two other technologies. In addition to co-liquefying coal with scrap tires, preliminary work has been conducted to address the problem of co-liquefying coal and scrap plastics. The data on plastic-waste availability, disposal and economics have been compiled. Furthermore, initial research has been conducted to examine the technical and economic performance of a commercial-scale process for co-liquefying coal and plastic wastes.

2. SURVEY OF SCRAP TIRE DISPOSAL AND CONVERSION

A comprehensive survey have been accomplished to review the current status of scrap-tires disposal and conversion. At present, there are serious environmental problems attributed to the annual generation of 244 million scrap tires in the United States. Furthermore,

Approximately two billion scrap tires are currently scattered throughout the nation in landfills, stockpiles or illegal dumps. These tires pose various problems. They provide breeding grounds for mosquitoes. In addition, piles of scrap tires constitute major fire hazards. They also take up valuable land filling space, especially around cities. The foregoing problems have led to several legislations affecting the disposal of scrap tires. Currently, many states have laws mandating the shredding of tires prior to land filling. The costs associated with landfilling scrap tires (whole or shredded) vary throughout the country. These costs range from $0.35/tire in the West Coast to $1.08/tire in the North East of the United States. Many states have now imposed surcharges on the retail prices of new tires to account for future disposal costs. For instance, Florida, Kentucky, Maine, Nebraska, Oklahoma and Oregon require a surcharge of one dollar of its retail cost per tire for disposal. In Arizona, a two percent sales tax is imposed on the retail of tires to be allocated for disposal.

It is worth discussing current disposal and conversion methods employed in tackling scrap tires. As has been mentioned earlier, 244 million scrap tires are generated each year in the United States. Almost 78% of these scrap tires are landfilled, stockpiled or illegally dumped. The current leading technique for utilizing scrap tires is combustion. About 11% of the scrap tires in the United States are burnt primarily in power plants, cement kilns and pulp and paper mills. This method is motivated by the relatively high heat of combustion (~300,00 Btu/tire). At present, two processes employ tire combustion in power plants. The first power plant in the United States to use scrap tires operates in Modesto, California. It burns about five million tires/year and generates 14 MW of power. the second power plant is located in Sterling, Connecticut which burns 11 million tires/year and generates 33 MW of power. Scrap tires can also be burned in cement kilns. At present, seven cement kilns in the United States use 14 million tires/year. This number may potentially grow to 40 kilns burning up to 80 million scrap tires/year. The process of burning scrap tires as a source of fuel in kilns is relatively straightforward. Therefore, it involves low fixed and operating costs. In addition, the iron which exists in the scrap tires is used in cement manufacture. The high operating temperature (2600 °F), the long residence time and the excess oxygen environment minimize the generation of hazardous species such as dioxins and furans.

Another alternative for utilizing scrap tires is the use of crumb rubber as an additive for asphalt. This option is particularly important in light of the "Intermodal Surface Transportation

Efficiency Act" which has been recently passed by the United States Congress. According to this Act, asphalt pavements should contain a minimum percentage of recycled rubber. This percentage is five percent for 1994, 10% for 1995, 15% for 1996 and 20% for 1997. This alternative may use up to 80 million tires/year. States that do not comply with this act may lose part of their federal funding for highways. Asphalt-rubber costs almost twice as much as standard asphalt. In addition, recycle of asphalt-rubber may not be feasible by heating since rubber may catch fire. On the other hand, asphalt-rubber offers longer lifetime than standard asphalt, thereby providing lower cost on a life-cycle basis. Nonetheless, in many states the decision of constructing a new highway is typically based on initial cost rather than life-cycle cost.

An additional option is to gasify rubber under high temperature and pressure into liquid fuels. A commercial-development run by Texaco started operation in December 1992 in Montebello, California. First, the shredded tires are cooked at 700 °F for 30 minutes for melting purposes and then passed through to a gasification reactor. A hydrocarbon mixture is created as the heat breaks the vulcanization bonds formed in the tire manufacturing process. This mixture goes to a reactor for gasification into a syngas. The syngas has relatively low sulfur content due to the low sulfur content of the tires. The gasifier is operated at 2500 °F and 500 - 900 psi. The syngas is used to produce electricity and is less harmful to the environment than a conventional coal-fired power plant. A gas steam is withdrawn and partially condensed to yield gas and a light oil product which can be further processed to yield gasoline, diesel oil and other feed stocks. This plant liquefies 500,000 tires/year.

3. TECHNICAL AND ECONOMIC ASSESSMENT OF CO-LIQUEFYING COAL AND SCRAP TIRES

The problem that has been addressed can be stated as follows:

Given a steady flow of 10,000 scrap tires per day, it is desired to develop a technical and economic evaluation of a process that co-liquefies the scrap tires with an equal mass of coal. The technical assessment has involved material and energy balances along with plant-wide simulation. Material and energy balances for the plant have been conducted. In addition, a plantwide simulation has also been undertaken using the software ASPEN Plus. Optimization of some units/systems has been carried out to minimize capital and operating costs. These technical

results have been used in undertaking an economic feasibility study for the proposed process. The economic assessment of this plant was undertaken. The fixed and working capital investments were found to be $118,461,000 and $139,687,000, respectively. By determining depreciation costs from these investment costs and calculating labor costs, utilities and the cost of raw materials, the total cost of co-liquefaction is $14,669,527/yr. On the other hand, revenue is generated by the annual sales of useful products and by-products to recover $1,769,489. Based on these findings, it was shown that in order for this plant to break even at current prices of $18/bbl of crude oil, an average tipping fee of $2.44/scrap tire must be collected. With this in mind, if this processing plant was looked upon as a waste-management facility for helping the nation with its growing problem of scrap tire disposal while producing useful transportation fuels, then this technology may be deemed feasible. Furthermore, co-liquefaction was compared with existing scrap-tire processing technologies. These technologies include combustion in power plants and cement kilns. It was found that co-liquefying scrap tires with coal provides a gross profit per tire that is higher than combustion. Nonetheless, due to the relatively high investment cost of co-liquefaction, it has a payback period that is much longer than combustion of scrap tires.

4. AVAILABILITY AND DISPOSAL OF PLASTIC WASTES

A comprehensive survey has been initiated to compile data on the disposal and conversion of scrap plastics in the United States. In addition, preliminary work has been undertaken to assess the economic feasibility of a process for co-liquefying coal and scrap plastics. Future plans include the refining of the current work by incorporating any new experimental data on the co-liquefaction of coal and scrap tires. In this context, the current endeavors of the Consortium for Fossil Fuel Liquefaction Science can be instrumental. In addition, a similar approach will be adopted to investigate the feasibility of co-liquefying coal with other polymeric wastes and cellulosic materials.

During the third and fourth quarters, efforts have been made to initiate technical and economic assessment for the co-liquefaction of coal with plastic wastes. The objective has been to provide answers to the following important questions: "what will be the cost per barrel or oil produced via co-liquefaction of coal and waste materials?", "how much total capital investment is needed?", "what are some of the profitability criteria of the process?", "how does a complete cost-benefit analysis for the process look like?", and "how sensitive is the economic evaluation of the process

to potential variations in feed characteristics and operating conditions".

The following activities have been undertaken:

1. Developed a comprehensive survey on the generation and fate of plastic wastes in the United States. Data on characterization, current utilization technologies and disposal costs have also been compiled. Postconsumer plastic wastes generated annually in the U.S. are estimated to be 14 million tons, or 80 million m^3 per year. These amounts make up about 8% by weight and 20% by volume of the 180 million tons of municipal solid waste generated annually in the United States. At present, less than 1% of the plastic wastes are being reclaimed/reutilized. In the context of economic data, there is a major discrepancy in cost information. Various conflicting data are reported for the collection, sorting, landfilling and recycle of plastic wastes. We have attempted to verify these data based on contacts with a variety of sources. In addition, a complete analysis of a material recovery facility has been accomplished. The results of this analysis will be used to assess the cost of employing plastic waste in a co-liquefaction plant.

2. Developed a conceptual process for co-liquefying coal and plastic waste. A preliminary technical assessment of the process has also been undertaken. In this regard, experimental data from other Consortium members have been included. Over the next few months, additional results obtained by the CFFLS groups will be efficiently assessed and integrated into the plant design so as to maximize the economic potential of the process. The proposed research will also be instrumental in identifying process variables wit the highest economic impact and, thus, suggest additional research to be done by CFFLS teams in an attempt to reduce the cost involved with these cost-dominant aspects of the process.

5. PUBLICATIONS RESULTING FROM THIS PROJECT

To date, this project has resulted in one paper and two technical presentations:

Warren, E. A. and M. M. El-Halwagi, "Technical and Economic Assessment of a New Process for Co-Liquefying Coal and Scrap Tires", Proceedings of Coal Liquefaction and Gas Conversion-Contractors Review Conference, Vol. 1, 45-69 (1994).

Warren, A. and M. M. El-Halwagi, "Conceptual Design of a New Precess for Co-Liquefying Coal and Scrap Tires", AIChE Annual Meeting, St. Louis, Nov. 7-12, 1993.

Warren, A. and M. M. El-Halwagi, "Technical and Economic Assessment of the Co-liquefaction of Coal and Scrap Tires", CFFLS Annual Meeting, Callaway, GA, July, 1993.

TASK I

Project I.9

COLIQUEFACTION OF COAL AND PLASTICS TO LIQUID FUELS

Larry L. Anderson and Wisanu Tuntawiroon
University of Utah

Disposing of waste is one of the country's major economical and environmental problems. Waste contains substantial amount of plastics and polymers. These materials are cleared away mainly by disposal in landfills. While our landfills are overflowing, there is also a great resistance in most communities to starting new landfills because of possible water supply contamination by toxic substances leaching from the landfills. Although recycling is possible for only some types of plastics, it is not economical to produce material that is inferior to the original. Only about 3 to 4 percent of all plastics are now recycled, primarily in the states where such recycling is enforced by law.[1] Liquefaction of coal with waste polymer (coliquefaction) would have the beneficial effect of utilizing hydrogen from plastic waste. The relationships of product yield to reaction variables (temperature, time, catalyst and the plastic to coal ratio) were investigated by a series of laboratory coliquefaction experiments.

The commingled plastic used was obtained from a recycling center in Utah in the form of detergent or soft-drink bottles. The samples then were washed to remove labels. The plastic was ground to -8 +25 mesh by a kitchen mill before analysis and use in coliquefaction experiments. A second batch of commingled plastic was also obtain from Oregon through the American Plastics Council. Analytical data are included in Tables I.9.1, I.9.2 and I.9.3. Polyethylene and polystyrene were acquired from Aldrich Chemical Co. Samples of -100 mesh DECS6 Blind Canyon Coals were obtained from the Penn State Coal Bank and stored at 0°C until experiment. The mixture of coal and polymer waste was shaken in an ultrasonic bath for about 1 hour before being put into a tubing reactor. It was then pressurized by hydrogen gas to 1000 psig. Samples were then reacted in a shaken tubing reactor at 160 rpm in a fluidized sand bath for various lengths of time.

The first set of experiments done last year was involved the use of polyethylene, polystyrene and polymer waste. These experiments were run in order to determine the effect of temperature and the ratio of coal and polymer on the coal liquefaction yields. Analyses of product liquids on the basic of their solubility (in THF and cyclohexane) show that co-liquefaction does produce increased yields of liquids. Experiments were complete to determine the effect of various parameters on the composition of liquids obtained by coliquefaction of commingled plastics and DEC-6 coal. From Figures I.9.1 - I.9.5, the maximum oil product from coliquefaction of commingled plastic with DECS-6 coal was obtained at 450 °C and 30 min.

A separation method is established for identification of organic compounds in coliquefaction product. All samples were extracted with cyclohexane (Oils Yield) and were characterized by simulated distillation (ASTM D-2887-84).

Table I.9.1

Ultimate analysis of High-density Poly Ethylene Polymer Wastes.

Elemental Analysis

	DECS-6	*DECS-17*	*Plastic1*	*Plastic2*
Carbon	81.72	82.05	8634	84.65
Nitrogen	1.56	1.39	0.05	0.65
Hydrogen	6.22	6.18	14.04	13.71
Oxygen	10.10	9.94	ND	0.98
Sulfur	0.44	0.44	0.22	0.01

Table I.9.2

Proximate Analysis of High-density Poly Ethylene Polymer Wastes.

Proximate Analysis

	DECS-6	*DECS-17*	*Plastic 1*	*Plastic 2*
Fixed Carbon	47.31	44.93	0.45	0.74
Volatile Matter	42.40	45.00	97.69	98.80
Ash	5.56	6.32	1.81	0.45
Moisture	4.73	3.74	0.06	0.01

Table I.9.3

Trace Elemental Analysis (ICP)of Polymer Wastes and Coal

Metal	DECS-6	DECS-17	Plastic1
Cr	6.0	6.0	0.77
Cd	*	*	0.19
Cu	<2.0	9.0	*
Pb	*	*	3.21
Ni	*	*	3.21
Zn	4.0	3.0	*

Figure I.9.1. Coliquefaction of DECS-6 Coal and Comingled Plastic at 350 °C

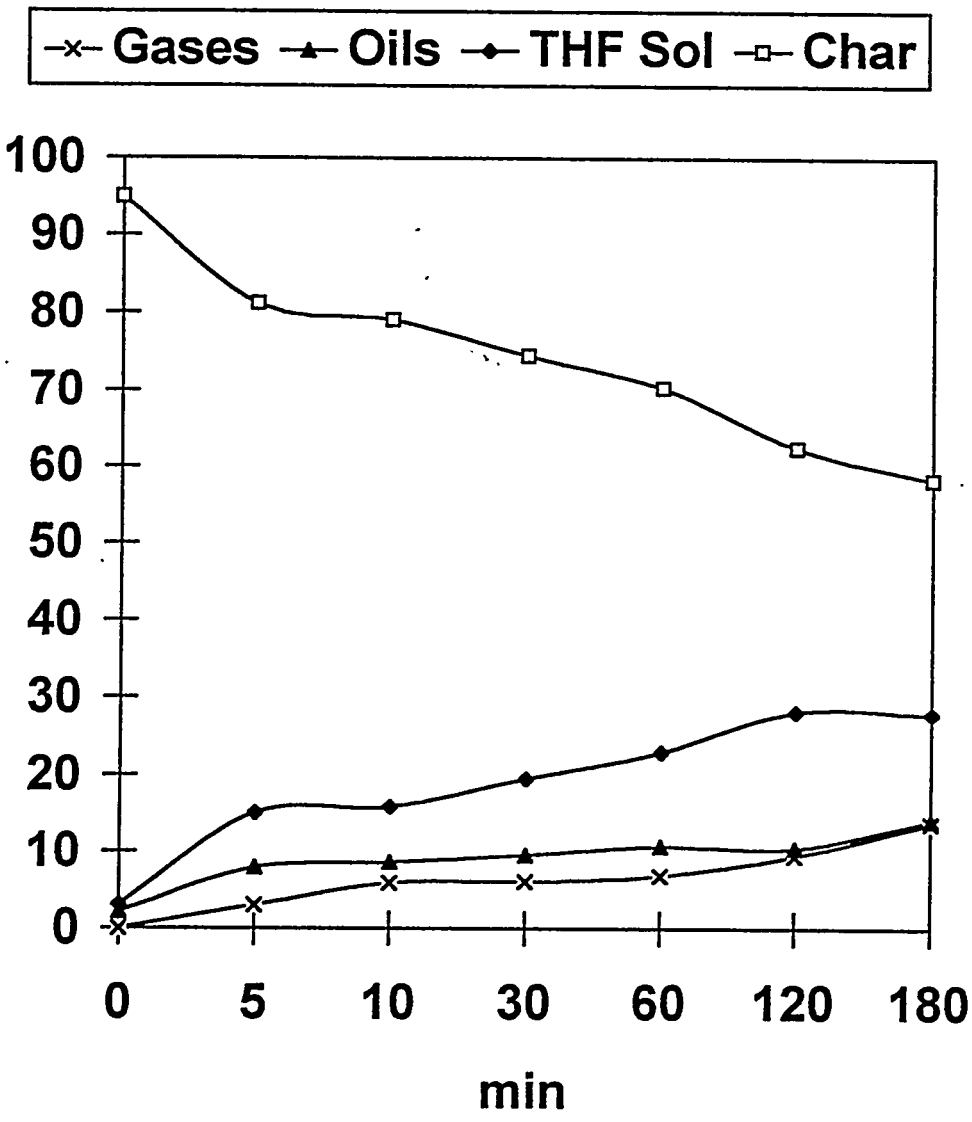

Figure I.9.2. Coliquefaction of DECS-6 Coal and Comingled Plastic at 400 °C

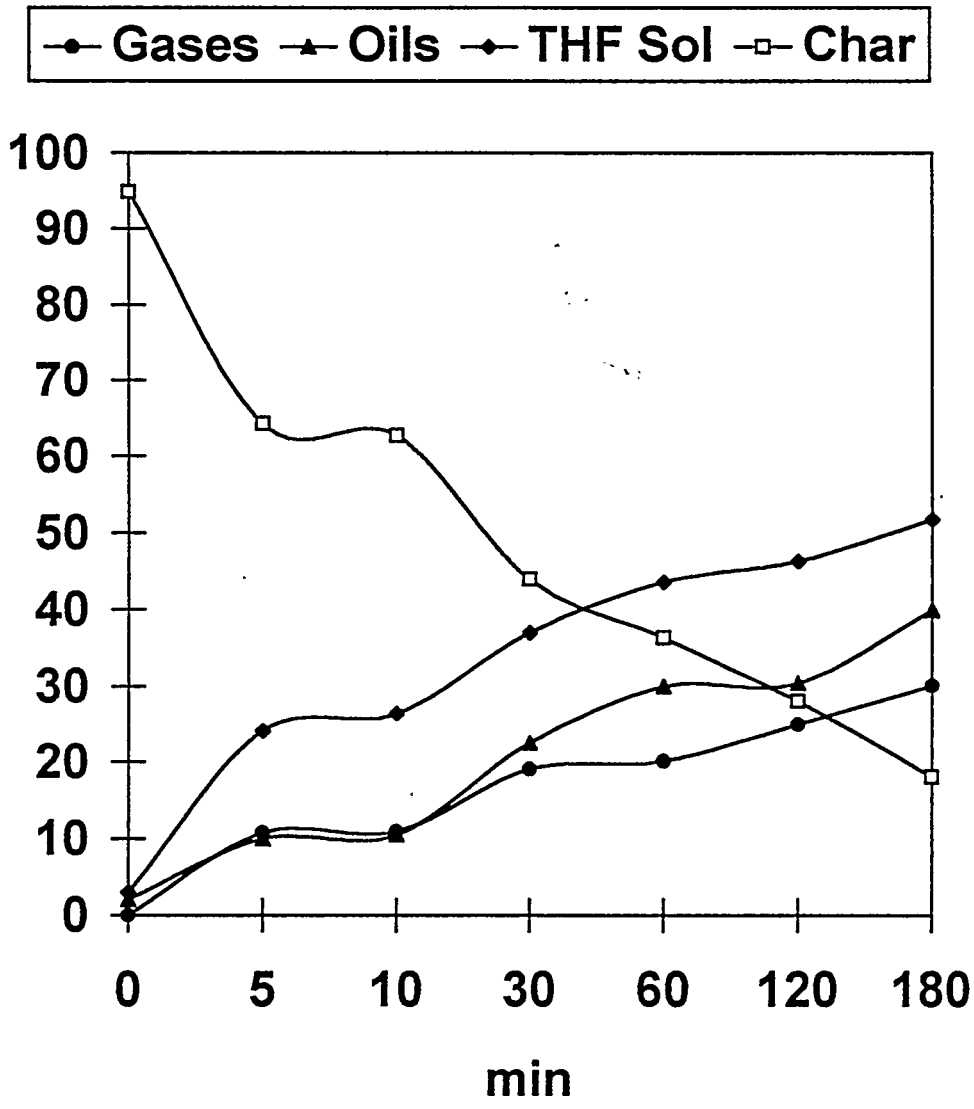

Figure I.9.3. Coliquefaction of DECS-6 Coal and Comingled Plastic at 450 °C

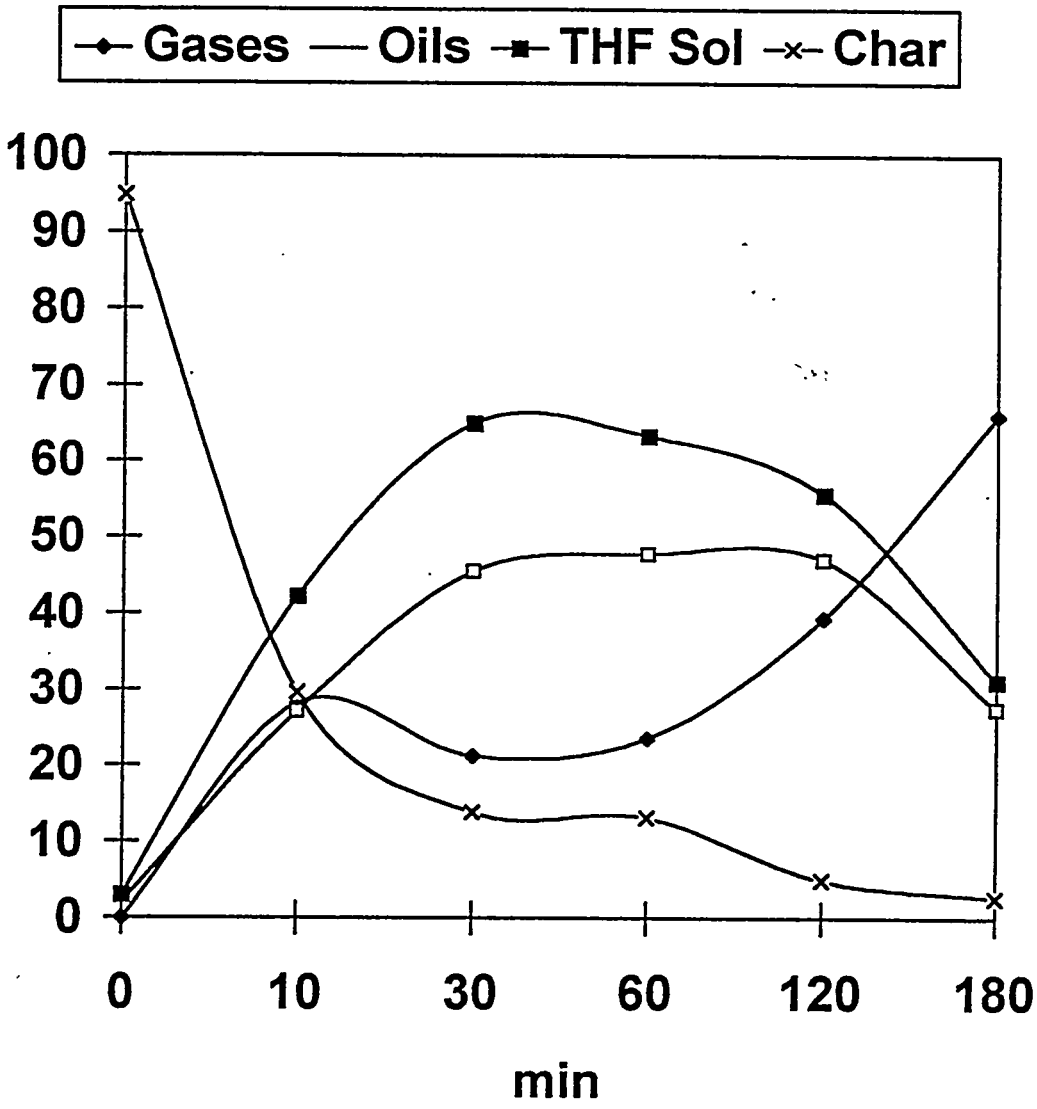

Figure I.9.4 Hydroliquefaction of DECS-6 Coal at 400 °C

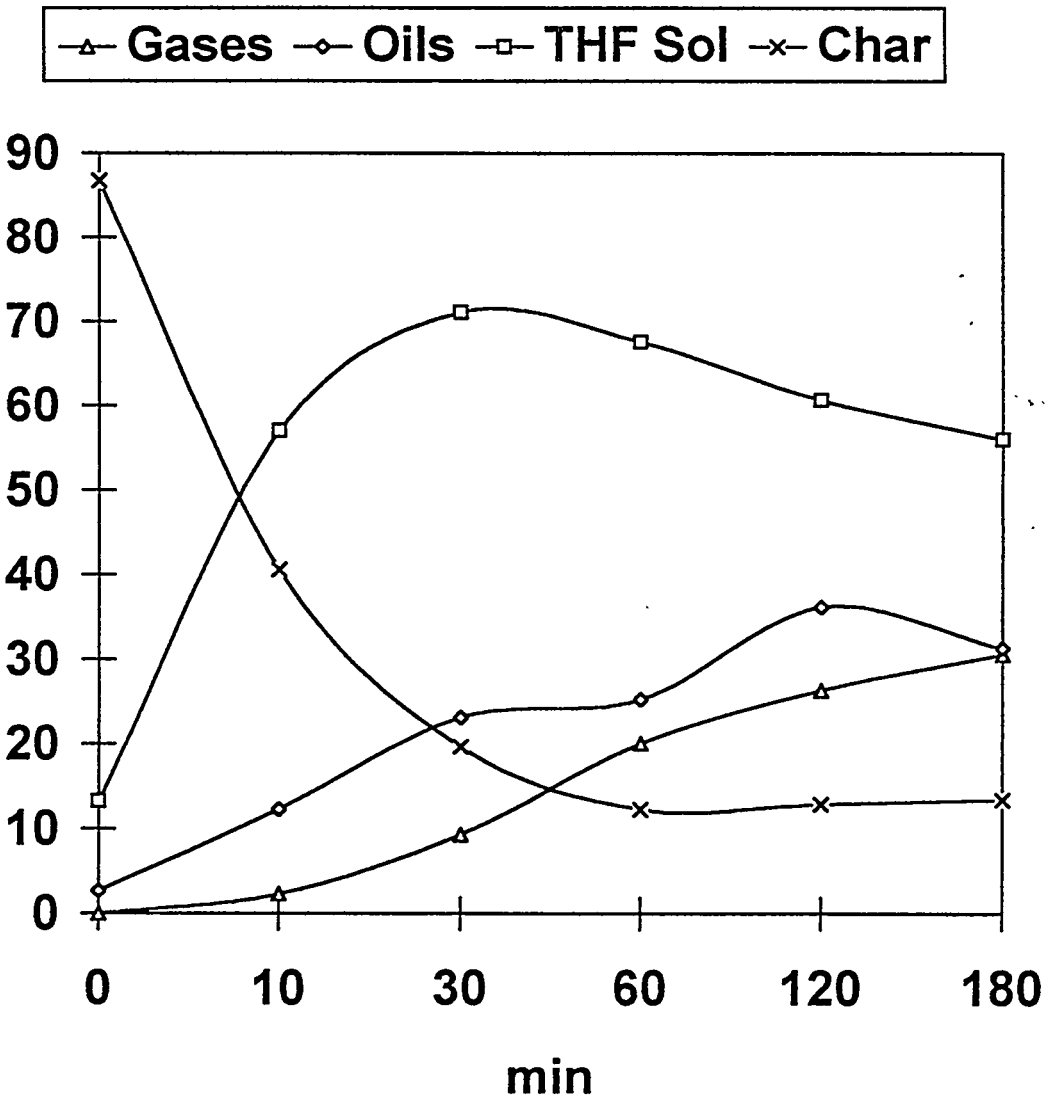

Figure I.9.5 Hydroliquefaction of Comingled Plastic at 400 °C

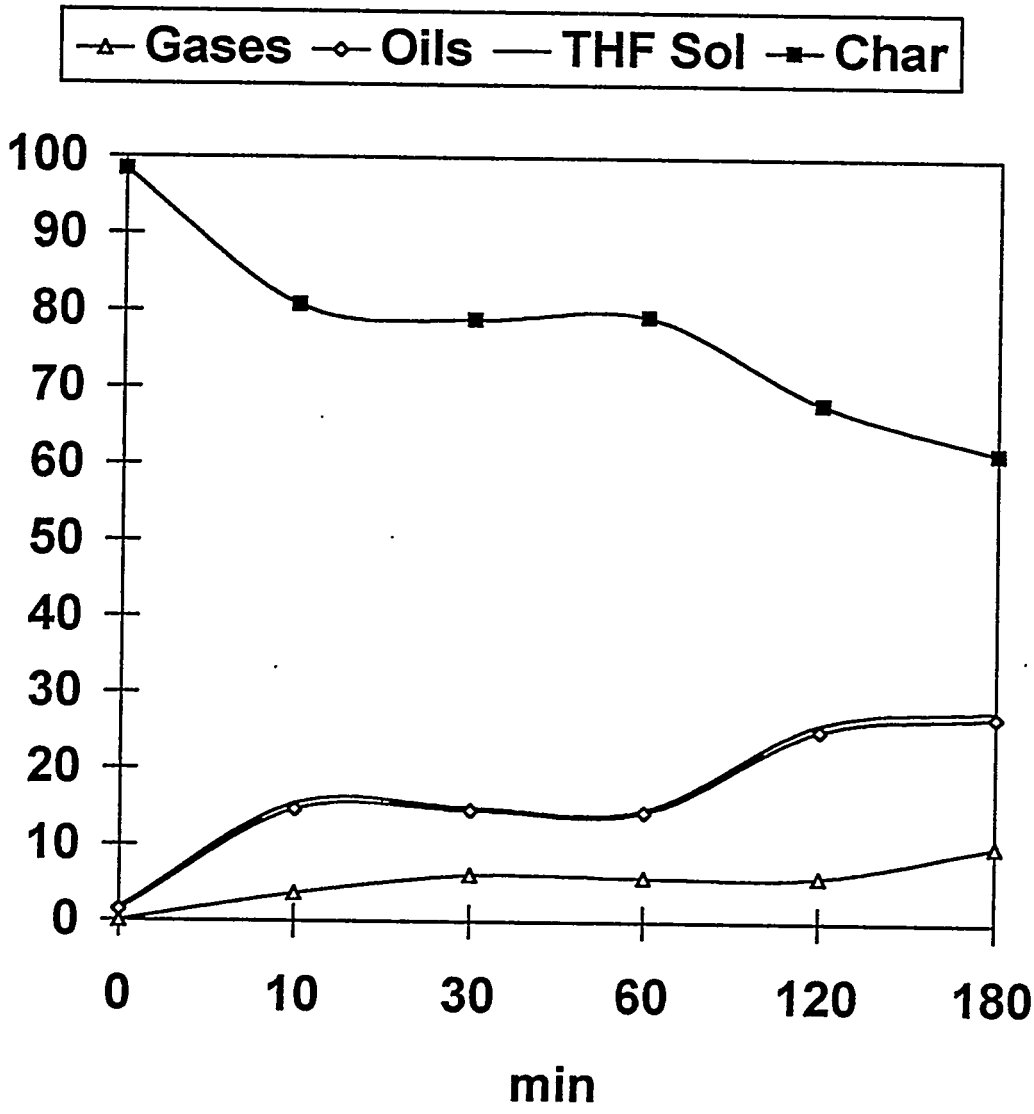

TASK II

CATALYSTS FOR COAL LIQUEFACTION TO CLEAN TRANSPORTATION FUELS

Coordinators: James Guin and Larry Anderson

TASK II

Project II.1

CATALYSTS FOR COAL LIQUEFACTION TO CLEAN TRANSPORTATION FUELS HYDROLIQUEFACTION OF COAL TO CLEAN TRANSPORTATION FUELS

Larry L. Anderson, W. H. Yuen
University of Utah

Tubing reactors were used to carry out catalytic hydroliquefaction of coals. To avoid the interference of external solvent on liquid yield and quality, vehicle solvent was not used. Water soluble compounds of iron, cobalt, nickel, tungsten, and molybdenum were used as coal hydrogenation catalysts. Blind Canyon coal (high volatile bituminous A coal) and Wyodak coal (subbituminous C coal) from the Pennsylvania State University Coal Sample Bank were used for catalyst effectiveness comparisons. Argonne Premium coal samples were used to study the influence of coal rank on conversion. In this research all reactions were operated in the following ranges: 500~3000 psi, 380~450 °C, and 15~90 min. Most of the reactions were operated at 2000 psi, 400 °C and 60 min for catalyst comparisons.

Among the tested iron catalyst precursors, ammonium iron (III) sulfate dodecahydrate gave the best coal conversions. When it was used with Blind Canyon coal, the impregnation of 0.56 wt% [Fe] on coal could yield 62 wt% coal liquids (tetrahydrofuran soluble) with 41 wt% oil (cyclohexane soluble). When Wyodak coal (PSOC-1520) was used under the same conditions, the impregnation of 0.56 wt% [Fe] on coal yielded 48 wt% coal liquids with 40 wt% oil (cyclohexane soluble).

Cobalt (II) nitrate hexahydrate was found to be better than cobalt (II) sulfate. Nickel (II) nitrate hexahydrate gave better coal liquid yield than other tested nickel precursors. The impregnation of 0.59 wt% [Ni] on coal resulted in 79 wt% coal liquids with 42 wt% oil. Oil yields from three tested nickel precursors were similar. Ammonium tetrathiomolybdate was an effective catalyst even at low concentration; the impregnation of 0.05 wt% [Mo] on DECS-17 coal gave a yield of 75 wt% coal liquids with 40 wt% oil. Ammonium tetrathiotungstate and tungstic acid were also tested, but they were found to be poor in improving the coal conversion.

GC and TG/MS were used to determine oil quality. Results from GC analyses showed that oils from catalytic hydroliquefaction of DECS-17 coal had a boiling range of 200 to 500 °C. By TG/MS analysis, the average molecular weight of the total liquids (tetrahydrofuran soluble) was found to be 280 g/mole, the average molecular weight of the oils was found to be 206 g/mole.

Besides the research results mentioned above, studies in liquid quality, liquid yield, effect of catalyst, and influence of reaction condition (temperature, pressure, and time) on coal conversion were also made. It was found that for Fe, Co, and Ni catalyzed hydroliquefaction of Blind Canyon coal (0.0001 mol [Metal]/g maf coal), the quality of obtained oils were in the following order: Fe > Ni > Co (by both GC and TG analyses), and the order of oil yields were: Ni >Fe > Co. Oils obtained from nickel or iron catalyzed reactions were lighter than oils from Mo catalyzed reactions.

INTRODUCTION

In this research, water soluble iron catalyst precursors were applied by incipient wetness impregnation to insure good dispersion of catalysts in coal particles. Besides iron catalysts, compounds of cobalt, nickel, molybdenum, and tungsten were also tested.

Tubing reactors were used to conduct catalytic coal hydroliquefaction. A fluidized sand bath was used to supply heat and to control the reaction temperature. The use of vehicle solvent was avoided, so interference by an external solvent on coal liquid yield and quality was avoided.

Blind Canyon coal samples (DECS-6 and DECS-17, high volatile bituminous A coal) and Wyodak coals (PSOC-1520, subbituminous C coal) were obtained from the Pennsylvania State University Coal Sample Bank and were used as the feed coals for catalyst effectiveness research and coal hydroliquefaction kinetic studies. Eight coal samples from the Argonne Premium Coal Sample Bank were used to study the influence of coal rank on coal conversion.

Mixtures of solid and coal liquid products were extracted by Soxhlett extraction. Coal liquid products from Soxhlett extraction were collected, and both quantitative results (liquid yield) and qualitative results (average molecular weight from TG/MS and simulated distillation curves from GC) were obtained. Studies were done in the following areas:[12,13,14]

1. Effects of different catalyst precursor of Fe, Co, Ni, Mo, and W on coal conversion and on the yields of coal liquids, gas, asphaltol, asphaltene, and oil.

2. Effects of an iron catalyst (ammonium iron (III) sulfate dodecahydrate as precursor) on the conversion of eight different Argonne premium coals.
3. Effects of catalyst concentration on hydroliquefaction yields.
4. Effects of reaction temperature, pressure, and time on coal conversion during catalytic hydroliquefaction.
5. Characterization of coal derived oil by GC simulated distillation.
6. Characterization of coal derived oil by TG/MS.
7. Kinetic studies for dry catalytic hydroliquefaction of Blind Canyon coal using ammonium iron (III) sulfate dodecahydrate as catalyst precursor.

EXPERIMENTAL

In this research, the hydropyrolysis reaction was usually controlled at 2000 psi, 400 °C. Incipient wetness impregnation was used to add the water soluble catalyst precursors to the coal samples.

First, a catalyst precursor was dissolved in de-ionized water. For Blind Canyon coal, (DECS-6 and DECS-17) the amount of water required was 50 wt.% of the coal sample (as received); and for Wyodak coal (PSOC-1520), the water required was 36 wt.% of the coal sample (as received). The aqueous solution of the dissolved catalyst precursor was then added to the coal sample and vacuum dried under -60 kPa at 60 °C overnight. After the coal sample was dried, it was ready to be used as the feed for coal hydroliquefaction experiments.

After the coal sample had been transferred into the tubing reactor, the reactor was then sealed. The gas inlet valve was then opened and the reactor purged with hydrogen to expel the air from the reactor. The reactor was then pressurized with hydrogen to 1100 psi at room temperature (at 400 °C the reaction pressure was 2000 psi). As soon as the hydrogen pressure reached the required value, the gas inlet valve was closed.

The reactor was then attached to a shaking mechanism and immersed into a sand bath at the desired reaction temperature (usually at 400 °C). Reactions were usually conducted for 1 h with shaking at 160 cycles/min.

After reaction, the reactor was taken out of the sand bath and quenched in air. The mixture of liquid and solid products were taken out of the reactor. The weight of gas product was

obtained by difference (between the feed coal and the mixture of liquid and solid products), which was used to calculate the gas yield.

The mixture from the reactor was then extracted with THF for 72 h. After extraction, both the soluble (coal liquid) portion and insoluble (residue) portion were vacuum dried (at 104 °C, 60 kPa). The weight of THF soluble was obtained by difference (between the weight of feed coal and the sum weight of gas and THF insoluble), which was used to calculate the yield of coal liquids.

The dried THF soluble portion was extracted with toluene for 24 h. Both the toluene soluble (asphaltene plus oil) and toluene insoluble (asphaltol or preasphaltene) were dried under vacuum (at 120 °C, 60 kPa). The weight of toluene insoluble was used to calculate the yield of asphaltol.

The vacuum dried toluene soluble portion of the products was extracted by cyclohexane for 24 h. Both the cyclohexane insoluble (asphaltene) and the soluble portions (oil) were dried under vacuum (at 104 °C, 60 kPa). The cyclohexane soluble portion was analyzed by GC and TG.

Coal conversion values were calculated by the following equations:

Gas Yield (% maf coal)= G =100 (B C) / A

Liquid Yield (% maf coal) = H =100% (C D)/A

Asphaltol Yield (% maf coal) = I= 100 E /A

Asphaltene Yield (% maf coal) = J= 100 F /A

Oil Yield (% maf coal) = H I J

Total Conversion (% maf coal) = G + H

where:

A = maf coal feed (g)

B = weight of coal and impregnated catalyst after vacuum drying (g)

C = solid & liquid mixture after reaction (g)

D = weight of char or THF insoluble (g)

E = weight of asphaltol or toluene insoluble (g)

F = weight of asphaltene or cyclohexane insoluble (g)

RESULTS

Some important findings of this research are listed below:

1. Ammonium iron(III) sulfate dodecahydrate was found to be effective in increasing the liquid yields for catalytic hydroliquefaction of lignite (Beulah-Zap coal), subbituminous coal (Wyodak coal), and some high volatile bituminous coals (Blind Canyon coal, and Lewiston-Stockton coal). All of these coals were low in sulfur content (0.6 - 0.8 %).
2. For high volatile bituminous coals with high sulfur contents, such as Illinois #6 (S% = 4.8) and Pittsburgh #8 (S% = 2.2), the impregnation of ammonium iron(III) sulfate dodecahydrate did not significantly change the coal conversion. The hydroliquefaction of these coals gave high liquid yields even if catalysts were not added.
3. By simulated distillation using GC, coal liquids from iron or nickel catalyzed hydroliquefaction of Blind Canyon coal (400 °C, 2000 psi, for 1 h) were found to be lighter than liquids from cobalt or molybdenum catalyzed hydroliquefaction.
4. By GC and TG analyses, the oil from Blind Canyon coal was found to be lighter than the oil from Wyodak coal.
5. Oils from Blind Canyon coal hydroliquefaction have a boiling point range from 200 to 500 °C (by GC simulated distillation analysis).
6. When reaction temperatures were increased (from 380 to 450 °C), both gas yield and coal conversion increased. Liquid yield normally increased at higher reaction temperatures in the range of 380 - 430 °C. At longer reaction times (90 min) liquid yields decreased due to gas production.
7. Total coal conversion and liquid yield was promoted by increasing hydrogen pressure. The gas yield was not distinctly influenced by increasing the hydrogen pressure from 500 psi to 3000 psi.
8. In this research ammonium iron(III) sulfate dodecahydrate was found to be more effective than iron(III) sulfate pentahydrate. This might due to the fact that ammonium iron(III) sulfate has more Bronsted acid sites in its active catalytic form.

$$NH_4Fe(SO_4)_2 \cdot 12H_2O \quad HFe(SO_4)_2 + NH_4OH + 11H_2O$$

Where the site on iron atom in $HFe(SO_4)_2$ by donating a proton away could be a Bronsted Acid Site, and the vacant space generated by removing water and ammonium from $NH_4Fe(SO_4)_2 \cdot 12H_2O$ could be Lewis Acid sites (electron pair acceptors).

9. The reactions in iron catalyzed coal hydrogenation is suggested as a six-step sequence, in which the surface reaction between hydrogen and free radicals (from larger coal units) on catalyst sites is considered the most important stage for production of liquids. The recombination of free radicals from larger coal units is considered as a competing reaction.

(1). Rij Ri + Rj (thermal cracking)

(2). $H_2 + X \quad H_2X$ (adsorption of H_2 on catalyst sites)

(3). $Ri + H_2X \quad H_2XRi$ (surface reaction)

(4). $H_2XRi \quad RiH + HX$ (dissociation)

(5). Ri + Rj Rij (recombination)

(6). Rj + HX RjH + X (termination)

Where

Rij = unreacted coal particles or larger coal units.

RiH or RjH = product of hydroliquefaction (smaller coal units or coal liquids).

Ri or Rj = free radicals produced by thermal cleavage of C-C bonds in coal.

H_2 = hydrogen molecules.

X = hydrogen adsorption sites of catalyst.

H_2X = hydrogenated sites.

H_2XRi = reaction intermediate produced by reaction of Ri and H_2 on X.

HX = half dehydrogenated sites.

In this six-step reaction sequence step 3 (surface reaction) and step 5 (recombination) are competing reactions. When the amount of effective catalytic sites are low, then less reactions by step 3 occur. That means more recombination reactions (step 5) and lower liquid

yield. The smaller units (RiH and RjH) produced from these steps may repeat the reaction from step 1 again and reduce their molecular size again.

CONCLUSIONS

Based on present research results, the following conclusions are obtained:

1. Longer reaction times for coal hydrogenation means more thermal decomposition; the amount of light hydrocarbon gases and char production will increase at longer reaction times.
2. The iron catalyzed hydroliquefaction of Blind Canyon coal (15 to 90 min) was first order with respect to the unliquefied coal, and the global activation energy is 9 to 12 kcal/mol.
3. A six-step reaction sequence presents the general reactions taking place in hydroliquefaction. The surface reaction between hydrogen and free radicals (from larger coal units) on catalyst sites is important for liquid production. Recombination reactions of free radicals from larger coal units are considered as competing reactions to the reactions which produce liquid or gaseous products.

Table I.9.1: Coal Conversions for Iron Catalyzed Coal Hydroliquefaction

Ammonium iron(III) sulfate dodécahydrate as precursor
Blind Canyon Coal (DECS-17, -60 mesh, 2000 psi)
x = coal conversions

T (K)	1/T (1/K)	x at 15 min	x at 30 min	x at 60 min	x at 90 min
653	0.00153	0.530	0.614	0.713	0.766
673	0.00149	0.619	0.717	0.801	0.842
703	0.00142	0.721	0.806	0.878	0.918
723	0.00138	0.788	0.860	0.921	0.952

Table I.9.2: The Relation Between -Ln(1-x) and t for Iron Catalyzed Coal Hydroliquefaction

Ammonium iron(III) sulfate dodecahydrate as catalyst precursor.
Blind Canyon Coal (DECS-17, -60 mesh, 2000 psi)
x = coal conversions

Time (second)	-Ln(1-x) at 653 K	-Ln(1-x) at 673 K	-Ln(1-x) at 703 K	-Ln(1-x) at 723 K
900	0.755	0.965	1.277	1.551
1800	0.952	1.262	1.640	1.966
3600	1.248	1.614	2.104	2.538
5400	1.452	1.845	2.501	3.037

Table I.9.3: The Relation Between -Ln(k) and 1/T for Iron Catalyzed Coal Hydroliquefaction

Ammonium iron(III) sulfate dodecahydrate as catalyst precursor.
Blind Canyon Coal (DECS-17, -60 mesh, 2000 psi)
x = coal conversions
k = rate constant = -Ln(1-x)/time

T (K)	1/T (1/K)	Ln(k) at 900 s	Ln(k) at 1800 s	Ln(k) at 3600 s	Ln(k) at 5400 s
653	0.00153	-7.083	-7.545	-7.967	-8.221
673	0.00149	-6.838	-7.263	-7.710	-7.982
703	0.00142	-6.558	-7.000	-7.445	-7.677
723	0.00138	-6.363	-6.819	-7.257	-7.483

Plot of Ln(k) vs. 1/T for Iron Catalyzed
Coal Hydroliquefaction

Ammonium iron(III) sulfate dodecahydrate as catalyst precursor.

Blind Canyon Coal (DECS-17, -60 mesh, 2000 psi)

k = rate constant = -Ln(1-x)/time

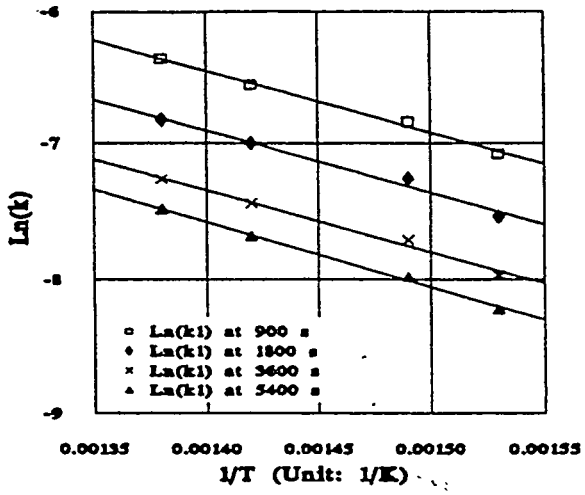

15 min: y = 0.06584 - 4656.93431x r^2 = 0.99435
30 min: y = -0.45350 - 4605.83942x r^2 = 0.98351
60 min: y = -0.93599 - 4576.64234x r^2 = 0.98916
90 min: y = -0.89051 - 4817.51825x r^2 = 0.99610

Hydroliquefaction of Argonne Premium Coals

Ammonium iron(III) sulphate dodecahydrate on Argonne Coals

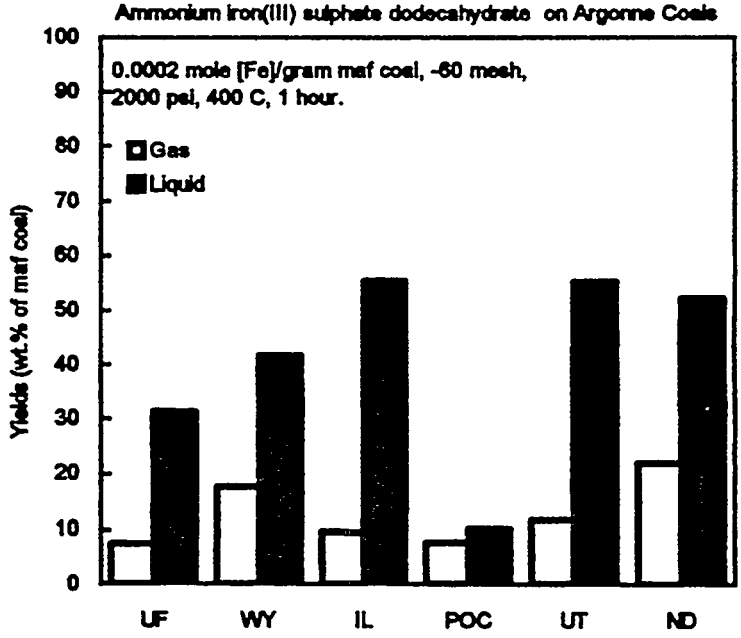

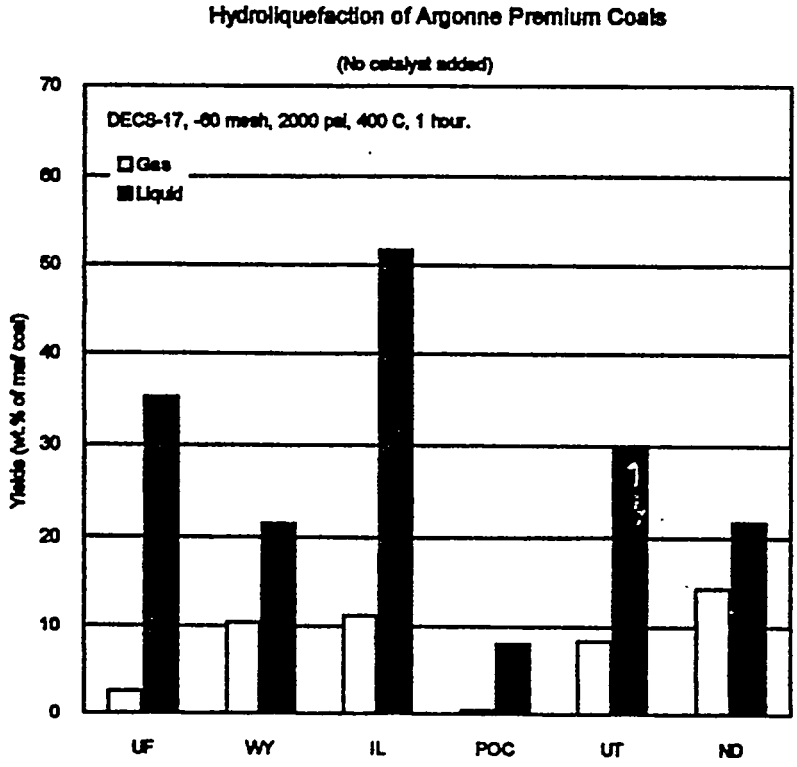
Hydroliquefaction of Argonne Premium Coals
(No catalyst added)
DECS-17, -60 mesh, 2000 psi, 400 C, 1 hour.
Gas
Liquid
Yields (wt.% of maf coal)
70
60
50
40
30
20
10
0
UF
WY
IL
POC
UT
ND

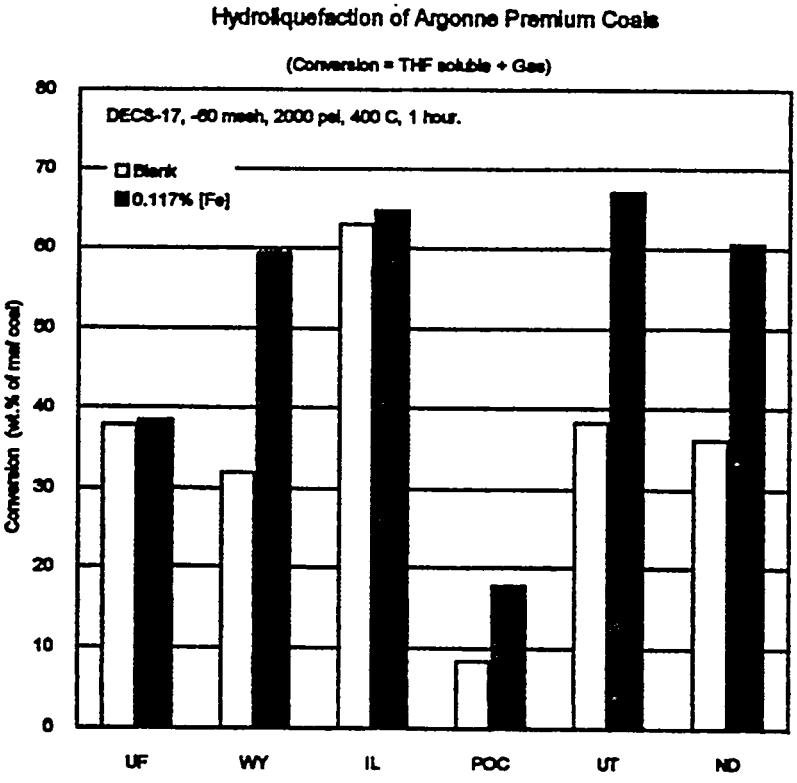
Hydroliquefaction of Argonne Premium Coals
(Conversion = THF soluble + Gas)
DECS-17, -60 mesh, 2000 psi, 400 C, 1 hour.
Blank
0.117% [Fe]
Conversion (wt.% of maf coal)
80
70
60
50
40
30
20
10
0
UF
WY
IL
POC
UT
ND

TASK II

Project II.2

HIGHLY DISPERSED BIMETALLIC CATALYSTS FOR DIRECT COAL LIQUEFACTION AND COPROCESSING

Irving Wender, John W. Tierney and Gerald D. Holder
University of Pittsburgh

Introduction

The activity of highly dispersed, anion-modified metal oxide catalysts for reactions of direct coal liquefaction and coal-heavy oil coprocessing at temperatures as high as 400°C and initial hydrogen pressures up to 1000 psig have been reported by us previously[1,2]. Their high activity at the conditions employed for coal liquefaction was explained on the basis of their transformation (in the presence of sulfur) to non-stoichiometric pyrrhotites ($Fe_{1-x}S$), which could be a precursor to the active form of the catalyst[3]. Certain anion-modified iron oxides (such as $Mo/Fe_2O_3/SO_4$) are bifunctional[3]; i.e., they possess a strong acidic component[4] along with a hydrogenation metal function. At the severe conditions employed in coal liquefaction and coprocessing, the SO_4^{2-} group on these catalysts decomposes, so that the catalyst loses its acidity. It was of interest to attempt to discover whether the acidity of these catalysts played a part in reactions at mild conditions, such as those during the heatup periods involved in direct coal liquefaction. Since the products of coal liquefaction are so chemically diverse and numerous, model compounds representing possible coal structural units were employed in acid-catalyzed reactions over these strongly acidic, bifunctional anion-modified metal oxides at conditions expected during the heatup part of the liquefaction reaction.

Results and Conclusions

The model compounds employed for our reaction studies include: long-chain alkylaromatics such as 1-phenyldecane and p-dodecylphenol, polynuclear aromatics such as 1-methylnaphthalene, bibenzyl, anthracene and heteronuclear polyaromatics such as benzyl phenyl ether. Experiments with a low-sulfur DECS-17 (Blind Canyon) coal were also carried out over the sulfated iron oxide catalysts. The sulfated iron oxides (with and without promoters such as Mo) and sulfated Fe-Sn oxides ($SnO_2/Fe_2O_3/SO_4$) were the catalysts mainly used in our reaction

experiments.

All reactions were carried out in a 27 cc stainless steel microautoclave reactor (tubing bomb) which is horizontally shaken while being immersed in a fluidized sand bath which is at the reaction temperature. Model compound reactions were conducted at 200°C and 500 psig (cold) H_2 pressure and reaction time was 60 min in all cases. The products obtained were identified by a GC-MS and were later quantified by a GC.

Results and Discussion

Reactions of 1-phenyldecane were carried out primarily with $Mo/Fe_2O_3/SO_4$ and $Pt/ZrO_2/SO_4$ catalysts. As expected, cracking of the C_{10} side chain occurs to form lower molecular weight paraffins. But we observed significant amounts of highly substituted alkylated benzenes among the products. These products were predominant when the $Pt/ZrO_2/SO_4$ catalyst, which is a stronger superacid than $Mo/Fe_2O_3/SO_4$, was used. Significant amounts of saturated compounds such as cyclohexanes were also observed. These are probably due to the presence of a hydrogenation metal function on the catalyst. The same reactions carried out with p-dodecylphenol yielded higher conversions and higher selectivities to alkylated phenols than with 1-phenyldecane. This may be due to the activating effect of the OH group on the aromatic ring which increases the electron density of the ring, making it more vulnerable to alkylation by electrophilic groups, viz. alkyl carbocations.

Reactions of two-ringed compounds such as 1-methylnaphthalene over $Mo/Fe_2O_3/SO_4$ yielded smaller conversions compared to results with single-ring aromatic compounds. However, we observed small amounts of alkylated naphthalenes (such as 1,5-dimethylnaphthalene) and small amounts of hydrogenated products (methyltetralins). Very low conversions were also observed with three-ringed compounds such as anthracene and phenanthrene where the main products identified were partially hydrogenated anthracene and phenanthrene. Though we observed a significant number of peaks near anthracene/phenanthrene in the chromatogram, which we suspect to be alkylated three-ring structures, we could not confirm them using GC-MS. The low conversions of polyaromatic compounds is probably be due to the high electron density of such compounds which are easily adsorbed onto the acid sites of the catalyst, thus reducing the number of free sites available. However, benzyl phenyl ether gave conversions exceeding 50%

over $Mo/Fe_2O_3/SO_4$ indicating that the acidity of the catalyst is sufficient to cause cleavage of the C-O bond in benzyl phenyl ether.

The results with model compounds led us to conduct similar experiments with coal over the sulfated iron oxides. The conversions and selectivities obtained from low-temperature coal experiments over sulfated iron oxide, compared to those obtained in a non-catalytic run, are shown in Table 1. It is evident that, though the overall conversions were low (expected at such mild conditions), the selectivity of pentane-soluble products increased significantly due to the presence of the sulfated iron oxide catalyst. As Table 1 shows, there seems to be no significant difference in the (H/C) atomic ratio of asphaltenes obtained from the two experiments. However,

Table 1 Mild temperature reaction results of a DECS-17 (Blind Canyon) coal with dodecane (1:2), 250°C, 800 psig H_2, 1 hr.

Catalyst Used	Conversion (%)	Oils + Gases % Yield (% Selectivity)	$(H/C)_{atomic}$ of Asphaltenes	$(H_\gamma/H_\beta)_{alkyl}$ ratio of oils from ^{1}H-NMR
No catalyst	15.6	8.5 (54.7)	0.986	0.457
Fe_2O_3/SO_4	19.2	12.8 (66.7)	0.987	0.561

the (γ/β alkyl) ratio of the hydrogens present in the proton NMR spectra of oils indicated that the oils from the catalytic reaction possibly contained shorter chain or isomerized paraffins than the noncatalytic run. The differences are not significantly high implying that the sulfated iron oxide catalyst helps in obtaining high selectivities to pentane-solubles but does not seem to greatly affect the quality of the liquefaction products.

Future Work

Based on our low-temperature coal depolymerization experiments, we intend to conduct a two-stage coal liquefaction experiment which involves a low-temperature first stage, utilizing the acidity of the catalyst, followed by a high temperature liquefaction stage in which the depolymerized coal cracks to form liquid products. We will also work with model compounds

in order to understand more about the nature of reactions occurring over the anion-modified bimetallic catalysts. The effects of promotion of metals such as Ru, Ni, W onto sulfated iron oxides will be investigated with coal model compounds and later, in coal liquefaction and coprocessing.

References

1. Pradhan, V. R., Hu, J., Tierney, J. W. and Wender, I., *Energy & Fuels*, **7**, pp. 446-454, (1993).

2. Pradhan, V. R., Herrick, D. E., Tierney, J. W. and Wender, I., *Energy & Fuels*, **5**, pp. 712-720 (1991).

3. Pradhan, Vivek Ravikant, "Catalysis by Novel Anion-Modified Metal Oxides in Coal Liquefaction", Ph.D. Dissertation, School of Engineering, University of Pittsburgh, Pittsburgh, PA 15261.

4. Tanabe, K., Hattori, H. and Yamaguchi, T., *Critical Reviews in Surface Chemistry*, **1**, No. 1, pp. 12-13 (1990).

TASK II

Project II.3

USE OF AEROSOL-GENERATED FINE PARTICLE MIXED-METAL CATALYSTS FOR DIRECT COAL LIQUEFACTION TO TRANSPORTATION FUELS

D.B. Dadyburjor, A.H. Stiller,
C.D. Stinespring and R. Sharma
Department of Chemical Engineering
West Virginia University

OBJECTIVES

The overall objective is to obtain catalytic clusters of metal sulfides in optimum proportions suspended in an appropriate hydrogen donor for coal liquefaction. Specific objectives are to determine the effect of catalyst preparation on the performance of the catalyst during coal liquefaction. Further objectives include surface analyses of the composition and structure of iron sulfide and mixed-metal catalysts as functions of synthesis, handling and pretreatment conditions. A final set of objectives involves coal liquefaction tests using solvents which have fewer donatable hydrogen atoms. Such solvents more closely resemble recycle oils expected to be used in practice.

Earlier, we have prepared and characterized iron-based catalysts starting from the generation and disproportionation of ferric sulfide precursor under various conditions. These materials are small in size, and contain varying amounts of pyrite (PY), pyrrhotite (PH) of various compositions, and elemental sulfur. The best liquefaction results have been obtained when the ratio PH/PY is unity. This generally corresponds to the hydrothermal disproportionation of ferric sulfide at 200°C for 1 h. In this report, we present results of preparation, characterization, and liquefaction experiments using two families of catalysts: one a series of (non-aerosol) mixed-metal catalysts containing cobalt, nickel, magnesium or molybdenum, in combination with iron sulfide; and the other a series of aerosol-generated catalysts.

RESULTS

1. Mixed-Metal Catalysts

a. Preparation and Procedures

The Co- and Ni-containing iron-sulfide catalysts were prepared by adding appropriate amounts of the chloride to the ferric chloride and sodium sulfide solution. Values of disproportionation temperature (T_d) ranging from 200° to 375°C were used. These catalysts were mixed with the coal prior to liquefaction. Additional details are available in the literature [1,2].

The Mg-containing catalysts are designated as types A and B1-B3. Catalysts of type A were prepared by reacting ferric hydroxide and acetic acid to produce ferric acetate which was dried to a powder. Later, it was dissolved in water and reacted with magnesium acetate and sodium sulfide. The resulting suspension was dried to obtain the mixed-metal catalyst. Catalyst type B1 was prepared in a similar way except that the ferric acetate was reacted as an aqueous solution with sodium sulfide. Types A and B1 were mixed with coal prior to liquefaction, in loadings of 8.4% and 1.86% respectively. To prepare types B2 and B3, the catalyst was made and impregnated *in-situ* on coal. The catalyst loading was 1.67 wt% for B2 and 8.4% for B3. The Mg fractions (f_{Mg}, Mg/(Mg+Fe) ratios) used were 0.01, 0.05, 0.1 and 0.5.

Preparation of the molybdenum-containing catalysts Bx1 was similar to the *in-situ* Mg catalysts, except that ammonium heptamolybdate solution was used in place of the magnesium acetate solution. Here x is 2 or 3, depending upon the loading, as for the Mg-containing catalysts. Mo-containing catalysts designated Bx2 (x = 2,3) were prepared by adding the heptamolybdate solution after filtering and drying the iron-sulfide/coal slurry. Values of f_{Mo} used were 0.05, 0.08, 0.1, 0.15 and 0.25.

b. Liquefaction.

The coal used was a high-volatile A bituminous coal from the Blind Canyon seam in Utah (DECS-6), ground to -60 mesh under N_2. Its analysis and pretreatment have been described in earlier reports. Techniques for liquefaction have also been described earlier. Results are reported as conversion, asphaltene yield and oil+gas yield, defined using tetrahydrofuran (THF) and hexane as described earlier.

The addition of Co appears to result in no improvement, in either total conversion or oil yield. Results for the addition of Ni are shown in Figure 1. For catalysts prepared at low T_d values (less than 300°C), Ni too improves neither the total conversion nor the oil yield. At higher T_d values, the conversion and oil yield improve when f_{Ni} is 0.1 or 0.5.

Preliminary runs with Mg-containing iron catalysts showed that catalyst types B2 and B3

with f_{Mg} equal to 0.01 and 0.05 were superior to the others. Therefore, results from catalysts with these two f_{Mg} values are shown in Table I. Most of the points in the table represent averages of two or more runs.

Table I indicates that, when tetralin is used as the solvent, 57% of the coal is converted without using any catalyst (#1). On the other hand, with phenanthrene as the solvent (#2), the conversion is much lower. Similarly, the yield of asphaltenes is higher with tetralin than with phenanthrene. The yield of oil+gas is about 7% in each case. Clearly the solvent has a significant effect on the product slate and the conversion. Because of the lower values of conversion and yield obtained with noncatalytic runs using phenanthrene as the solvent, experiments using this material can more easily differentiate between different catalysts than can experiments using tetralin.

Using iron-alone catalysts of type B2, the conversion increases with both the solvents (Table I, #3, 4). The increase in conversion due to the catalytic activity is 6 percentage points in the case of tetralin, while the increase is 23 percentage points in the case of phenanthrene. The yield of asphaltenes also increases correspondingly in both cases. Catalyst B3, with the higher loading, has an even more dramatic effect on the results (#5): the conversion is 8 percentage points higher than that with B2, and the oil+gas yield increases by almost 5 percentage points. Significantly, in the presence of the catalyst, conversions and yields for the two solvents are almost indistinguishable. In other words, this catalyst may make it economically advantageous to use a cheaper, lower hydrogen-donating, solvent.

The CS_2 may be helpful in presulfiding of the catalyst. Runs #5-7 indicate that the conversion and oil+gas yield increase with increasing CS_2, but by a maximum of 1 percentage point. It appears that the activity and selectivity of these catalyst improve only slightly in the presence of CS_2.

An increase in f_{Mg} does not affect conversions and yields using catalyst B2 and 0.1 ml CS_2 (#3, 9, 15). When the higher-loaded catalyst (type B3) is used at the same CS_2 level (#6, 12, 18), the conversion and asphaltene yield decrease with increasing f_{Mg}. On the other hand, the yield of oil plus gas fraction passes through a minimum at 11% when $f_{Mg} = 0.01$. Similar observations can be made when CS_2 is not added (#5, 11, 17). However, when the amount of CS_2 is 0.5 ml (#7, 13, 19), the decrease in the conversion and yields at high Mg content is found to be small, at 2-3 percentage points. The above results show that when magnesium is introduced in the

catalyst, the product slate and conversion are almost unchanged.

Results with molybdenum-containing iron catalysts are summarized in Table II, again with most points representing an average of two or more runs. For runs at 350°C, when the catalyst loading is 1.67 wt%, the conversion of coal is 2-3 percentage points higher with the lowest f_{Mo} catalysts (#1, 3 in Table II) than with iron-alone catalyst (#4 in Table I), and the conversion to asphaltenes is 6-7 percentage points higher. When the catalyst loading is increased to 8.4 wt%, conversions and oil+gas yields in the presence of molybdenum (#2, 4 in Table II) are lower than in runs without molybdenum (#5 in Table I). For the Fe-alone catalyst, loadings higher than 3% have been shown [1] to increase the oil+gas yield significantly. Finally, the activity of the catalyst is independent of the stage at which Mo is added to the catalyst, i.e. before filtration (Table II, #1, 2) or after filtration (#3, 4).

For experiments at 400°C, the conversion and yield of asphaltenes increase with the iron-alone catalyst, relative to the noncatalytic case (Table II, #5, 6). With the introduction of Mo, the conversion and asphaltene yield increase further, depending on f_{Mo}. A maximum conversion of 88% is achieved when $f_{Mo} = 0.15$ (#16, 17). The oil+gas yield is a maximum at 25%, when $f_{Mo} = 0.1$.

Some experiments were carried out using tetralin as solvent with the Fe-Mo-S catalysts. In the absence of CS_2 (Table II, #20), the conversion of coal is about 4 percentage points higher than the average conversion in the corresponding runs with phenanthrene (#6 and #9). The increase in conversion with tetralin is accompanied by an increase in the yield of oil+gas. Interestingly, in the presence of CS_2 (#21), the conversion increases significantly, whereas the yield of asphaltenes decreases; this leads to a dramatic increase in the yield of oil+gas.

It is not clear if the activity and selectivity of the catalysts are affected by exposure to air. To study this aspect, preliminary runs have been made in which the catalyst was not exposed to air at any time during or after the impregnation on coal. The results indicate that the conversion with iron-alone catalyst increases by 3 percentage points when the catalyst is prepared and stored in N_2 (Table II, #7). The oil+gas yield also increases, but by 4 percentage points. Similar observations can be made with catalysts containing Mo (#10, 15, 18). However, the relative increases in conversion and in oil+gas yield are smaller for the Fe-Mo-S catalysts than for the Fe-S catalysts.

c. Characterization

Results for the Fe-Ni-S (high T_d) and the Fe-Mo-S series of catalysts only will be reported. For the Fe-Ni-S series, x-ray diffraction (XRD) was carried out in the laboratory of Professor M.S. Seehra at WVU. Figure 2 indicates that material with $f_{Ni} = 1$ shows peaks of Ni_3S_2. When $f_{Ni} = 0$, PY and PH peaks can be noted. At $f_{Ni} = 0.5$, the characteristic peaks are those of $(Fe,Ni)_9S_8$. This indicates that our preparation technique can in fact yield mixed metal sulfides.

Auger electron spectroscopy (AES) results for the Fe-Ni-S series are shown in Figure 3. The nickel fraction on the surface is never higher than the fraction in the bulk. This implies that, at all levels of nickel formulation, the nickel is preferentially found in the bulk, not the surface. S is enriched on the surface relative to the bulk, since almost all values can be seen to be greater than 1.5 (expected from Fe_2S_3). However, comparing the values with that for zero nickel fraction indicates that there is less S on the surface when Ni is present than when it is absent. Finally, it is worth noting the complementary nature of the curves for S and for O. If the S and O fractions are added, the numbers are relatively constant. Since oxygen is not present in the formulation, oxidation must be occurring during handling. The role, if any, of the surface oxygen on the catalytic properties of the materials needs investigation.

A focus of surface science investigation of the Fe-Mo-S series was to select a specific catalyst ($f_{Mo} = 0.1$) and characterize this catalyst prior to and after precipitation on the coal, and after the liquefaction run. However, charging of the impregnated coal was a major difficulty for AES; some samples could be analyzed, while many could not. To remedy this, the catalyst was impregnated on comparable graphite particles. Spectra of catalyst/coal particles, where obtained, were comparable to those of the corresponding catalyst/graphite samples, which could be more routinely obtained. Some samples were subjected to liquefaction conditions as in Table II, and then analyzed by AES. In some cases, the carbonaceous material after "liquefaction" was removed by dissolution in n-methyl pyrrolidone (NMP), and the sample was then subjected to AES.

Table III summarizes AES results for these systems. Here, the "catalyst/graphite" refers to the as-impregnated catalyst, while "THF-insoluble" refers to the residue after "liquefaction" and "NMP-insoluble" refers to the solid after washing with NMP. Finally, some Fe-Mo-S catalysts were precipitated during preparation in the absence of coal or graphite; this corresponds to the "precipitated catalyst." The first item of note in Table III is that the surface is S-poor in

all cases, relative to the bulk values of 3/2. On the other hand, the surface of the fresh catalyst is enriched with Mo, relative to the value of 0.1 expected. Both these effects are counter to those observed with the Ni addition. The presence of graphite does not appear to change the S ratio appreciably; the Mo ratio is diminished, but that is probably because of the small Mo signal from the sample. (The data of Figure 1 were obtained without the presence of coal or graphite.) After "liquefaction," the Fe signal is negligible but reappears after the NMP wash. This indicates the presence of significant carbonaceous material on the Fe during liquefaction. The S signal is reduced after "liquefaction," but to a lesser extent, and it too reappears after the NMP wash.

2. Aerosol-Generated Catalysts

a. Preparation and Procedure

Details of the design and construction of the aerosol reactor and the method of preparation of aerosol catalysts have been described in the literature [3]. The majority of the catalysts made, characterized and run during this period were iron-alone materials. However, preliminary preparation of some multi-metal materials has been attempted. These include Fe-Al-S ($f_{Al} = 0.01$), Fe-Zn-S and Fe-Cu-S (f_{Zn} and f_{Cu} values of 0.05 and 0.10 each), and Fe-Cu-Zn-S ($f_{Zn} = 0.05$, $f_{Cu} = 0.10$).

b. Characterization

XRD data indicate interesting effects when conditions are changed. At low precursor concentrations, 0.01M, when aerosol reactor conditions are maintained at 200°C and 200 psi, peaks are observed corresponding to FeS_2, monoclinic pyrrhotite (Fe_7S_8, i.e., x = 1.143) and elemental S. This is consistent with XRD patterns from hydrothermal disproportionation [1,4]. However, as mentioned in an earlier final report, when the precursor concentration is higher, 0.1M, and the temperature is 165°C, peaks observed include FeS_2 and S, as before, and also greigite (Fe_3S_4, x = 1.333). But greigite is stable typically only below 100°C [5]. Perhaps the thermodynamically unstable form is trapped in the particle due to the rapid quenching that takes place in the aerosol reactor. The role of the higher precursor concentration in facilitating the unstable form is not clear.

Other characterization data can be found in Table IV. The ratio of pyrrhotite to pyrite (PH/PY) was found by atomic adsorption spectrometry as described in earlier reports. Values reported are mainly around unity, as expected. Density was measured using He pycnometry. For sample A9, grinding the solid increased the density measurement by 0.1 g/cc, probably within

the accuracy of the measurement. Accordingly, the changes in density between samples A8 and A9 and between samples A9 and A12 are related to the different solids produced under those two conditions, not changes in the inner and/or outer diameters of the particles. Note that increasing the temperature of the aerosol reactor causes less change than increasing the precursor concentration.

The mean diameter in Table IV is measured using multiple-angle laser light scattering with photon correlation spectroscopy. For these measurements, the particles were suspended in tetralin, the same solvent used for the DCL experiments. In addition, a transmission electron microscope (TEM) in Professor G.P. Huffman's laboratory at UK was used. In the latter measurements, the particles were suspended in ethyl alcohol, which was then evaporated on the TEM slide. Sizes measured by TEM range from 3 - 580 nm, with a majority of particles in the lower portion of the range. The 1-2 orders of magnitude by which the two techniques differ is probably due to clumping of the particles in the tetralin. Since the physical situation with tetralin is closer to the conditions during liquefaction, the values in Table IV are probably more realistic than TEM values. The larger particle size observed in sample A9 relative to sample A8 is probably due to the increased concentration of precursor used.

Bulk ratios of S to Fe and the corresponding surface ratios, obtained from energy-dispersive x-ray spectroscopy (EDX) and AES respectively, are also shown in Table IV. Bulk ratios for samples A7 and A8 are similar, and greater than 1.5, the value expected for Fe_2S_3. A smaller value is obtained for sample A12, and the value decreases further for sample A9. The decreasing values may be due to loss of elemental S (found after disproportionation of the Fe_2S_3) in sample handling. Hence the decreasing values may indicate increasing amounts of elemental S formed, and increasing amounts of PH relative to PY. The decreasing bulk values are consistent with decreasing surface S/Fe values as well. The ratios are higher on the surface than in the bulk, again consistent with the formation of elemental S and its migration to the surface. For AES on the aerosol catalysts, the peak shape corresponding to S is, in fact, characteristic of that ascribed to elemental sulfur. Further, comparing the S/Fe values with that from Figure 3 when $f_{Ni} = 0$ indicates that an aerosol catalyst typically contains more S on the surface.

Preliminary AES and EDX data on the multi-metal Fe-Al-S material indicate that relatively little Al is found. The PH/PY ratio obtained is approximately 2. The presence of Al seems to move Fe from the PY form to the PH form.

c. Liquefaction

The performance of the catalysts characterized in Table IV is shown in Table V. The experiments were carried out under conditions similar to those described above. Full experimental details have been provided earlier [3,4]. All catalyst samples used show noticeable improvements in conversion and asphaltene yield relative to the thermal runs, although oil yields are not improved. The improvement in conversion is most striking for catalysts prepared using the lower precursor concentration, and the oil+gas yield is best for the catalyst prepared at the highest temperature. The lowest oil+gas yield corresponds to the lowest PH/PY ratio in Table IV.

Preliminary results on the Fe-Al-S catalyst indicate significant improvement in both conversion and oil+gas. Compared to sample A12 in Table V, conversion is 3% higher, and the oil+gas yield is 6% higher. These numbers need confirmation, however.

SUMMARY AND FUTURE WORK

Iron-based catalysts have been prepared and characterized by XRD, AA, AES, EDX, and other methods. The catalysts have been used in liquefaction runs using a poor solvent, with and without sulfiding. The non-aerosol mixed-metal catalysts prepared to date are not appreciably more effective than the iron-alone catalysts. Possible exceptions are the Fe-Ni-S and Fe-Mo-S series, for which the product slate and conversion depend on the Ni and Mo fraction. The activity is not affected by the stage at which Mo is added to the coal/catalyst mixture, but may be affected by the presence of air. Aerosol catalysts have been shown to be of nanometer dimension in the TEM. Preparation conditions have been correlated with results of characterizations and liquefaction runs. Preliminary liquefaction experiments with multi-metal aerosol catalysts are promising.

Future work will concentrate on multi-metal and iron-alone catalysts made by aerosol techniques. These will be characterized and used in liquefaction runs.

REFERENCES

1. Dadyburjor, D.B., Stewart, W.E., Stiller, A.H., Stinespring, C.D., Wann, J.-P. and J . W . Zondlo, Energy and Fuels **8**, 19 (1994).

2. Dadyburjor, D.B., Stiller, A.H., Stinespring, C.D., Zondlo, J.W., Wann, J.-P., Sharma, R.K., Tian, D., Agarwal, S. and Chadha, A., Prepr. ACS Div. Fuel. Chem. Washington, DC (1994).

3. Stiller, A.H., Agarwal, S., Zondlo, J.W. and Dadyburjor, D.B., Proc. 10th Ann. Intern. Pittsburgh Coal Conf., Chiang, S.-H., Editor (1993).

4. Stansberry, P.G., Wann, J.-P., Stewart, W.R., Yang, J., Zondlo, J.W., Stiller, A.H. and Dadyburjor, D.B., Fuel **72**, 793 (1993).

5. Power, L.F. and Fine, H.A., Miner. Sci. Eng. **8**, 106 (1976).

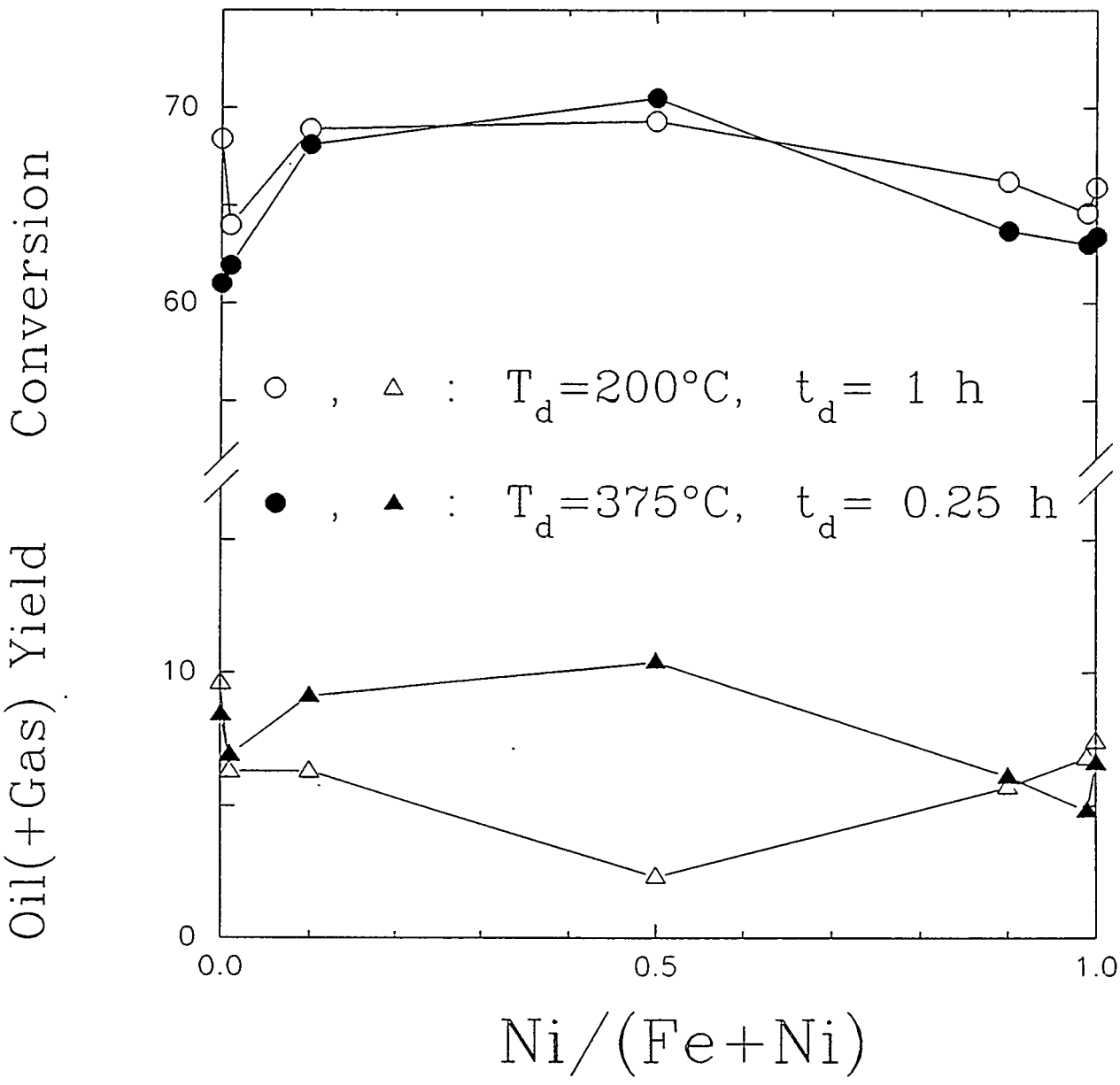

Figure 1. Liquefaction conversion and oil+gas yield over a series of Fe-Ni-S catalysts as a function of Ni fraction and disproportionation conditions.

Figure 2. XRD peaks for catalysts disproportionated at T_d = 375°C in 1500 psig H_2 (hot) for t_d = 0.25 h. Ni fractions: 1.0 (top), 0.5 (middle), 0.0 (bottom).

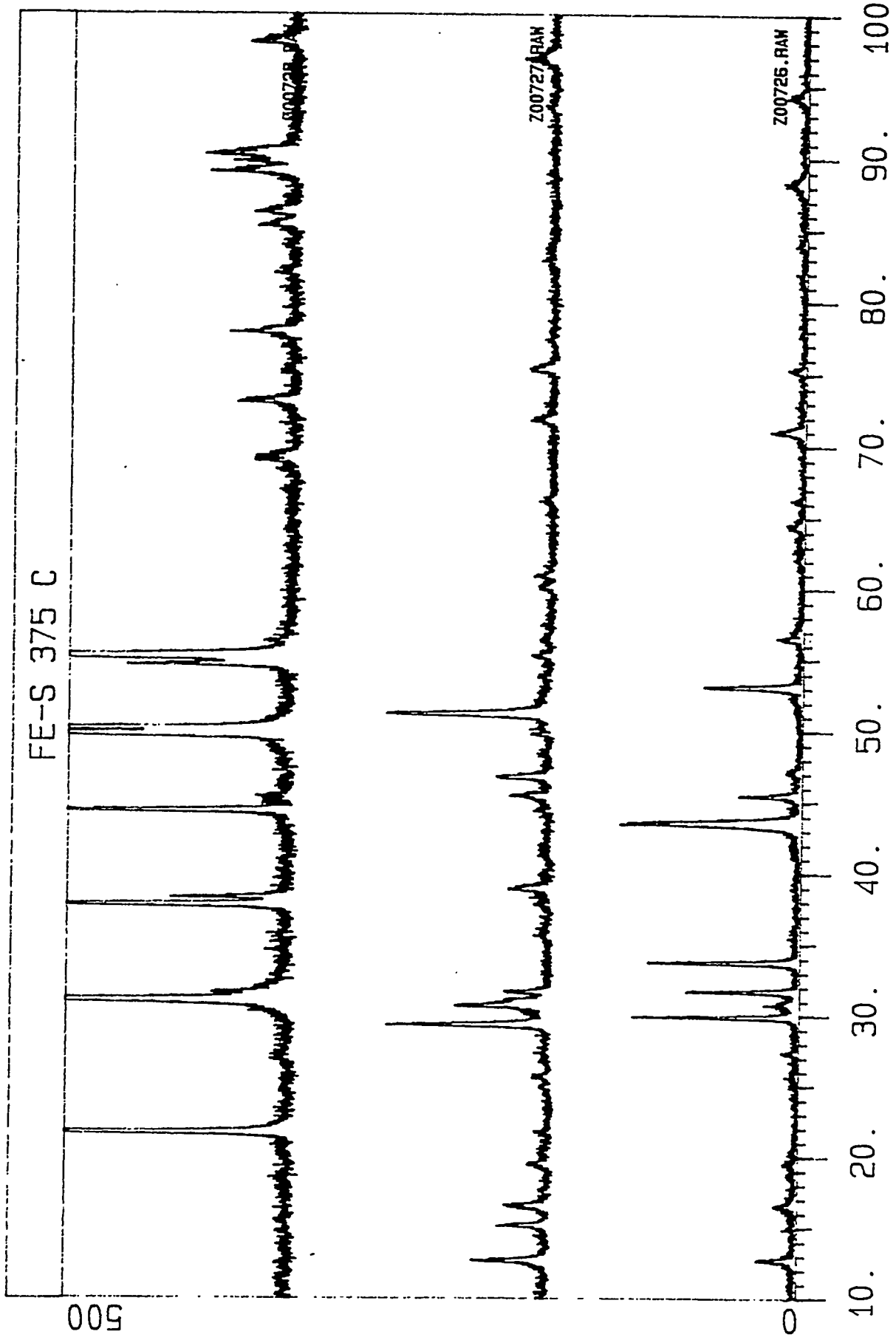

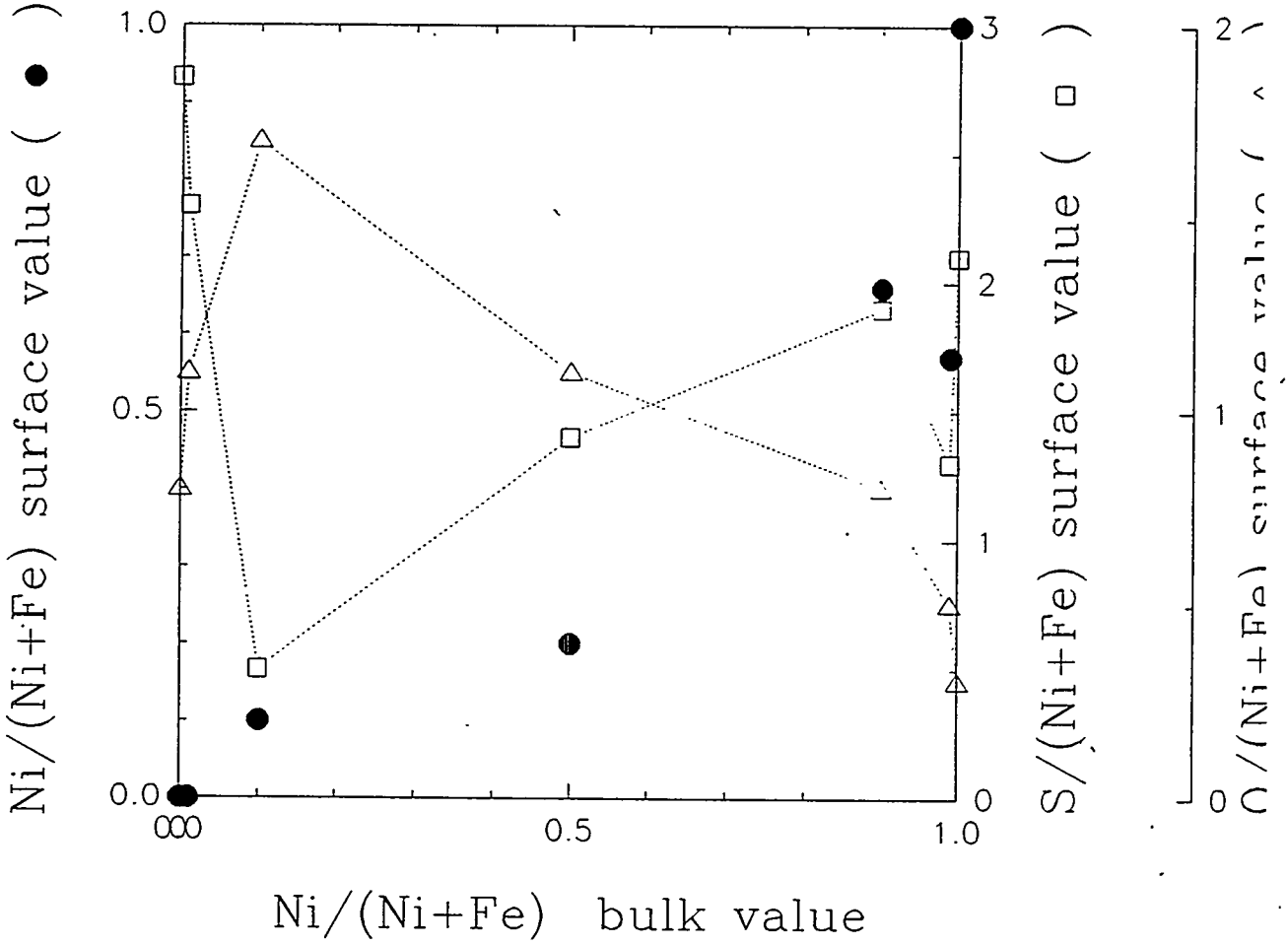

Figure 3. Summary of AES results for a series of catalysts prepared as in Figure 2 as a function of Ni fraction.

Table I

Coal Liquefaction Using Fe-Mg-S Catalysts

DECS-6 coal, 350°C, 1000 psi (cold) H_2, 60 min, 500 cpm.

RUN #	PREP TYPE	f_{Mg}	SOLVENT USED	CS_2 ml	CONVN %	ASPHLTN YIELD,%	OIL+GAS YIELD,%
1	thermal	--	tetralin	0.0	57.0	50.0	7.0
2	thermal	--	phenanthrene	0.0	41.6	33.4	7.5
3	B2	0.00	tetralin	0.1	63.3	55.6	7.7
4	B2	0.00	phenanthrene	0.1	64.0	56.2	7.8
5	B3	0.00	tetralin	0.0	71.2	58.5	13.2
6	B3	0.00	tetralin	0.1	71.6	58.5	13.0
7	B3	0.00	tetralin	0.5	71.9	57.7	14.2
8	B3	0.00	phenanthrene	0.1	72.9	61.0	11.8
9	B2	0.01	tetralin	0.1	62.2	54.0	8.5
10	B2	0.01	phenanthrene	0.1	53.5	43.6	9.9
11	B3	0.01	tetralin	0.0	70.5	59.7	10.8
12	B3	0.01	tetralin	0.1	71.5	60.5	11.0
13	B3	0.01	tetralin	0.5	71.8	59.0	12.8
14	B3	0.01	phenanthrene	0.1	73.3	61.9	11.2
15	B2	0.05	tetralin	0.1	63.6	55.5	8.2
16	B2	0.05	phenanthrene	0.1	64.3	57.1	7.2
17	B3	0.05	tetralin	0.0	65.7	53.5	12.6
18	B3	0.05	tetralin	0.1	65.2	52.6	13.1
19	B3	0.05	tetralin	0.5	70.4	58.7	11.7
20	B3	0.05	phenanthrene	0.1	72.5	61.7	10.8

Table II

Coal Liquefaction Using Fe-Mo-S Catalysts.
DECS-6 coal, 1000 psi (cold) H_2, 500 cpm.

(A) T = 350°C, t = 1 h

RUN #	PREP TYPE	f_{Mo}	SOLVENT USED	CS_2 ml	CONVN %	ASPHLTN YIELD,%	OIL+GAS YIELD,%
1	B21	0.05	phenanthrene	0.1	67.1	63.7	3.4
2	B31	0.05	phenanthrene	0.1	69.2	64.4	4.8
3	B22	0.05	phenanthrene	0.1	66.7	62.3	4.4
4	B32	0.05	phenanthrene	0.1	66.9	63.0	3.9

(B) T = 400°C, t = 0.5 h

RUN #	PREP TYPE	f_{Mo}	SOLVENT USED	CS_2 ml	CONVN %	ASPHLTN YIELD,%	OIL+GAS YIELD,%
5	thermal	--	phenanthrene	0.0	69.8	48.7	21.1
6	B22	0.00	phenanthrene	0.1	84.5	61.8	22.7
7[1]	B22	0.00	phenanthrene	0.1	87.3	61.0	26.3
8	B21	0.05	phenanthrene	0.1	86.8	64.9	21.9
9	B22	0.05	phenanthrene	0.1	86.5	64.1	22.4
10[1]	B21	0.05	phenanthrene	0.1	90.0	66.4	23.6
11	B21	0.08	phenanthrene	0.1	88.1	64.1	24.0
12	B22	0.08	phenanthrene	0.1	88.4	64.7	23.7
13	B21	0.10	phenanthrene	0.1	86.3	60.9	25.4
14	B22	0.10	phenanthrene	0.1	87.2	62.0	25.2
15[1]	B21	0.10	phenanthrene	0.1	90.9	64.0	26.9
16	B21	0.15	phenanthrene	0.1	88.8	64.1	24.7
17	B22	0.15	phenanthrene	0.1	88.2	63.1	25.1
18[1]	B21	0.15	phenanthrene	0.1	89.5	63.5	26.0
19	B22	0.25	phenanthrene	0.1	83.6	61.5	22.1
20[2]	B42	0.02	tetralin	0.0	89.6	62.5	27.1
21[2]	B42	0.02	tetralin	0.5	93.2	51.7	41.5

[1] Coal, catalyst not exposed to air.
[2] catalyst loading 2 wt%, not 1.67 wt% as for catalyst B22

TABLE III

AES Characterization of A Series of Fe-Mo-S catalysts, $f_{Mo} = 0.1$

CATALYST TYPE	SURFACE S/(Fe+Mo)	SURFACE Mo/(Fe+Mo)
precipitated	1.2	0.17
catalyst/graphite	1.1	0.0
THF-insoluble	0.5	1.0
NMP-insoluble	1.8	0.17

TABLE IV

Characterization of Aerosol-Generated Fe-S Catalysts

#	PRECURSOR CONCN M	PREP PRES psi	PREP TEMP °C	PH PY	DENSITY g/cc	DIA nm	BULK S/Fe EDX	SFCE S/Fe AES
A7	0.01	200	200	0.96	---	---	2.5	3.6
A8	0.01	100	200	0.66	4.60	507	2.5	3.3
A9	0.10	100	200	0.92	4.27	1200	0.9	2.0
A12	0.01	100	250	---	4.66	---	1.9	---

TABLE V

Coal Liquefaction with Aerosol-Generated Fe-S Catalysts
DECS-6 coal, tetralin, 0.1 ml CS_2, 5% catalyst loading
350°C, 1000 psi (cold) H_2, 60 min, 500 cpm

SAMPLE #	CONVERSION [%]	ASPHALTENE YIELD [%]	OIL + GAS YIELD [%]
thermal	54.9	41.2	13.6
A8	64.9	55.6	9.3
A9	63.0	52.1	10.8
A12	64.4	54.8	10.9

TASK II

Project II.4

STUDIES IN CATALYTIC HYDROPROCESSING FOR UPGRADING PRIMARY COAL DERIVED LIQUIDS TO CLEAN TRANSPORTATION FUELS

J. A. Guin, X. Zhan, H. S. Joo, and R. Menon
Auburn University

During the past year work has proceeded in several areas. The first five months of this new project mainly concentrated on finishing the iron based catalyst work and literature review on catalytic upgrading of coal liquids. Our iron based catalyst work has been summarized in two recent publications.[1,2] Two PhD students are now working in the new project involving the promotion of hydrotreating catalysts with noble metals. A new masters student has also joined the project and is just beginning her work in the area of new catalyst supports. In the following we summarize our completed work on iron-based catalysis and new work on improved upgrading catalysts for clean transportation fuels.

IRON-BASED CATALYST STUDIES

During the course of our investigation of iron as a potential dispersed phase catalyst for coal liquefaction, it was found that the H_2-reduced form of iron yielded a particularly active catalyst for the hydrogenation of aromatic ring compounds. A literature review revealed that kinetic studies using iron catalysts were sparse, especially in the high pressure reaction regime representative of coal liquefaction. For these reasons we examined the hydrogenation activity of the iron particle catalyst in the high pressure region.

Trickle-bed Reactions. Hydrogenation of naphthalene (NAPH) yielding tetralin (TET), trans- and cis-decalin (DEC) was examined in trickle bed reactions. An extent of hydrogenation A_H was defined as eq. (1) based on the stoichiometry.

$$A_H = \frac{2M_{TET} + 5M_{DEC}}{5(M_{NAPH} + M_{TET} + M_{DEC})} \quad (1)$$

Here the M_i are the moles of compound i in the reaction products.

Figure 1 shows the extent of hydrogenation A_H vs. time for Ni-Mo/Al_2O_3 extrudate and

iron at 250°C and 300°C. No significant deactivation was observed for Ni-Mo/Al_2O_3 after 340 hours. For Fe_2O_3 at 300°C, the catalyst activity increased gradually to a maximum followed by significant deactivation. The initial increase in activity is believed to reflect an activation of the iron catalyst by H_2 reduction. This view is further confirmed by the results of experiments at 250°C also shown in Figure 1. With Fe_2O_3 at 250°C, there was essentially no conversion for the first 6 hrs. A_{II} then increased rapidly during the next 18 hours and reached a relatively stable level without further deactivation in the following 54 hours. In contrast, the H_2 pre-reduced catalyst showed immediate high activity at 250°C without obvious deactivation for 150 hrs. It is concluded that the original Fe_2O_3 has little hydrogenation activity while in-situ pre-reduction in hydrogen yields a highly active catalyst. The iron based catalysts are more susceptible to deactivation than the Ni-Mo/Al_2O_3.

Results of three runs at 250°C with a sulfur source (CS_2) added to the feed in different periods are shown in Figure 2. The iron catalyst was charged in its original oxide form. In the first run, liquid feed without CS_2 was charged for the first 72 hours at which time the liquid feed was spiked with 2 wt% CS_2. A_{II} then fell continuously to zero after 32 hours indicating sulfur poisoning of the hydrogenation sites. The other two runs were performed by feeding CS_2 spiked feeds from the beginning and then switching to a CS_2-free feed. No conversion was observed until introduction of CS_2-free feeds at 48 and 92 hours respectively, following which both runs showed small, but stable A_{II} as the residual H_2S concentration in the reactor became depleted. This small activity indicates that the sulfided iron has finite, albeit significantly lower aromatic hydrogenation activity than H_2 pre-reduced iron. Conclusions from these experiments are that the aromatic hydrogenation activity of the iron catalyst decreases in the order Fe>FeS_x>Fe_2O_3.

Fixed-bed Vapor-phase Reactions. Vapor-phase hydrogenation of naphthalene using an iron particle catalyst was examined using cyclohexane as solvent at 1000 psi and 160-300°C. The empirical power-law rate model shown in eq. (2) was used to fit the vapor-phase experimental data.

$$r_N = k_{app} C_N^a C_H^b \qquad (2)$$

Figure 3 shows the first order kinetics of naphthalene. When the initial concentration of H_2 was reduced to 70% of the baseline condition for both reduced iron and Ni-Mo/Al_2O_3 catalysts, the

slopes of the plots are reduced correspondingly to about 70% of those under baseline conditions indicating that hydrogen also follows first order. Figure 4 shows the Arrhenius plots based on the observed apparent rate constants at temperatures of 160-300°C. For Ni-Mo/Al_2O_3 catalyst, the apparent activation energy (40.2 kJ/mol) is approximately the same as that of reduced iron (43.2 Kj/mol), and the frequency factor ($1.18x10^9$), is about twice that of reduced iron ($6.06x10^8$). The surface area of Ni-Mo/Al_2O_3 is about 60 times that of the original iron oxide catalyst. Assuming that the surface area of the pre-reduced iron catalyst is not too different from the original Fe_2O_3, then on a per unit surface area basis, the reduced iron is more active than the Ni-Mo/Al_2O_3.

Iron Catalyst Surface Area Studies. As shown in Figure 5, the surface area of Mach-I iron catalyst decreases gradually with the calcining temperatures in air. In advance of calcination of the catalyst, pretreatment with water and then drying in vacuum oven did not influence the surface area. Also as shown in Figure 5, when the catalyst was placed in a TBMR in the presence of tetralin and hydrogen with and without CS_2 at various temperatures, a decrease in the surface area was observed similar to that of simple calcination in air. In an attempt to minimize the loss of surface area, the Mach-I catalyst was doped with various amounts of sulfate ion to determine if the sulfate would deter the agglomeration of the catalyst and subsequent loss of surface area. A further study was done to examine the effect of sulfate ion on the maintenance of surface area of the Mach-I disposable iron catalyst. The BET surface area of the Mach-I disposable iron catalyst was found to drop dramatically in the coal liquefaction reactor from about 215 m^2/g to about 4 m^2/g. Promotion of the Mach-I catalyst with various concentrations of ammonium sulfate resulted in an increase in the surface area maintenance of the catalyst, if calcined in air at 500°C, from about 35 m^2/g to about 120 m^2/g. There was optimal surface area maintenance at 0.3-0.6 M ammonium sulfate promotion of the Mach-I. However, when the sulfate promoted iron catalyst was exposed to coal liquefaction conditions, the surface area dropped to about 12 m^2/g independent of the concentration of ammonium sulfate promoter, as compared to that of 4 m^2/g for untreated Mach-I iron catalyst.

UPGRADING CATALYST DEVELOPMENT STUDIES

Introduction. Three types of commercial Al_2O_3 supported catalysts (Criterion 424

NiMo, Cyanamid 1442B CoMo and Crossfield 550S NiW) and samples of coal liquid (courtesy of Exxon) were procured for this study. Experiments have been performed to examine hydrogenation and HDN activities of three different Pt promoted catalysts for upgrading coal liquid.

Continuous Reactor Upgrading Studies. The continuous reactor has been modified for *upflow* of liquid and gas through a fixed bed of catalyst, as recommended by industrial workers who do this type of catalyst development. The flooded upflow mode is thought to give better wetting and flow distribution for upgrading studies than the previously used downward trickle flow. Several runs have been made with a Wilsonville coal middle distillate; however, they had to be terminated after 10-30 hours on stream due to reactor system plugging. Further modification of the continuous reactor is in progress and the test results will be reported later. It is felt that the plugging problem can be solved in the near future thus allowing longer term runs to study catalyst activity maintenance.

Catalyst Preparation. Catalysts used in tubing bombs were crushed and sieved to between 100 and 200 mesh, and then presulfided with dimethyldisulfide (DMDS) in a tubing bomb at 300 °C for 2 h. Pt promoted catalysts were prepared by an incipient wetness technique and were then dried in air overnight and calcined at 450 °C for 3 h. The Pt doped catalysts were presulfided by the above procedure.

Experimental. 6 g of reactant solution contained 2 wt% naphthalene and (or) 2 wt% pyridine in hexadecane were used for model compound studies and 3 g of coal liquid for upgrading. The experiments in 15.5 cc tubing bomb reactors charged with 1000 psig cold hydrogen pressure were performed at 350 °C using 0.1 g catalyst and 0.09 g DMDS for model compound reactions and at 375 °C for 1 hr using 0.4 g catalyst for upgrading coal liquid.

Analysis. Analysis was performed on a temperature programmed Varian 3200 GC with 30 m x 0.32 mm x 0.25 μm J & W DB-5 capillary column for products of naphthalene reactions and 30 m x 0.32 mm x 1.0 μm Restek Stabilwax-DB capillary column for products of pyridine reactions. GC-MS and spiking were performed to identify the products.

Reaction Network. Naphthalene hydrogenation is sequential with naphthalene hydrogenation to tetralin and tetralin hydrogenation to decalin. Pyridine HDN also occurs through a sequential pathway. Pyridine is saturated to form piperidine, followed by

hydrogenolysis to form pentylamine and subsequent removal of nitrogen to form pentane and ammonia. Pentyl-piperidine is formed from the alkyl-transfer reaction of piperidine and pentylamine. Di-n-pentylamine was also found to a minor extent.

Results. The hydrogenation activities (A_H) of the NiMo catalysts were examined for sulfur effects on the hydrogenation reaction as shown in Fig. 7. While the A_H of the NiMo (0.89) is higher than that of the presulfided NiMo (0.43) under the reaction without sulfur, the two values of A_H in reactions with sulfur added were the same (0.47). The A_H of the Pt promoted NiMo (PtNiMo) at 310 °C was much superior to that of the NiMo. This indicates that the Pt has adequate dispersion on the NiMo catalyst. The A_H of the SPtNiMo with sulfur added was lower than that of the PtNiMo showing that the hydrogenation function of the PtNiMo is poisoned to some extent by sulfur as was the original NiMo.

HDN of pyridine at several different Pt wt% in the catalyst was examined at 350 °C for 30 min and the results are in Fig. 8. It is seem that the Pt doped NiMo and CoMo catalysts are more active for HDN than the original catalysts. % HDN's of the presulfided Pt promoted NiMo and CoMo were about 100 % at the Pt wt% above 0.8 % but NiW did not show any positive effect of Pt doping. Based on these results, the experiments described below were conducted using 0.8 wt% Pt catalysts.

Experiments using a reactant solution which consists of naphthalene and pyridine in hexadecane were performed at 350 °C. The product distributions and % HDN from pyridine reactions are shown in Fig. 9-11. Comparing the Pt promoted and unpromoted (no Pt) catalysts shows that with Pt promoted catalysts, pyridine reacted faster with more effective hydrogenation, except with NiW catalyst. Lower pentylamine and higher N-pentane concentrations in the reaction with Pt promoted catalysts yields a more effective nitrogen removal rate as compared to the unpromoted one. The activity of the NiW catalyst was not enhanced by Pt doping. In the experiments where naphthalene and pyridine were used as reactants, all catalysts showed very low activities for naphthalene hydrogenation.

Coal liquid was upgraded with the catalysts above and % nitrogen was analyzed as shown in Table 1. The % HDN of each run is shown in Fig. 12. The order of HDN activities is PtNiMo > PtCoMo > (NiMo = NiW = PtNiW) ≅ CoMo. This result shows that Pt promoted catalyst has more effective HDN activity than an unpromoted one except for NiW. The PtNiMo

was best for upgrading coal liquid among the six types of catalysts tested.

Catalyst Support Studies. The objective of this part of our project is to explore the performance of metal phosphates of aluminum, titanium and zirconium as potential new supports for stage 2 upgrading catalysts. There is considerable evidence of metal phosphate utility as a possible catalyst support material in light of their high stable surface area, pore geometry, surface acidity properties and surface chemistry.[3] Phosphate anions are known to promote hydrogenation/dehydrogenation. Based on these promising possibilities, we plan to begin our studies using $AlPO_4$ - metal oxide systems such as alumina-aluminum phosphate, titania - $AlPO_4$ and Zirconia - $AlPO_4$. We also plan to check the catalytic activity of supports such as titania-$TiPO_4$, Zr_2O_3-$ZrPO_4$, etc. A literature review for catalyst preparation methods is given below.

(1) Alumina-Aluminum phosphate (AAP) support preparation

To prepare a series of alumina-aluminum phosphate supports, coprecipitation methods as reported in previous works[4,5] will be examined. Chen et al[4] used AAP as a support of CoMo catalyst for hydrodesulfurization reactions of residual oils in a trickle bed reactor. The samples were characterized by X-ray diffraction, BET surface area and mercury-penetration pore volume measurements. Controlling the stoichiometry of the Al/P atomic ratio allowed a desired AAP composite to be obtained. It was shown that surface area increases and average pore diameter decreases as the Al/P atomic ratio increases. The acidity of AAP decreased as the Al/P atomic ratio increased. It was shown that larger surface area, smaller acid amount and weaker interaction of AAP supports make the metal more highly disperse, produce more active sites and result in high initial HDS activity.

Marcelin et al[5] studied the preparation of several compositions of AAP and their resulting physical properties. It was observed that by varying the stoichiometry of the precipitates, Al/P atomic ratio from 1 to 20, surface areas and pore size distributions could be controlled. High alumina content invariably yielded materials with high surface area and small pores while high aluminum phosphate resulted in smaller surface area and larger pores. Some of the large-pore support gels were mixed with nickel salts to produce catalysts which were found to be highly active for the liquid phase hydrogenation of 2-ethyl hexenal. The BET surface area and pore size distribution of the unreduced catalyst were measured using nitrogen adsorption at 77 K. As the Al/P ratio increased, a decrease in the pore size and an increase in surface area were observed.

A review by Moffat[3] discusses the physical and catalytic properties of aluminum phosphate and includes AAP, but makes no mention of its utility as a catalyst support.

$AlPO_4$ - metal oxide preparation:

Blanco et al[6] studied the catalytic activity and selectivity of a series of $AlPO_4$ and $AlPO_4$ - metal oxide systems (Al_2O_3, TiO_2 and ZrO_2) as catalysts for the gas-phase micro catalytic alkylation of toluene with methanol. Campelo et al[7] discusses the preparation of $AlPO_4$ for making AAP. The texture and surface chemistry of $AlPO_4$ were also studied. Use of aluminum phosphate-zirconia catalysts in cyclohexene isomerization was mentioned by Blanco et al[8]. An increase in ZrO_2 content and/or calcination temperature decreases the surface area and pore volume.

A series of $AlPO_4$ - TiO_2 (APTi) catalysts containing different weight compositions was prepared by Campelo et al[9] by precipitation of $AlPO_4$ on commercial TiO_2 using propylene oxide and characterized with respect to crystallinity, textural properties and surface chemistry. The surface area and pore volume of the final APTi catalysts depend largely upon the weight composition and to a lesser degree, upon the post precipitation heat treatment under 1273 K. When the TiO_2 content was increased, the decrease in surface properties due to calcination temperatures is greater. Another study on $AlPO_4$ / TiO_2 catalysts[6] mentioned that the surface area, pore volume, crystal structure and surface acid character were dependent on the precipitation agent, chemical composition and calcination temperature. It was found that both the apparent rate constant and the selectivity in cyclohexene skeletal isomerization were dependent on the catalyst composition, i.e. the $AlPO_4$ / TiO_2 weight ratio. These were shown to have a relatively high surface area (109 - 319 m^2/g). Other textural properties like pore volume and pore-size distribution (vol %) were also mentioned.

Our objective is to prepare $AlPO_4$ - metal oxide systems and to measure the textural properties. Catalyst activity decline is a major problem in the upgrading of coal liquids, and the effects of metal phosphates as catalyst supports on this aspect of catalytic performance will be examined.

REFERENCES

1 Guin, J.A., Zhan, X., and Linhart, R.S., **Energy and Fuels**, 8(1), 105-112, 1994.

2 Guin, J.A., Zhan, X., **AIChE Spring Meeting, Atlanta, GA, April 17-21, 1994.**

3 Moffat, J.B. **Catal. Rev.- Sci. Eng.,** 18(2), 199-258, 1978.

4 Chen, et al. **Ind. Eng. Chem. Res.,** 29, 1830-1840, 1990.

5 Marcelin, et al, **J. Catalysis**, 83, 42-49, 1983.

6 Blanco, et al, **J. Catalysis**, 137, 51-68, 1992.

7 Campelo, et al, **Chem. Soc. Faraday Trans I,** 85(8), 2535-2553, 1989.

8 Blanco, et al, **J. Catalysis,** 53, 135-156, 1989.

9 Campelo, et al, **J. Colloid and Interface Sci.**, 118 (1), July 1987.

Table 1. % Nitrogen of Original and Upgraded Coal Liquid.

Catalyst	Nitrogen wt%
original coal liquid	0.62
NiMo	0.30
PtNiMo	0.10
CoMo	0.32
PtCoMo	0.23
NiW	0.30
PtNiW	0.30

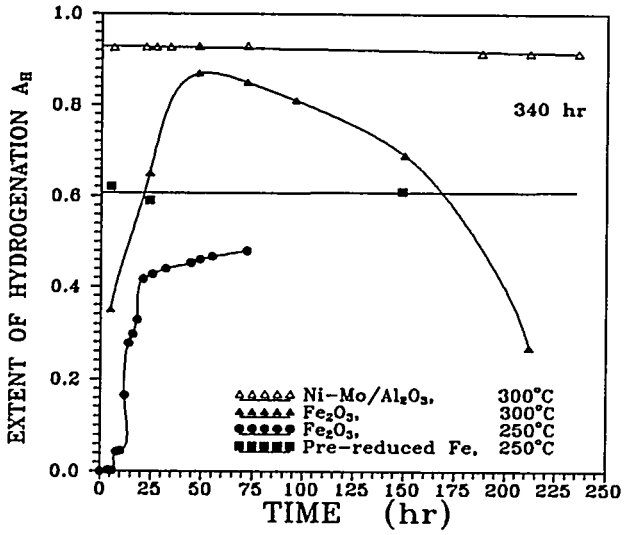

Figure 1 Extent of Hydrogenation of Ni-Mo/Al_2O_3 and Pre-reduced Iron Catalysts at Different Temperatures in the Trickle-bed Reactor

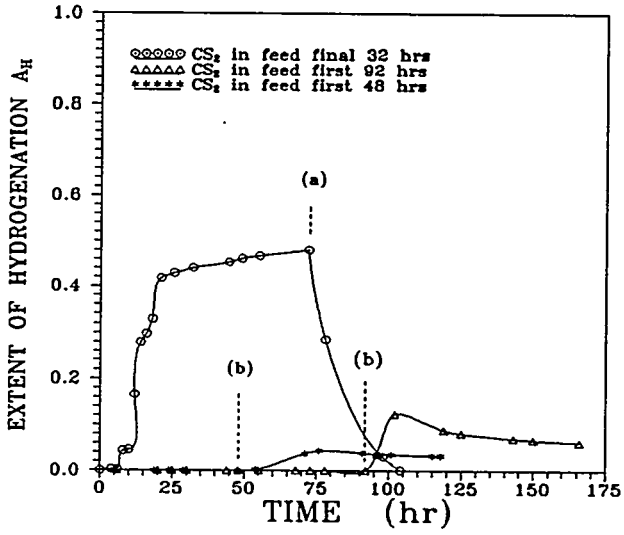

Figure 2 Effects of Fe_2O_3 Catalyst Sulfidation on the Extent of Hydrogenation at 250°C in the Trickle-bed Reactor. (a) CS_2 introduced. (b) CS_2 removed.

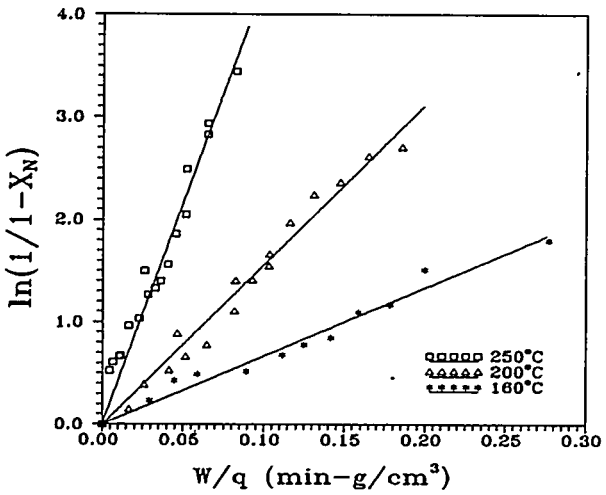

Figure 3 First Order Kinetic Plots of Reactions on Pre-reduced Iron.

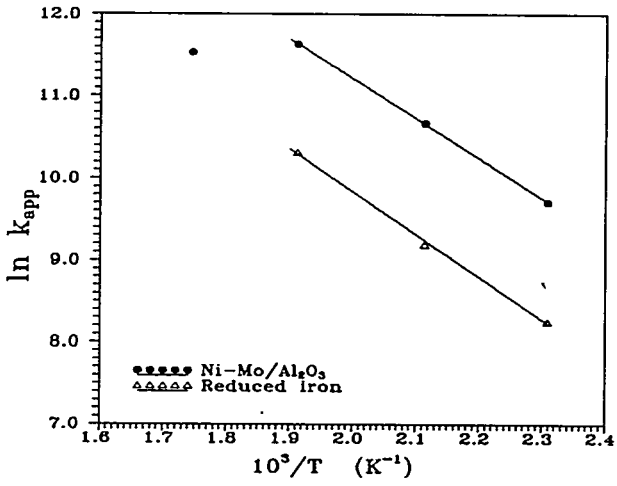

Figure 4 Arrhenius Plots Based on the Apparent Rate Constants.

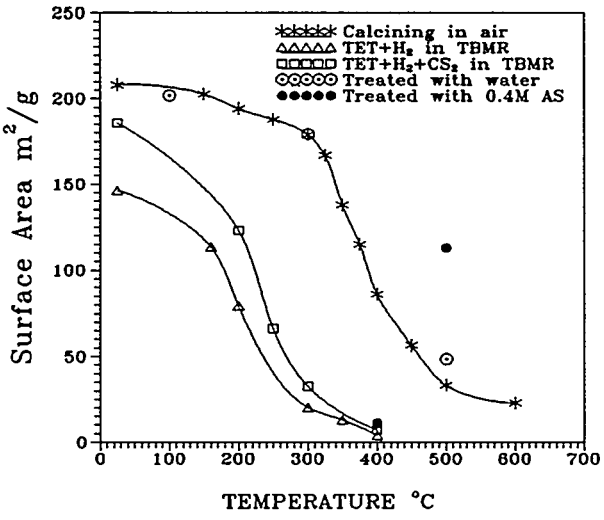

Figure 5 Dependence of Surface Area on Pretreatment conditions.

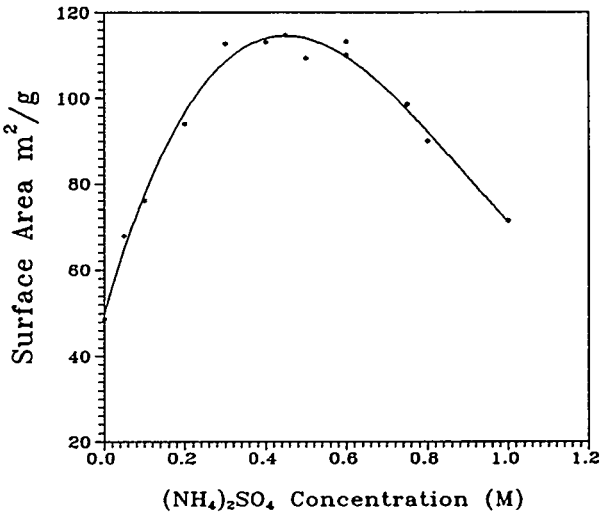

Figure 6 Effect of the Concentration of $(NH_4)_2SO_4$ Solution on the Surface Area of Iron Catalyst.

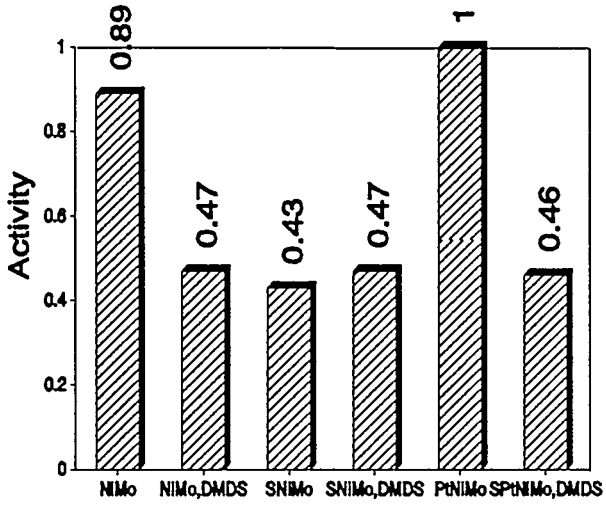

Figure 7 Hydrogenation Activities of Naphthalene Reactions.

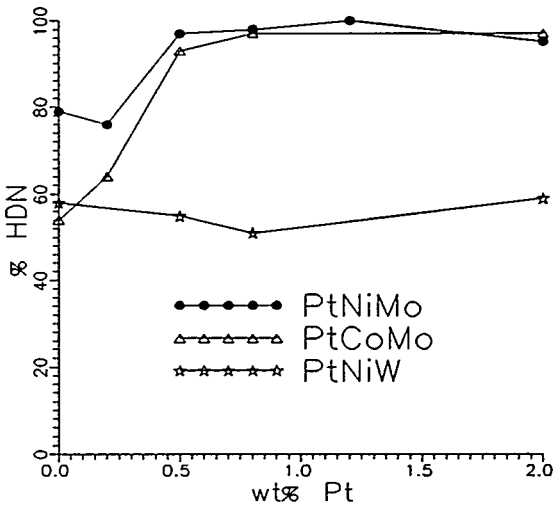

Figure 8 % HDN of Pyridine Reactions vs. wt% Pt

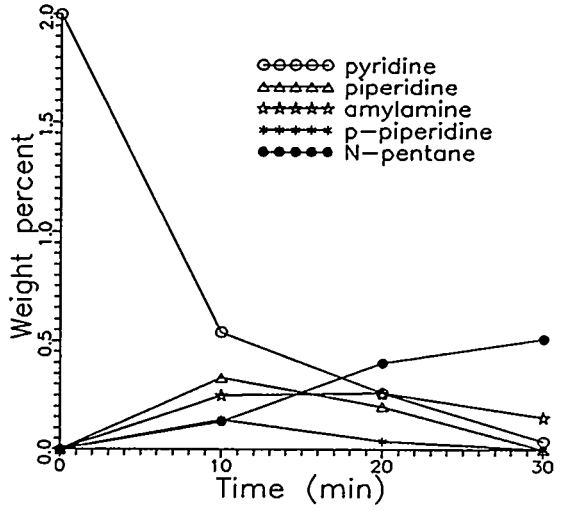

Figure 9 Product Distribution of Pyridine HDN Reactions with NiMo.

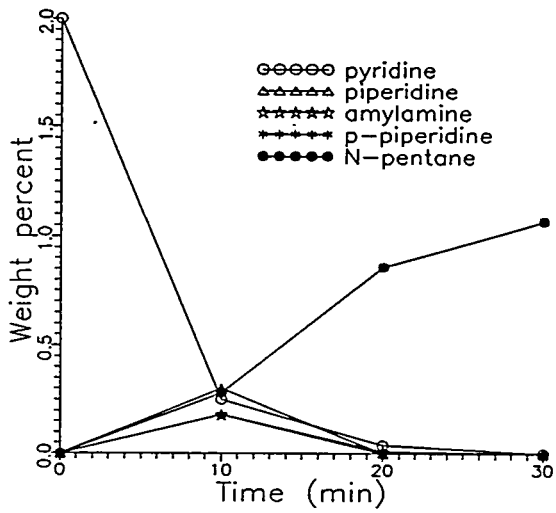

Figure 10 Product Distribution of Pyridine HDN Reactions with PtNiMo.

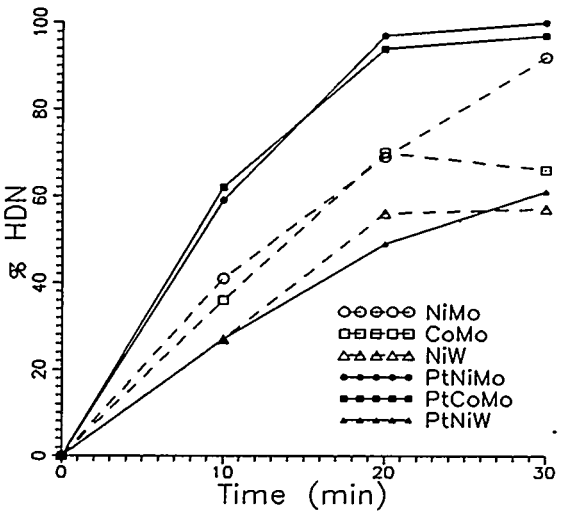

Figure 11 % HDN of Pyridine Reactions with Six Types of Catalysts.

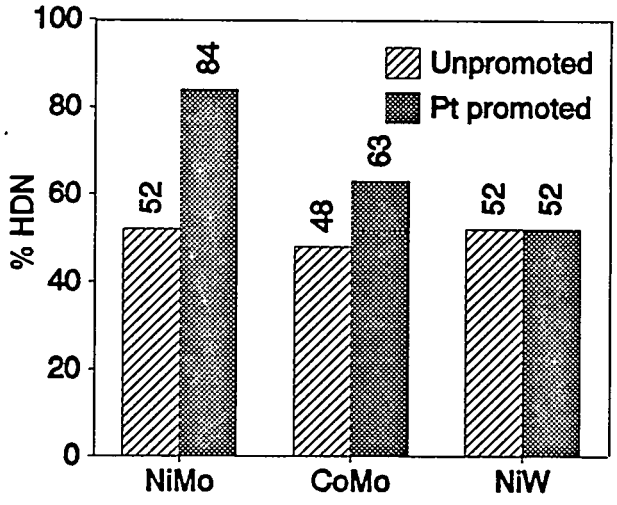

Figure 12 % HDN of Coal Liquid Upgrading Reaction

TASK II

Project II.5

LASER PYROLYSIS PRODUCTION OF NANOSCALE CATALYSTS FOR COAL LIQUEFACTION

Peter C. Eklund
Center for Applied Energy Research
University of Kentucky

Summary

During the first half of the past year our efforts were devoted to optimize the conditions for the laser pyrolysis synthesis of a variety of Mo-, Co-, Fe- and W- ultrafine particle (UFP) catalysts. These particles were prepared in the form of sulfides, nitrides, carbides and oxides in a pure, crystalline monophasic form. By modifying the reaction parameters and chemical precursors, we were able to prepare not only pure binary catalysts (e.g. MoS_2) as ultrafine particles, but also ternary UFP catalysts (e.g. $Fe_xMo_yS_z$) and a few supported ones (Mo_2N/SiO_2).

The first part of this report contains the results of the characterization of two of the systems recently prepared (MoS_2 and WS_2) using TEM, X-ray diffraction, Raman Spectroscopy and BET surface area. The remaining compounds are still being characterized.

The second part of this report contains the preliminary results obtained from the testing of the catalytic activity and selectivity of Mo_2N, Mo_2C and MoS_2 UFP catalysts during various model reactions to assess their benefit for coal liquefaction. The catalytic properties of the molybdenum based catalysts have been compared to those of a molybdenum-promoted sulfated hematite, the latter has been shown to be very active during coal liquefaction [1]. In addition, stability of these catalysts against chemical change has been examined using x-ray diffraction. Results from the activity and selectivity of these catalysts in various model compound reactions in which hydrogenation, desulfurization and deoxygenation occur, show that all molybdenum UFP catalysts prepared by laser pyrolysis are more active, on a per-surface-area basis, than the sulfated hematite, and that the MoS_2 is the most active.

In the next quarter, it is intended to complete the catalyst characterization via the study of quinoline hydrodenitrogenation and naphthyl-methyl bibenzyl hydrogenolysis. In addition, we will further explore the synthesis and testing of $Fe_xMo_yS_z$. We will investigate the synergistic benefit of having Mo and Fe on the same nanoparticle. Furthermore, additional efforts will be expended to investigate ways of improving the catalyst dispersion in coal. First, the coal will be impregnated by a colloidal suspension of the catalyst using a surfactant, and second, a means of depositing the as-synthesized particles directly onto a high surface area support will be investigated. Preliminary testing of some of our catalysts for processing plastic waste into hydrocarbon liquids may be initiated if time permits.

I. Synthesis and Characterization of crystalline Mo and W sulfide nanoparticles (MoS_2 and WS_2)

Our laser pyrolysis system is shown schematically in Fig. 1. The reactant gas mixture contains H_2S, C_2H_4 and a organometallic precursor. H_2S is introduced at the input to a cell heated close to the sublimation temperature of $Mo(CO)_6$ (150 °C) or $W(CO)_6$ (150 °C) (Aldrich, 99.9%) at 1 atm. C_2H_4 is then mixed into the reactant gas stream above the sublimation cell, as shown. The reactant gas mixture then flows vertically out of a central stainless steel tube (or nozzle) where it intersects a 120 Watt cw CO_2 laser (Laser Photonics Model 150), tuned to an absorption band (P20 line) of C_2H_4, forming a pyrolysis zone. The particles are thereafter entrained in inert gas and flow upward into a pyrex trap.

No evidence of carbide formation (Mo_2C) was detected by XRD or Raman scattering when H_2S was present in sufficient quantities. However, in the absence of H_2S Mo_2C (a superconducting carbide) forms readily. Similar to our studies of the formation of $Fe_{1-x}S$ (pyrrhotite) [3], we propose that the reaction pathway involves the thermal decomposition of $Mo(CO)_6$ to elemental Mo and CO, followed by the reaction of Mo with the H_2S to form the sulfide, while the C_2H_4 acts as a passive, heat absorbing species.

The nanoparticle production rate is approximately 2 g/h depending of the diameter of the nozzle. This large production rate makes it possible to evaluate these nanoparticles for practical applications as lubricants or catalysts. The as-synthesized nanopowders were handled in air after an "in situ" T = 300 K surface passivation in flowing 5% O_2 balanced by He. The reaction conditions used in the synthesis of Mo and W-disulfides, including laser intensity, chamber pressure, and reactant gas flow rate are given in Table 1.

II. Characterization of Mo and W sulfide nanoparticles

In Fig. 2 we display XRD data (dots) for nanocrystalline 2H-MoS_2 (Fig. 2a) and 2H-WS_2 (Fig. 2b) produced in our LP system. The average crystallite size was found to be 2.2 nm (MoS_2) and 3.6 nm (WS_2), estimated from the width of (002) diffraction peak using the Debye-Scherrer (DS) equation. The solid curve in each figure represents a sum of Lorentzian lineshapes riding on an exponential background βe^{-x} . The values used for the diffraction peak positions and peak areas were taken directly from a standard powder diffraction file. A single linewidth is used for all the peaks, and the curve was normalized to the height of the (002) diffraction intensity of our particles.

The powder diffraction file data are also plotted as thick vertical lines in the figure to indicate the standard line intensities and positions. It is clear from the figure that most peak positions match well with the standard powder data, indicating that our identification of the respective majority phase is correct. However, significant differences exist in the relative intensities of several diffraction lines between our nanoparticles and standard bulk powder data, which suggests either a lattice distortion, perhaps near the skin of the particle, or missing atoms.

In Fig. 3 is shown a TEM image of 2H-MoS_2 nanoparticles whose XRD data appear in Fig. 2. The particle size, as determined directly by bright field TEM, is about 5 nm (2H-MoS_2). In the same manner, the average particle size of 2H-WS_2 was estimated to be 9 nm. Thus it

appears that the TEM size exceeds the DS estimated size by a factor of two. However, the DS estimate is along the c-axis, and if platelets of these layer compounds have formed in LP, then the TEM image might be associated with the characteristic basal plane dimension. Higher resolution TEM studies are in progress to see if these nanoparticles are indeed platelets.

In Fig. 4a are displayed the Raman spectra at T=10K and 300K for LP-generated 2H-MoS_2 (Fig. 4a) and 2H-WS_2 (Fig. 4b) nanoparticles. The data were taken using the 488 nm Argon ion laser line in the Brewster-angle-backscattering configuration with the powder in a He atmosphere. At T=300 K, lines at 288, 351, 381 and 407 cm^{-1} are observed in the MoS_2 spectrum. The mode frequencies at 288 (E1g), 381 (E2g(1)) and 407 (A1g) are found in good agreement with those observed in the bulk, where the symmetry assignments for these 1st order intralayer modes appear in parentheses. At 10K, these modes upshift to higher frequency by ~ 2 cm^{-1}. Note that the linewidth of the E2g(1) and A1g modes is not T-sensitive, and this might be identified with a particle size-effect, i.e., the T-independent scattering of phonons from the particle surface. The mode at 351 cm^{-1} has not been reported in bulk MoS_2 , and exhibits resonant enhancement at the shortest excitation wavelengths. In Fig. 4b are displayed the Raman spectrum at T= 10K and 300 K for WS_2 nanoparticles also taken with the 488 nm line. Intralayer modes are observed at 356 and 420 cm^{-1} (A1g) mode, in agreement with data taken on bulk WS_2 , but the broader line at 356 cm^{-1} has been identified previously with second order scattering. The A1g mode in WS_2 exhibits a weak T-dependent contribution, indicative of the usual bulk thermal phonon scattering, which is consistent with the fact that the WS_2 particles are, on average, a factor of two larger than the MoS_2 nanoparticles [3].

In Fig. 5, we show the UV-vis absorption spectrum (solid line) at T= 300K for a colloidal suspension of MoS_2 particles in cyclohexane. For comparison, we display the a-face absorption spectrum (dots) of a bulk single crystal sample. Several peaks (A, B, C and D) appear in the bulk phase spectrum which have been identified with band-edge excitons. The full width at half maximum of the A and B exciton peaks at 300 K are 0.1 and 0.2 eV, respectively, indicated in the figure by the short vertical bars. It is clear from Fig. 5 that the excitonic features in our particles are significantly broadened. This broadening might be attributed to a particle size effect, i.e., the quantum confinement of excitons. An exciton size effect has been reported in thin single crystal MoS_2 plates with a ~100 nm thickness, about 20 times larger than our TEM-derived particle size.

III. Relative catalytic activity and selectivity of nanoscale Mo_2N, MoS_2, Mo_2C and Mo-promoted sulfated hematite in model compound reactions.

This section contains preliminary results of the catalytic activity and selectivity of Mo_2N, MoS_2, Mo_2C UFP and of a molybdenum-promoted sulfated hematite (denoted as $Mo/Fe_2O_3/SO_4$ or E5) for the hydrogenation of naphthalene, deoxygenation of diphenyl ether, hydrodesulfurization of benzothiophene and hydrogenolysis of bibenzyl. These model reactions were chosen to provide fundamental information useful in designing a ternary $Fe_xMo_yS_z$ catalyst.

The activity of Mo_2N for these model reactions listed above has been characterized at 380°C, 800 psig of H_2 and as function of reaction time. Results from the activity of the Mo_2C and MoS_2 catalysts have been obtained only for a reaction time of 30 minutes.

A. Catalyst Preparation

The sulfated hematite used for the model compound reactions was prepared by the aqueous precipitation of ferric ammonium sulfate and ammonium molybdate by the thermal decomposition of urea, followed by calcination in air at 475°C for 15 minutes [1]. The resulting catalyst is mainly composed of α-Fe_2O_3 with α-Fe as a minority phase and has a BET surface area of 150 m^2/g.

The experimental procedure for the preparation of the UFP catalysts has already been described in section I of this report. Table 2 summarizes the laser pyrolysis parameters for the Mo-based catalysts. The crystalline phases of the molybdenum UFP catalysts have been identified by x-ray diffraction as 2H-MoS_2, Cubic-Mo_2C and Gamma-Mo_2N

B. Experimental Procedure

The reactions were carried out using a 22 ml stainless steel horizontal microautoclave reactor. Five grams of a solution that contained 5 wt% of model compound in hexadecane were charged into the reactor for each reaction run. Note that no hydrogen donor solvent was added to the reaction mixture. Thermal runs were conducted to determine the background conversion. In addition, experiments using only hexadecane, with and without catalyst, were carried out to determine the extent of cracking under the reaction conditions. The catalyst was loaded at 5 wt% with respect of model compound. For the sulfiding experiments, dimethyl disulfide (DMDS) was added as a sulfur source at 20% excess of the stoichiometric amount to convert all the Fe in the hematite catalyst to FeS_2. In the case of Mo_2N, DMDS was added at three times the stoichiometric amount of sulfur required to form MoS_2. After loading, the reactors were purged and pressurized to 800 psig (cold) with hydrogen and then placed in a heated fluidized sand bath set at 380°C and agitated vertically at 400 cycles/min. The reaction time was varied between 15 to 60 minutes after which the reactor was quenched in a cool sand bath. The liquid products were analyzed with a Hewlett Packard 5890 Series 2 gas chromatograph equipped with a 30 m fused silica capillary column (DB5) and a 30 m carbowax column.

C. Results

C.1. Naphthalene Hydrogenation

Mo_2N, Mo_2C, MoS_2 and the sulfated hematite (E5) were tested for naphthalene hydrogenation activity under identical reaction conditions. In the case of naphthalene hydrogenation the main reaction product was tetralin and only trace amounts of decalin were found.

Figure 6 shows the naphthalene conversion for the sulfated hematite (E5) and for Mo_2N with and without DMDS added. It is observed that under thermal conditions 7% of naphthalene was converted to tetralin after 60 minutes of reaction time, while addition of sulfur as DMDS increased the conversion to 19%. This indicates the catalytic effect of the sulfur alone on the conversion of naphthalene to tetralin. The reaction over the sulfated hematite did not induced any increase in conversion compared to the thermal background whereas the addition of DMDS to the reaction mixture increased the conversion to 82%. X-ray diffraction of this catalyst showed

the transformation of the hematite to the pyrrhotite form which is considered to be the active phase of the iron catalysts for coal liquefaction.

In the case of the unsulfided molybdenum nitride the overall napthalene conversion was 59% and addition of sulfur did not affect the conversion of the reactant. Suggesting that the Mo_2N is not transformed to the sulfided phase. This has been confirmed by x-ray diffraction analysis of this catalyst which shows that the Mo_2N is still the majority phase after one hour of reaction time.

In order to compare the relative activity of the different molybdenum-based catalysts, the hydrogenation of naphthalene was carried out over MoS_2 and Mo_2C at 380°C for 30 minutes. Table 3 shows the results of the activity under these conditions

Table 3

Naphthalene hydrogenation activity after 30 minutes of reaction at 380°C

Catalyst	Surface Area (m^2/g)	Conversion	($mol_{react}/mol_{fed}.m^2$).$10^{4*}$
E5	150	4.03	2.7
E5+S	150	43.6	29.0
Mo_2N	63	26.8	42.5
Mo_2N+S#	63	28.7	45.5
MoS_2	84	45.9	62.9
Mo_2C	75	27.3	40.1

* mol of naphthalene reacted/(mol of naphthalene added).(meter of catalyst).
# sulfur added as DMDS

Notice that the molybdenum based catalysts were found to exhibit higher specific activity than the sulfated hematite even with sulfur added. Furthermore, the most active catalyst under these reaction conditions was found to be the molybdenum disulfide. A

comparison of these results to those reported on the same reaction but using molybdenum naphthenate and commercial $NiMo/Al_2O_3$ shows that our UFP and the sulfated hematite are not as active hydrogenation catalysts as the Mo naphthenate. In those cases, conversions close to 100 % and the presence of decalin were observed but higher hydrogen pressures were employed. In addition, all catalysts exhibited low selectivity to hydrocracking of the tetralin to butyl benzene as the mechanism suggested [4].

One of the possible reasons is the low degree of dispersion that the UFP catalysts may have during the reaction conditions precluding the total exposure of the active sites and decreasing their activity.

C.2. Diphenyl Ether Deoxygenation

Figure 7 presents the conversion of diphenyl ether (DPE) versus reaction time under thermal and catalytic conditions. It is observed that for this reaction, UFP Mo_2N is a more active catalyst than the sulfated hematite (E5) even in the presence of added sulfur. Under thermal conditions, the conversion reached 21% without sulfur, whereas in the presence of excess sulfur, it decreased to 12%. In the case of E5, the conversion reached 26% after 60 minutes of reaction time, and as in the case of the naphthalene reaction, the addition of excess sulfur proved to be beneficial for E5 since the conversion increased to 39%. This effect was the opposite seen for the reaction using Mo_2N, in this case the conversion reached 53% without sulfur and only 20% when sulfur was present.

Selectivity

Figure 8 shows the normalized product distribution for the iron and molybdenum based UFP catalysts reacted at 380°C for 30 minutes. It is observed that the main products of the DPE reaction are benzene and phenol. In the case of E5, the concentration of both benzene and phenol is about 10% whereas in the case of the sulfided hematite their concentrations reached about 16%. Overall the most active catalyst was the MoS_2 followed by Mo_2N and Mo_2C. In the case of MoS_2 benzene was almost 4 times more abundant than phenol. In addition, MoS_2 gave higher concentration of hydrogenated compounds, cyclohexanol and cyclohexane (11mol %) than Mo_2N and Mo_2C (5 mol% and 6 mol% respectively).

C.3. Bibenzyl Hydrogenolysis

Under the reaction conditions employed during this study, bybenzyl showed to be very stable both thermally and in the presence of the catalyst. The overall conversion, less than 2%, yielded toluene as main product. No hydrogenation products were detected from this reaction even when tetralin was added as a hydrogen donor. Increase in bond cleavage was observed when the reaction temperature was raised from 380°C to 400°C. This is probably due to the higher bond strength of the C-C bond in the bibenzyl molecule compared to the C-O in the diphenyl ether.

C.4. Hydrodesulfurization of Benzothiophene

Figure 9 presents the time dependence of the activity of Mo_2N and E5 for benzothiophene conversion. Both catalysts exhibited high activity for benzothiophene (BZT) conversion even after short periods of reaction time. The addition of excess sulfur in the form of DMDS to both catalysts produced an increase in the conversion of benzothiophene whereas for the thermal reactions, it caused a decreased in conversion by almost 50%. After 30 minutes of reaction time the conversion over Mo_2N was 77%, 95% for Mo_2N+S, 95% for E5 and 100% for E5+S. Thus, E5+S has the highest overall activity for BZT conversion. After 60 minutes BZT reacted completely over Mo_2N and E5 with and without sulfur added.

Selectivity

Finally, Figure 10 presents the normalized product distribution of the reaction products formed at 380°C after 30 minutes of reaction time. The main product of the reaction over all catalysts is ethylbenzene followed by dihydrobenzothiophene(HBZT), which constitutes an intermediate in the reaction pathway to ethylbenzene [4]. It is observed that in case of Mo_2N alone, about equal amounts of benzothiophene and dihydrobenzothiophene are produced. When DMDS was added to this catalyst, the conversion of benzothiophene increased (reflected by the reduction in the height of the BZT bar) but also that the fraction of dihydrobenzothiophene decreased thus producing more ethylbenzene. In the case of the MoS_2, all the benzothiophene was converted to ethylbenzene with ethylcyclohexane and methylcyclohexane present in less quantity. Similar to the case of the Mo_2N, addition of sulfur to the E5 catalyst induced an increase in conversion of the benzothiophene to ethylbenzene with less formation of the hydrogenated intermediate.

IV. References

1. G.T. Hager, E. Givens, F.J. Derbyshire, ACS Preprints, Div. Fuel Chemistry 38(3) 1087(1993).

2. P. C. Eklund, Xiang-Xin Bi, and F.J. Derbyshire, Preprints of Fuel Division, American Chemical Society, Vol. 37(4), 1781(1992).

3. Xiang-Xin Bi, Y. Wang, W.T. Lee, Kai-An Wang, S. Bandow and P. C. Eklund, Proc. of Mater. Res. Soc. Meeting, Symposium N, Boston, Nov.28-Dec.3, 1992.

4. H. Kim and C.W. Curtis, Energy & Fuel 4(2) 20 (1990).

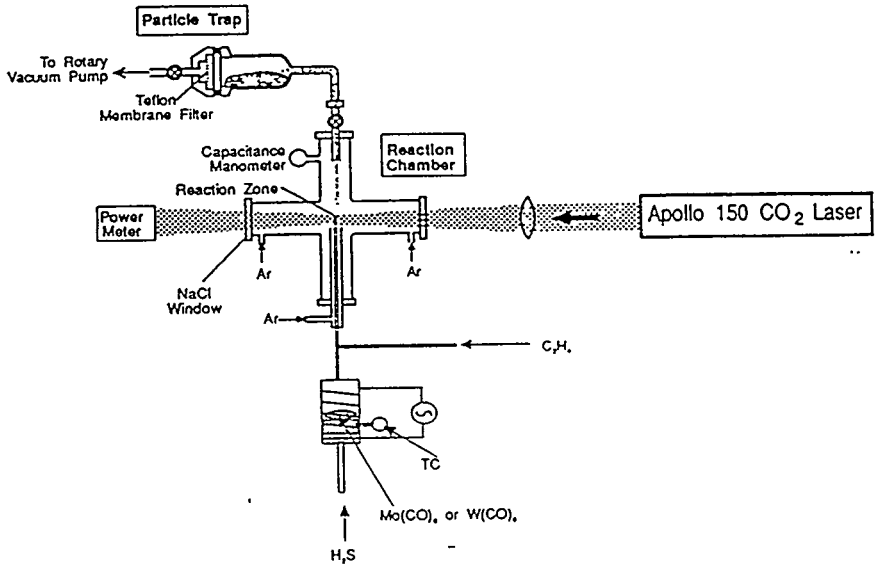

Fig. 1 CO_2 laser pyrolysis system.

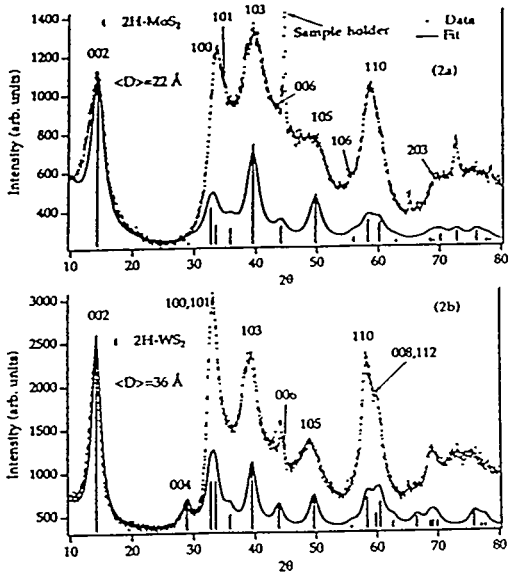

Fig 2 Cu(Kα) X-Ray diffraction data(dots) for nanocrystalline MoS2(2a) and WS2(2b). Solid lines are calculated (see text) from standard powder diffraction data represented by thick vertical lines.

Table 1 Typical laser pyrolysis reaction parameters used to generate MoS_2 and WS_2 nanocrystalline particles.

	MoS_2	WS_2
Laser Intensity (W)	100	100
Beam Width (mm)	1	1
Chamber Pressure (Torr)	200	200
C_2H_4 Flow Rate (sccm)	70	70
H_2S Flow Rate (sccm)	70	70

Table 2

Laser Pyrolysis Preparation Parameters of Mo_2N, MoS_2 and Mo_2C

	Mo_2N	Mo_2C	MoS_2
Laser Intensity	114W	110W	110W
Beam Width (mm)	1	1	1
Chamber Pressure(Torr)	200	200	200
C2H4 Flow Rate(sccm)	-	80	60
H2S Flow Rate(sccm)	-		70
NH3 Flow Rate(sccm)	80	-	-

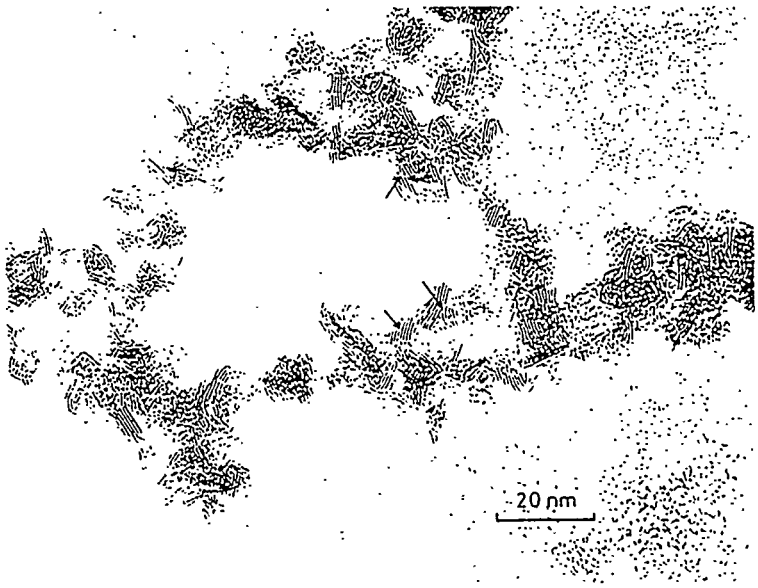

Fig. 3 Bright field TEM images for nanocrystalline MoS_2

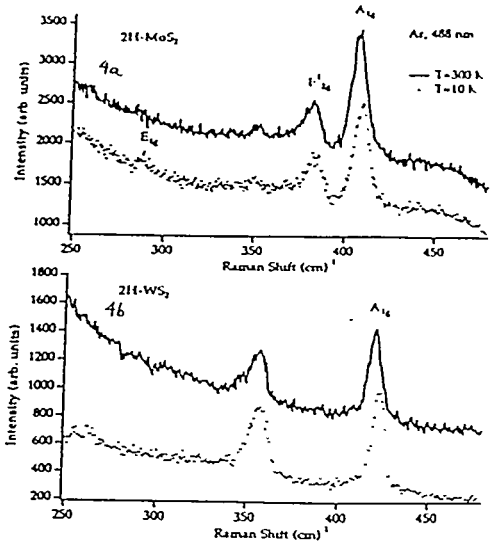

Fig. 4 Raman spectra of MoS_2(4a) and WS_2(4b) nanoparticles at T=300 and 10 K.

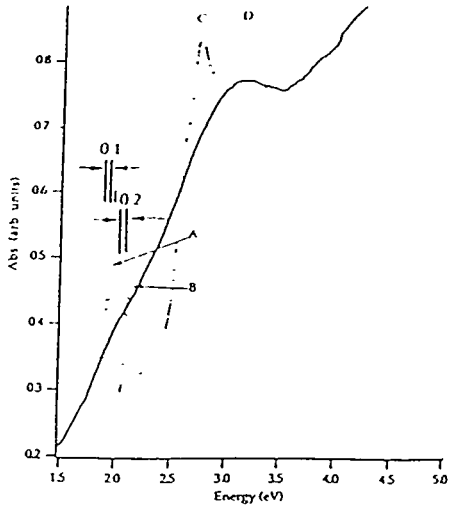

Fig. 5 UV vis. absorption spectrum(solid line) for a colloidal suspension of MoS_2 particles in cyclohexane The dotted line is the absorption spectrum for bulk phase MoS_2 single crystal at 5K. The full width at half maximum of the excitonic peaks for bulk MoS_2 at 300K are indicated in the figure.

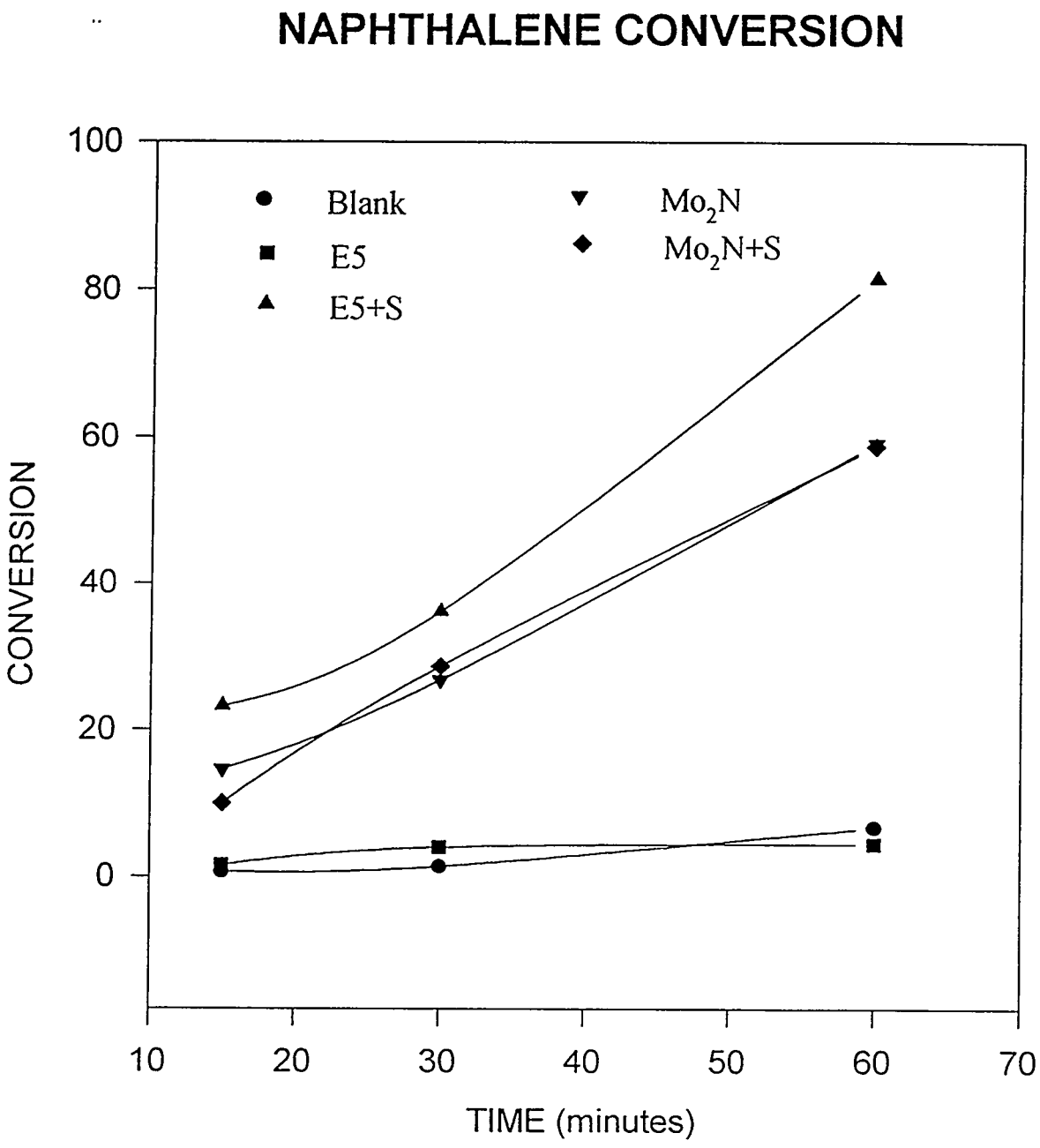

Fig. 6 Naphthalene Conversion over molybdenum nitride and a molybdenum promoted sulfated hematite.

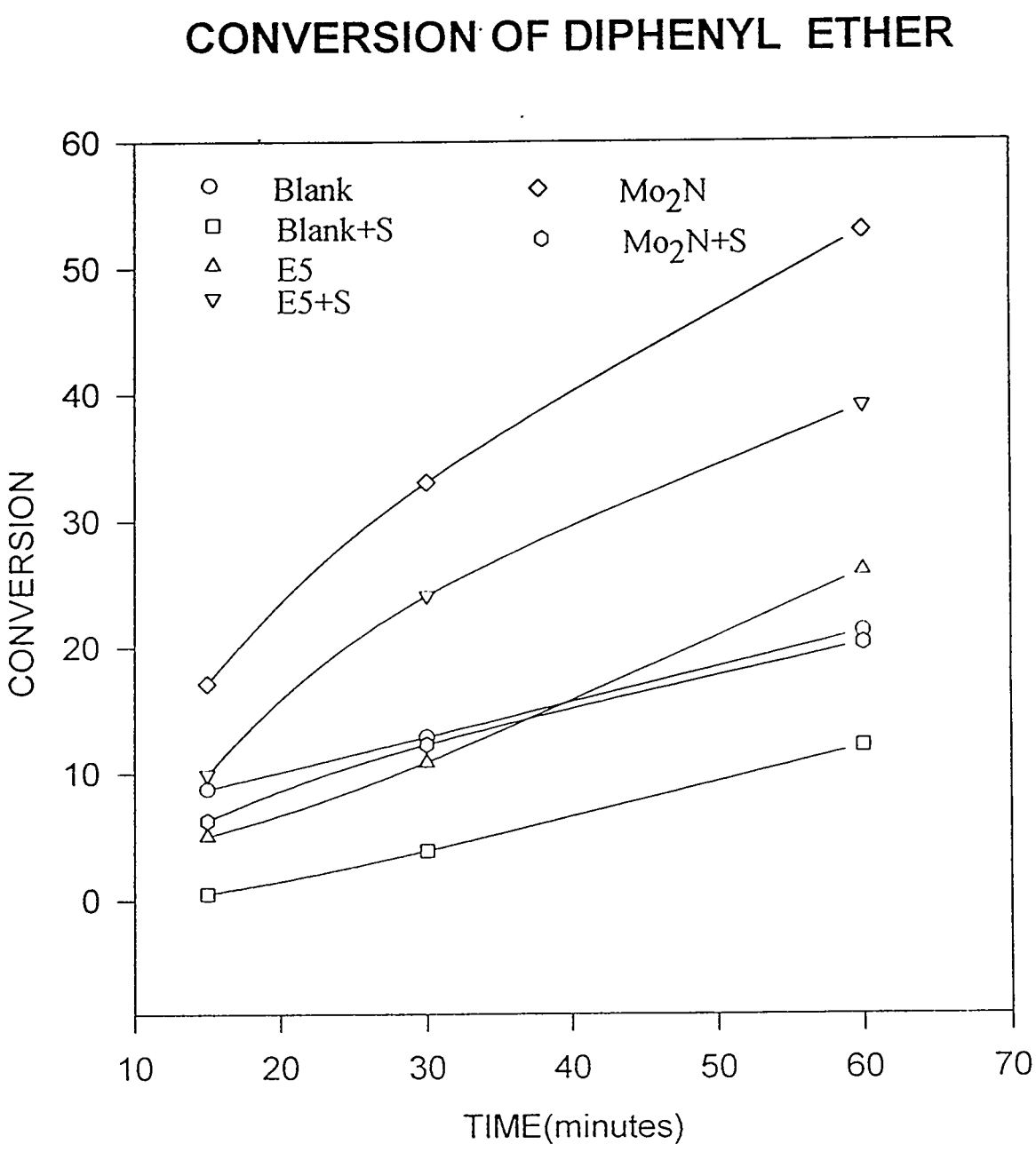

Fig. 7 Conversion of Diphenyl ether over molybdenum nitride and a molybdenum promoted sulfated hematite (E5) as a function of reaction time.

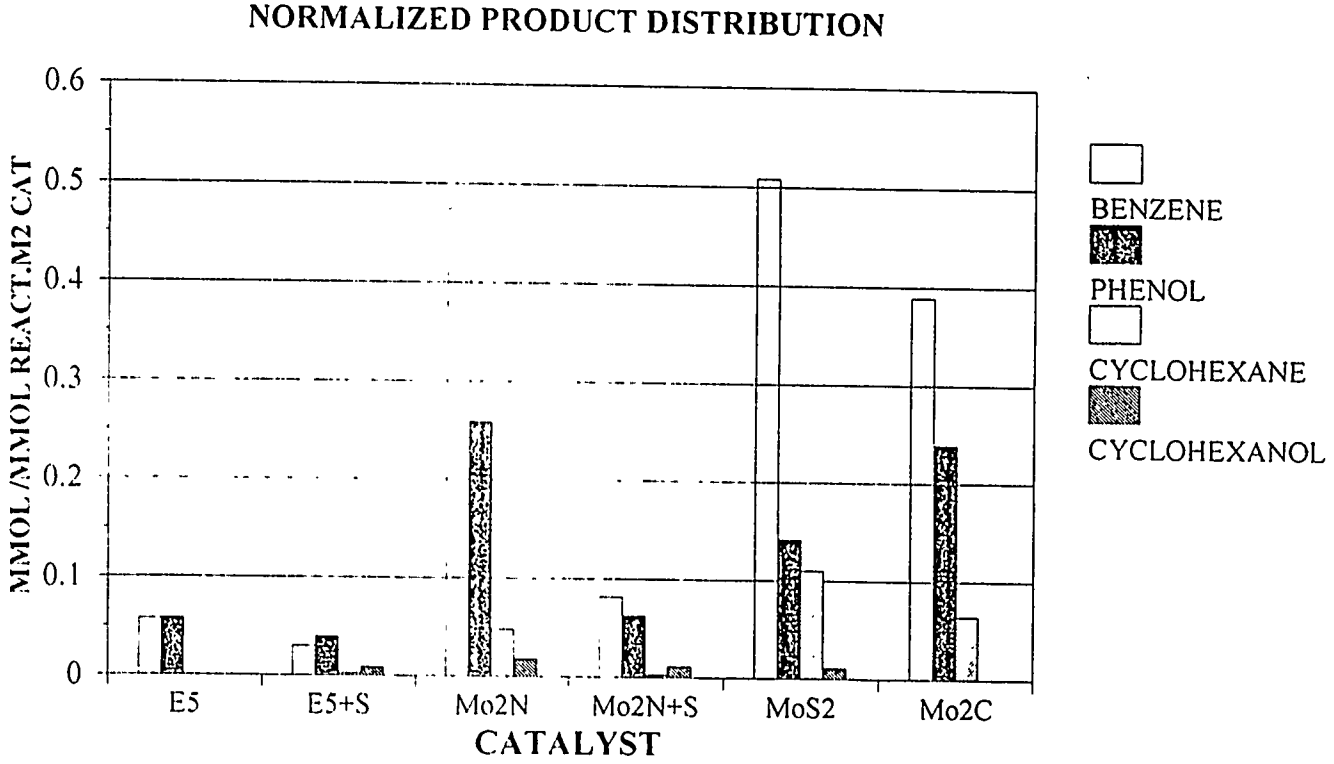

Fig. 8 Normalized product distribution from the reaction of diphenyl ether over Mo_2N, MoS_2 and Mo_2C and E5.

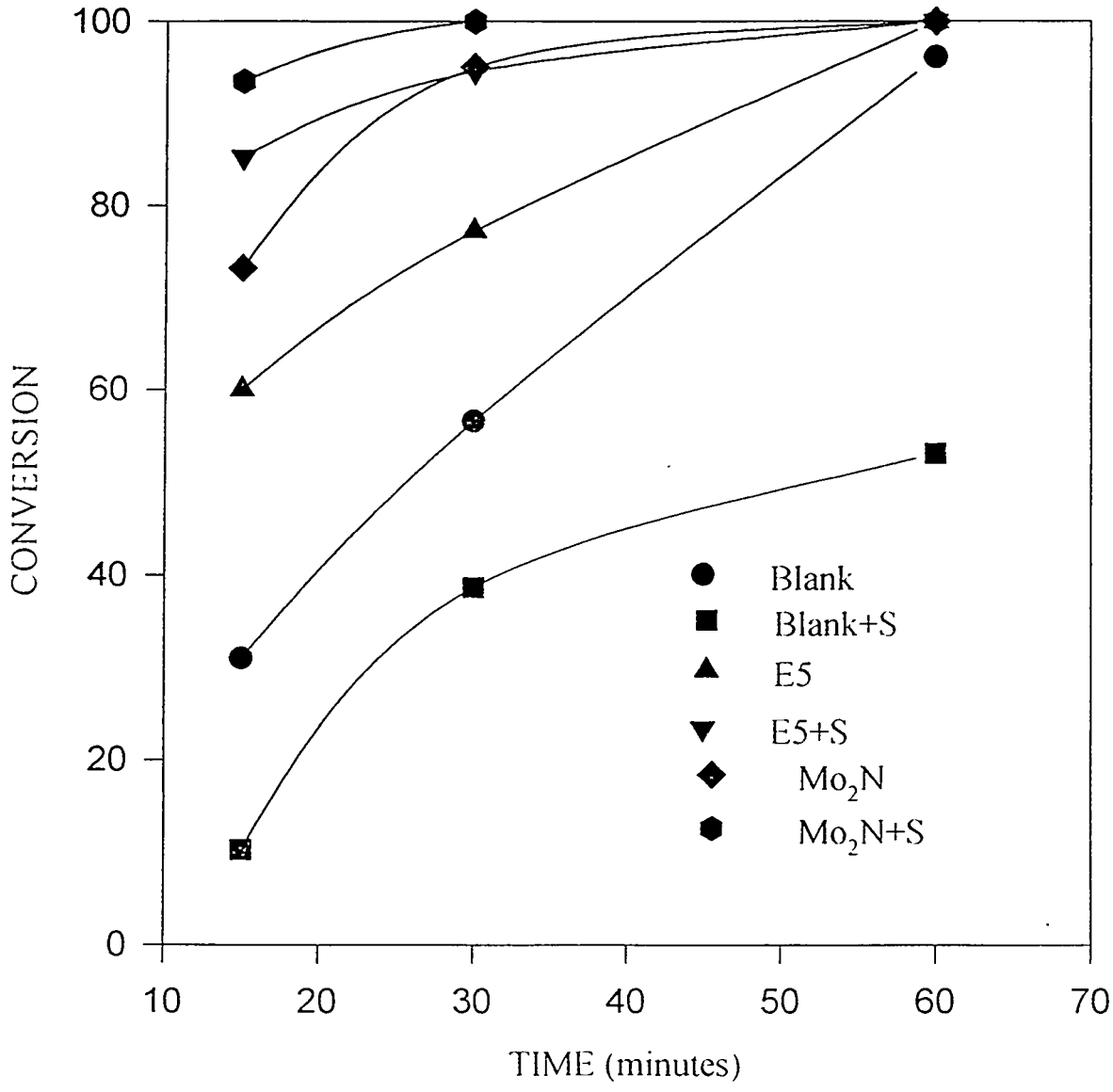

Fig. 9 Conversion of Benzothiophene over Mo_2N and E5.

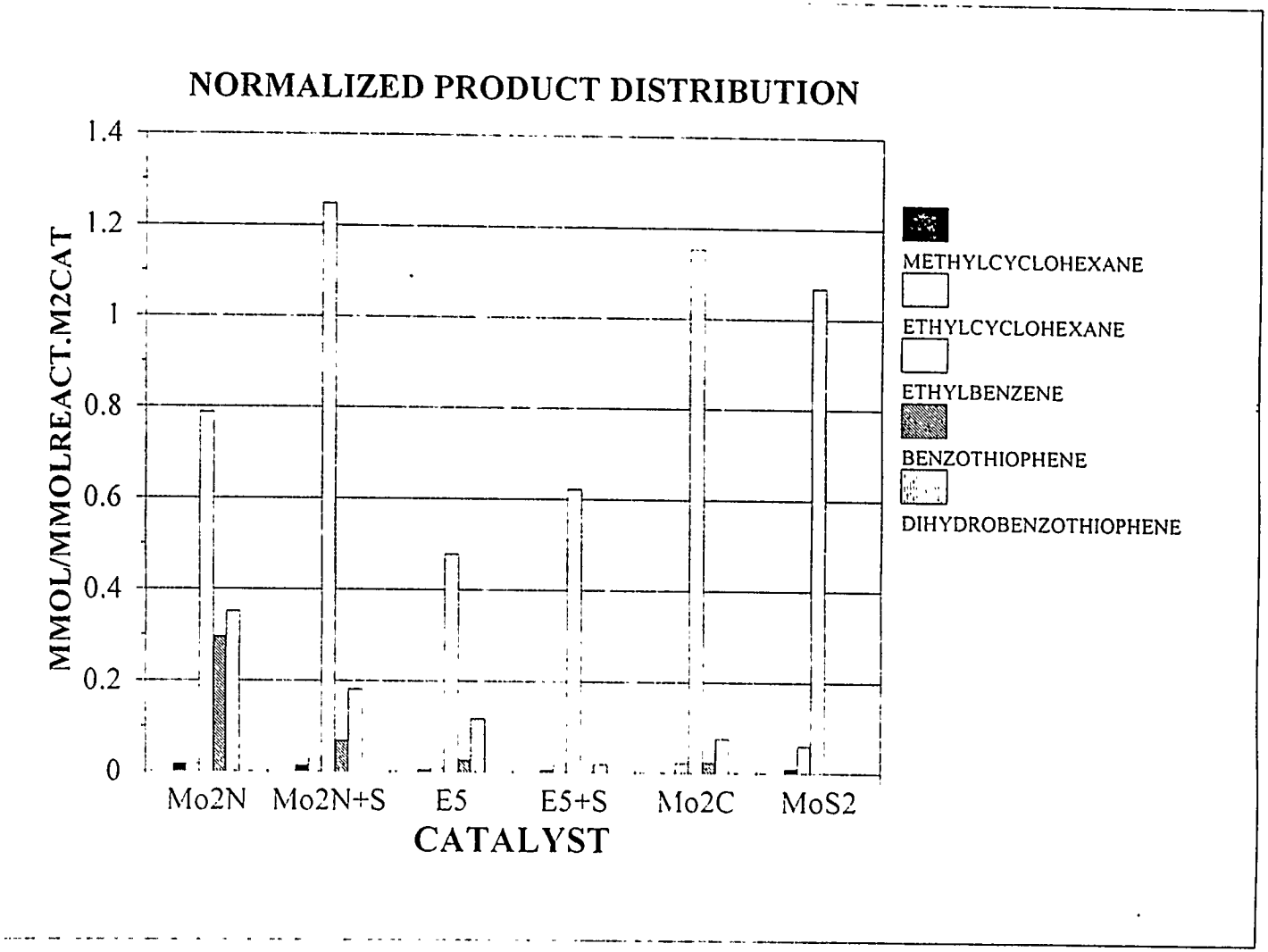

Fig. 10 Normalized product distribution from the reaction of benzothiophene over Mo_2N, MoS_2 and Mo_2C and E5.

TASK II

Project II.6

NOVEL CATALYSTS FOR COAL LIQUEFACTION

Jianmin Zhao, Zhen Feng, M.M. Taghiei, F.E. Huggins, G.P. Huffman
University of Kentucky

Development of new binary ferrihydrite catalysts

We started our investigation with characterization studies of the Mach I, 30-A catalyst, a pure ferrihydrite phase [1,2]. Although the catalyst has a very high surface area (>200 m^2/g), it is not able to maintain its dispersion at high temperatures; it quickly agglomerates and transforms to hematite of much lower surface area at temperatures >250°C [3, 4]. This problem has been resolved by adding a small amount of impurity cations (M) during precipitation to form a binary ferrihydrite catalyst (M/FHYD). The adsorbed impurity ions effectively inhibit particle agglomeration at higher temperature, allowing the catalyst to maintain its dispersion, which results in more active catalysts for DCL [4-7].

A number of binary ferrihydrite catalysts with M = Si, Al, Mo, P, Zn, and organic acids (M/Fe $\approx$ 5%) have been synthesized in our laboratory. These catalysts are structurally similar to that of pure ferrihydrite, but with a modified surface due to chemisorbed impurity anions (M). The chemical environment of the Mo in Mo/FHYD has been investigated using XAFS spectroscopy [6]. The radial structure functions (RSFs) of the EXAFS spectra for two Mo/ferrihydrite catalysts and a $Mo/Fe_2O_3/SO_4$ catalyst provided by Dr. Wender are shown in Figure 1. The spectra indicate the chemical environments of Mo in the samples are very similar. Least square fitting of the spectra shows that Mo is coordinated by 3 - 4 oxygens at ~ 1.7 A. This distance is very close to that observed for tetrahedrally coordinated Mo in Mo^{6+} oxides and molybdates. The spectra also show little structure beyond the first oxygen shell, suggesting that Mo probably has incomplete coordination shells beyond the first oxygen shell. Therefore, Mo is likely to be at the ferrihydrite surface and the $Mo/Fe_2O_3/SO_4$ catalyst surface. ESR and SQUID measurements conducted by Dr. Seehra (WVU) and XPS measurements conducted by Dr.

Reucroft (UK) on a series Si/ferrihydrite samples have also confirmed that Si is concentrated at the surface.

The presence of impurity anions at the ferrihydrite surface inhibits the phase transformation of ferrihydrite to hematite. With Si : Fe = 0.05, the Si/FHYD catalyst can maintain its dispersion to as high as 425°C, whereas the 30-Å catalyst readily converts to large particle hematite at 250°C, as shown in Figures 2 and 3.

DCL tests have been performed on Si/FHYD and citric acid-treated ferrihydrite CA/FHYD catalysts with DECS-17 and Black Thunder coals. The results, along with those for thermal reactions and reactions using the Mach I catalyst, are summarized in Table 1. Improvement of both total yields and oil yields are obtained with the binary ferrihydrite catalysts.

The advantages of the binary ferrihydrite catalysts may be summarized as follows: (i) low cost: it requires only low grade chemical compounds (ferric nitrate) and is synthesized with one step precipitation; (ii) it is DCL active; (iii) has the potential for further improvement by choosing the proper impurity anions to make the catalyst more active and selective.

Studies of the $Fe_{1-x}S$ formed by sulfidation of binary ferrihydrite catalysts

Most studies of iron catalysts for direct coal liquefaction (DCL) have focused on the oxide phases. In a precise definition, however, the iron oxide catalyst is actually the catalyst precursor. It converts to a pyrrhotite ($Fe_{1-x}S$) under DCL reaction conditions, and it is generally believed that $Fe_{1-x}S$ is the active catalyst. Therefore, the dispersion of the oxide phase does not guarantee the dispersion of the pyrrhotite phase. Srinivasan et al [8] showed that, after sulfidation, the highly dispersed ferrihydrite catalyst, (30-A), converts to large size (> 1000 A), hexagonal shaped crystals of pyrrhotite. It is therefore of interest to study the structure, dispersion and morphology of the pyrrhotite phase formed from the binary ferrihydrite catalysts under the sulfidation condition present in DCL.

Sulfidation experiments were conducted in a tubing bomb reactor under simulated coal liquefaction conditions, but without the coal. Three catalysts, a pure ferrihydrite (30-A), a Si/ferrihydrite with Si:Fe = 0.05 ($Si_{0.05}$/FHYD), and a citric acid treated ferrihydrite (CA/FHYD) were tested. The samples after sulfidation were analyzed with X-ray diffraction (XRD), Mossbauer spectroscopy, and transmission electron microscopy (TEM).

The XRD patterns of the three sulfided samples, together with a $Fe_{1-x}S$ standard, are shown in Figure 4. The XRD patterns for the sulfided Si/FHYD and CA/FHYD catalysts show broad diffraction peaks as compared to those exhibited by the sulfided pure ferrihydrite; such broadening is usually an indication of smaller particle size. The XRD for the sulfided Si/FHYD also has broad shoulders on the high 2θ side of the diffraction peaks, which may be attributed to disorder effects caused by incorporation of the Si in the $Fe_{1-x}S$ structure.

After sulfidation at 350°C, TEM for the 30-A catalyst show that the catalyst converted to a well crystallized pyrrhotite, $Fe_{1-x}S$, in agreement with a previous investigation carried out at 400°C [8]. The $Fe_{1-x}S$ phase formed from the binary ferrihydrite at 400°C exhibits much smaller and more irregularly shaped particles than those formed from the 30-A catalyst at 350°C. These TEM results indicate that the binary ferrihydrite catalysts promote the formation of a dispersed $Fe_{1-x}S$.

We plan to investigate further the effect of the sulfidation conditions on the structure and morphology of $Fe_{1-x}S$ phases synthesized with various binary ferrihydrites and test the DCL activity of these $Fe_{1-x}S$ phases.

Studies of the iron phase for an impregnated iron catalyst on coal

The effectiveness of impregnation of iron catalysts on coal for direct coal liquefaction (DCL) has been known since 1950 [9]. The technique has been modified recently by PETC scientists [10]. The major disadvantage of the technique is that the procedure requires pretreatment of coal in a solvent.

The idea and the method of impregnation of catalysts on coal are in fact derived from synthesis of supported catalysts. It is generally believed that the impregnation improves catalyst dispersion, a matter of fact for the supported catalysts [9, 10]. However, there is a doubt whether impregnation indeed takes place on coal. The success of impregnation depends not only on the procedure, but also on the morphology of the supports: the support must have a pore structure to provide favorable for impregnation. Supports such as SiO_2 and Al_2O_3 have enormous surface areas of >200 m^2/g (measured by N_2 chemisorption) and 95% of the surface area is contributed by mesopores (2 - 50 nm) and macropores (> 50 nm). These mesopores and macropores are the sites for impregnation. Although coal does have pores, it has a much smaller surface area of ~ 2 m^2/g (measured by N_2 chemisorption).

The iron phase formed by the PETC impregnation method (incipient wetness precipitation/impregnation, [10]) is actually ferrihydrite. Based on our experience with this material, we reasoned that the activity of the impregnated catalyst on coal is probably similar to that for the binary ferrihydrite catalysts. As the coal powder is mixed with the solvent, a considerable amount of impurity anions will be dissolved into the solvent and subsequently adsorbed at the precipitated ferrihydrite surface. Therefore, the activity of the impregnated catalyst is due to anti-agglomeration of ferrihydrite particles, rather than dispersion by impregnation.

What we shall prove are as follows: (a) the surface of the ferrihydrite particles formed by impregnation is chemisorbed with impurity anions; (b) the ferrihydrite particles are not well separated as the name "impregnation" implies; (c) similar coal liquefaction results can be obtained using binary ferrihydrite catalysts.

Superparamagnetic measurements using Mossbauer spectroscopy for nanoscale particles provide information about the surface properties and the interaction between the particles. For small particles, as the temperature decreases, the Mossbauer spectra exhibit a transition from paramagnetic (2-line absorption lines) to magnetic (6-line absorption line) [11]. The superparamagnetic blocking temperature T_B is defined as the temperature at which a complex intermediate phase is seen,

$$T_B = \text{const} \cdot K\,V \qquad (1)$$

where K is the ansiotropy energy and V the volume of the particle. The anisotropy energy is a measure of the energy required to rotate the magnetization direction. The anisotropy energy K is contributed by interaction, exchange, and surface anisotropy energies. All these three anisotropy energies are influenced by surface adsorption.

From the temperature dependency of the Mössbauer spectra, T_B, for the pure FHYD, impregnated coal, and citric acid treated FHYD (CA/FHYD) are estimated to be 70 K, 38 K, and 35 K, respectively (Figure 5, 6). The temperature dependence of the first Mössbauer moment, a parameter obtained from the Mössbauer spectrum without fitting that shows promise for describing superparamagnetic transitions [12], is shown in Figure 7 for the three catalysts. The decrease of T_B is mainly attributed to surface adsorption of nonmagnetic ions

which leads to decrease of the surface anisotropy energy [13]. SQUID measurements by Prof. Seehra for a series of binary ferrihydrite catalysts also indicate that T_B decreases consistently as the surface adsorption of nonmagnetic ions increases. In addition to T_B, the spectra show the differences in the behavior of the magnetic phase transition among the samples. For the pure ferrihydrite, the transition from paramagnetic to magnetic occurs between 35 and 100 K, whereas for CA/FHYD and impregnated catalyst, it occurs at a narrower temperature range of 25 to 50 K. The complex features of the intermediate phases is mainly due to the exchange and interaction anisotropy energies. The rotation of the magnetization direction of a particle is influenced by the magnetization directions of its neighboring particles. For pure ferrihydrite, the particles are in intimate contact with each other, hence the exchange and interaction anisotropy energy is maximum. Therefore, free rotation of the magnetization direction is prohibited and the Mossbauer spectra exhibit a complex intermediate in wide temperature range. With chemisorbed impurities, the exchange and interaction anisotropy energy is weaker and the rotation of magnetization direction depends less on those of its neighbors. Therefore a sharper transition is seen. Again, the phase transition behavior for the impregnated catalyst is very similar to that for CA/FHYD. The results suggest that the particles in the impregnated catalyst is adsorbed with impurities. However, they are not completely separated from each other as the name "impregnation" suggests. If the particles were indeed impregnated, exchange and interaction will be virtually zero, and a much sharp transition is expected.

Comparison coal liquefaction experiments with the binary ferrihydrite catalyst and impregnated catalysts are in progress.

References

1. G. P. Huffman, B. Ganguly, J. Zhao, K. R. P. M. Rao, N. Shah, Z. Feng, F. E. Huggins, M. M. Taghiei, F. Lu, I. Wender, V. R. Pradhan, J. W. Tierney, M.S. Seehra, M. M. Ibrahim, J. Shabtai, E. M. Eyring, ***Energy & Fuels*** **7,** 285 (1993).

2. J. Zhao, F. E. Huggins, Z. Feng, F. Lu, N. Shah, G. P. Huffman, ***J. Catal.*** **143**, 499 (1993).

3. Z. Feng, J. Zhao, F. E. Huggins, and G. P. Huffman, ***J. Catal.*** **143,** 510 (1993).

4. J. Zhao, F. E. Huggins, Z. Feng, and G. P. Huffman, submitted to ***Clays and Clay Minerals.***

5. J. Zhao, Z. Feng, F. E. Huggins, and G. P. Huffman, ***Energy & Fuels*** **8**, 38 (1994).

6. J. Zhao, Z. Feng, F. E. Huggins, N. Shah, G. P. Huffman, and I. Wender, ***J. Catal.*** (1994), in the press.

7. J. Zhao, Z. Feng, F. E. Huggins,and G. P. Huffman, ***Energy & Fuels*** **8,** in press (1994).

8. R. Srinivasan, R. A. Keogh, and B. H. Davis, preprint paper, ACS, Div. Fuel Chemistry, 37, 1265 (1993).

9. S. W. Weller, ***Energy & Fuels*** **8,** 415 (1994).

10. A. V. Cugini, D. Krastman, D. V. Martello, E. F. Frommell, A. W. Wells,and G. D. Holder, ***Energy & Fuels*** **8,** 83 (1994); B. R. Utz and A. V. Cugini, ***U.S Patent*** 5,096,570, (1992).

11. B. Ganguly, F. E. Huggins, K. R. P. M. Rao, and G. P. Huffman, ***J. Catal.*** **142,** 552 (1993).

12. S. Mørup, B. S. Clausen, and H. Topsøe, H. ***J. Physique*** **40,** C2-78 (1979).

13. F. E. Huggins and J. Zhao, work in progress.

Table 1. DCL results of binary ferrihydrite catalysts

Coal: 5 g.
tetralin: 10 g.
Catalyst /coal: 0.6 : 100 (iron content)
DMDS/catalyst: 2/1
Reaction: 1 hour, 1000 psi.

(a) DECS-17 Coal, 410°C

catalyst	oil	gas	asph	preasph	total yield
thermal	31.2	2.4	37.6	9.5	80.9
30-Å	33.1	2.8	50.2	0.6	86.6
Si/FHYD	35.7	3.1	42.6	5.0	86.4
CA/FHYD	36.8	2.9	42.3	2.5	84.5

(b) Black Thunder Subbituminous Coal, 415°C

catalyst	oil	gas	asph+preasph	total yield
thermal	35.4	6.4	45.0	87.0
30-Å	40.3	6.6	44.2	91.1
CA/FHYD	44.7	6.2	40.2	90.5

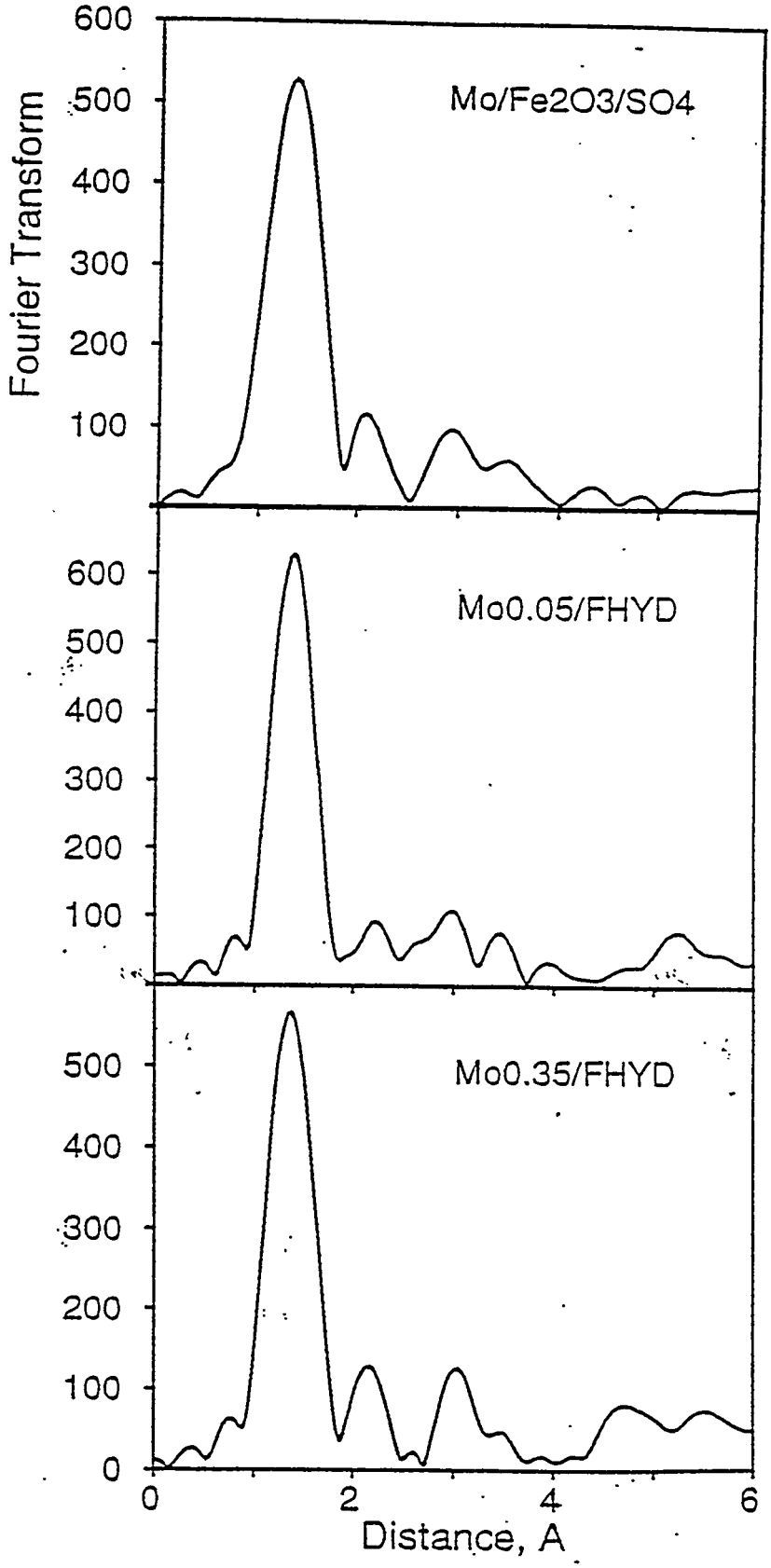

Fig 1. Mo K-edge XAFS radial structure functions for $Mo/Fe_2O_3/SO_4$, $Mo_{0.05}$/FHYD, and $Mo_{0.35}$/FHYD.

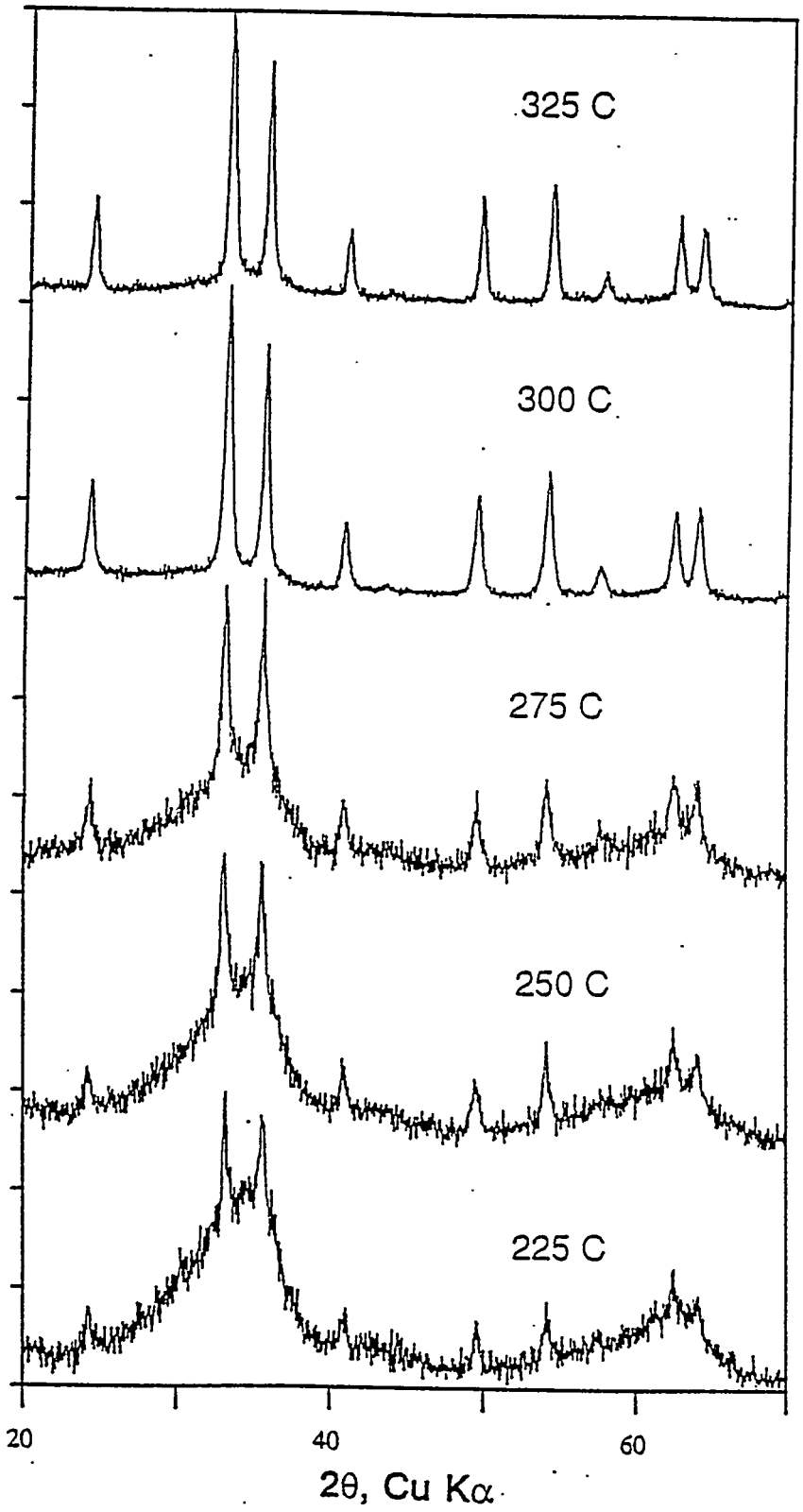

Fig 2. XRD patterns for the 30-Å catalyst after annealing at 225 - 325°C. Hematite (sharp diffraction lines) starts to form at 250°C.

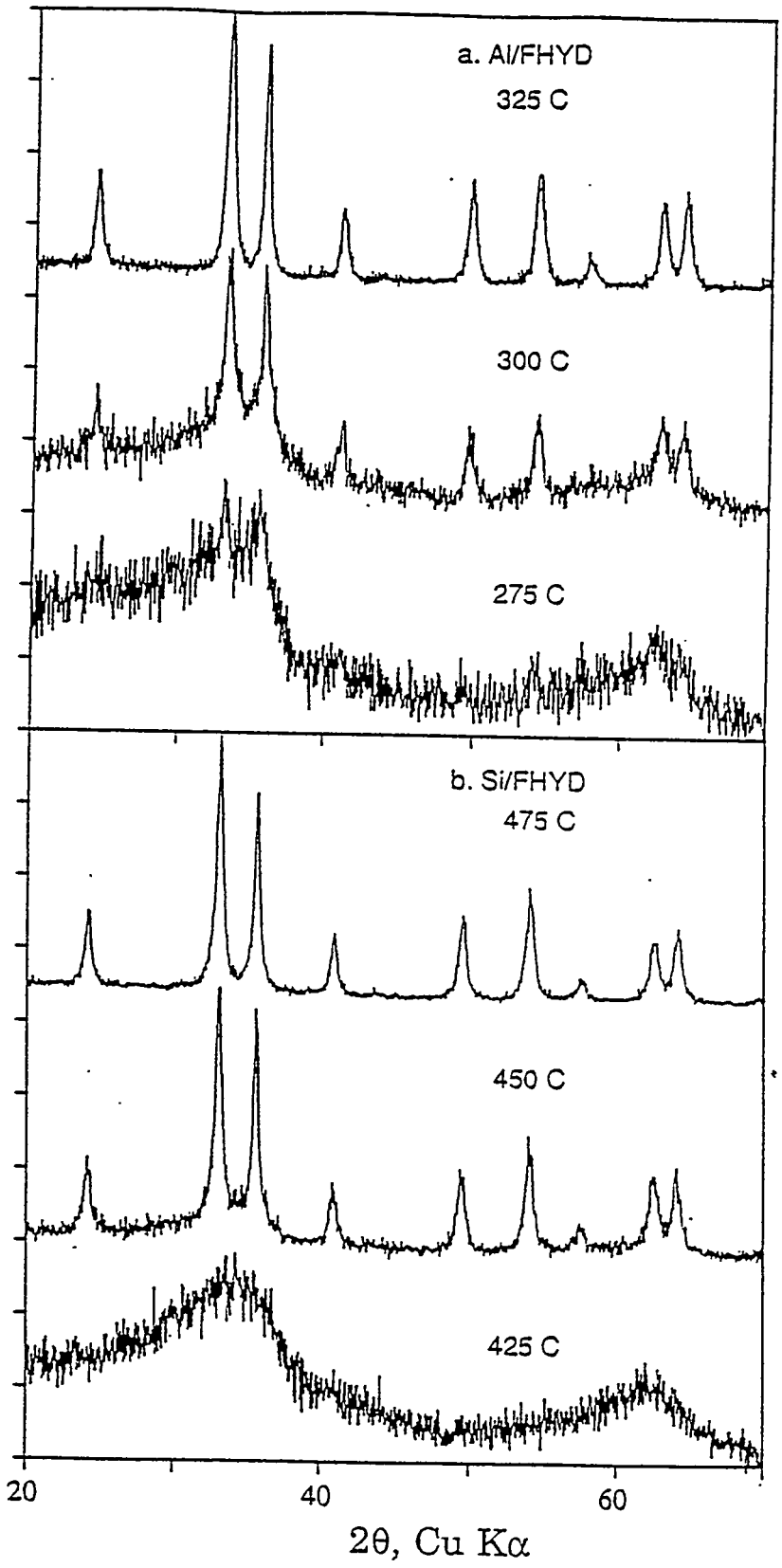

Fig 3. XRD patterns for the $Al_{0.05}$/ferrihydrite and $Si_{0.05}$/ferrihydrite catalysts after annealing. Formation of hematite is seen at 300°C for the $Al_{0.05}$/ferrihydrite and >425°C for the $Si_{0.05}$/ferrihydrite catalyst.

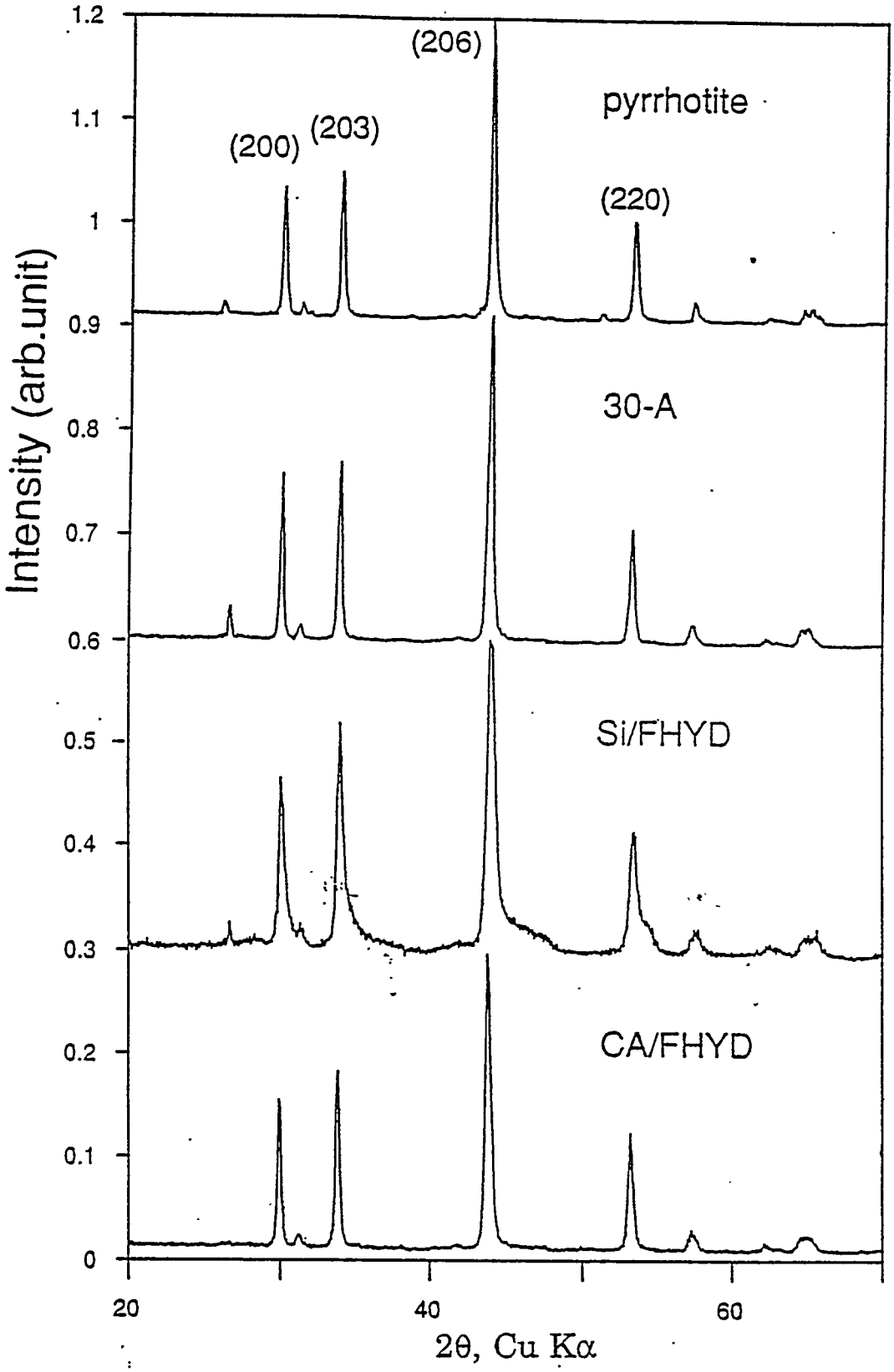

Fig 4. XRD patterns for the three ferrihydrite catalysts after sulfidation, as compared with that for pyrrhotite.

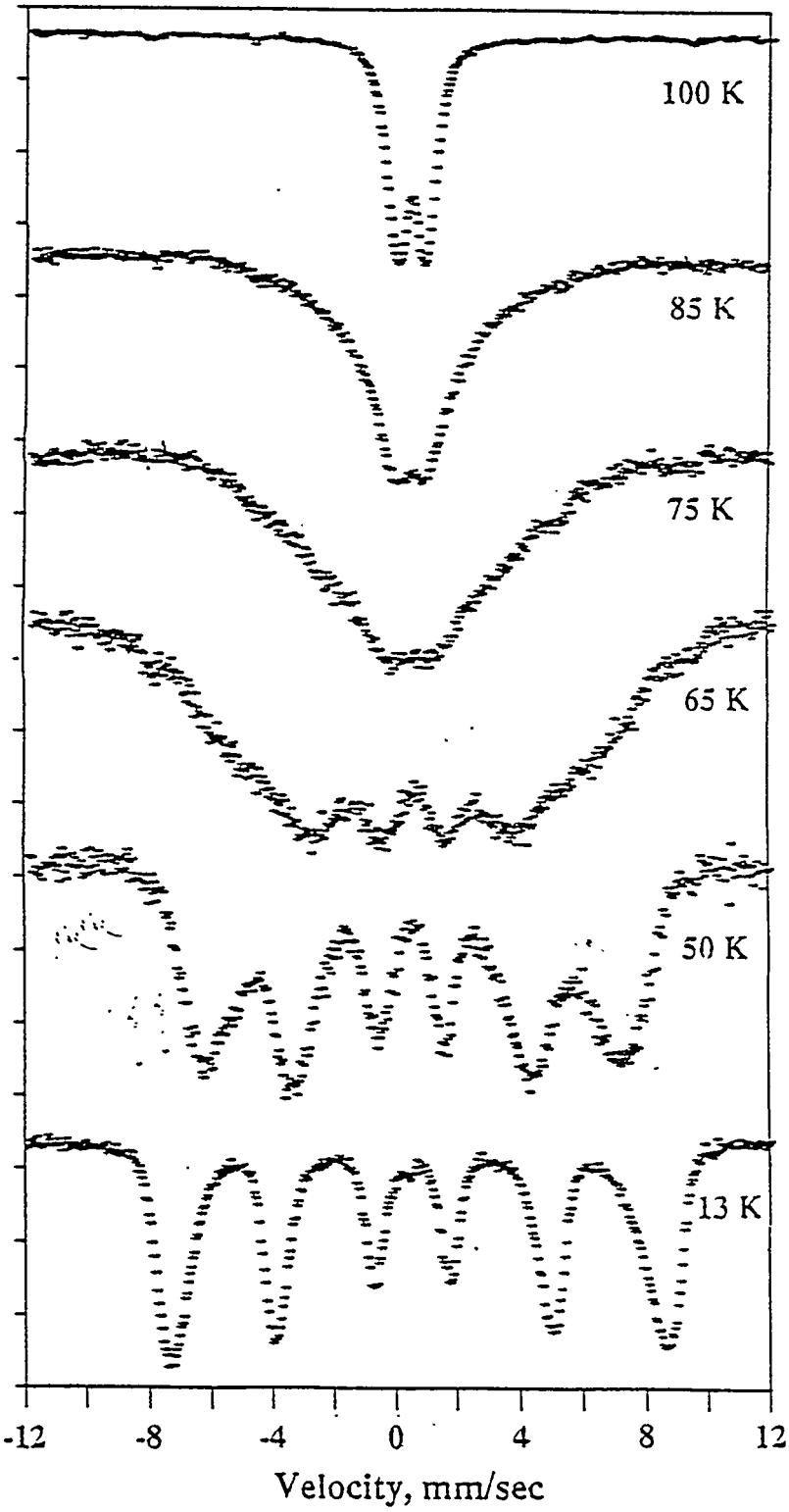

Fig 5. Temperature dependence Mossbauer spectra for the pure ferrihydrite catalyst (30-A).

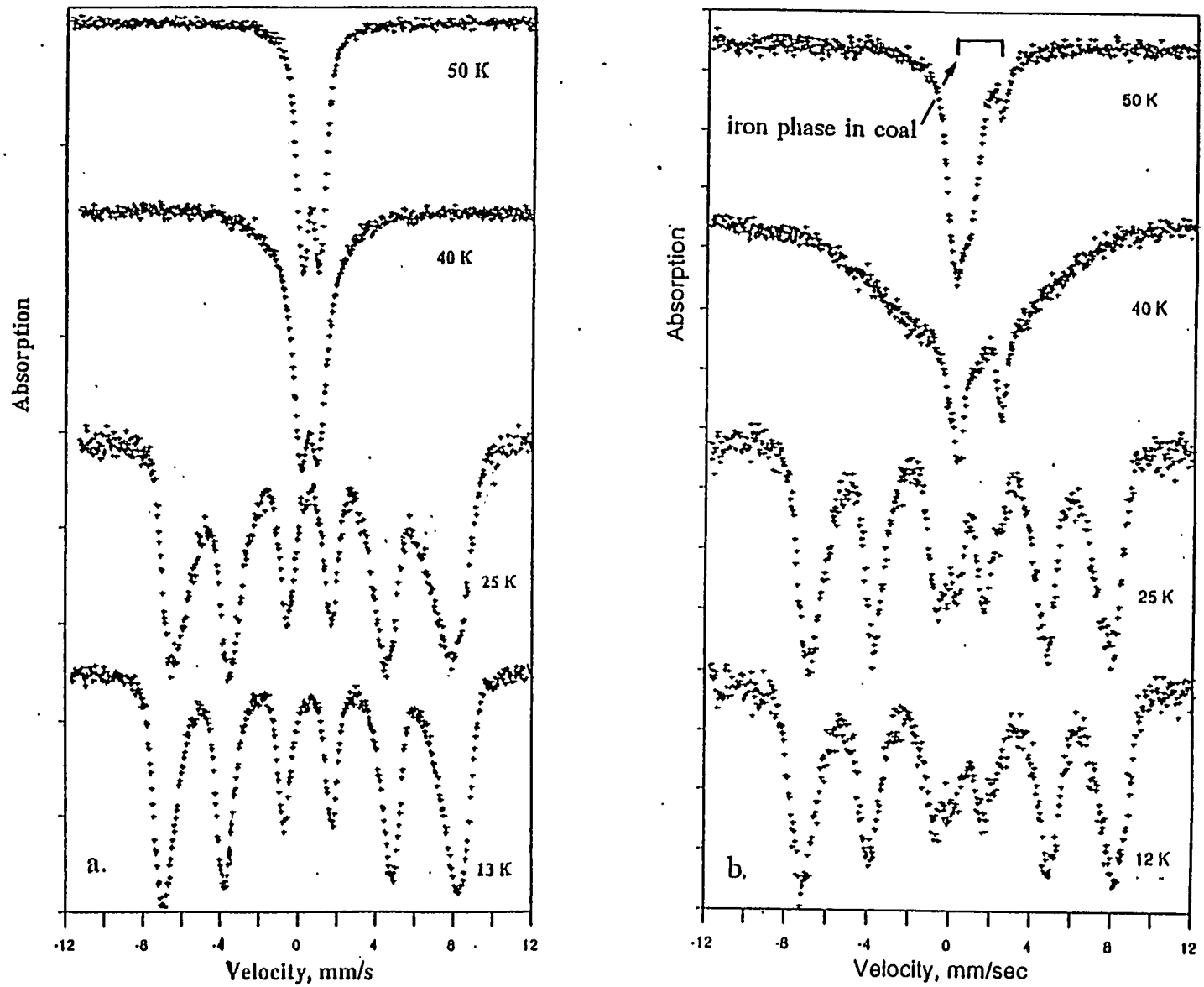

Fig 6. Temperature dependence Mossbauer spectra for: (a) CA/FHYD, and (b) the impregnated catalyst on coal.

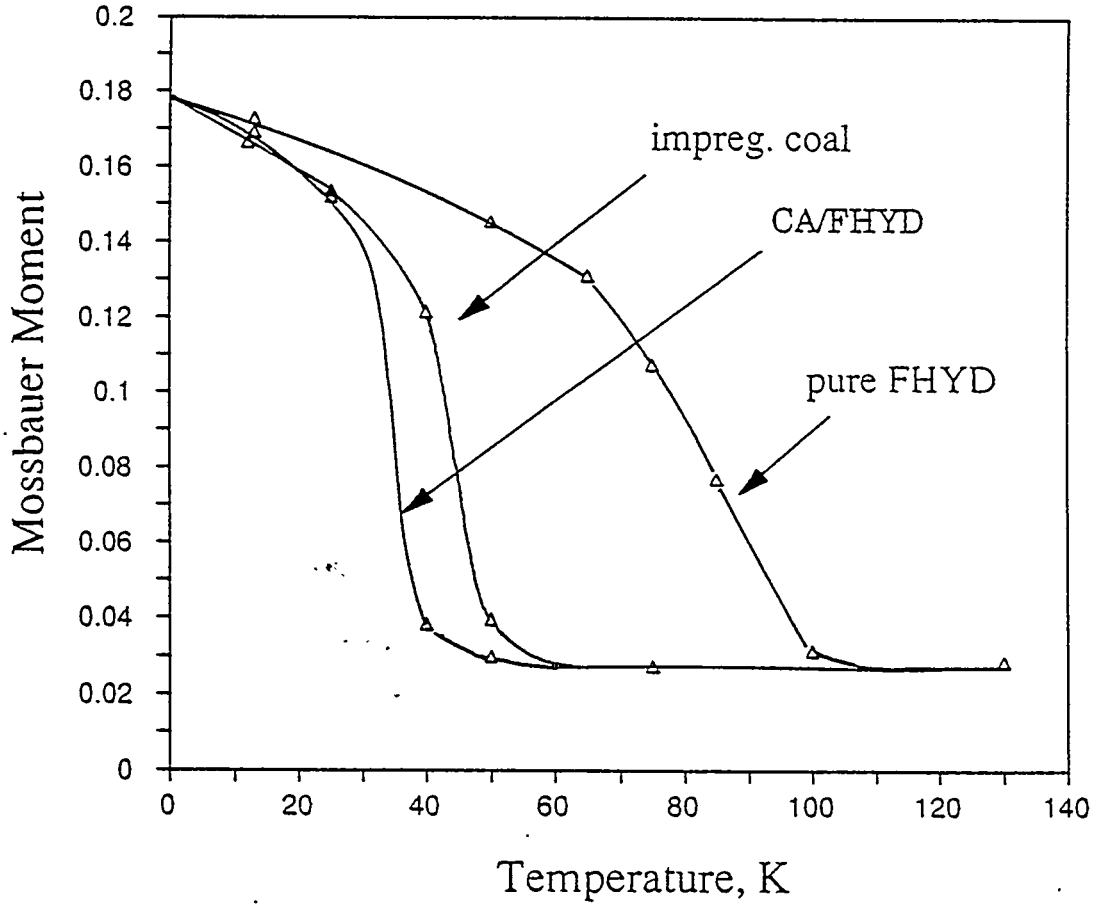

Fig 7. Temperature dependence Mossbauer moments for three ferrihydrite catalysts.

TASK III

FUNDAMENTAL RESEARCH IN COAL LIQUEFACTION

Coordinator: Frank Huggins

TASK III

Project III.1

GENERIC STRUCTURAL CHARACTERIZATION STUDIES

F.E. Huggins, J. Zhao, Z. Feng, K.R.P.M. Rao, and G.P. Huffman
University of Kentucky

As in previous years, the primary activity of this project is to supply a characterization service for the Consortium as a whole with element-specific spectroscopic techniques, viz. Mössbauer spectroscopy and XAFS spectroscopy. In addition, during this year, similar services were requested of the CFFLS program for closely allied projects from outside the CFFLS program. These projects include the DCL catalyst testing program at Sandia National Laboratory, New Mexico, (Dr. Frances Stohl), Mössbauer studies of red mud and related DCL residue samples from the Instituto de Carboquimica, Zaragoza, España (Srta. Carmen Mayoral and Dr. A. M. Mastral), and Mössbauer studies of catalysts in a chemical simulation of DCL (Drs. S. Petrosius, and Malvina Farcasiu). A brief synopsis of the results of these studies are given here, if they are not described elsewhere in this report.

1. Characterization of homogeneous DCL catalysts reacted with sulfur (Auburn University program, Prof. C. Curtis, P.I.):

Mössbauer and Mo K-edge XAFS spectroscopy were recorded from the residue of reaction of sulfur with iron naphthenate, iron acetylacetonate, molybdenum naphthenate, and a mixed 50% Mo - 50% Fe naphthenate.

Mo K-edge XAFS spectra were recorded from the Mo-containing naphthenate samples at the Stanford Synchrotron Radiation Laboratory (SSRL). As summarized below, the Mo XAFS spectra were quite different for the two samples.

It was found that both the XANES and EXAFS portions of the Mo XAFS spectrum of the residue from the reaction of sulfur with pure Mo naphthenate were similar to those reported for MoS_2, in which the Mo has 6 sulfur atoms as the molybdenum nearest neighbor environment. However, whereas the derived Mo-S and Mo-Mo bond distances from the EXAFS analysis were similar to those for MoS_2, coordination numbers were significantly smaller and indicative of a

4-coordinated sulfur environment as the nearest-neighbor shell. Such an environment has been reported previously for sulfided Co-Mo catalysts supported on γ-Al_2O_3 [1].

Molybdenum K-edge XAFS analysis of the 50% Mo - 50% Fe naphthenate residue sample indicated that the molybdenum was surrounded by four oxygen nearest neighbors with Mo-O distances of about 1.78 Å. Such a structure is compatible with tetrahedral MoO_4^{2-} anion complexes similar to those found in inorganic molybdate compounds and in Co-Mo/γ-Al_2O_3 before sulfidation [1].

Mössbauer spectra of the 50% Mo - 50% Fe and 100% Fe naphthenate residue samples showed that the iron was present in different forms. The 100% Fe sample showed a room-temperature Mössbauer spectrum similar to that of a nonmagnetic or superparamagnetic (spm) FeOOH phase. This was confirmed by a low-temperature measurement. The 50% Mo - 50% Fe naphthenate residue sample was much more complex and suggested the formation of both ferric and ferrous iron sulfates, although a significant presence of FeOOH could also have been present.

Mössbauer spectra were then run at both room temperature and at 13 K on sulfur-reacted residue samples of a second sample of pure iron naphthenate and of iron acetylacetonate. These samples were interpreted as mixtures of iron oxyhydroxide (probably goethite, α-FeOOH) and iron sulfates.

2. Mo XAFS studies of sulfated iron oxide catalysts with Mo promoters (University of Pittsburgh program, Prof. I. Wender, P.I.).

Results on these samples are included in the next section below in the discussion of Mo ferrihydrite binary catalysts.

A paper was prepared [2] on the results obtained from XAFS studies from Mo promoted catalysts and submitted as a Note to the J. Catalysis. This paper has been reviewed, modified, and re-submitted. We anticipate it will now be accepted and be published during the next quarter.

During the fourth quarter, new XAFS experiments were made at the Stanford Synchrotron Radiation Laboratory (SSRL) at the tungsten L edge and tin K edge for W/Fe_2O_3/SO_4 and Sn/Fe_2O_3/SO_4 catalyst formulations prepared at the University of Pittsburgh. These data have yet to be examined in detail.

3. Characterization of binary ferrihydrite catalysts (University of Kentucky program, J. Zhao and Z. Feng, P.I.s).

Both Mössbauer and XAFS spectroscopic measurements were made to characterize these samples and to complement XRD measurements. Results are included section II.6 of this report that describes both the synthesis and characterization of these catalysts.

4. Characterization of ion-exchanged low-rank coals (University of Kentucky program, M.M. Taghiei, P.I.).

Both Mössbauer and XAFS spectroscopies were used to characterize the iron present in ion-exchanged coals and to complement the significant enhancement of both oil and total conversion yields achieved with these coals. These data are discussed in section II.6 of this report.

5. Mössbauer characterization of iron phases in simulated DCL reactions (associated U.S. DOE project, S. Petrosius and M. Farcasiu, PETC, P.I.s).

Mössbauer spectroscopy has been used to characterize iron-bearing phases in a model chemical system designed to simulate DCL (M. Farcasiu, personal communication). The residues of various iron DCL catalysts, including those prepared in the CFFLS program, from reaction of the catalyst for 10 or 20 minutes with the model compound (4-(1-naphthylmethyl)bibenzyl - 41-NMBB) in a sulfur (from elemental sulfur) and hydrogen rich (from 9,10 dihydrophenanthrene - 910-DHP) environment at 320°C were analyzed by Mössbauer spectroscopy. The Mössbauer results showed that all of the oxide catalysts could be converted to 100% sulfides (mixtures of pyrite and pyrrhotite), if the particle size was sufficiently small enough and the conditions were not too hydrogen rich, or to mixtures of sulfides and oxides (unreacted catalyst?) for larger-sized material or more hydrogen-rich conditions. Surprisingly, excess 9,10-DHP appeared to retard the formation of sulfide phases.

These findings were reported to the Principal Investigators.

6. Characterization of red mud samples and residue samples from DCL tests at the Instituto de Carboquimica, Zaragoza, España (Srta. Carmen Mayoral and Dr. A. M. Mastral, P.I.'s).

Red mud (a natural soil comprised of primarily of fine-grained iron oxides and oxyhydroxides, silica, and minor clays) was used as a DCL catalyst in tests performed at the Instituto de Carboquimica, Zaragoza, España. As part of a student exchange program between U.S. DOE and equivalent European energy agencies, Srta. C. Mayoral was located at PETC for the summer of 1993 to work on DCL with M. Farcasiu. A week's visit to the Mössbauer laboratory at the University of Kentucky and Mössbauer characterization of her samples was included as part of this exchange program.

Mössbauer spectroscopy of the red mud sample before reaction showed that it consisted of fine-grained hematite as the major iron-bearing phase. The room temperature spectrum exhibited a strong magnetic and weaker spm components indicating that its average grain size was at least 150 Å. Residue samples from liquefaction tests using the red mud and other iron oxide materials as catalyst were also examined. These materials consisted of mixtures of pyrrhotite and spm magnetic oxides.

A second sample of red mud was also analyzed for comparison purposes. This sample was collected by Malvina Farcasiu during the Seventh Annual Technical Meeting of the Consortium for Fossil Fuel Liquefaction Science at Pine Mountain, Georgia. This Georgia red mud sample was significantly different from the red mud sample from C. Mayoral. It had considerably less total iron (based on relative Mössbauer intensity per unit weight) than the spanish sample, and the major iron-bearing phase was goethite, rather than hematite which was relatively minor. Both phases were largely spm at room temperature and hence the average particle sizes of the iron oxide phases in the Georgia red mud are smaller than those in the spanish red mud.

7. Characterization of residue samples from DCL catalyst testing program at Sandia National Laboratory, (Dr. Frances Stohl, P.I.).

To complement characterization studies of catalysts undertaken by Sandia National Laboratory as part of their DCL catalyst testing program, some samples of the coal, catalyst and DCL residue samples from these tests are being analyzed by Mössbauer spectroscopy at the University of Kentucky. Samples consisted of Blind Canyon coal (DECS-17), the Fe_2O_3/SO_4^{2-} catalyst (provided by I. Wender, University of Pittsburgh), and various residue samples from thermal and liquefaction runs carried out at 350, 375, and 400°C for various times.

The Mössbauer spectrum of the Blind Canyon coal is dominated by a quadrupole doublet attributed to iron in the carbonate mineral ankerite, $Ca(Ca,Fe,Mg)(CO_3)_2$. The measured quadrupole splitting value, 1.67±0.02 mm/s, is significantly smaller than that recorded for siderite, $FeCO_3$, 1.80 mm/s, which is commonly observed in low-sulfur coals of bituminous rank [3]. As expected, the isomer shift value is closely similar to those of other iron carbonate minerals. Iron in the form of pyrite could not be directly discerned from the spectrum because of the relatively poor signal/noise ratio of this spectrum as a result of the low iron content of this particular coal. It is estimated that iron in the form of pyrite is less than 5% of the total iron in the Blind Canyon coal. This is consistent with the reported forms-of-sulfur analysis of this coal.

The Mössbauer spectrum of the catalyst used in the catalytic DCL runs indicates that most of the iron is present as small particle hematite, α-Fe_2O_3. The room-temperature spectrum indicates significant superparamagnetic (spm) behavior and an average particle size of about 10 - 12 nm [4]. There appears also to be a significant fraction (13%) of the iron present in the sample as a ferric sulfate, $Fe_2(SO_4)_3$. This phase may have been formed during the pre-treatment of the catalyst at 450°C.

The iron-bearing phases present in the thermal residues must derive from the iron-bearing minerals present originally in the coal. The Mössbauer spectrum of the thermal residue at 350°C, 20 min., is dominated by the ankerite doublet. The Mössbauer parameters for this doublet are virtually unchanged from those for the doublet in the coal spectrum. However, there is also the presence of a single peak absorption in the residue spectrum that is not apparent in the coal spectrum. This peak is attributed to an austenitic iron (γ-Fe) formed by reduction of the iron in the carbonate mineral:

$$FeCO_3 \quad ---> \quad \gamma\text{-Fe} + CO_2$$

The γ-Fe phase is likely to be stabilized by substitutional carbon. There is also present a very weak magnetic phase, probably $Fe_{1-x}S$, which, although it can not be adequately fit, can just be discerned in the background. This particular phase is much more apparent in the Mössbauer spectrum of the residue from the 400°C thermal run; in this spectrum, the pyrrhotite iron exceeds 40% of the total iron. The austenitic iron is more obvious in this spectrum than in the lower-temperature spectrum, but still 37% of the iron is present in carbonate form. However, the Mössbauer parameters are somewhat different from those for the carbonate phase in the original coal, indicating, perhaps, that the composition of the carbonate has changed. It is conceivable

that only the carbonates of highest iron content have undergone reaction and that carbonates richer in calcium and poorer in iron still resist reaction under these conditions.

Despite having extra iron added to the coal samples, the Mössbauer spectra of the catalytic runs are quite similar to the spectrum of the thermal run at 400°C, except that the amount of pyrrhotite is always greater in the corresponding catalytic run. These data indicate that the catalyst is converted entirely to pyrrhotite in these experiments. Both the carbonate and the γ-Fe absorption derived from the original iron-bearing carbonate in the coal, diluted by the catalytic iron added to the DCL runs, persist in these DCL residues in about the same ratio as observed in the thermal residues. There is no trace of either the hematite or the ferric sulfate phase present originally in the catalyst in any of the catalytic residue samples.

To summarize the results of this investigation:, the iron mineralogy of the Blind Canyon coal has been examined and found to consist principally of ankerite. During DCL, it appears that this mineral is slowly converted to first austenitic iron (γ-Fe) and then pyrrhotite; the reaction is by no means complete at 400°C, even after 60 min. It is possible that there is a carbonate fraction, probably of higher Ca content and lower Fe content, that is resistant to reaction under these conditions. Conversion of the iron phases in the catalyst to pyrrhotite appears to be much more rapid as there is no remaining trace of either of the major iron-bearing phases that were originally in the catalyst, even after the mildest treatment at 350°C for 20 min. All of the catalyst appears to have been converted to pyrrhotite.

These Mössbauer data should provide a useful baseline for interpreting the behavior and transformations of the many different iron-based DCL catalysts to be tested at Sandia National Laboratory. These results have been forwarded to Dr. Stohl in an informal memorandum [5].

8. Characterization of iron phases formed in an aerosol reactor (West Virginia program, Prof. A. Stiller, P.I.).

Two iron-sulfur proto-catalyst samples from the aerosol reactor described by Stiller and co-workers (WVU) have been investigated by a combination of Mössbauer spectroscopy and STEM. The iron-sulfur phases were formed in the aerosol reactor at a temperature of 200°C, a pressure of 100 psi, and with iron concentrations in the spray solutions of 0.01M and 0.1M for the two syntheses. Mössbauer spectra were recorded at room temperature only.

Mössbauer spectra of the two catalysts showed that the major phase present in these samples was FeS_2. The Mössbauer parameters (IS = 0.31, QS = 0.60) for this phase formed from the 0.1M feed solution were exactly those for pyrite [3], however, the parameters (IS = 0.29, QS = 0.57) for the more dilute feed solution may indicate a mixture of mostly pyrite with some marcasite [3]. A very minor amount of the iron (3%) was present as a ferrous sulfate ($FeSO_4.H_2O$) in the product from the dilute feed solution, whereas a more significant amount of iron (13%) was present as hematite in the product from the concentrated feed solution

A brief investigation of these materials was also undertaken on the Hitachi H800 NA STEM at the University of Kentucky. Each catalyst was laid down on a TEM copper grid as a drop of a very dilute suspension of the catalyst in ethanol. A total of eight different areas for each material were examined in the STEM at 200 kV operating voltage. Photomicrographs of each area were taken at magnifications between 30kX and 80kX. Examination of the micrographs show that the particle size of the catalyst materials was variable: particles ranged in diameter from 3 nm to 580 nm.

Results from both Mössbauer and STEM experiments were relayed to Prof. Stiller in informal memoranda [6].

9. XAFS Investigation of Trace Elements in Waste Lubricating Oil and Residues of Co-processing Waste Oil with Coal, (Auburn University program, Prof. A. Tarrer, P.I.).

From a trace element analysis of waste lubricating oil (15W40), a significant amount (approx. 800 ppm) of zinc was found to be present in the oil. Other elements of significant concentration were calcium (1,025 ppm), magnesium (385 ppm), phosphorus (843 ppm) and copper (10 ppm); all other trace elements were less than 5 parts per million (ppm) by weight. The total ash content was 0.45 wt%, and the sulfur content was 1.01 wt%. XAFS spectroscopy of Zn and Cu has been carried out at the Stanford Synchrotron Radiation Laboratory (SSRL) (Feb. 2 - 14), while calcium, sulfur, and possibly phosphorus will be investigated at NSLS (June). The objective of this work is to identify the form of the element in the waste oil, and then determine whether it has altered significantly during the co-processing.

Although the XAFS analysis of Cu and Zn has not quite been completed, it is clear that Zn is present in the waste oil in the form of a dialkydithiophosphate. It was originally added to the oil in this form as an antiwear agent and apparently has not undergone significant change

as a result of the utilization of the oil in automotive engines. During coliqefaction of the oil with a bituminous coal (Blind Canyon, UT), the Zn ends up in the residue in the form of zinc sulfide, as a result of reaction of the Zn complex in the oil with sulfur released from the coal. XAFS data for copper in the oil and residues are much poorer in quality, because of its much lower concentration, and it may not be possible to interpret the data reliably. An attempt to detect arsenic (1 ppm) in the waste oil was also made, and, although an edge was observed, no effort will be made to interpret such a weak signal.

A detailed analysis of the Zn XAFS data will be presented at the Consortium Meeting in Snowbird, UT, in July 1994, and at the ACS IEC Meeting on Emerging Technologies in Hazardous Waste Management VI, to be held in Atlanta, GA, in September, 1994 [7].

10. XAFS Examination of Materials Prepared by Laser Pyrolysis, (University of Kentucky program, P. Eklund, P.I.)

XAFS spectra were obtained at SSRL of small particle Mo and W sulfide and carbide catalyst materials prepared by Dr. Peter Eklund and his group using their laser pyrolysis process. From these spectra, there are various qualitative differences between the spectra of the laser pyrolysis products and of those of bulk MoS_2 and WS_2 that appear to be derive from small particle effects. More experiments are planned for August 1994 in order to interpret the XAFS data for carbides produced by laser pyrolysis. A detailed report of the results of this investigation will be given after those experiments are completed.

11. New Method of Analysis of Superparamagnetic Mössbauer Spectra

We are still seeking improved methods for interpreting Mössbauer spectra of superparamagnetic (spm) iron oxides and oxyhydroxides. In the last month or so, we have been developing and testing a new parameter, the Mössbauer moment, that appears to have better potential for describing spm transitions than existing Mössbauer parameters. Such a method avoids the complexity of the procedure developed by Ganguly et al. [4]

A more detailed discussion of these developments will be presented after some more rigorous testing has been carried out.

References:

1. T. G. Parham and R. P. Merrill, *J. Catal.* **85**, 295, (1984).
2. J. Zhao, et al., submitted to *J. Catal.* (1994).
3. F. E. Huggins and G. P. Huffman, Chapter 50 in: *Analytical Methods for Coal and Coal Products*, Volume III, (C. Karr, Jr., ed.), Academic Press, New York, pp. 371-423, (1979).
4. B. Ganguly, F.E. Huggins, K.R.P.M. Rao, and G.P. Huffman, *J. Catalysis*, **142**, 552-569, (1993).
5. F.E. Huggins and K.R.P.M. Rao, Informal Memorandum on Results of Analysis, to Dr. F. Stohl, Sandia National Laboratory, Jan. 5th., 1994.
6. Z. Feng, K. R. P. M. Rao and G. P. Huffman, Informal Memorandum on Results of Analysis, to Prof. A. Stiller, West Virginia University.
7. F. E. Huggins, M. M. Taghiei, and G. P. Huffman, Extended Abstract for American Chemical Society (I&EC Division) Symposium, *Emerging Technologies in Hazardous Waste Management VI*, Atlanta, GA, (1994).

TASK III

Project III.2

COAL STRUCTURE/LIQUEFACTION YIELD CORRELATIONS BY MEANS OF ADVANCED NMR TECHNIQUES

Ronald J. Pugmire
University of Utah

INTRODUCTION

The ^{13}C CP/MAS experiment has proven to be a powerful technique for obtaining high resolution spectra in complex solids such as coal (1). MAS narrows the chemical shift anisotropy (CSA) to its isotropic shift when the sample spinning speed is greater than the anisotropy. While the isotropic chemical shift is useful in characterizing chemical structure, the principal values of the chemical shift tensor provide even more information. These principal values are available from the powder pattern obtained from a stationary or slowly spinning sample. Unfortunately, the overlap of many broad powder patterns in a complex solid often prevents the measurement of the individual principal values.

In an effort to address this problem of spectral overlap, many 2D techniques have been developed to simultaneously obtain the dispersion by isotropic shift, such as produced by MAS, in one dimension and the tensorial information as separate powder patterns in the second dimension (2-6). A very successful technique is the slow spinning modification of the magic angle hopping experiment (2) recently proposed by Gan (5), which we call the Magic Angle Turning (MAT) experiment (6). This experiment has a number of advantages over earlier 2D methods. The use of very slow spinning speeds (<50 Hz) favors the quantitative polarization of all carbons and allows the use of a large volume sample rotor resulting in a typical 2D spectrum acquisition requiring less than 24 hours. The mechanical device for slow spinning is very stable and high resolution in the isotropic chemical shift dimension can be easily obtained. The MAT experiment could be done on a suitably stable MAS probe. The only disadvantage of the original

MAT experiment is that data acquisition starts right after the last pulse, causing distortion in the evolution dimension (the second dimension) even if a delay as short as 20 μs is used.

We have recently improved the performance of the MAT experiment by employing a rotor synchronization device to trigger the pulse train at the appropriate rotor position. This improvement in experimental technique will improve the quality of the spectral information obtained.

In this report, the triple-echo MAT sequence is described which improves the 2D baseline (6, 7). Two additional experiments, using short contact times and dipolar dephasing techniques, are also described which further separate the powder patterns of protonated and nonprotonated carbons in complex compounds. Experimental results on representative model compounds as well as coals have been studied.

EXPERIMENTAL DETAILS

The experiments were performed on a Varian VXR-200 NMR spectrometer. A large-sample-volume slow-spinning MAS probe was constructed for the experiment. The probe holds approximately 5 cm^3 of sample and has a very stable sample spinning rate ranging from 20 to 300 Hz. A spinning rate of 44 Hz was used for the experiments discussed below. 1,2,3-trimethoxybenzene (TMB) and 2,3-dimethylnaphthalene were used as received from Aldrich and the coal samples were obtained from Argonne Premium Coal Sample Bank.

RESULTS AND DISCUSSION

The triple-echo and dipolar dephased MAT sequences are given in Figure III.2.1. The 2D spectrum obtained in this manner and plotted in a square has the bands inclined relative to the acquisition dimension axis at an angle arctan $(\omega_2/(3\omega_1))$, where ω_1 and ω_2 are the evolution and acquisition spectral widths, respectively. In order to obtain a 2D spectrum whose projection along one axis gives the isotropic shift spectrum, these data must be sheared through the inclination angle. For all experiments carried out during this reporting period, the evolution-time increments are chosen to be three times the acquisition dwell times, so that the spectral widths

for the acquisition dimensions are three times those for the evolution dimensions. This results in 2D spectra with bands inclined at an angle of arctan (1) = 45°. After a 45° shearing operation, the isotropic shift spectrum is obtained from the projection on one axis, while the powder patterns are taken as the perpendicular slices at the isotropic shift positions. The resultant contour plot spectrum of 1,2,3-trimethoxybenzene (TMB) is shown in Figure III.2.2. The resolution achieved for the isotropic chemical shift dimension is about 1 ppm, as illustrated in Figure III.2.2, where the resonance for M_1 and M_3, separated by 1 ppm, are resolved (8). The flat baseline in the isotropic shift projection of Figure III.2.2 indicates the quality of the 2D baseline achieved, which is essential for the quantitative measurement of the aromaticity (f_a) of coal. The individual powder patterns, from which the principal values of the chemical shift tensor can be extracted, are displayed in Figure III.2.3.

Results from a triple-echo MAT spectrum of 2,3-dimethylnapthalene (2,3-DMN) are given in Figure III.2.4 and Table III.2.1. The methyl carbon isotropic shift at 21 ppm is well-separated from those of the ring carbons, and is easily assigned. Assignment of the closely-spaced aromatic carbon shifts is more difficult. An expansion of the aromatic region of the MAT isotropic-shift projection and a similar portion of the MAS spectrum are shown in Figure III.2.4(a). These spectra are interpreted as showing isotropic shift peaks at 124 ppm, 128 ppm, 133 ppm, and 134 ppm. The 128 ppm peak has double intensity, but it is no wider than the single intensity peak at 124 ppm, indicating that two pairs of chemically equivalent carbons have virtually identical isotropic shifts in the solid. A dipolar-dephasing MAS spectrum (not shown) indicates that the nonprotonated carbons are those with isotropic shifts of 133 ppm and 134 ppm. A tentative assignment of the aromatic carbons can be made by assuming that the order of the solid isotropic shifts is the same as that in solution. The chemical shift assignments for 2,3-DMN in solution reported by Wilson and Stothers (9) are given in Table III.2.1. On the basis of the isotropic shift order the 124 ppm shift is assigned to $C_{6,7}$, the 133 ppm shift to $C_{2a,8a}$, and the 134 ppm shift to $C_{2,3}$. These assignments are consistent with the dipolar-dephasing MAS data. The isotropic shifts of $C_{1,4}$and $C_{5,8}$ have moved together in the solid to form the double-intensity peak at 128 ppm. Assignment of $C_{1,4}$ and $C_{5,8}$ requires examination of the principal values of the

tensors and the details for the assignments of all carbons are given in reference 6. The important point of note from the example of 2,3,DMN is that the triple-echo MAT experiment provides sufficient resolution to deconvolute overlapping tensor principal values.

The combination of triple-echo MAT, dipolar dephasing triple-echo MAT, and short-contact-time triple-echo MAT experiments can be used as a basic technique for extracting ^{13}C tensor information in complex powdered solids, e.g. coal. The flat 2D baseplanes produced by these modified sequences and the quantitative cross polarization of the MAT technique are especially important to this application. Shown in Figure III.2.5(a) is the 2D contour plot of a spectrum of Pocahontas coal obtained with the triple-echo MAT pulse sequence; the projection onto the isotropic shift axis is given in Figure III.2.5(b). The aromaticity (f_a) obtained by a volume integration of the spectrum in the aliphatic and aromatic regions is 0.86, in good agreement with the value of 0.86 obtained by a variable contact time of ^{13}C MAS experiment at a field of 2.35T (1). Selected Pocahontas coal powder pattern slices are shown in Figure III.2.6. The normal triple-echo MAT powder pattern at an isotropic shift of 20 ppm in Figure III.2.6(a) corresponds to methyl carbons on aromatic rings. The dipolar dephasing triple-echo MAT powder pattern at 139 ppm in Figure III.2.6(e) arises from the substituted aromatic carbons, some of which cluster in the 135-139 ppm range. Figure III.2.6(b) shows the normal triple-echo MAT powder pattern from the overlapping protonated and nonprotonated aromatic carbons at 124 ppm. These overlapping patterns are successfully separated in Figures III.2.6(c) and 6(d) by the short contact time and the dipolar dephasing experiments, respectively, into patterns characteristic of protonated and nonprotonated (bridgehead) carbons. Nonprotonated and protonated structural types can thus be distinguished in coal by these MAT techniques. The principal values of the tensors for different types of carbons obtained by measuring the shift at the peaks and half-heights of the breakpoints are given in Table III.2.2. The principal values are in good agreement with those obtained by a 1D variable-angle spinning experiment (10). The extraction of the methyl powder pattern, difficult to see in a coal by any other technique, further demonstrates the power of the MAT experiment.

With the MAT experiment we have examined a number of anthracite coals as well as the coals from the Argonne Premium Sample Bank. It is clear that a great deal of information is available in the experimental data and we are evaluating methods for analysis of the principal value data. The quantitative aspects of the MAT experiment on coals is portrayed in Figure III.2.7. The triple-echo MAT values of aromaticity correlate closely with those reported by Solum (1). A careful analysis of the quantitative nature of the experiment will be pursued in the future.

CONCLUSIONS

The data described in this report demonstrate that the Magic Angle Turning experiment enables the measurement of ^{13}C principal values in complex powdered solids by separating tensor powder patterns according to their isotropic shifts. Furthermore, the principal values of different types of tensors are recognizable even when the isotropic shifts overlap. The triple-echo MAT experiment produces 2D spectra with flat baseplanes which are well-adapted to quantitative analysis. Protonated and nonprotonated carbons may be separated by the short-contact-time and dipolar-dephasing variants of the triple-echo MAT experiment. The major problems associated with obtaining MAS spectra at high fields, the very high spinning speeds required to suppress or separate sidebands and the consequent difficulty in uniformly polarizing all spins, are eliminated by the MAT experiment. The triple-echo MAT experiment effectively suppresses spinning sidebands at low rotation frequencies, and the slowly rotating sample appears to promote the polarization of all spins. To date, none of the experiments performed in this laboratory on a wide range of model compounds exhibit recognizable magic angle holes. the MAT experiments described are particularly promising for the investigation of complex solids such as coal at high fields. Hence, it appears that the MAT experiment will be very useful in the study of a wide range of complex materials. A particular advantage is found in the relatively high resolution features of the experiment. In the isotropic chemical shift dimension the spectral resolution is comparable to that of a traditional CP/MAS experiment, while the uncertainty in the principal values in the powder pattern projections is estimated at ±2 ppm.

REFERENCES

1. Solum, M.S., Pugmire, R.J., and Grant, D.M., Energy & Fuels, 1989, 3, 187.

2. Bax, A., Szeverenyi, N.M., and Maciel, G.E., J. Magn. Reson., 1983, 52, 147.

3. Maciel, G.E., Szeverenyi, N.M., and Sardashti, M., J. Magn. Reson., 1984, 64, 365.

4. Kolbert, A.C. and Griffin, R.G., Chem. Phys. Lett., 1990, 166, 87.

5. Gan, Z., J. Am. Chem. Soc., 1992, 114, 8307.

6. Hu, J.Z., Orendt, A.M., Alderman, D.W., Pugmire, R.J., Ye, C., and Grant, D.M., Solid State Nucl. Magn. Reson., 1994, 3 (in press).

7. Pugmire, R.J., Hu, J.Z., Alderman, D.W., Orendt, A.M., Ye, C., and Grant, D.M., Proceedings, 7th International Conference on Coal Science, Sept. 12-17, 1993, Banff, Alberta, Canada, p. 485.

8. Hu, J.Z., Alderman, D.W., Ye, C., Pugmire, R.J., and Grant, D.M., Magn. Reson., 1993, 105, 82.

9. Wilson, N.K., and Strothers, J.B., J. Magn. Reson., 1974, 15, 31.

10. Orendt, A.M., Solum, M.S., Sethi, N.K., Pugmire, R.J., and Grant, D.M., Advances in Coal Spectroscopy, Meuzelaar, H.L.C., Editor, Plenum Press, 1992, page 250.

11. Sherwood, M.H., Facelli, J.C., Alderman, D.W., and Grant, D.M., J. Am. Chem. Soc., 1991, 113, 750.

Table III.2.1.

Carbon-13 Chemical Shift Tensors in 2,3-Dimethylnaphthalene and Naphthalene

Carbon	δ_{11}	δ_{22}	δ_{33}	$\delta_{iso.}$	$\delta_{sol.}$[b]
2,3-Dimethylnaphthalene[c]					
Methyl	30	25	8	21	20.1
$C_{1,4}$	218 [d]	132	34	128	127.3
$C_{2,3}$	232	157	14	134	135.2
$C_{5,8}$	222 [d]	142	20	128	126.7
$C_{6,7}$	225	135	11	124	124.8
$C_{4a,8a}$	207	197	-4	133	132.3
Naphthalene[e]					
C_1, C_4	224.7, 223.9	140.3, 145.6	22.8, 20.4	129.6	127.7
C_2, C_3	227.6, 227.6	139.3, 138.2	11.1, 10.4	125.7	125.6
C_{4a}	208.5	202.2	-5.9	134.9	133.3

a. Shift obtained from isotropic projection and MAS spectrum.
b. Solution shifts from Reference 9.
c. Solid shifts in ppm from TMS. Estimated error in solid data is ±2 ppm. The shifts are referenced via the methyl carbon of hexamethylbenzene at 17.3 ppm from TMS.
d. Calculated from δ_{22}, δ_{33}, and $\delta_{isotropic}$.
e. Solid shifts taken from Reference 11; the single crystal environment exhibits C_i symmetry and has two values for the alpha beta carbons.

Table III.2.2.

^{13}C Chemical Shift Tensors in Pocahontas Coal[a]

Carbon	δ_{11}	δ_{22}	δ_{33}	$\delta_{ave.}$	$\delta_{iso.}$
Methyl	35	22	5	20.7	20.3
Protonated	223	13	20	124.7	126.7
Nonprotonated	197	18	-8	124.3	124.0
Substituted	228	16	32	141.0	139.4

a. Shifts in ppm from TMS referenced via methyl carbon of hexamethylbenzene at 17.3 ppm from TMS.

b. Average of three principal value shifts.

c. Chemical shift of slice used.

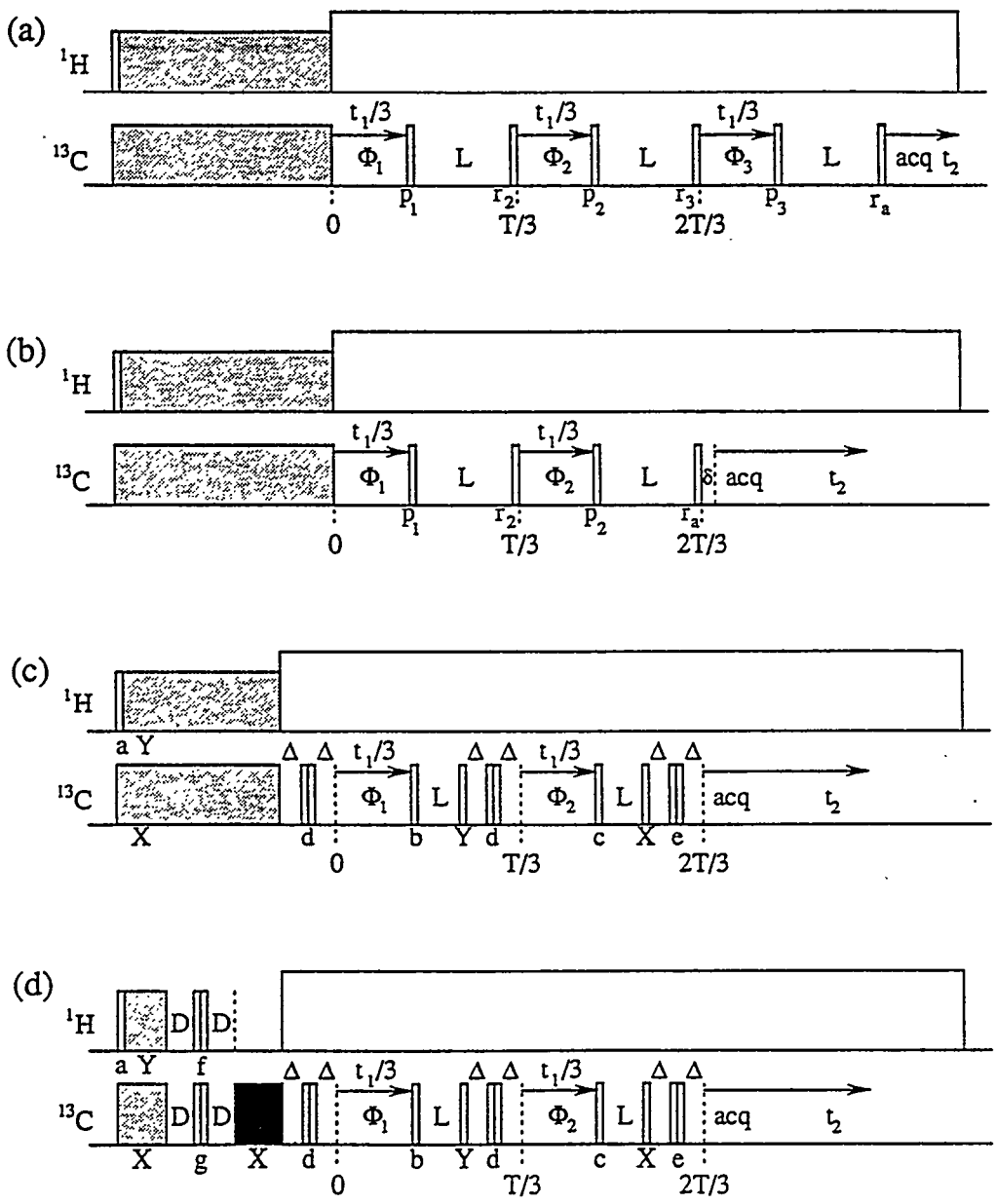

Figure III.2.1. Pulse sequences for the 2D MAT experiments. 90° pulses are represented by single rectangles; two adjacent rectangles denote a 180° pulse. The cross-polarization pulses are shaded. The time T is an integral number of rotor periods (excluding a multiple of three rotor periods). The magnetization precesses in the transverse plane during the periods labeled f_1 and f_2, and is along the longitudinal axis during the periods labeled L.
(a) Normal triple-echo MAT pulse sequence. Δ is an echo delay time determined by the probe ring-down and receiver recovery time. The character above each pulse indicates the entry in the phase cycle table (reference 6) which gives the phase of the pulse.
(b) Dipolar dephasing triple-echo MAT pulse sequence. The spin-lock pulse is darkened. The character above each pulse indicates the entry in the phase cycle table (reference 6) which gives the phase of the pulse.

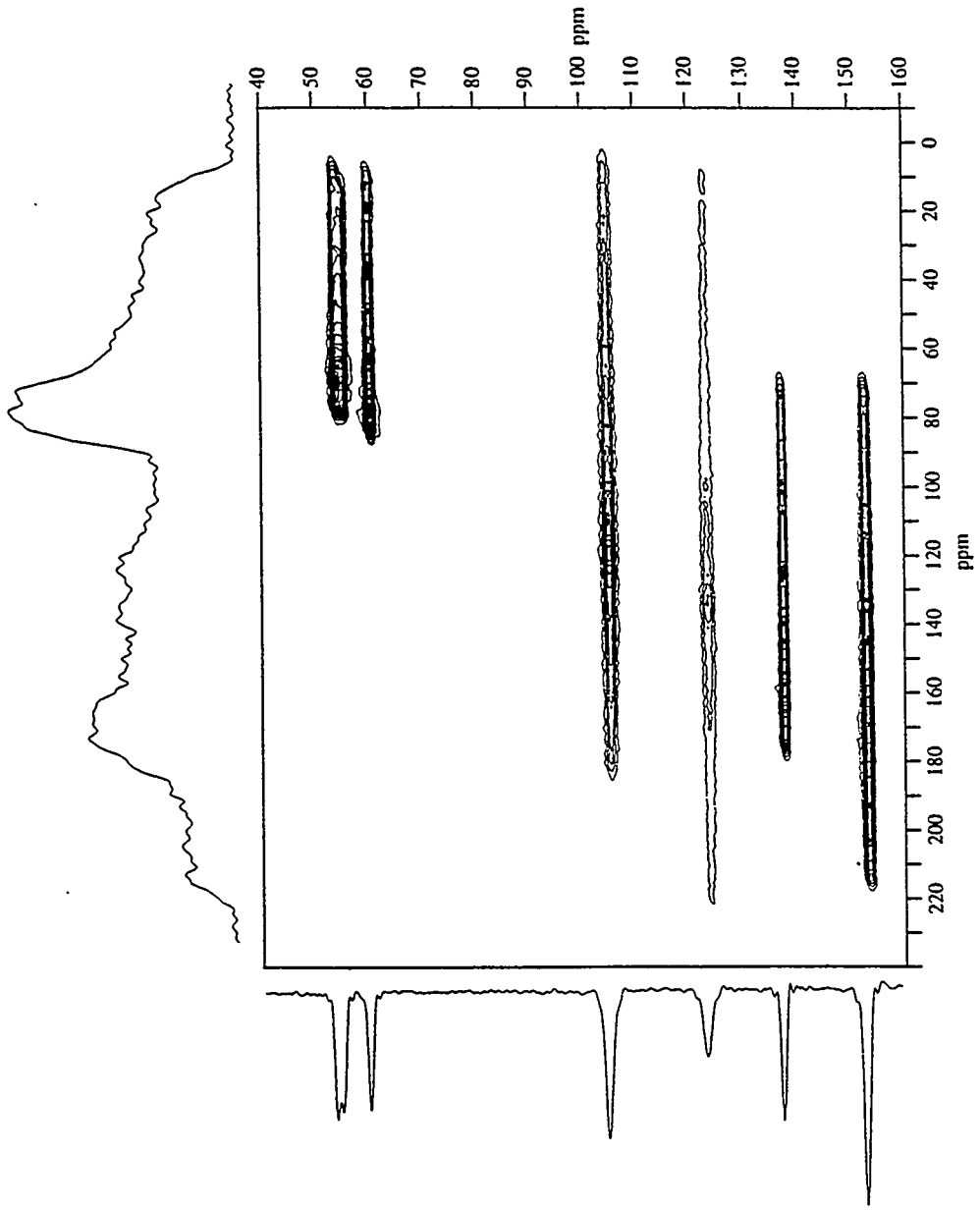

Figure III.2.2 Contour plot of the central portion of the 1,2,3, -TMB 2D spectrum obtained by shearing the spectrum by 45°. The contour interval is 4% of the maximum peak height. The position of the breakpoints and peaks in the bands are given correctly by the ppm scale on the horizontal acquisition dimension axis. The isotropic shifts of the carbons can be read from ppm scale on the vertical axis. A 1.5 ppm Gaussian line broadening was applied in both dimensions, except that the isotropic shift projection was prepared from a 2D spectrum with no line broadening.

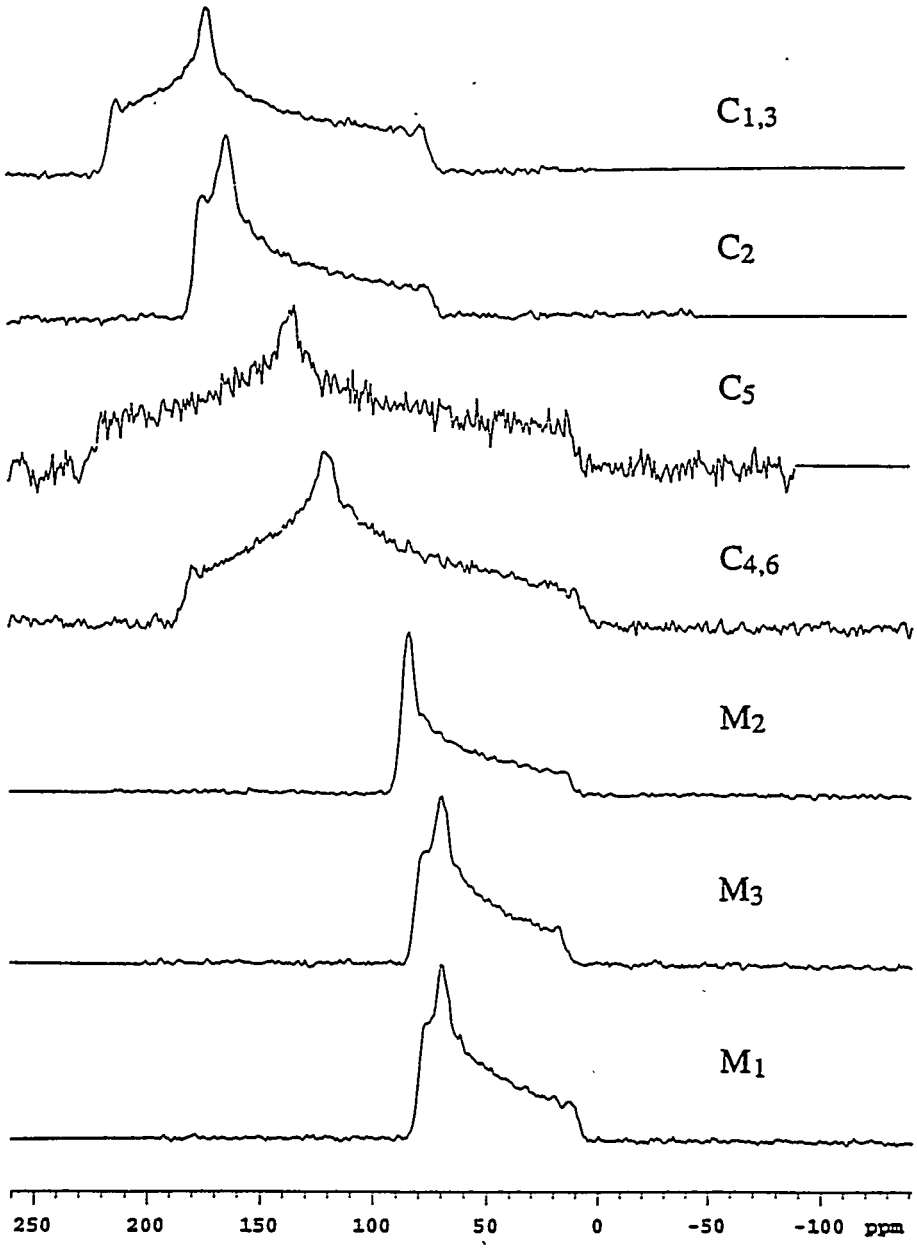

Figure III.2.3. 1,2,3,-TMB powder patterns from slices of the triple-echo MAT 2D spectrum in Figure 2.

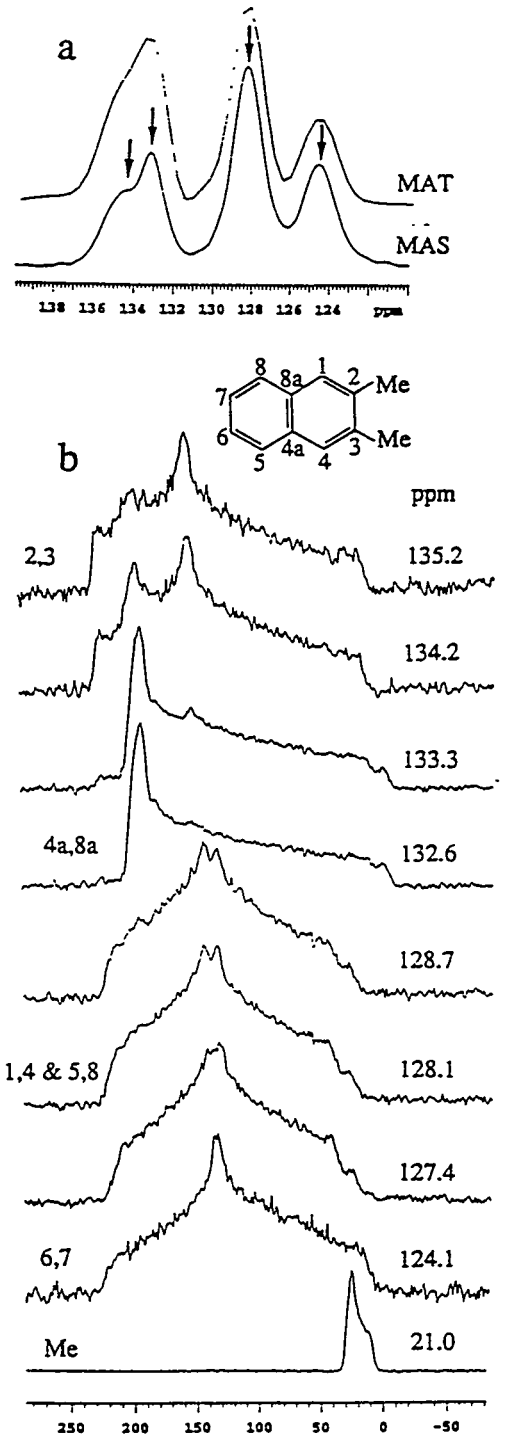

Figure III.2.4. (a) The projection along the isotropic shift dimension and the CP/MAS spectrum of the aromatic carbons of 2,3-DMN with the isotropic shifts of the resolved resonances highlighted. (b) Powder pattern slices taken from normal triple-echo MAT spectrum of 2,3-DMN at indicated values of the isotropic chemical shift. The spectrum was obtained using a 4 ms contact time, spectral widths of $\omega_2=3\omega_1=3200$ Hz, a 12 s recycle delay, 32 scans for both real and imaginary FIDs, 120 evolution increments with a 93.75 μs increment time, and 26 hours total experimental time.

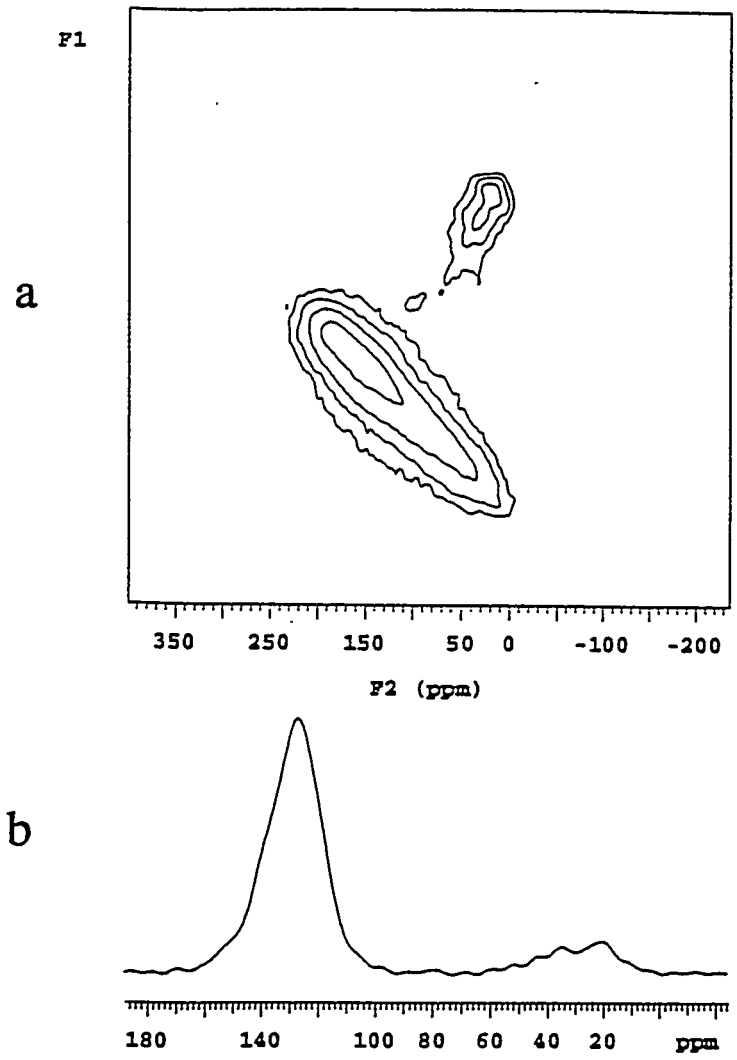

Figure III.2.5. Pocahontas coal triple-echo MAT spectra. (a) 2D spectrum obtained using a sample rotation rate of 44±0.025 hz, a Δ of 60 μs, a contact time of 2 ms, a recycle delay of 2 s, an acquisition dwell time of 31.25 μs, a t_1 increment of 93.75 μs, and 25 t_1 increments. Data was acquired for 512 scans in the real data set and 512 scans in the imaginary data set for a total measuring time of approximately 8 hr. A 2 ppm full-width-at-half-maximum Gaussian line broadening was applied in both dimensions. (b) Projection of the 2D spectrum in (a) onto the isotropic shift axis.

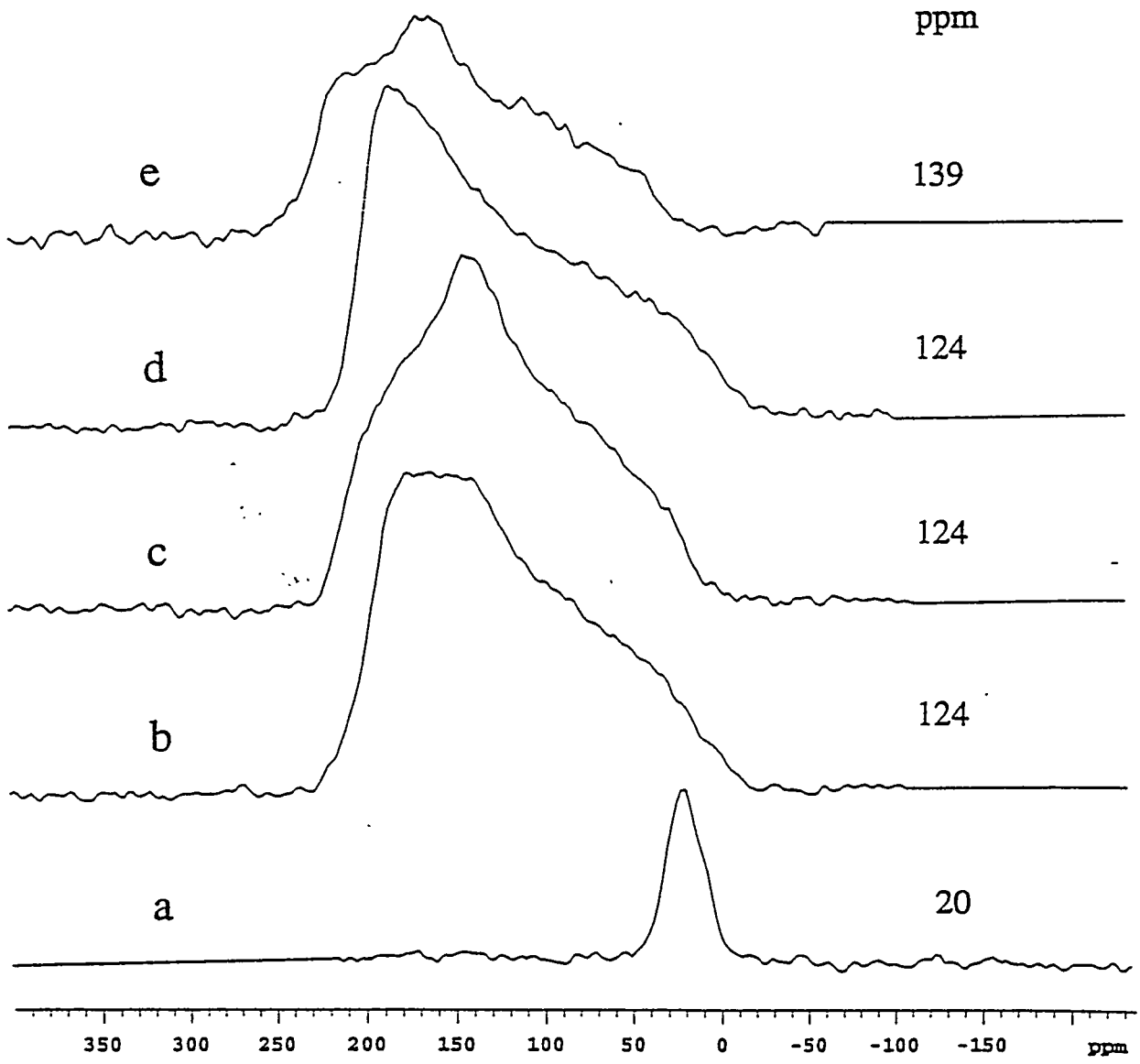

Figure III.2.6. Pocahontas coal triple-echo MAT spectrum slices at selected isotropic shift values. (a) Normal triple-echo MAT spectrum slice showing the aliphatic carbons centered at 20 ppm. (b) Normal triple-echo MAT spectrum slice showing the overlapping protonated and nonprotonated (bridgehead) carbons centered at 124.0 ppm. (c) 50 μs contact time triple-echo MAT spectrum slice showing the protonated carbons centered at 124 ppm. (d) Dipolar dephasing triple-echo MAT spectrum slice with D = 30 μS and a spin lock pulse of 1.5 ms showing the nonprotonated carbons centered at 124 ppm. (e) Dipolar dephasing triple-echo MAT spectrum slice with D = 30 μs and a spin lock pulse of 1.5 MS showing the nonprotonated carbons centered at 139 ppm.

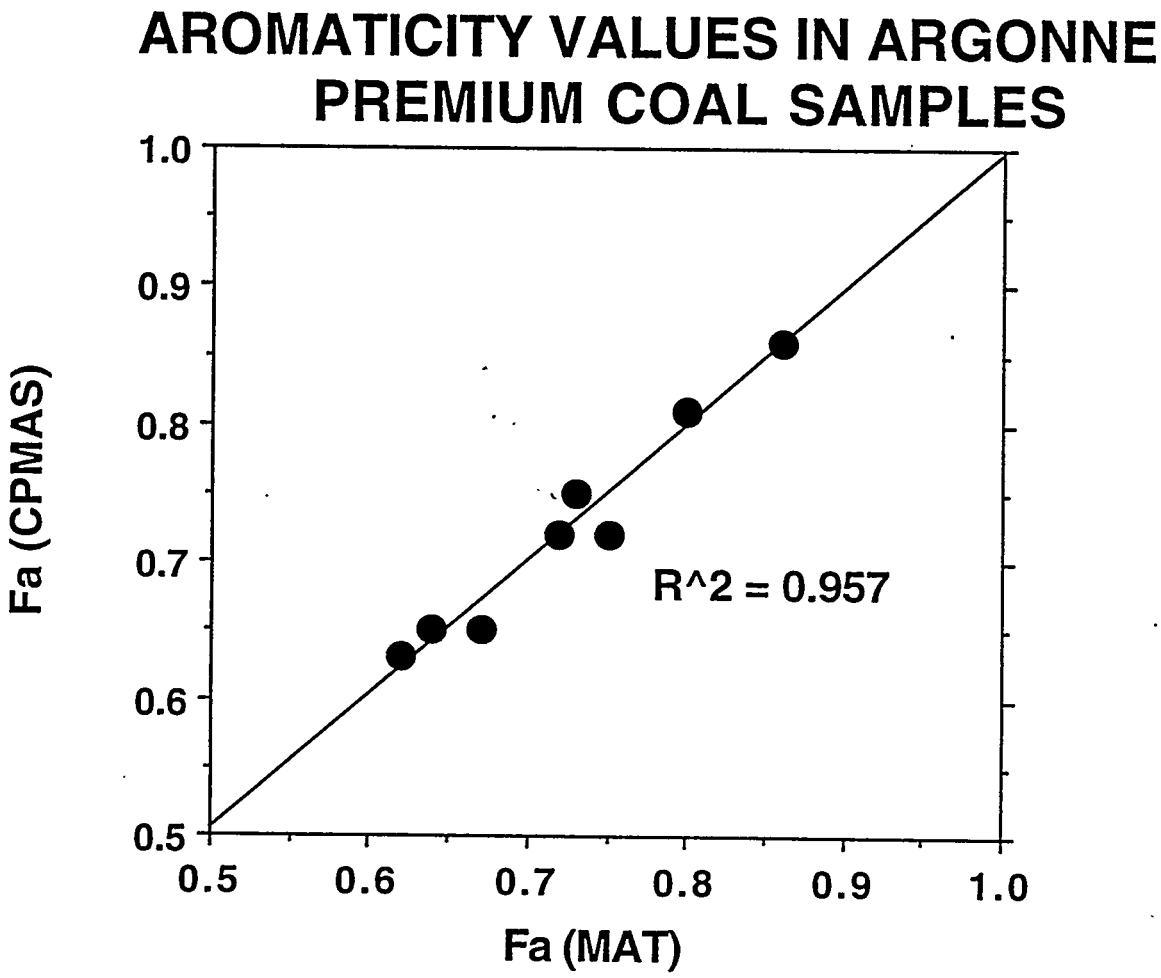

Figure III.2.7. Comparison of the carbon aromaticity values (fa) for the Argonne Premium coals as determined by the variable contact time CP/MAS technique (reference 1) and the triple-echo mat technique.

TASK III

Project III.3

CHARACTERIZATION OF COAL LIQUIDS BY HIGH PERFORMANCE LIQUID CHROMATOGRAPHY IN COMBINATION WITH GAS CHROMATOGRAPHY/MASS SPECTROMETRY AND SUPERCRITICAL FLUID CHROMATOGRAPHY/MASS SPECTROMETRY

Ramesh Subramanian, David Padlo and Edwin Kugler
Department of Chemical Engineering
West Virginia University

INTRODUCTION

Due to the complex composition of fossil fuels, separation of these liquids into their compound classes provides a major challenge. One of the tools used to characterize fossil fuels is liquid chromatography. Open column liquid chromatography (OCC) and high performance liquid chromatography (HPLC) are the most widely used of these techniques.

OCC is used for separating larger samples whose fractions can then be collected for further analysis. Quantifying the separated compounds can be done gravimetrically, after evaporating the volatile mobile phase. In spite of this advantage, OCC has a lot of drawbacks. Most of the OCC schemes are complicated, tedious, and are highly "operator dependent" [1]. Since pretreatment, cleaning, and preparation of resins and adsorbent packings are required for each run, the technique is time consuming. Finally, OCC schemes suffer from incomplete separation of compound classes and overlap of compounds into the adjacent fractions.

HPLC eliminates most of these drawbacks. The technique uses a small amount of sample (in μg) and involves little sample preparation. Precise control over solvent flow rate and composition ensure rapid elution and sharp peaks. With the advent of computer control, complete automation of the scheme can be achieved thereby providing the capability of making multiple unattended runs.

Matsunaga [2] studied the HPLC separation of aromatic from polar model compounds which are known to be present in fossil fuels. He evaluated the effectiveness of commercially available HPLC packings including silica, alumina, and polystyrene gels. Matsunaga found that alumina gave the best separation of aromatics whereas silica did the

best job of resolving polars from aromatics. Similar work was carried out by Grizzle and Thomson [3] who investigated the separation of aromatics by ring size, again using model compounds which were known to be present in petroleum, coal, and shale liquids. Of the various commercially available stationary phases, they concluded that DNAP (dinitroanilinopropyl silica) gave the best separation of the aromatics by ring size with only small effects from the substituents on the aromatic rings.

A rapid and automated analytic HPLC scheme for separating saturates and aromatics in lube oils was developed by DiSanzo and coworkers [4]. They reported that their technique worked well for lube based feedstocks with high viscosity. Hsu et al. [5] pointed out the advantage of using on line LC/MS for characterizing complex mixtures of hydrocarbons. They used this technique for in depth molecular level characterization of high boiling petroleum and processed oil fractions [6].

HPLC separation of heavy vacuum oil residue was reported in preparative scale by Carbognani and Izquierdo [7]. Alfredson [8] developed an HPLC scheme to achieve group-wise separation of petroleum model compounds. Other investigations on the separation of aromatic hydrocarbon mixtures are described in the literature [9-15].

In spite of all the schemes put forward in the past decade there exists room for improvement. Many of these schemes suffer from the inability to separate polars from aromatics. The techniques which do achieve separation between these two compound classes are very complicated and use 2-3 switching valves. In this paper we report the initial results obtained using a column switching technique developed in our laboratory which has the capability of achieving compound class separation of fossil fuels. The aromatics present are further separated by their ring size in this simple scheme which takes under an hour for completion.

EXPERIMENTAL

A Varian 9000 series HPLC was used for these measurements. The equipment consisted of a Varian 9010 pump with three proportioning valves for running solvent gradients with up to three solvents, a Varian 9095 autosampler, a Varian 9065 diode array detector and a VAREX IIA evaporative light scattering detector (ELSD). Nitrogen was used as the nebulizing gas for the ELSD. A Gilson 203 model fraction collector was used in series

with the whole set up to collect the separated fractions when needed. One six-port switching valve was used to direct flow through the columns. The columns used were a DNAP column (30 cm X 0.46 cm, ES Industries), an LC-DIOL column (25 cm X 0.46 cm, SUPELCO) and a DIOL precolumn. The whole process was automated and controlled by a computer using Varian Star software (Fig. 1).

The basic technique developed by Kugler was used to achieve separation [16]. The DNAP-silica column was analyzed in detail by Grizzle and Thomson [3] for separating aromatic molecules. The DNAP phase has a strong affinity for the aromatic solutes differing in the number of aromatic rings. This affinity is due to charge transfer from the column to the electron deficient aromatic rings. The DIOL column on the other hand was used to separate the polar compounds. The DIOL column separates by hydrogen bonding to oxygen and nitrogen compounds and provides the basis for polar - nonpolar separations.

The solvents used were pentane, methylene chloride, and isopropyl alcohol. Hexane was used in the early stages of this work but was replaced by pentane because it had a lower boiling point which was an advantage when working with the ELSD. A methylene chloride gradient was used to elute the multi-ring aromatics. Isopropyl alcohol flushed out the hard to elute polars from the DIOL column.

The mobile phase was pumped at a constant flow-rate of 1.5 ml/min. This flow-rate ensured good separation and reduced peak broadening. The initial column configuration used for the analysis is shown in Fig. 2a. The sample first is passed through a filter to trap any particulate impurities which could plug the column or damage the switching valves. The sample then passed through the DIOL precolumn. The precolumn trapped the polars but allowed the aliphatics and aromatics to pass through. The aliphatics and the aromatics then entered the DNAP column. In a series of tests we determined the optimum time needed for the complete separation of the polars from the aliphatics and aromatics as two minutes. In this time, the aliphatics and the aromatics got out of the DIOL precolumn but remained completely within the DNAP column. Pentane was used as the mobile phase for this stage.

After two minutes the configuration was switched to analyze the polars. The six-port valve was switched to route the flow through the LC-DIOL column thereby isolating the compounds in the DNAP column. The configuration is shown in Fig. 2b. and was run from two to twenty seven minutes. A solvent gradient of pentane to methylene chloride and 5%

isopropyl alcohol was used. After all the polars passed through the DIOL column and the detector (shown by the occurrence of a flat baseline in the chromatogram) the solvent was changed back to pentane.

The final stage involved the separation of aliphatics and aromatics. For this the switching valve was reset back to its original configuration (Fig. 2c). The mobile phase was now used to flush out the aliphatics and aromatics trapped in the DNAP column. For eluting the aliphatics pentane was used. The single and the double ring aromatics were then eluted using a gradient of up to 40% methylene chloride in pentane. The multi-ring aromatics (2+ rings) are separated using 100% methylene chloride. The total analysis time is fifty minutes. The solvent gradient used is given in tabular form in Table 1.

After the analysis was complete, the columns were allowed to equilibrate for ten minutes. Pentane is used as the mobile phase. Any residue present on the lines is also flushed out at this time.

RESULTS AND DISCUSSION

Fig. 3 shows the trace obtained when a polynuclear aromatic hydrocarbon (PAH) mix obtained from SUPELCO was run using our scheme. From Table 2 it can be seen that the retention times correlate with the number of double bonds. Polars are resolved on the basis of their functional groups (Fig. 4).

Commercial feeds -- both the oil fractions from coal and petroleum -- were run using our analysis technique and excellent separation was obtained. The chromatograms obtained when separating vacuum gas oils (VGO) are shown in Figures 5a and 5b. Figure 5c shows a trace of the compound class separation achieved with a Wilsonville Heavy Diesel (WHD) fraction.

The polars and the aromatics were completely separated. Baseline separation was obtained between the single and the double ring aromatics. Excellent resolution was obtained between the double ring and the multi-ring aromatics. The aliphatics overlapped with the single ring aromatics. Work is presently being done in separating these two compounds by extending our analysis scheme.

The uv detector proved to be useful in identifying the separated compounds but failed in two major areas. Quantifying the separated samples was difficult to achieve using the uv

detector due to the vast number of compounds involved. The refractive index (RI) detector, the detector of choice for quantification, could not handle solvent gradients which were essential for good clean separation. The uv detector also did not detect the aliphatics as they do not absorb uv light. We tried collecting the separated fractions in a fraction collector and then injecting the fractions into a gas chromatograph (GC) for quantification. This attempt did not succeed as the GC failed to respond to the collected fractions due to the large dilutions of sample after HPLC analysis. We feel that collecting fractions for further analysis will only work in semi-preparative scale HPLC which can handle larger samples.

Due to these problems, we opted for an evaporative light scattering detector (ELSD) for on-line quantification. An ELSD works well with a volatile mobile phase. Hence we chose pentane as our mobile phase, instead of hexane due to its lower boiling point. A lot of recent work has been done with the ELSD for analyzing non- volatile compounds. This detector has been used in the analysis of carbohydrates [17], phospholipids [18,19], surfactants [20], triglycerides and fatty acids [21]. The light scattering detector has been used as a mass detector in size exclusion chromatography of coal extracts [22]. Couloumbe compared the RI detector and the ELSD in terms of linearity, sensitivity and response factors [23]. Theoretical analyses of the functioning of the ELSD and investigation of the different variables which affect its response have been carried out [24,25]. The detector response has been simulated and various equations are available in literature [26-27].

We feel that the ELSD can be used as a detector for high boiling hydrocarbons, with boiling points greater than 300 °C. The detector gives on-line quantification and its response is approximately proportional to the mass of the sample. The response is non-linear but can be linearized for specific compounds as is shown in Figure 6.

Dealing with response ELSD obtained when running complex mixtures is much more complicated. A comparison between the light scattering detector and uv detector is shown in Figures 7a and 7b for a vacuum gas oil sample. The ELSD response points out that the amount of high boiling aliphatics in the VGO is much more than the multi-ring aromatics. The single ring aromatics which show up in the trace are probably ones with long side chains which increase their boiling points. The chromatogram obtained when the Wilsonville Heavy Diesel sample was run through the ELSD is shown in Figure 7c. Most of the polars which show up in the uv trace are not seen here. This suggests that the strong uv signals are

produced by small quantities of strong absorbers.

To determine whether the ELSD will respond to a particular feed we suggest running a simulated distillation [28] of the feed before running it though the ELSD. The GC response to the three feeds are shown in Figures 8a,8b and 8c. All three samples had a boiling range which was greater than the lower detection limit of the ELSD.

Due to the non-linear response of the ELSD it was imperative to determine the optimum conditions for operation of the ELSD, where the response will be similar for all compounds. To determine the optimum operating conditions we looked at three variables - drift tube temperature, flow rate of the nebulizer gas, and mobile phase used for separation.

The effect of nebulizer gas flow rate on sample response is shown in Figure 9. Two solvent compositions were used. The response to a fluoranthene sample varied steeply at lower flow rates before a flat profile is obtained at approximately 4.8 l/min (65 mm on the instrument rotometer). Keeping this as our optimum flow rate, we studied the dependence on temperature. The dependence on temperature was very distinct and the ELSD was very sensitive to small variations in temperature. As most of our compounds of interest had normal boiling points that lay between 300-550 °C, we ran a series of linear paraffins (C_{12} to C_{40}) at different ELSD temperatures and with different mobile phases, to try to optimize the response. The best results were obtained at an operating temperature of 50 °C and with pentane as the mobile phase (Figure 10).

Although these conditions give the best response we are still handicapped by the dependence of the ELSD response on the mobile phase being used. Work is being done in trying to remove this constraint and optimize the ELSD performance with solvent gradients.

CONCLUSIONS

This HPLC technique is very useful for rapid analysis of fossil fuel liquids. Compound class separation is obtained with the polars resolved by functional groups and the aromatics separated by ring size. The scheme works well for identification, but work needs to be done in the area of quantification for want of a universal mass detector. The ELSD holds a lot of promise but further research needs to be done in understanding the dependence of the ELSD on the mobile phase used, before it can be used as a tool for routine quantification of unknown fuel mixtures.

REFERENCES

1. D.W. Later, M.L. Lee, K.D. Bartle, R.C. Kong, and D.L. Vassilaros, Anal. Chem., 53, 1612 (1981).

2. A. Matsunaga, Anal. Chem., 55, 1375 (1983).

3. P.L. Grizzle and J.S. Thomson, Anal. Chem., 54, 1071 (1982).

4. F.P. DiSanzo, S.P. Herron, B. Chawla and D. Holloway, Anal. Chem., 65, 3359, (1993).

5. C.S. Hsu, M.A. McLean, K. Qian, T. Aczel, S.C. Blum, W.N. Olmstead, L.H. Kaplan, W.K. Robbins, and W.W. Schulz, Energy and Fuels, 5, 395 (1991).

6. K. Qian and C.S. Hsu, Anal. Chem., 64, 2327 (1992).

7. L. Carbonanani and A. Izquierdo, Fuel Sci. and Tech. Int'l., 8(1), 1 (1990).

8. T.V. Alfredson, J. Chromatogr., 218, 715 (1981).

9. S.A. Wise, S.N. Chesler, H.S. Hertz, L.R. Hilpert, W.E. May, Anal. Chem., 49, 2306 (1977).

10. J.S. Thomson, J.W. Reynolds, Anal. Chem., 56, 2434 (1984).

11. P.L. Scolla, R.J. Hurtubise, J. Chromatogr., 357, 127 (1986).

12. J.F. Schabron, R.J. Hurtubise, Anal. Chem., 49, 2253 (1977).

13. S.C. Ruckmick, R.J. Hurtubise, J. Chromatogr., 321, 343 (1985).

14. S.C. Ruckmick, R.J. Hurtubise, J. Chromatogr., 331, 55 (1985).

15. R. Matthias, H. Willsch, and D.H. Welte, Anal. Chem., 56, 2538 (1984).

16. S. L. Kugler and E. L. Kugler, CFFLS Review meeting (1991).

17. R. Macrae and J. Dick, J. Chromatogr., 210, 138 (1991).

18. L. Brenton, B. Serkiz, J.P. Volland, and J. Lepagnol, J. of Chromatogr., 497, 243 (1989).

19. P. Van Der Meeren, J. Vanderdeelen, M. Huys, and L. Baert, J. Chromatogr., 447, 436 (1988).

20. G.R. Bear, J. Chromatogr., 459, 91 (1988).

21. J.L. Robinson, M. Tsimidou, and R. Macrae, J. Chromatogr., 35 (1985).

22. K.D. Bartle, T. Norman, M.J. Mulligan, D.G. Mills, and C. Gibson, Fuel, 62, 1181 (1983).

23. S. Couloumbe, J. Chromatogr. Sci., 26, 1 (1988).

24. A. Stolyhwo, H. Colin., and G. Guichon, J. Chromatogr., 265, 1 (1983).

25. A. Stolyhwo, H. Colin, M. Martin, and G. Guichon, J. Chromatogr., 288, 253 (1984).

26. T.H. Mourney, and L.E. Oppenheimer, Anal. Chem., 56, 2427 (1984).

27. P. Van der Meeren, J. Vanderdeelen, and L. Baert, Anal. Chem., 64, 1056 (1992).

28. ASTM Designation D 2887, Annual book of ASTM standards, Vol 05.02.

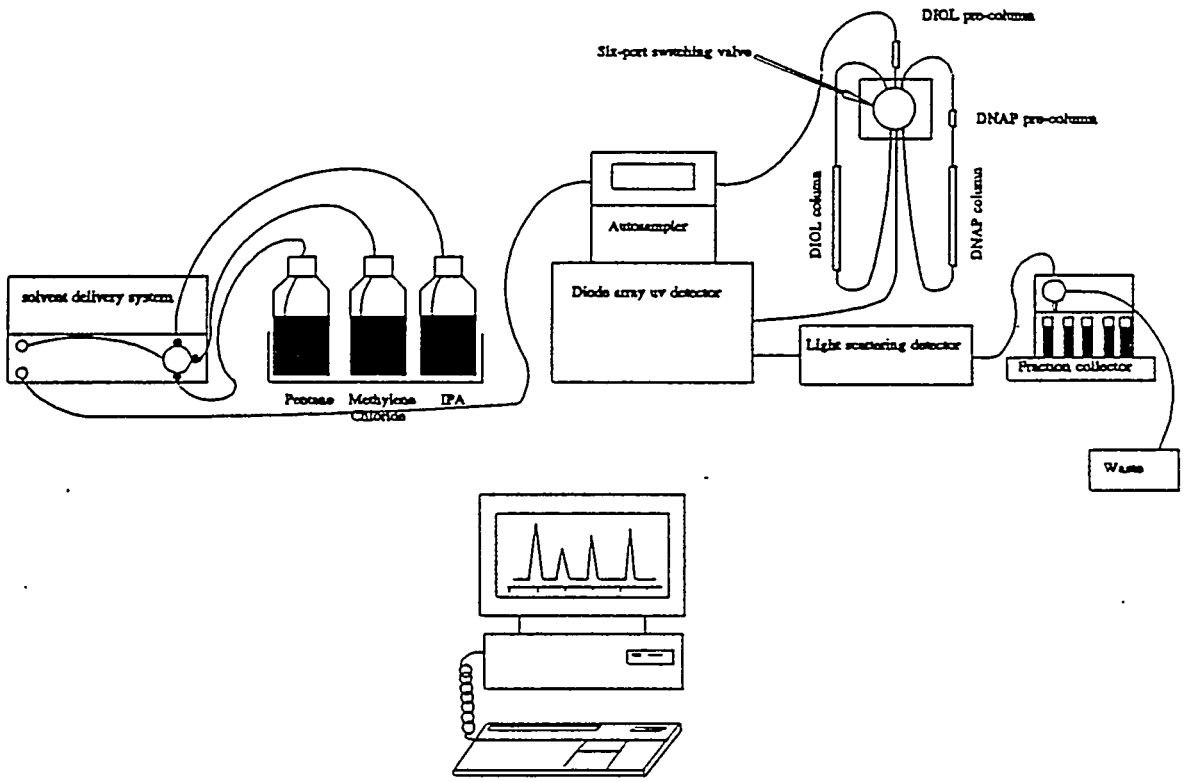

Figure 1: Schematic of HPLC experimental setup

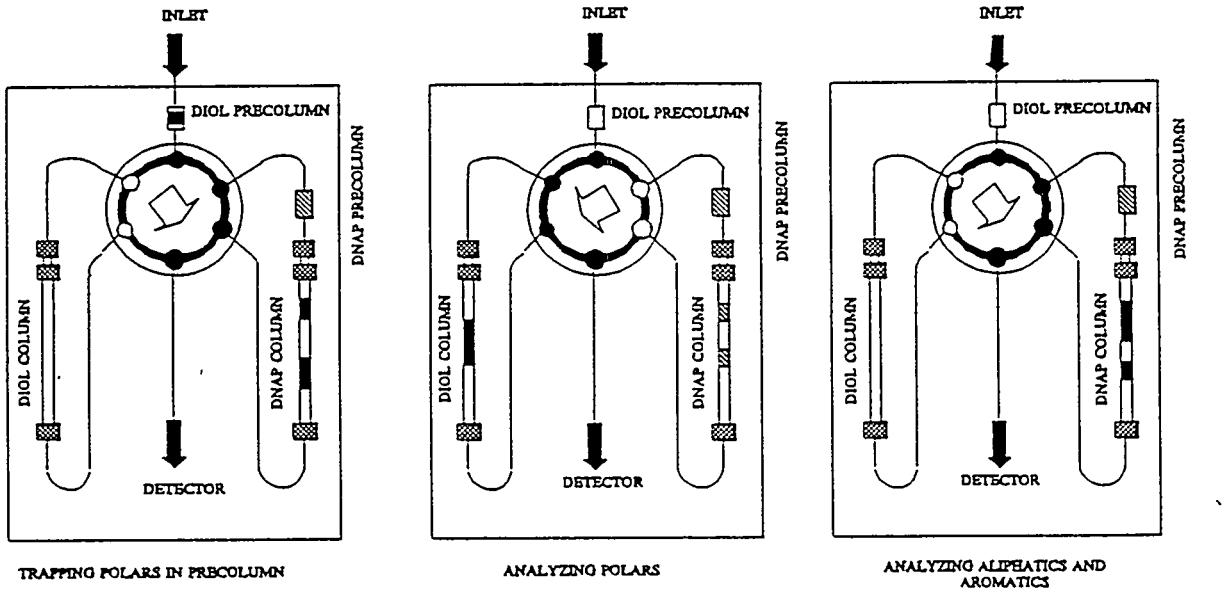

Figure 2a,2b,2c: Column configurations used for analysis

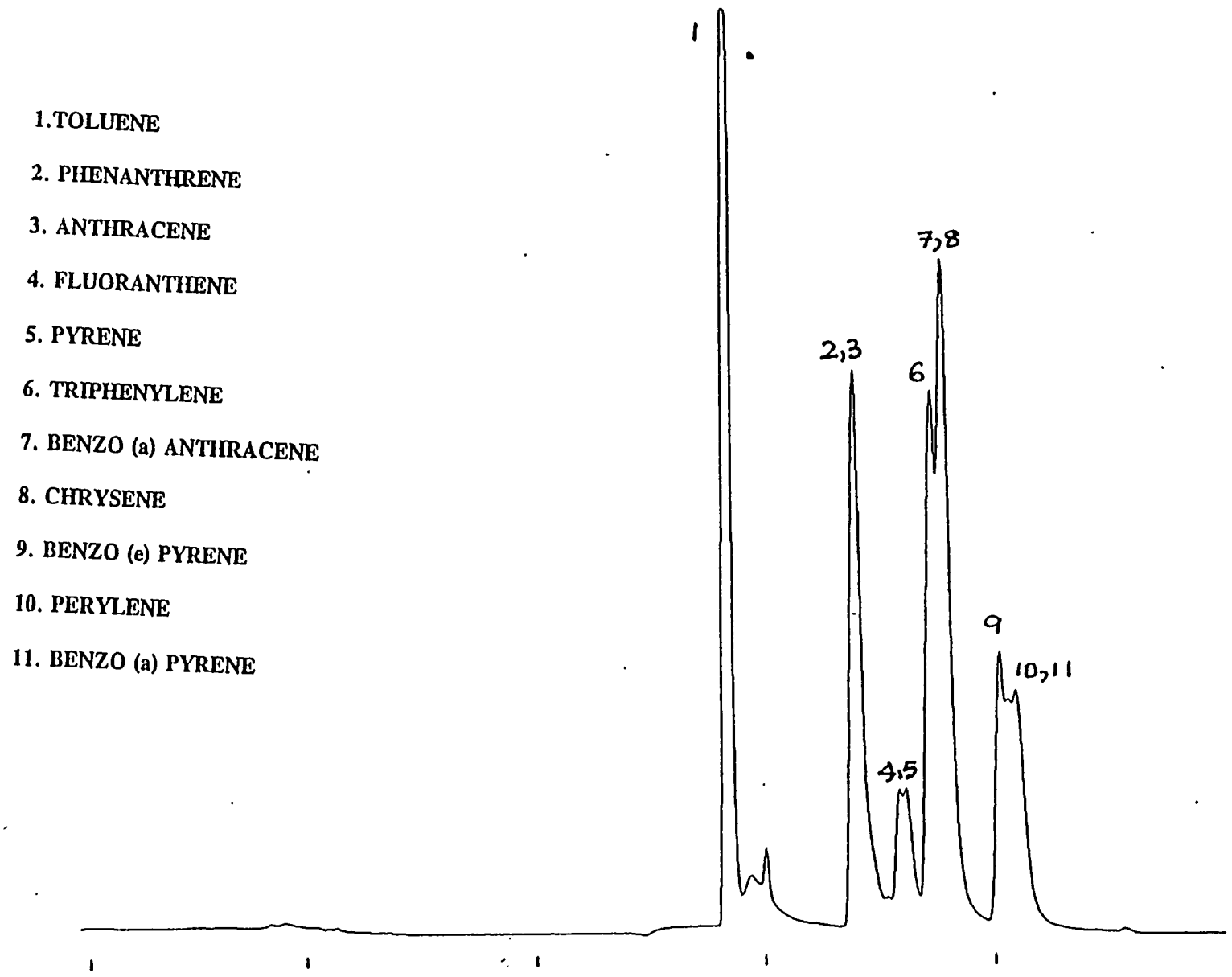

Figure 3: Separation of polynuclear aromatics using our HPLC scheme

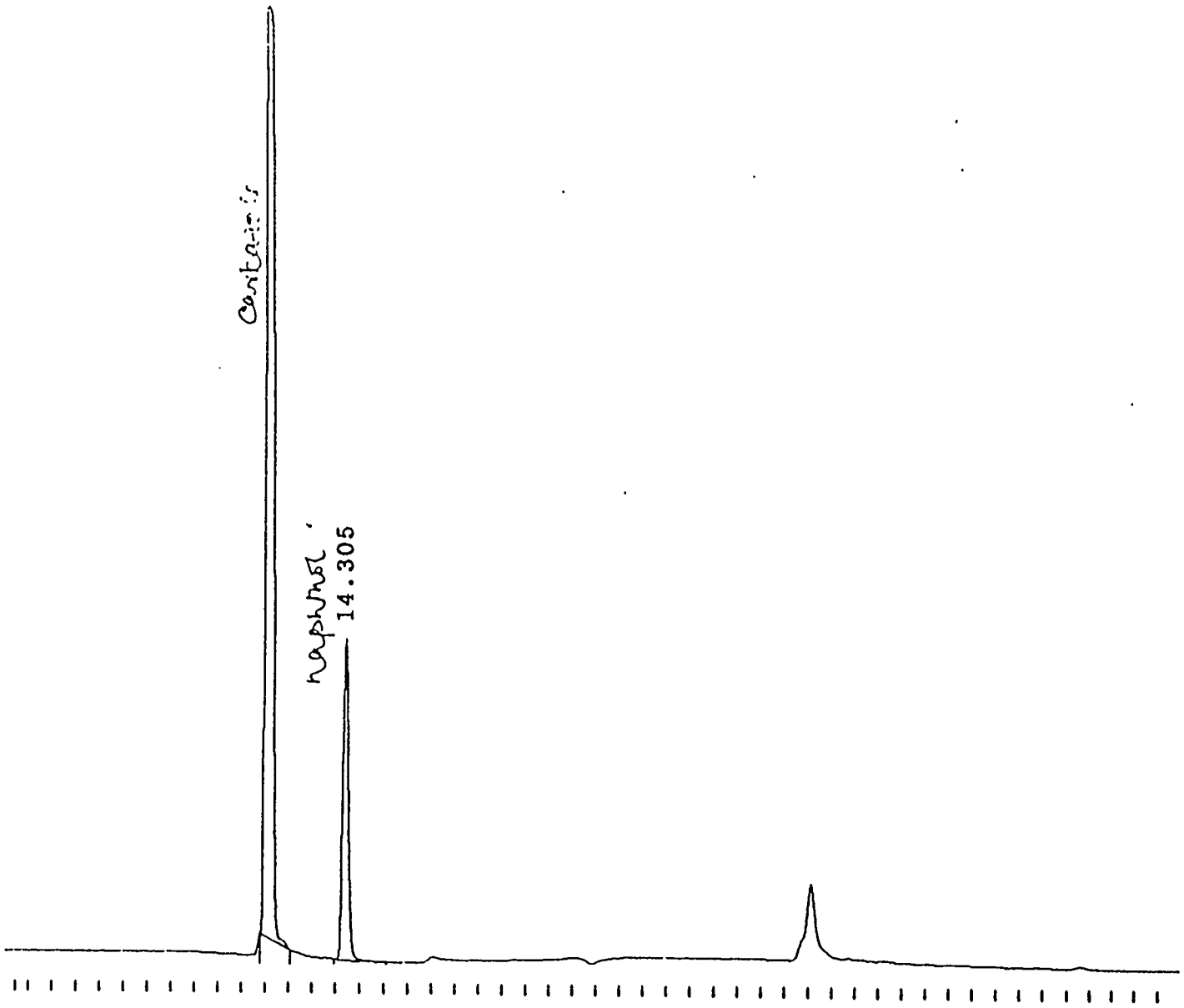

Figure 4: Functional group separation of polars

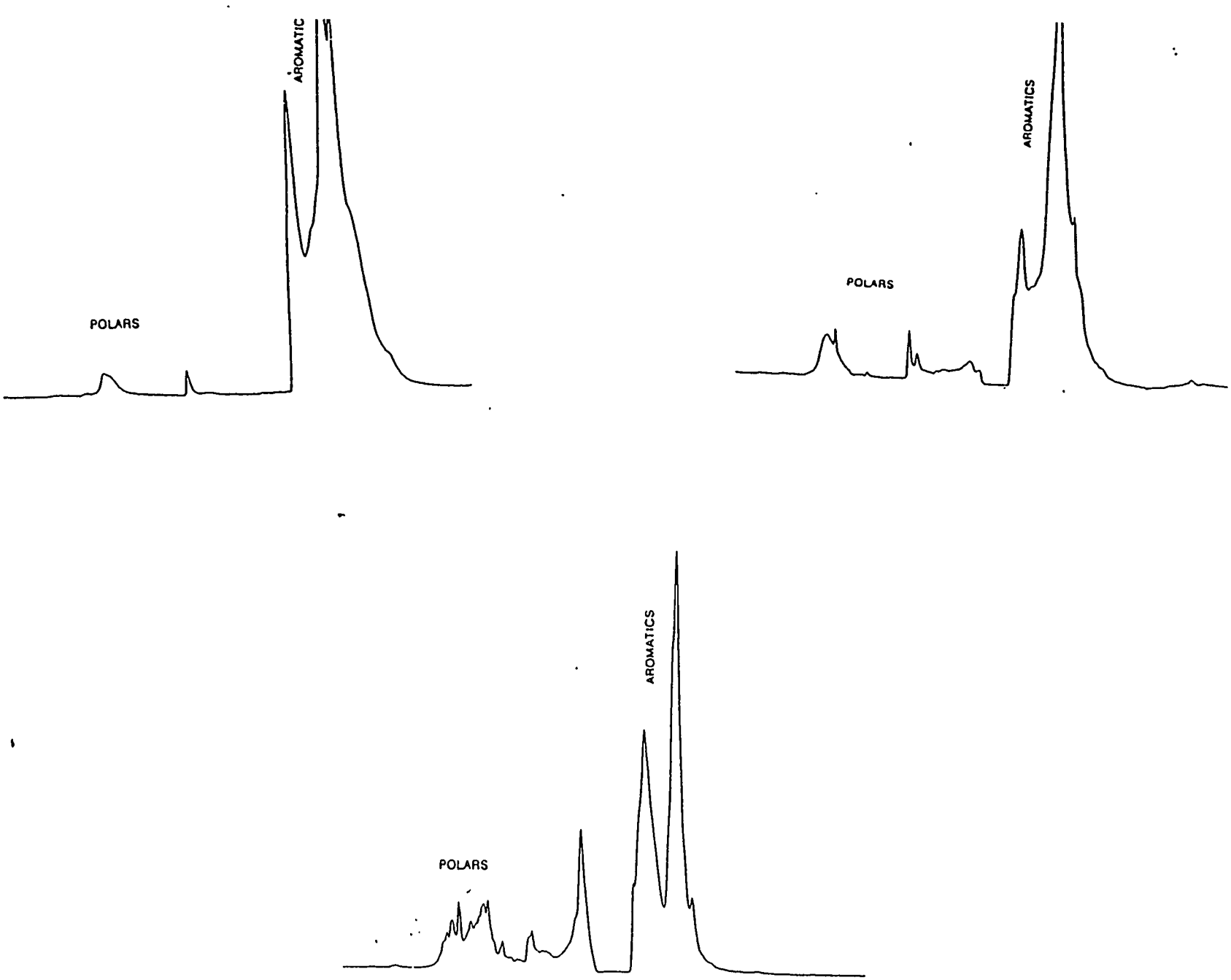

Figure 5a,5b,5c: Commercial crudes resolved by compound class (uv response)

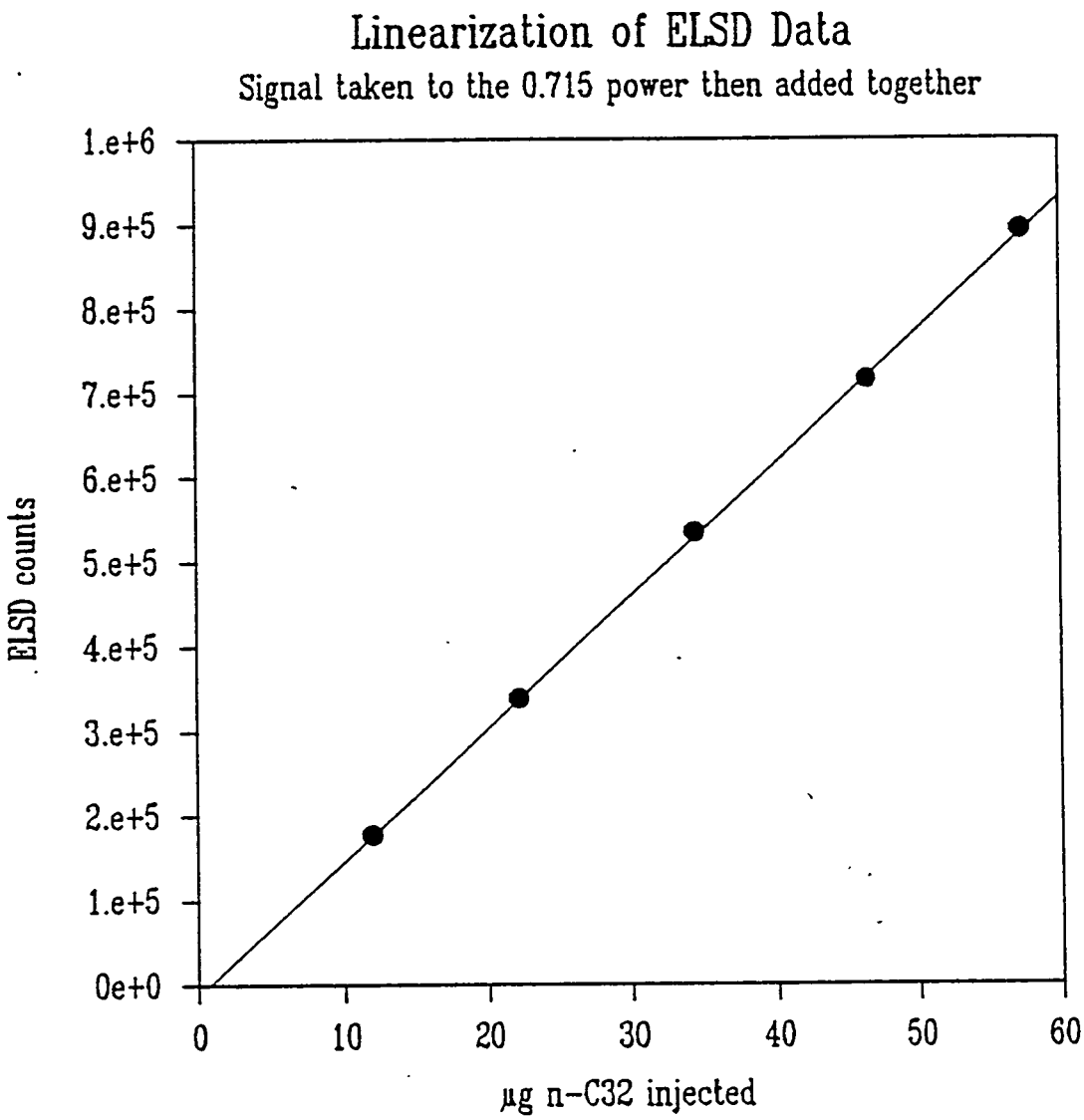

Temp= 50 deg C; N_2 flow = 2.9 l/ min ; mobile phase: 1.5 ml/min pentane

Figure 6b: Linearization of C_{32} response using ELSD.

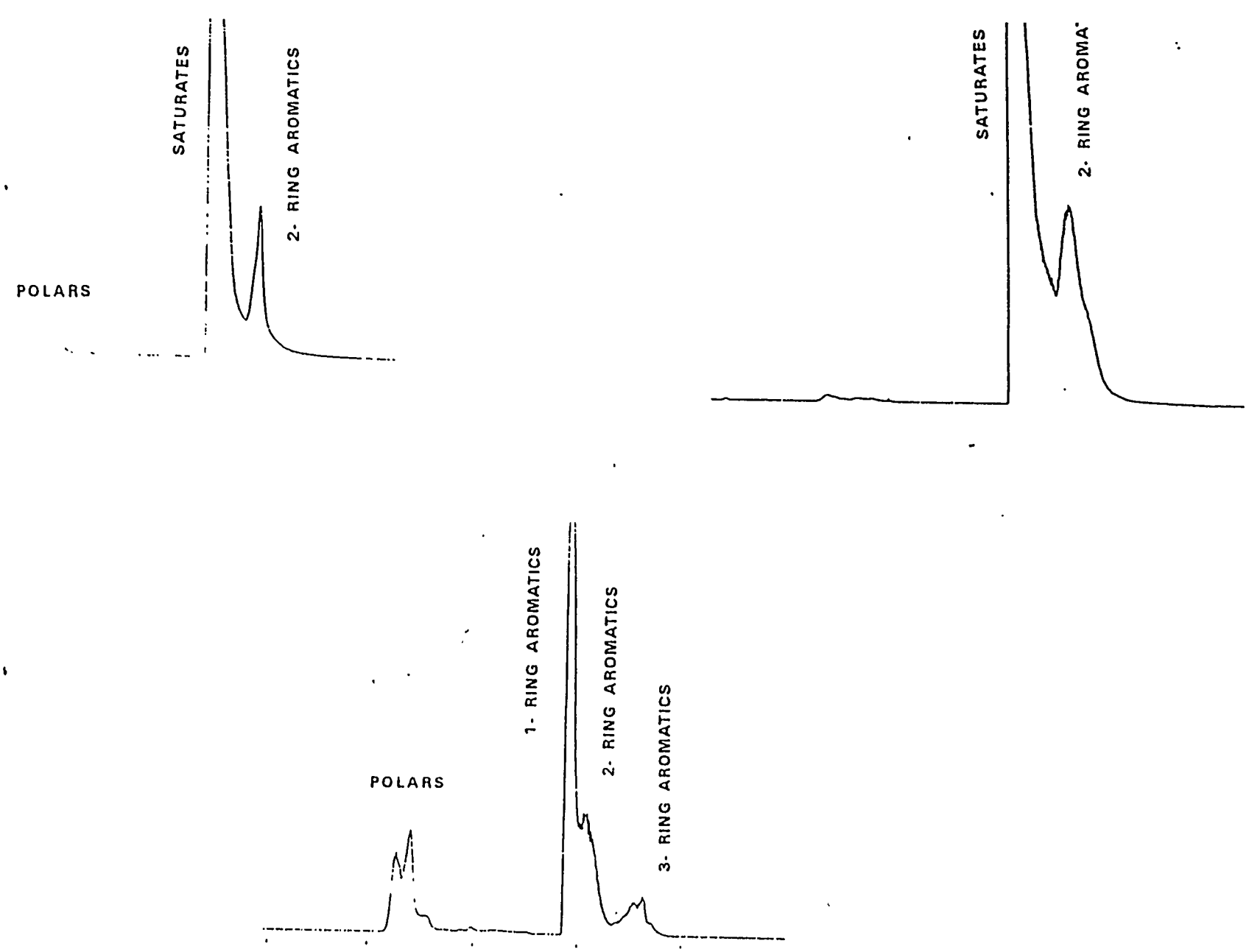

Figure 7a,7b,7c: Commercial crudes resolved by compound class (elsd response)

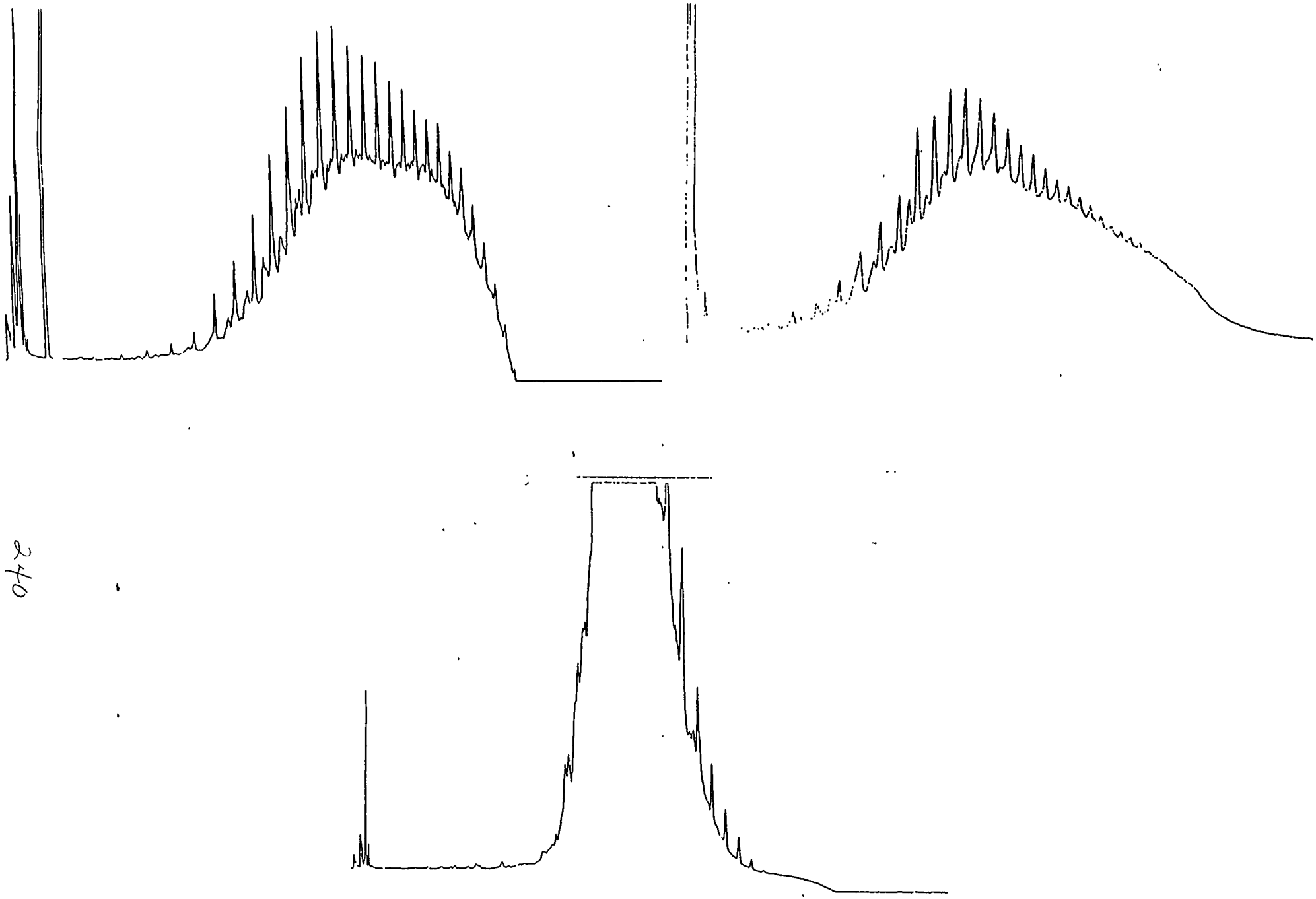

Figure 8a,8b,8c: Simulated distillation of a commerical crude oil feedstock

ELSD Response to N_2 Flow Rate and Solvent Composition

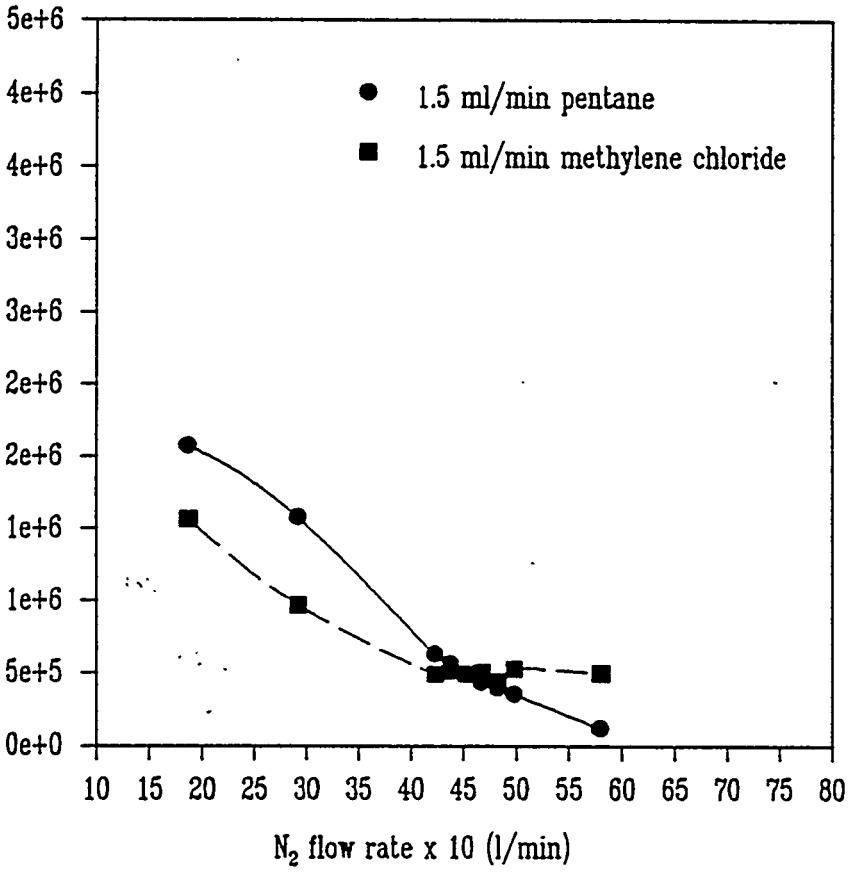

21.0 µg Fluoranthene injected Temp = 50 deg C

Figure 9: Optimizing the nebulizer gas flow rate for the ELSD.

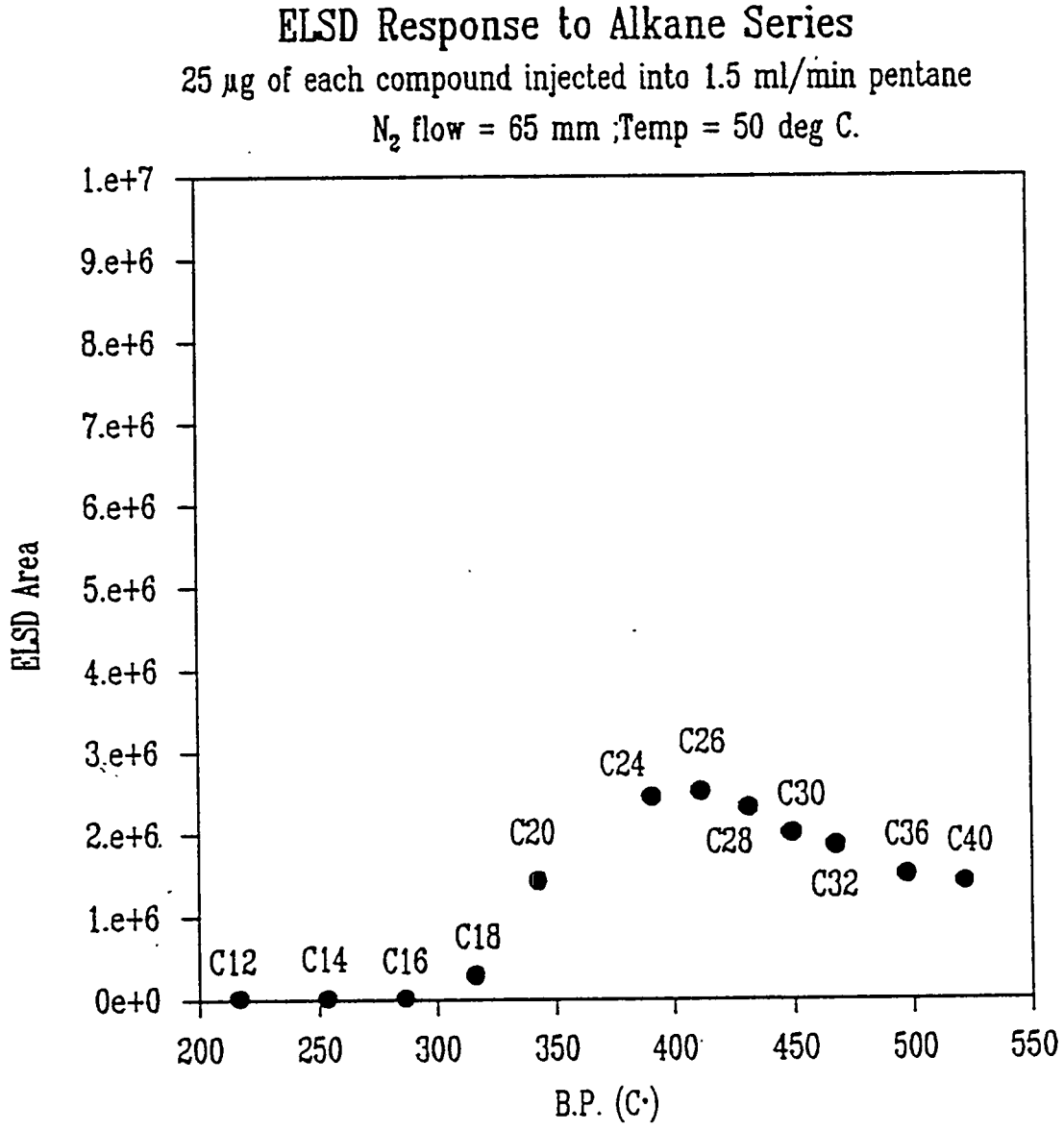

Figure 10: ELSD response to alkane series

TIME	PENTANE	METH. CHL.	IPA
0.00	**DNAP COLUMN**	**DNAP COLUMN**	**DNAP COLUMN**
0.00	100	0	0
2.00	**DIOL COLUMN**	**DIOL COLUMN**	**DIOL COLUMN**
2.00	100	0	0
3.33	100	0	0
13.33	0	0	100
20.00	0	95	5
20.67	0	100	0
21.33	100	0	0
26.67	**DNAP COLUMN**	**DNAP COLUMN**	**DNAP COLUMN**
26.67	100	0	0
40.00	40	60	0
43.33	0	100	0
50.00	**DNAP COLUMN**	**DNAP COLUMN**	**DNAP COLUMN**
50.00	0	100	0

Table 1: Solvent gradient used in the separation scheme

	COMPOUND NAME	DOUBLE BOND	RETENTION TIME (min)
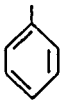	TOLUNENE	3	28.24
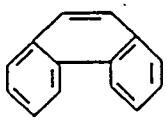	PHENATHRENE	7	33.919
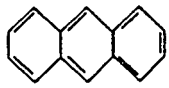	ANTHRACENE	7	35.841
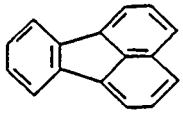	FLUORANTHENE	8	36.084
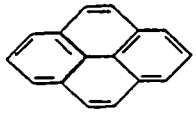	PYRENE	8	36.084
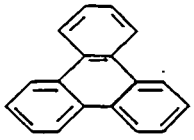	TRIPHENYLENE	9	37.300
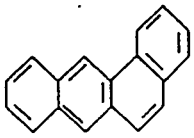	BENZO (a) ANTHRACENE	9	37.789
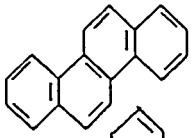	CHRYSENE	9	37.789
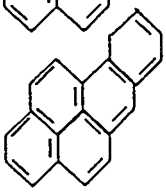	BENZO (e) PYRENE	10	40.205
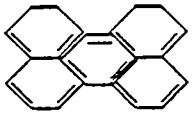	PERYLENE	10	40.569
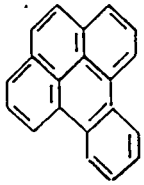	BENZO (A) PYRENE	10	40.891

Table 2: Retention time cor-relates with number of double bonds

TASK III

Project III.4

COMPUTATIONAL CHEMISTRY OF DCL CATALYSTS AND MODEL COMPOUNDS

K.R. Subbaswamy
University of Kentucky

During the 93-94 contract year, we have worked on the following topics: (1) modeling of Fe-based DCL catalysts; (2) investigation of catalytic mechanisms for model compounds; and (3) modeling binary catalysts.

1. Fe-based Catalysts

We continued our initial work[1] on the adsorption of small aromatic compounds on FeS surfaces. We have investigated the effect of adsorption sites on adsorption energy and bond dissociation energies for both pristine FeS surfaces and surfaces with vacancies. We have also done studies of the effect of H adsorbed in vacancies on bond dissociation energies of the aliphatic-aromatic bond of adsorbates to investigate the possible role of adsorbed hydrogen on bond cleavage.

One of the additional sites we considered is one in which the midpoint of the $C_{(aromatic)}$-$C_{(aliphatic)}$ bond is initially placed above the center Fe atom of the cluster. This geometry is referred to as midpoint hereafter. In this configuration the iron atom is in an ideal position to insert into the carbon-carbon bond and promote dissociation of this bond. A typical minimized geometry of the adsorbate with respect to the surface is shown in Figure 1.

For comparison, we also investigated sites in which the ring carbon atom of the $C_{(aromatic)}$-$C_{(aliphatic)}$ linkage was initially placed directly above the Fe atom in the center of the cluster, one in which the center of the aromatic ring system of toluene is placed over the center Fe atom, and one in which the C of the methyl group of toluene is positioned above an Fe atom. These geometries are referred to respectively as atop, centered, and methyl-atop hereafter. The centered position is the so-called η^6 site, usually observed for low coverages of aromatics on transition metal surfaces. In all of the calculations the methyl group is oriented with one hydrogen down towards the surface and the other two up.

Our computed results for the adsorption energy, BDE, and charge transfer for the different cases studied for the smooth (0001) surface are summarized in Table 1. The adsorption energy of toluene to the surface for the midpoint case is exothermic by 3.35 eV. With the parameters used, we observe a transfer of electron charge from the adsorbed molecule to the FeS cluster with a resultant decrease in the $C_{(ring)}$-CH_3 overlap population and bond breaking energy as compared to unadsorbed (free) toluene. The bond dissociation energy for toluene decreases upon chemisorption from 4.25 to 2.77 eV. Using unadsorbed toluene as a reference point, it is observed that electron density is removed from the p_z (π) orbitals of the ring system and from

the σ bond of the $C_{(aromatic)}$-$C_{(aliphatic)}$ linkage, thereby weakening the affected bond. The bond dissociation energy decreases to 0.6 eV when the reference point for the bond dissociation energy calculation is a methyl group adsorbed on a next nearest neighbor Fe atom. However, this does not include the barrier for surface diffusion of the methyl group.

For the pristine FeS cluster considered here the iron d-levels extend down to -13.05 eV, and the top of the sulfur p-band is at -14.1 eV. The HOMO of the free toluene is at -13.1 eV, and the level that contributes most to the Ph-CH_3 bond is at -13.5 eV. The adsorption involves the overlap of the iron d_z^2 orbitals with the Ph-CH_3 sigma-orbitals corresponding to these closely lying levels.

As discussed in our earlier report, similar results are observed for the atop geometry. The adsorption energy of toluene to the surface is exothermic by 3.07 eV and the bond dissociation energy is 2.96 eV, again a decrease as compared to unadsorbed toluene. Electron density is removed from the $p_z(\pi)$ orbitals of the ring system and from the σ bond of the $C_{(aromatic)}$-$C_{(aliphatic)}$ linkage for the atop geometry also. In the centered case we observe that even though the toluene molecule is more strongly adsorbed by the surface in this conformation, increasing to 3.89 eV, the bond dissociation energy increases to 3.23 eV when compared to the midpoint and atop configurations. Electron density is removed from the pi orbitals of the ring system, but the electron density for the sigma linkage is unchanged as compared to that of the unadsorbed toluene molecule.

In the methyl-atop case, we again see a stronger adsorption energy, in this case 3.99 eV, but the bond dissociation energy has increased to 3.15 eV as compared to the atop and midpoint configurations. Electron density is removed from the pi orbitals of the ring but not from the sigma linkage as compared to that of the unabsorbed toluene molecule.

The BDE appears to decrease the most when an Fe atom is underneath the $C_{(aromatic)}$-$C_{(aliphatic)}$ bond. There are some geometries in which this bond lies between two Fe atoms, and is not weakened as much.

In order to simulate the pyrrhotite iron deficient structure, various Fe atoms in the top layer of the smooth surface have been removed, thereby creating a vacancy. For the atop geometry, three possible vacancies have been considered, one in which the iron atom immediately under the ring C of the aromatic-aliphatic linkage has been removed, one in which the Fe near the methyl group is removed and one in which the Fe at the rear of the ring is removed. These are hereafter referred to as ring, front, and rear, and are shown in Figure 2. For the ring and rear cases, the energy of adsorption of toluene decreases to 2.07 and 2.68 eV, respectively. Also, the bond dissociation energy increases to 3.23 eV for the ring case as compared to when there is no vacancy.

In the ring case, as in the centered case, electron density is removed from the π orbitals of the aromatic system but not from the σ bond linkage leading to an increase in the bond dissociation energy. In the rear and front cases, electron density is removed from the sigma bond linkage, and hence the BDE is largely unaffected. These results are summarized in Table 2.

We also considered the effect of an Fe vacancy for the midpoint and methyl-atop initial geometries. In the midpoint case the Fe vacancy occurs for the Fe initially at the midpoint of the aromatic-aliphatic bond (i.e., the atom numbered 3 in Figure 1), and for the methyl-atop case the Fe vacancy is underneath the methyl group. The adsorption energies increase for the midpoint case and are largely unaffected for the methyl-atop vacancy case when compared to similar surfaces with no vacancies. However, the bond dissociation energies for the midpoint case have increased as compared to the case with no vacancy. The electron density is not removed from the σ linkage. These results are summarized in Table 3.

We also studied a stepped surface in which Fe atoms instead of sulfur form the top layer. Preliminary results indicate that the bond dissociation energy for adsorbed toluene has been decreased to 2.5 eV as compared to 4.25 eV for free toluene. The adsorption energy is about 2.3 eV. This, combined with the fact that adsorption does not occur for the zig-zag surface, seems to suggest that a critical number of clustered iron atoms on the surface is essential for adsorption to occur.

When a H atom is placed in a vacancy in the smooth Fe cluster, the H moves to 1.36 A from a sulfur atom in the second layer. Preliminary results indicate that in this geometry the H in the vacancy has no effect on the adsorption energy of bond dissociation energy for toluene.

Transition metal sulfides are used extensively as hydrotreating catalysts. To investigate the effect of FeS in such processes, we have studied the adsorption of H_2 on FeS clusters. When a hydrogen molecule is placed parallel to the stepped surface, one hydrogen atom directly above a sulfur atom and at a distance of 2.4 A from the surface we find that the hydrogen molecule escapes from the vicinity of the surface as a hydrogen molecule. However, when the hydrogen molecule was pushed down to 1.4 A above an exposed sulfur atom, the hydrogen molecule dissociates and forms a pseudo-H_2S species on the surface of the stepped surface. The optimized geometry after dissociation has a H-S-H bond angle of 106° and a H-S bond distance of 1.4 A.

We find that a hydrogen molecule (with the molecular axis parallel to the surface) is weakly physisorbed 2.4 A above an Fe atom on the smooth surface. The adsorption energy is only 0.05 eV. Both hydrogen atoms of the molecule were allowed to move to lower energy positions. No tendency for the hydrogen molecule to dissociate into atoms or to leave the vicinity of the surface was observed. When the hydrogen molecule is pushed down to 1.4 A above the surface and again, both hydrogen atoms were allowed to seek lower energy positions, another minimum position is found for the molecule about 1.6 A above the surface and 2.5 A from the nearest Fe atom and with an adsorption energy of 0.10 eV. Again, no dissociation of the hydrogen molecule into hydrogen atoms is noted.

A similar result is seen when the initial geometry has the midpoint of the hydrogen bond over the center Fe atom. The optimized geometry puts the hydrogen molecule 1.6 A above a surface interstitial position; the corresponding adsorption energy is 0.1 eV. No tendency for the dissociation of the hydrogen molecule is observed. For the FeS cluster considered here, the sulfur s-band extends down from -19.9 eV. The free hydrogen molecular

level is at -19.3 eV. However, on the FeS (0001) surface the sulfur atoms are well beneath the exposed iron atoms, giving little possibility of overlap with the relevant sulfur orbitals. This explains the weak adsorption of hydrogen.

In conclusion, we observe that molecules with aromatic ring systems are strongly chemisorbed by Fe atoms of the FeS (0001) catalyst surface as well as the Fe atoms of the stepped surface, suggesting that there is a critical number of exposed Fe atoms necessary in order for stable adsorption to occur. A transfer of charge from the adsorbed molecule to the catalyst is observed, creating a radical cation-substrate complex and leading to a decrease in bond dissociation energies of bonds between aromatic rings and aliphatic carbons. This appears to be similar to the mechanism proposed by Farcasiu, *et al.* in the context of the catalytic decomposition of 4-(1-naphthylmethyl)bibenzyl in the presence of carbon black. The decrease in bond dissociation energies is greatest when electron density is removed from both the sigma bond of the $C_{(aromatic)}$-$C_{(aliphatic)}$ linkage and from the pi system of the aromatic ring system.

To explain[1] the preferential bond cleavage at a polycyclic condensed ring-$C_{aliphatic}$ linkage over that of a monocyclic ring-$C_{(aliphatic)}$ linkage, one can envision a synergistic effect wherein the polycyclic condensed ring, instead of a monocyclic ring, is preferentially adsorbed on an exposed iron surface of FeS, followed by a transfer of charge from the polycyclic ring system to the surface, weakening the bond adjacent to the adsorbed ring system. Further, the sulfur surfaces can, under pressure, aid in the dissociation of molecular hydrogen into atomic species. The hydrogen molecule, dissociated into atoms by the sulfur interaction and perhaps trapped in a Fe vacancy is then available to cap off the free radicals formed upon dissociation. This preferential adsorption of polycyclic condensed rings should lead to a weakening of the aromatic-aliphatic bond adjacent to the polycyclic rings. Bonds not in the immediate vicinity of the surface should be unaffected by the adsorption process.

2. Radical Hydrogen Transfer Mechanism

Farcasiu and coworkers[2-5] have recently studied a series of model compounds with structural similarities to coal molecule fragments. They have found that carbon black catalysts (e.g., Black Pearl BP2000) show remarkable selectivity for the cleavage of the strong bond linking a condensed polycyclic aromatic ring to an aliphatic carbon, rather than weaker carbon-carbon single bonds. The mechanism for this catalysis is still the subject of much debate.[2,5-7] Combining reactivity studies with a charge distribution analysis of the catalyst Farcasiu and coworkers have proposed that in the presence of the catalyst, the reaction proceeds via the transfer to the catalyst surface of an electron, derived mostly from orbitals concentrated on the polycyclic aromatic ring.[2-4] Penn, et al.,[6] studying the photochemistry of naphthyl and phenyl compounds in solution and in the gas phase concluded that there was no indication of differences in reactivity of naphthyl and phenyl radical cations with the cleavage being that of the weaker carbon-carbon single bond rather than the stronger aliphatic-aromatic bond. Malhotra and McMillen,[7] from their study of the effect of C_{60} on the cleavage rate of strong bonds of 1,2'-dinaphthylmethane and selectivity of the bond cleavage, suggested that the increase in reactivity and selectivity results from the more efficient utilization of hydrogen in the presence of the catalyst.

Radical hydrogen transfer[7-18] (RHT) has been proposed as a possible mechanism for the cleavage of strong bonds in this context. RHT basically involves two steps: the bimolecular transfer of a hydrogen atom from a solvent derived radical to the ipso position of an aryl-alkyl linkage of the substrate, followed by the elimination of the substituent.[19] Free hydrogen atom transfer may also compete with the RHT process; the outcome of the competition is governed by many factors including aromaticity of the hydrogen donor.

Calculations of radical hydrogen transfer as a possible mechanism to explain the catalytic cleavage of model compound I have been continued. The AM1 calculations have been done with the quantum chemical program, MOPAC 5.0, of Stewart.[20] The calculations have been done with the RHF option with the half-electron correction and for completeness we extended the calculations to include the UHF (unrestricted Hartree-Fock) option of the MOPAC program. We have performed calculations modeling both hydrogen atom addition and bimolecular transfer of hydrogen from a C_6H_7 radical to model I. Autrey, et al.[21] have shown that for the ethyl+ ethylene RHT reaction the barrier calculated with AM1 semiempirical method is in agreement with *ab initio* calculation. They have, in fact, used such semiempirical calculations for higher hydrocarbon systems in assessing the importance of RHT pathway for cleaving strong bonds in coal and have concluded from their mechanistic studies that RHT need not be invoked to explain bond cleavage.[22] Rather the experimental results can be explained by reverse radical disproportionation and free hydrogen addition. On the other hand, McMillen and Malhotra[23] felt that Autrey chose the poorest solvent system for RHT for their mechanistic modeling and that RHT is needed to explain the selective cleavage of 1,2'-dinaphthylmethane.

The positions at which we consider hydrogen addition or transfer to Model I are shown and labeled in Figure 3. Our results for radical hydrogen transfer are summarized in Table 4 and for hydrogen atom addition and subsequent bond cleavage in Table 5. In the series A calculations the C_6H_7 radical was allowed to approach Model I at the four different transfer sites considered until the energy became slightly repulsive. At this point the distance between the relevant carbon atom of the radical and the attack site of the carbon atom of Model I was fixed and the transfer of the hydrogen atom between the two components allowed to occur. In series B calculations the C_6H_7 radical was allowed to approach the attack sites of Model I with no constraints along the transfer path, i.e., potential energy curves were calculated point by point by fixing only the distance between the relevant H and the position on Model I to which it is being transferred.

The second step in RHT, namely the cleavage of the ipso bond of the radical complex, is generally the fast step.[9] Therefore the barrier height of the first step, i.e. the addition or transfer of the hydrogen atom, considered to be the slow step, should control the final product distributions. The product distributions that result from the consideration of the relative activation energies of this first step are listed in Tables 4 and 5. The AM1 results for bond cleavage through radical hydrogen transfer do not reproduce the selective bond cleavage found in the experimental results (cleavage of the bond adjacent to the naphthyl group, bond a). We conclude that radical hydrogen transfer, while a possible mechanism for the cleavage of the strong bonds, does not seem to be the dominant mechanism operating in

the catalytic cleavage by carbon black of Model I.

3. Modeling Binary DCL Catalysts

A.Effect of adding molybdenum to FeS based catalysts.

It is known that the addition of small amounts of molybdenum leads to increased liquefaction yields.[24] Molybdenum also produces a more highly hydrogenated product.[24] Therefore, we have investigated, with the ASED-MO method, the influence of molybdenum impurities in FeS clusters. We investigated the bond breaking energy of the aromatic-aliphatic bond in toluene in the presence of Mo impurities and also considered the effect of the impurity on hydrogen molecule adsorption. In our modeling a Fe atom in the FeS cluster is replaced by a Mo atom. No relaxation of the surface around the vacancy is allowed. Two initial configurations were considered. In one (Case B) the Mo impurity atom is place initially at the midpoint of the Ph-CH_3 bond. The Mo impurity atom for the other initial geometry (Case A) is in front of the methyl group. These are shown in figures 4 and 5.

We find that for both initial geometries the favored adsorption site for is the so-called η^6 site, with the Mo in the center of the aromatic ring. However, when the Mo is initially at the midpoint the final geometry has the methyl group between two Fe atoms. For the other case an Fe atom is underneath the Ph-CH_3 bond. Strong adsorption occurs for both cases but the bond energy is lowered most when the Fe atom is underneath the Ph-CH_3 bond. These results are summarized in Table 6. The results for the adsorption of toluene (midpoint case) on a pristine FeS surface are included for comparison. We conclude therefore that the presence of the Mo impurity has no effect on the cleavage of bonds and the experimental results on increased yields is probably due to increased efficiency of hydrogenation.

Table 6

Case	Ph--CH_3 BDE(eV)	Adsorption Energy (eV)
Free	4.25	
FeS(mid)	2.77	3.44
Mo(A)	2.85	5.62
Mo(B)	3.23	5.84

B. Effect of Mo on H_2 chemisorption

Since the addition of Mo seems to have no synergistic effect on bond dissociation energies we investigated the effect of the impurity atom on hydrogen molecule adsorption. When the midpoint of the H_2 molecule was placed over the Mo impurity of the (0001) surface a weak adsorption of 0.2 eV at 2.2 A above the surface was observed. If the H_2 is initially placed 1.4A above the surface, the minimum is found again 2.2 A above the surface, unlike the case

for the adsorption of H_2 on the pristine FeS (0001) where a new minimum was found closer to the surface. When a stepped surface was considered with two Mo impurities underneath (for symmetry) and the S on top we found H_2 dissociates and forms an "H_2S" species as in the stepped surface of pure FeS cluster. However, with the two Mo atoms in the subsurface, the binding of the H_2S species is 0.27 eV less than when only pure FeS is present. Thus, release of these hydrogen atoms in a hydrogenation reaction should be easier in the presence of the Mo impurities

C. The effect of SiO coating of the Fe surface

Zhao et al.[25] have found that adding a small amount of impurity anions (M) during precipitation of in the preparation of ferrihydrite catalysts causes the formation of a new surface layer consisting of Fe-O-M. This surface layer inhibits agglomeration of small ferrihydrite particles at high temperature. In order to see if the inclusion of this surface layer would affect bond dissociation energies and adsorption of toluene on the FeS surface we performed ASED-MO calculations in which an -O-Si moiety is placed perpendicular to the (0001) smooth FeS surface. We find that SiO co-adsorption, if it is still present when the catalysis occurs, has no effect on liquefaction chemistry. Our results are summarized in Table 7.

Table 7

Case	Ph--CH_3 BDE(eV)	Adsorption Energy (eV)
Free	4.25	
FeS(mid)	2.77	3.44
SiO (A)	2.84	3.18
SiO (B)	2.83	3.28

SiO co-adsorption has no effect on liquefaction chemistry.

REFERENCES

1. Ades, H.F.; Companion, A.L.; Subbaswamy, K.R. *Energy Fuels*, **1994**, *8*, 71
2. Farcasiu, M.; Smith, C. *Prepr., Div. Fuel Chem., Am. Chem. Soc.*, **1990**, *35*, 404.
3. Farcasiu M.; Smith, C. *Energy Fuels*, **1991**, *5*, 83.
4. Farcasiu M.; Smith, C.; Hunter, E. A. (to be published).
5. Farcasiu,M.; Petrosius, S.C. *Prepr., Div. Fuel Chem., Am. Chem. Soc.* **1994**, *39*,723.
6. Penn, J.; Wang, J. *Energy Fuels*, **1994**, *8*, 421.
7. Malhotra, D. R.; McMillen D. F. *Energy Fuels*, **1993**, *7*, 227.
8. Malhotra, R.; McMillen, D. F.; Tse, D. S.; Lorents, D. C.; Ruoff, R. S.; Keegan, D. M. *Energy Fuels*, **1993**, *7*, 685.
9. McMillen, D. F.; Malhotra, R.; Tse, D.S. P*repr., Div. Fuel Chem., Am. Chem. Soc.*, **1991**, *36*, 498.
10. Malhotra, R.; McMillen, D. F.; *Energy Fuels*, **1990**, *4*, 184.
11. Autrey, T.; Gleicher, G. J.; Camaioni, D. M.; Ferris, K. F.; Franz, J. A. *Prepr., Div. Fuel Chem., Am. Chem. Soc.*, **1991**, 36, 521.
12. McMillen, D. F.; Malhotra, R.; Chang, S-J.; Ogier, W. C.; Nigenda, S. E.; Fleming, R. H. *Fuel*, **1987**, *66*, 1611.
13. Metzger, J. O. *Angew. Chem., Int. Ed. Engl.*, **1986**, *25*, 80.
14. McMillen, D. F.; Malhotra, R.; Nigenda, S. E. *Fuel*, **1989**, *68*, 380.
15. Freund, H.; Matturo, M. G.; Olmstead, W. N.; Reynolds, R. P.; Upton, T. H. *Energy Fuels*, **1991**, *5*, 840.
16. Smith, C. M.; Savage, P. E. *Energy Fuels*, **1991**, *5*, 146.
17. Smith, C. M.; Savage, P. E. *Energy Fuels*, **1992**, *6*, 195.
18. Autrey, T.; Franz, J. A. *Prepr., Div. Fuel Chem., Am. Chem. Soc.*, **1990**, *35*, 381.
19. Poutsma, M. L. *Energy Fuels*, **1990**, *4*, 113.
20. Stewart, J. J. P.; et al. Quantum Chemistry Program Exchange No. 581, vers. 5.0, (Indiana University, Bloomington).
21. Autrey,S.T.; Camaioni, D.M.; Ferris, K.F.; Franz, J.A. Proc., 7th Int. Conf. Coal Sci., Banff, Alberta, Canada, **1993**, Vol. I, 336.
22. Autrey, T.; Alborn-Cleveland, E.; Camaioni, D.M.; Franz, J.A. *Prepr., Div. Fuel Chem., Am. Chem. Soc.*. **1994**, *39*, 627.
23. McMillen, D.F.; Malhotra, R. *Prepr., Div. Fuel Chem., Am. Chem. Soc.*. **1994**, *39*, 632.
24. Pradhan, V.R.; Herrick, D.E.; Tierny, ,J.W.; Wender, I.; *Energy Fuels*, **1991**, *5*, 712.
25. Zhao, J.; Feng, Z.; Huggins, F.E.; Huffman, G.P. *Energy Fuels*, **1994**, *8*, 38.

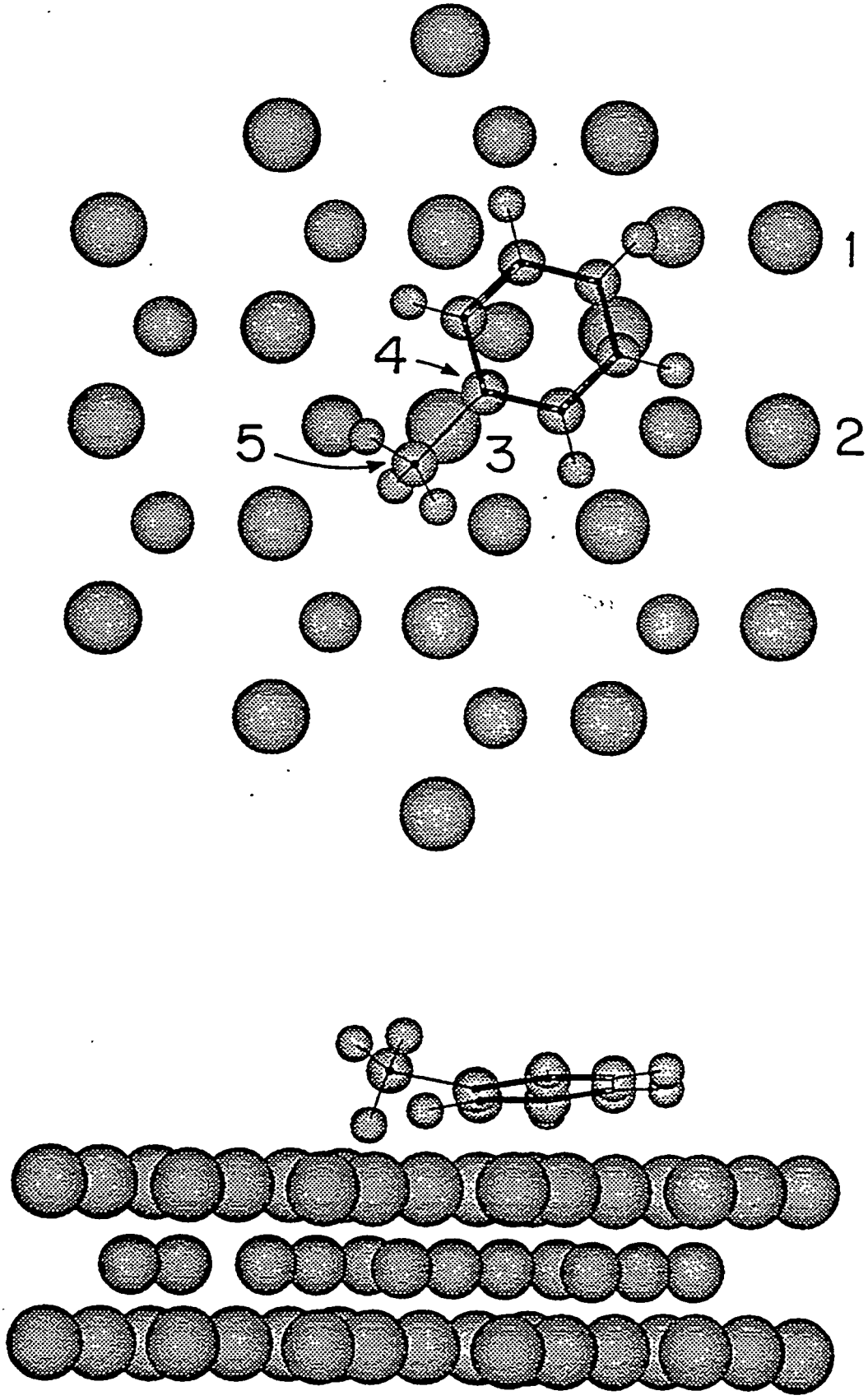

FIGURE 1

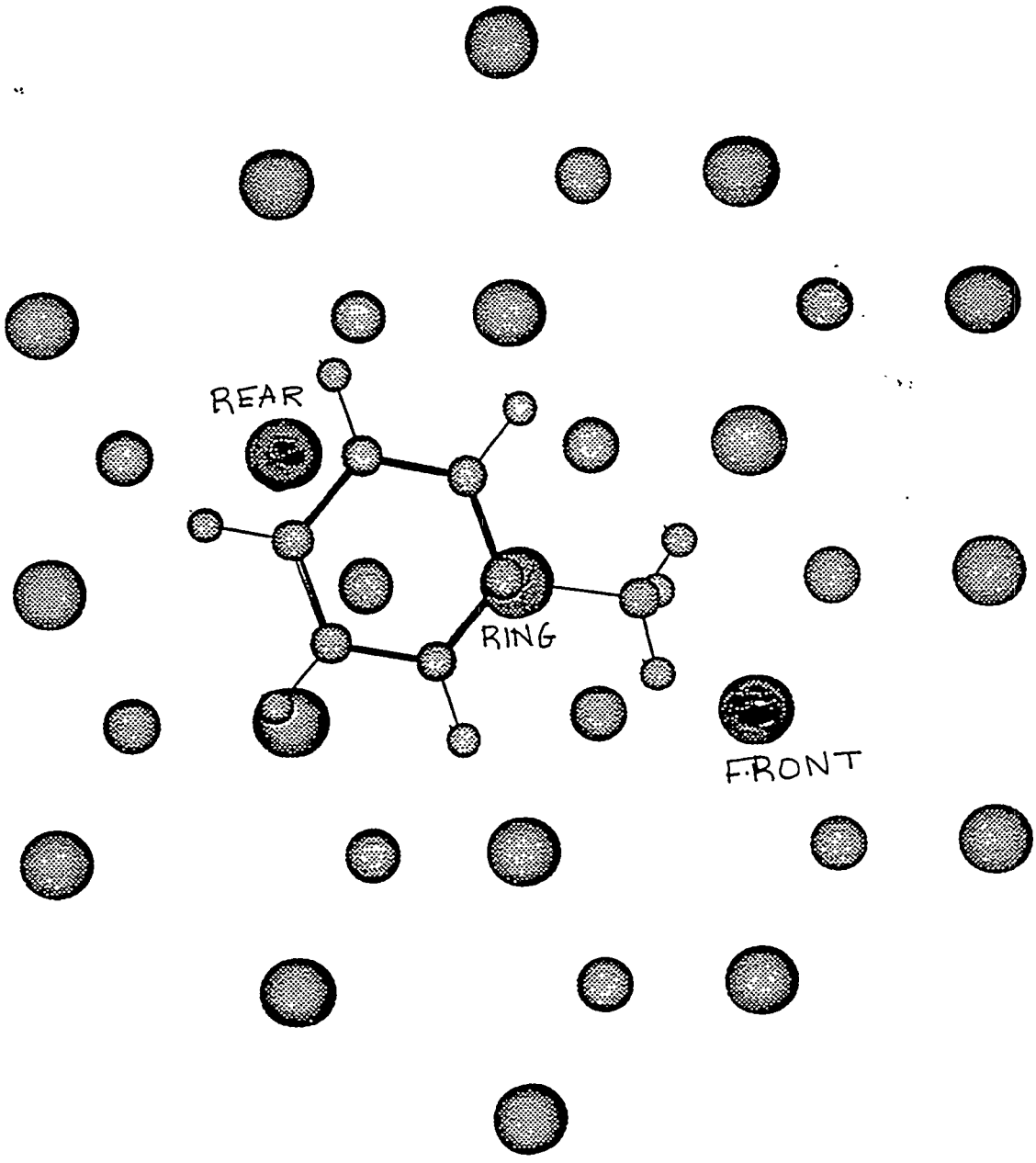

FIGURE 2

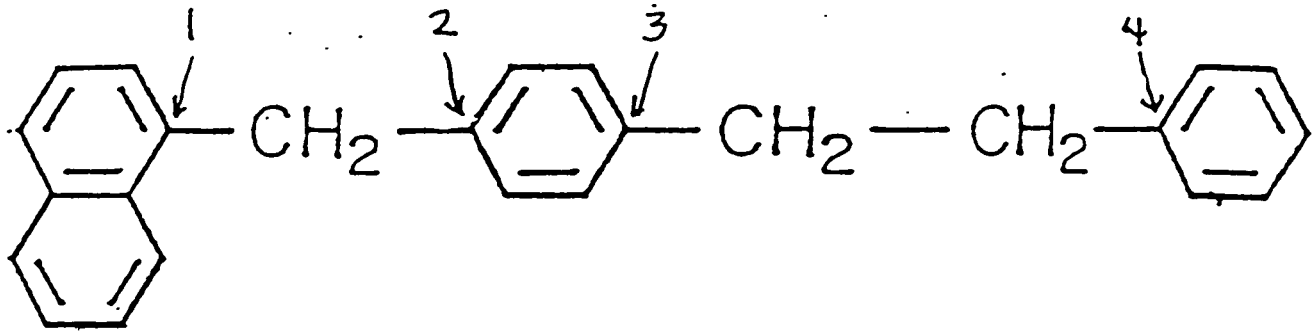

FIGURE 3

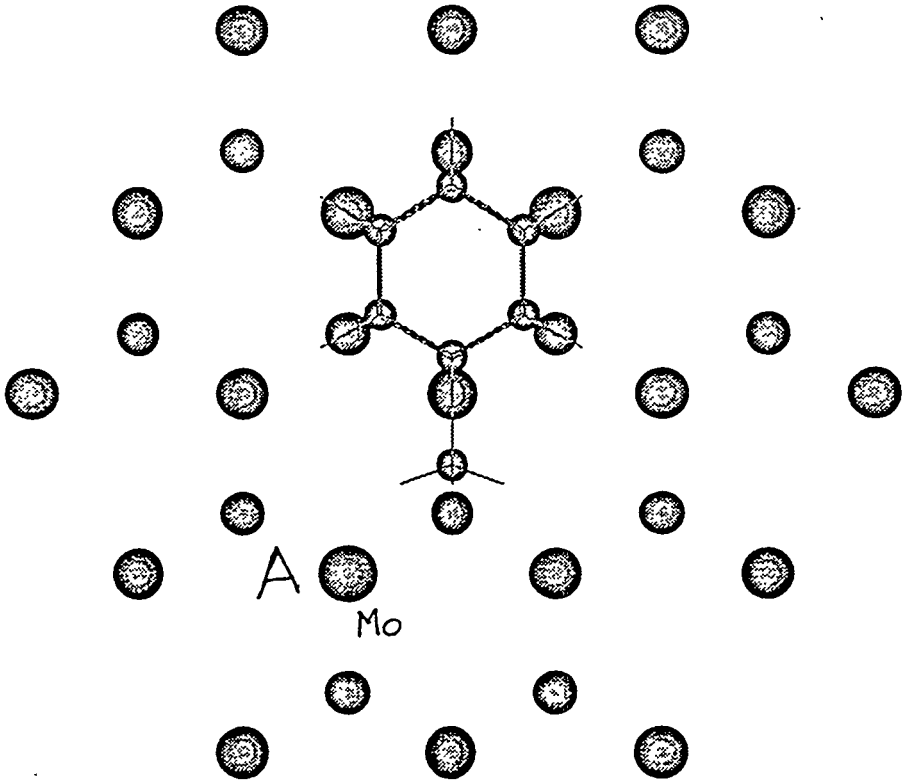

Fig. 4: Initial and final geometries with Mo near the CH_3 unit.

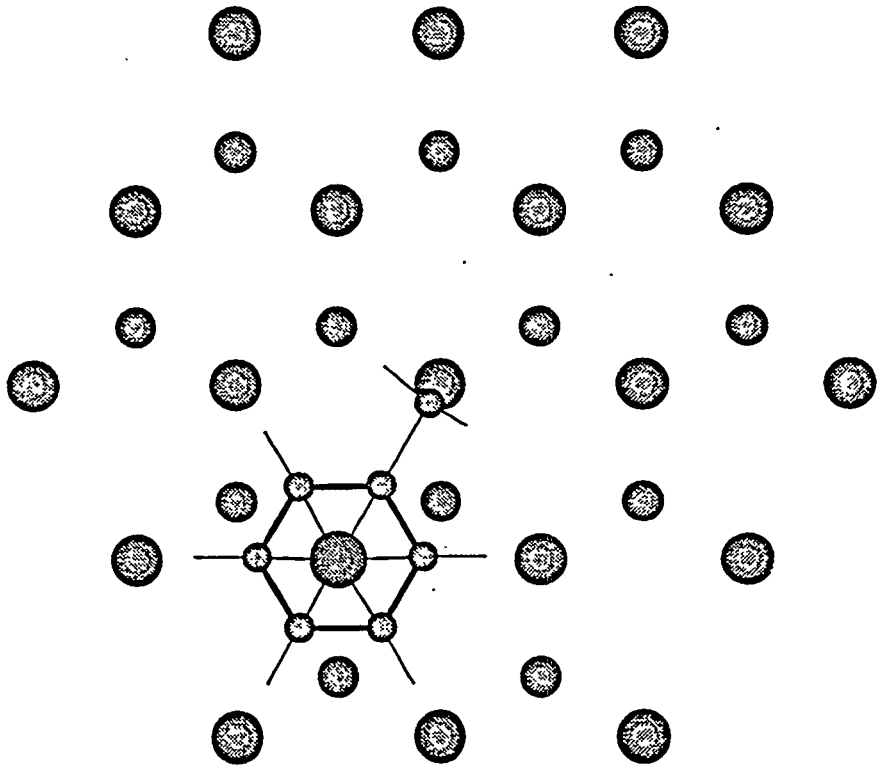

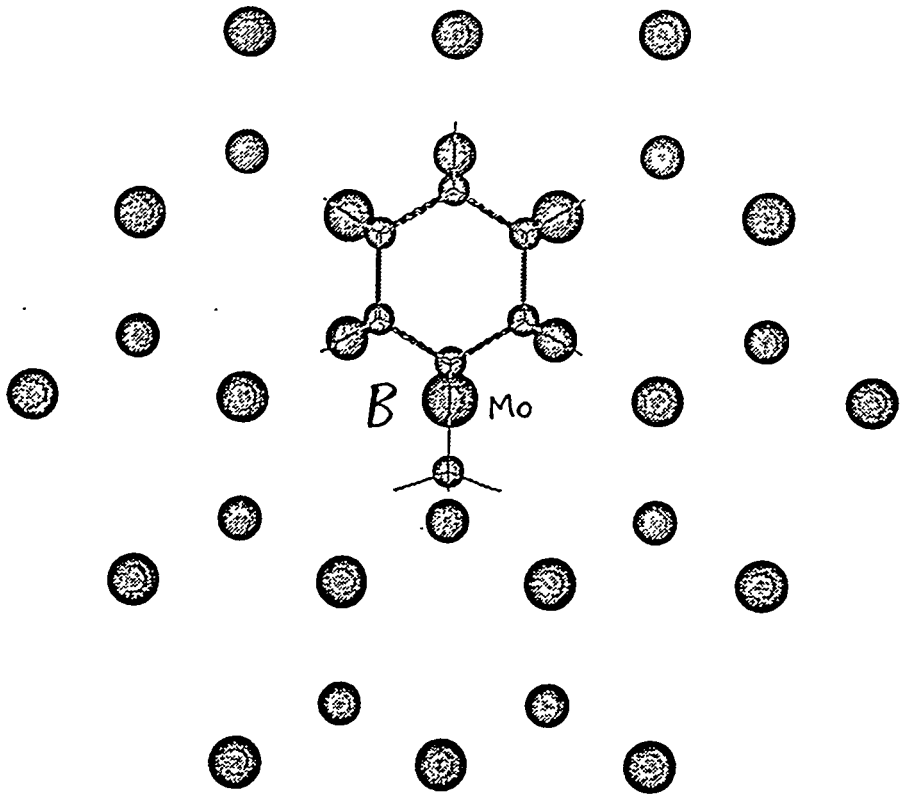

Fig. 5: Initial and final geometries with Mo near the Ph-CH_3 bond.

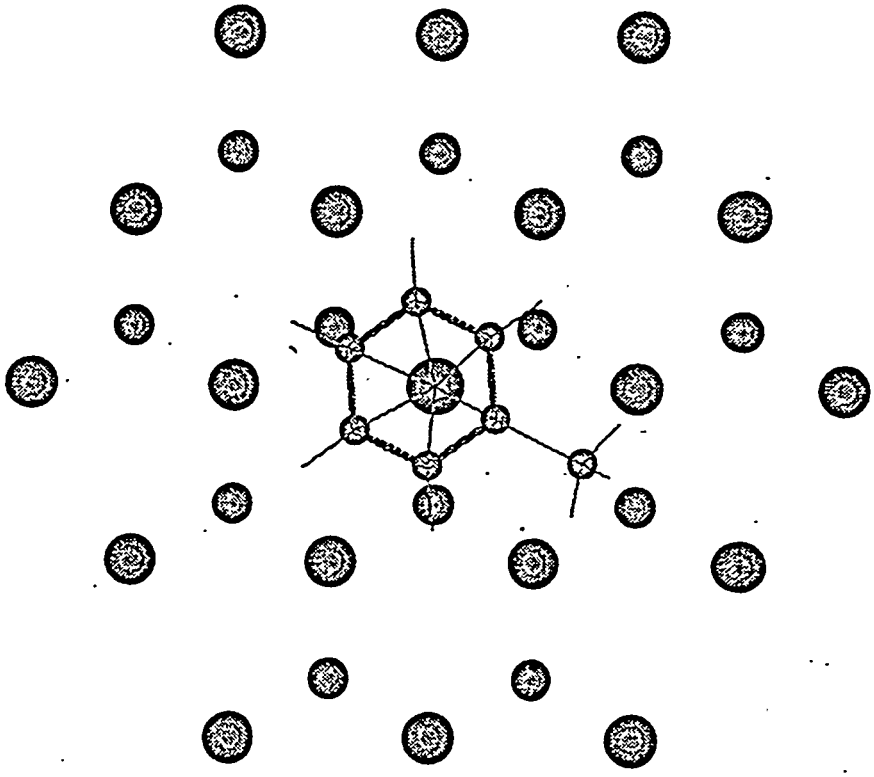

Site	Free	Atop	Midpoint	Centered	Methyl-atop
$-\Delta E_{adsb.}$ (eV)		3.07	3.44	3.89	3.99
BDE (eV)	4.25	2.96	2.77	3.23	3.15
ΔQ to surface		$0.87e^-$	$1.16e^-$	$0.75e^-$	$0.60e^-$
$\Delta\rho_e$ from $C_{aromatic}$		0.1587	0.1804	0.1406	0.1110
$\Delta\rho_e$ from $C_{aliphatic}$		0.0663	0.1380	0.0005	-0.002

Table 1: Summary of results of adsorption of toluene on FeS (0001) surface. Results for free (unadsorbed) species are included for comparison. ΔQ is the charge transfer to the surface; the last two rows give the total electron density removed from the aromatic carbon and the aliphatic carbon of the $C_{aromatic}$-$C_{aliphatic}$ linkage, respectively.

Site	Front	Ring	Rear
$-\Delta E_{adsb.}$ (eV)	3.10	2.07	2.68
BDE (eV)	2.88	3.23	3.03
ΔQ to surface	$0.78e^-$	$0.55e^-$	$0.78e^-$
$\Delta\rho_e$ from $C_{aromatic}$	0.1311	0.0875	0.1616
$\Delta\rho_e$ from $C_{aliphatic}$	0.0478	-0.0060	0.0549

Table 2: Summary of results of adsorption of toluene on FeS (0001) surface in the presence of an iron vacancy when toluene is in the atop position. The vacancy site lables are illustrated in Figure 2. The various quantities are the same as in Table 1.

Site	Midpoint	Methyl-atop
$-\Delta E_{adsb.}$ (eV)	3.84	3.88
BDE (eV)	3.12	3.08
ΔQ to surface	$1.02e^-$	$0.861e^-$
$\Delta\rho_e$ from $C_{aromatic}$	0.1447	0.1346
$\Delta\rho_e$ from $C_{aliphatic}$	0.016	0.008

Table 3: Summary of results of adsorption of toluene on FeS (0001) surface in the presence of an Fe vacancy. The site labels designate the configuration of the adsorbate. The positions of the vacancy in the two cases are described in the text. The quantities are the same as in Table 1.

Position	E_1	E_2	d_{C-H}	%Distribution
Series A				
1	1.87	-0.49	1.77	20.9
2	1.88	0.17	1.75	29.5
3	1.89	0.11	1.76	24.8
4	1.88	0.11	1.76	24.8
Series B				
1	1.81	-0.06	1.37	6.9
2	1.76	0.16	1.37	16.2
3	1.74	0.09	1.37	22.9
4	1.69	0.14	1.37	54.0

Table 4: Activation barriers (E_1), bond formation energies (E_2), for the bimolecular transfer of a hydrogen atom from a C6H7 radical to Model I. Energies are reported in eV's and bond distances in Å. The distributions were calculated assuming a Boltzmann distribution at 400° C. See Figure 3 for bond labels.

Position	E_1	E_2	E_3	E_4	%Distribution
1	0.53(0.57)	-1.62(1.55)	1.28(1.30)	0.65(0.59)	9
2	0.44(0.51)	-1.33(1.41)	1.22(1.21)	0.39(0.48)	42.3
3	0.44	-1.42	1.36	0.52	42.3
4	0.55	-1.35	1.29	0.51	6.4

Table 5: Activation barriers (E_1), bond formation energies (E_2), dissocation energy barriers (E_3), and bond cleavage energies (E_4) for radical hydrogen transfer. Energies are reported in eV's. A negative bond formation energy represents an exothermic process. See Figure 3 for bond labels. The numbers in parentheses refer to energies for the approach path from the other side of the molecule, when different. The percent distributions are given for the lowest energy approach path only.

TASK III

Project III.5

SURFACE CHARACTERIZATION OF BINARY FERRIHYDRITE LIQUEFACTION CATALYSTS

J.Y. Kim, P.J. Reucroft, and J. Zhao*
Department of Materials Science and Engineering
University of Kentucky

* The Consortium for Fossil Fuel Liquefaction Science
University of Kentucky

Introduction

In recent years, efforts have been made to produce highly dispersed iron oxide catalysts for direct coal liquefaction (DCL).[1-6] Under the DCL conditions normally employed, the iron oxide undergoes phase transformations to sulfided forms, such as $Fe_{1-x}S$, during which agglomeration of fine particles may occur, resulting in a lower surface area and reduced catalytic activity. Under these conditions, a catalyst, to remain active, has to be able to maintain its dispersion.[2] Secondary components are added to the iron oxide catalyst in order to accomplish this and a binary system is thereby produced. The properties of the binary catalyst can be controlled by choosing an appropriate element as the secondary component and by varying the doping level. The degree of dispersion of the binary system usually increases with addition of the secondary component due to the discrepancy between the ionic radii of the two components causing the secondary component to accumulate at the catalyst particle surface.[7,8] It is also possible to have the secondary component (M) adsorbed at the catalyst surface to form a new M-O-Fe surface layer. Since the performance of a catalyst is determined mainly by its surface structure and condition, a reconstructed surface may significantly improve the activity of the catalyst, even at low-levels of doping (M/Fe < 5%). Wender *et al.* have reported on the DCL performance of Fe_2O_3/SO_4^{2-} catalyst systems.[2] They observed that the catalysts maintain their dispersion under the reaction conditions due to the acidity of the S-O-Fe layer, which prevents small α-Fe_2O_3 particles from agglomerating. Recently, Zhao *et al.* have described the DCL performance of binary ferrihydrite catalysts (M/FHYD). Preliminary results with added Si to

FHYD have shown that both the oil yield and total conversion are increased in the direct liquefaction of DECS-17 (Blind Canyon) coal at 410°C.[9,10] The catalyst dispersion and the resulting intimate contact between the catalyst surface and coal can play an important role in coal liquefaction. Since the catalyst surface is the primary site of catalytic activity, past efforts have been directed at characterizing fresh catalyst surfaces and catalyst surfaces in coal liquefaction environments.[11] In the present work, X-ray photoelectron spectroscopy (XPS) has been used to investigate the surface characteristics of a series of binary ferrihydrite catalysts (M/FHYD) where secondary metallic- or non-metallic components are added to the particle surface to inhibit particle agglomeration at high temperatures.

Experimental

A pure ferrihydrite sample and 5 different binary ferrihydrite catalysts were investigated in the surface characterization studies. A citric acid treated ferrihydrite catalyst was also investigated. The estimated particle size was 30 Å in the case of the pure ferrihydrite catalyst. The particle size has not been determined for the rest of the samples. The detailed sample preparations have been described in previous papers.[9,10] The catalysts are briefly summarized in Table 1.

The samples were examined by XPS employing a Kratos XSAM 800 spectrometer using Mg Kα (1253.6 eV) radiation. The XPS experimental set-up employed in this work has been described previously.[11,12] The spectrometer was run in fixed analyzer transmission (FAT) mode at a pass energy of 11 kV and 13 mA. Under these conditions, the full width half maximum (FWHM) of the Ag ($3d_{5/2}$) peak is ~1.0 eV. All binding energies were referred to carbon 1s at 285 eV to compensate for sample charging. Atomic concentrations were estimated from the area of peaks by applying the appropriate atomic sensitivity factors.[13]

Results

Fig. 1 shows typical XPS wide scan spectra of a binary ferrihydrite catalyst (Si/FHYD) and a citric acid treated ferrihydrite catalyst (FHYD/CA). The spectra showed distinct peaks for the major elements, oxygen and iron in each catalyst sample. A strong carbon peak was observed in all catalysts which can be ascribed to carbon contamination. Relatively weak peaks of secondary components were observed in wide scan spectra due to the low concentrations of the added secondary components relative to Fe (see Table 1).

Separate narrow survey scans were carried out on each element peak to determine both

the oxidation states and elemental concentrations at the particle surface. The binding energies of the Fe 2*p*, Si 2*p*, P 2*p*, Mo 3*d*, Al 2*s*, and Zn 2*p* peaks showed the expected values for the most stable oxidation states of these elements. Figs. 2, 3, 4, and 5 show the spectra of Fe 2*p*, Si 2*p*, P 2*p*, and Mo 3*d*, respectively. Multiple splitting was observed in the transition element signals, such as Fe and Mo. No significant changes in chemical states for the Fe 2p regions were observed between the citric acid treated FHYD and the secondary component modified FHYD samples. The Fe 2*p* showed the 13.6 eV splitting between the $2p_{1/2}$ and $2p_{2/3}$ peaks. This was observed in all FHYD containing catalysts. The surface chemical state of Fe in FHYD can thus be ascribed to either Fe_2O_3 or FeOOH. Mo 3*d* showed the characteristic 3.2 eV splitting between the $3d_{2/3}$ and $3d_{2/5}$ peaks and can thus be attributed to the MoO_3 state at the catalyst surface. These results corresponded well with previous XPS studies on iron-oxide based catalysts.[11]

To determine the relative concentrations of the various constituents observed in the samples, peak area sensitivity factors have been employed. The surface elemental concentrations of the catalyst samples are shown in Table 2. The atomic ratio of both the added secondary components and oxygen to the FHYD (Fe) are also shown in Table 3. The surface concentration of Fe was not significantly affected by the added secondary components. Relatively high surface concentrations of both secondary components and oxygen were determined compared to the bulk values due presumably to surface oxidation and the surface enhancement of secondary components. Enhancement of secondary components at the surface of the FHYD particles may be due to the discrepancy between the ionic radii of the two components. From the values of the O/Fe ratio of the samples, the surface composition of FHYD appears to be closer to FeOOH (O/Fe=2.0), rather than Fe_2O_3 (O/Fe=1.5). XPS depth profiling studies will be employed to further define the nature of the FHYD surface and any difference between the surface and bulk concentrations of various elements. These studies are currently in progress.

REFERENCES

1. G.P. Huffman, B. Ganguly, J. Zhao, K.R.P.M. Rao, N. Shah, Z. Feng, F.E. Huggins, M.M. Taghiei, F. Lu, I. Wender, V.R. Pradhan, J.W. Tierney, M.S. Seehra, M.M. Ibrahim, J. Shabtai, and E.M. Eyring, *Energy & Fuels* **7**, 285 (1993).

2. V.R. Pradhan, J.W. Tierney, I. Wender, and G.P. Huffman, *Energy & Fuels*, **5**, 497 (1991).

3. J.S. Shabtai and Y. Zhang, *Proc. 1989 Int. Conf. Coal Sci., Tokyo*, **2**, 807 (1989).

4. M.M. Taghiei, F.E. Huggins, B. Ganguly, and G.P. Huffman, *Energy & Fuels*, **7**, 399 (1993).

5. B.R. Uts and A.V. Cuzini, U.S. Patent 5,096,570, 1992.

6. D.W. Matson, J.C. Linehan, and J.G. Darab, *Prepr. Pap.-Am. Chem. Soc., Div. Fuel Chem.*, **38**, 14 (1993).

7. U. Schwertmann, R.M. Cornell, *Iron Oxides in the Laboratory*, VCH, Weinheim, Germany, 1991, and references in therein.

8. T.G. Quin, G.J. Long, C.G. Benson, S. Mann, R.J.P. Williams, *Clays Clay Miner.*, **36**, 165 (1988).

9. J. Zhao, Z. Feng, F.E. Huggins, and G.P. Huffman, *Energy & Fuels*, **8**, 38 (1994).

10. J. Zhao, Z. Feng, F.E. Huggins, and G.P. Huffman, Submitted to *Energy & Fuels.*

11. J.Y. Kim, P.J. Reucroft, V.R. Pradhan, and I. Wender, *Fuel Proc. Technol.*, **34**, 207 (1993).

12. J.Y. Kim, P.J. Reucroft, M. Taghiei, V.R. Pradhan, and I. Wender, To be published in *Energy & Fuels, 1994.*

13. J.F. Moulder, W.F. Stickle, P.E. Sobol, and K.D. Bomben, *Handbook of X-ray photoelectron spectroscopy*, J. Chastain ed., Perkin Elmer Corp. Phys. Elec. Div., Eden Prairie, MN, 1992.

Table 1. Summary of Catalysts

Catalyst	Symbol	Elemental analysis
FHYD	I	30 Å particle size
Si/FHYD	II	Si/Fe = 0.05 (atomic ratio)
Si/FHYD	III	Si/Fe = 0.1 (atomic ratio)
Mo/FHYD	IV	Mo/Fe = 0.05 (atomic ratio)
P/FHYD	V	P/Fe = 0.08 (atomic ratio)
Al/FHYD	VI	Al/Fe = 0.05 (atomic ratio)
Zn/FHYD	VII	Zn/Fe = 0.05 (atomic ratio)
FHYD/CA	VIII	Citric acid treated FHYD

Table 2. Surface concentration (at.%) for FHYD catalysts

Elements	I	II	III	IV	V	VI	VII	VIII
C	15.9	17.2	18.8	18.9	13.3	17.4	27.4	19.7
O	60.6	53.5	54.0	56.9	59.7	59.8	49.4	56.4
Fe	23.5	23.0	19.1	22.7	23.2	20.7	19.2	23.9
Si		6.3	8.1					
Mo				1.5				
P					3.8			
Al						2.1		
Zn							4.0	

Table 3. Atomic ratios of secondary components and oxygen to Fe in FHYD catalysts

	I	II	III	IV	V	VI	VII	VIII
M*/Fe		0.27	0.42	0.07	0.16	0.10	0.21	
O/Fe	2.58	2.33	2.83	2.51	2.57	2.94	2.56	2.38

M* represents the added secondary component (see Table 1)

Figure 1 XPS wide scan spectra of (a) a binary ferrihydrite catalyst (Si/FHYD) and (b) a citric acid treated ferrihydrite catalyst (FHYD/CA)

Figure 2 Fe 2p XPS narrow scan spectra for (a) citric acid treated FHYD and (b) secondary component modified FHYD

Figure 3 Si 2p XPS narrow scan spectra for the Si modified FHYD

Figure 4 P 2p XPS narrow scan spectra for the P modified FHYD

Figure 5 Mo 3d XPS narrow scan spectra for the Mo modified FHYD

Table 1. Summary of Catalysts

Catalyst	Symbol	Elemental analysis
FHYD	I	30 Å particle size
Si/FHYD	II	Si/Fe = 0.05 (atomic ratio)
Si/FHYD	III	Si/Fe = 0.1 (atomic ratio)
Mo/FHYD	IV	Mo/Fe = 0.05 (atomic ratio)
P/FHYD	V	P/Fe = 0.08 (atomic ratio)
Al/FHYD	VI	Al/Fe = 0.05 (atomic ratio)
Zn/FHYD	VII	Zn/Fe = 0.05 (atomic ratio)
FHYD/CA	VIII	Citric acid treated FHYD

Table 2. Surface concentration (at.%) for FHYD catalysts

Elements	I	II	III	IV	V	VI	VII	VIII
C	15.9	17.2	18.8	18.9	13.3	17.4	27.4	19.7
O	60.6	53.5	54.0	56.9	59.7	59.8	49.4	56.4
Fe	23.5	23.0	19.1	22.7	23.2	20.7	19.2	23.9
Si		6.3	8.1					
Mo				1.5				
P					3.8			
Al						2.1		
Zn							4.0	

Table 3. Atomic ratios of secondary components and oxygen to Fe in FHYD catalysts

	I	II	III	IV	V	VI	VII	VIII
M*/Fe		0.27	0.42	0.07	0.16	0.10	0.21	
O/Fe	2.58	2.33	2.83	2.51	2.57	2.94	2.56	2.38

M* represents the added secondary component (see Table 1)

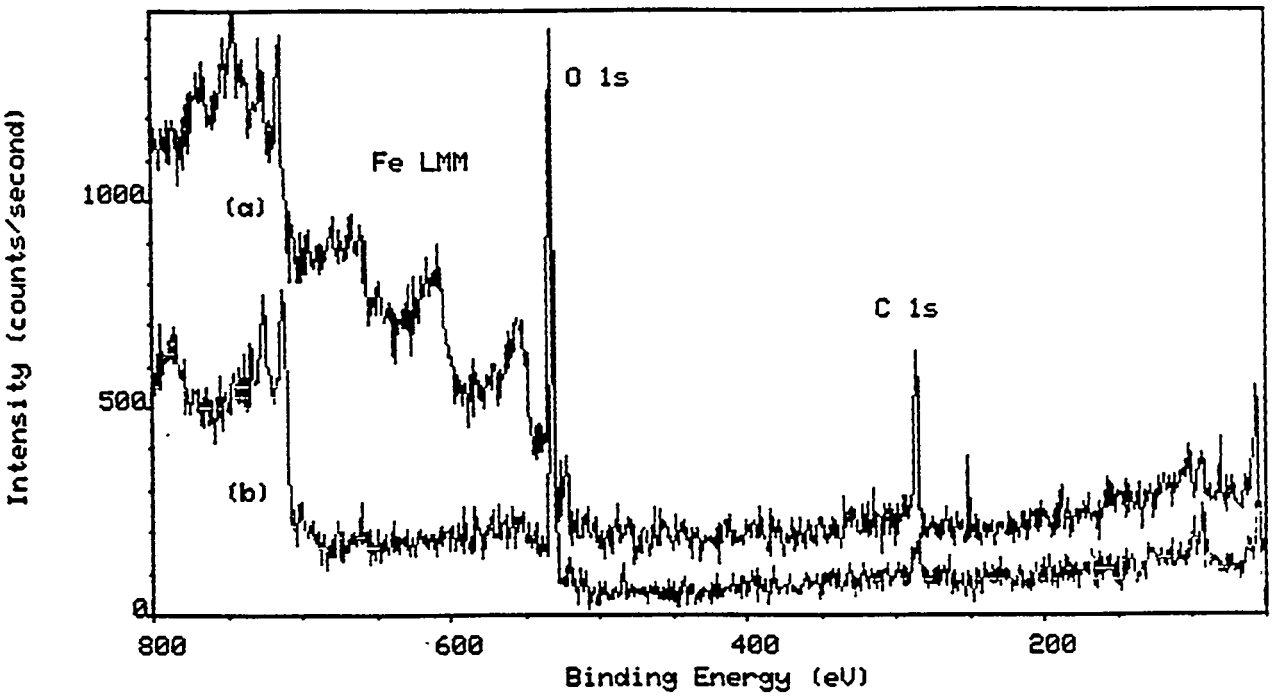

Figure 1 XPS wide scan spectra of (a) a binary ferrihydrite catalyst (Si/FHYD) and (b) a citric acid treated ferrihydrite catalyst (FHYD/CA)

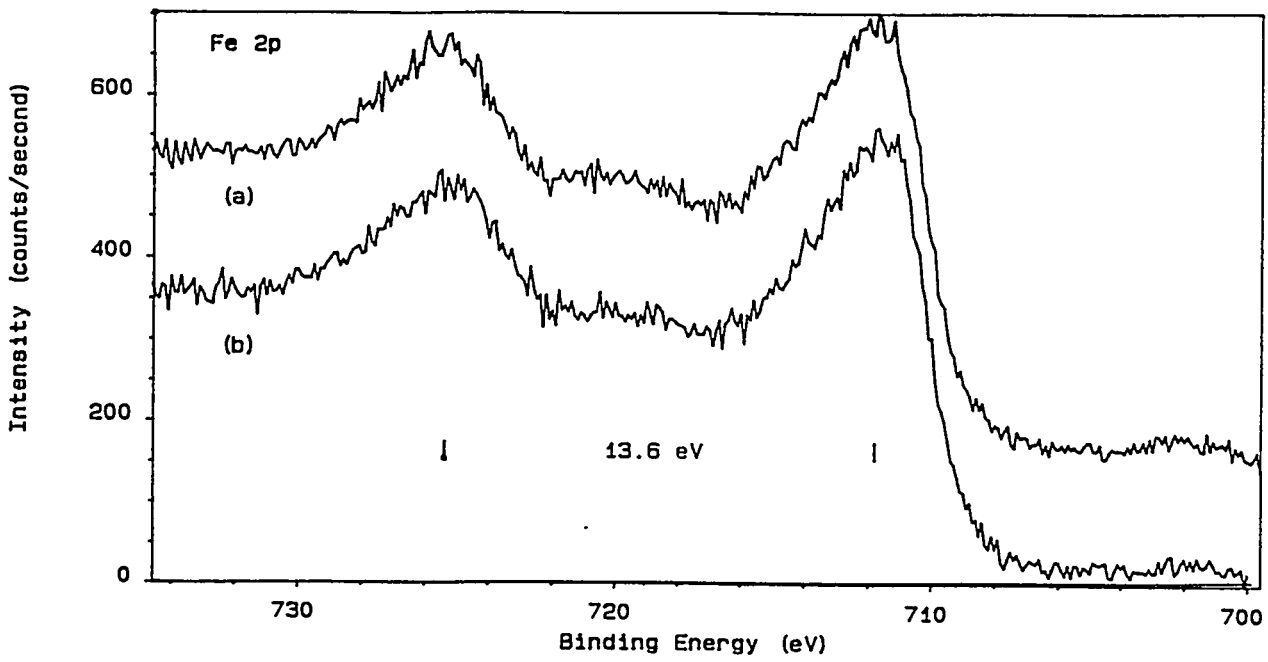

Figure 2 Fe 2p XPS narrow scan spectra for (a) citric acid treated FHYD and (b) secondary component modified FHYD

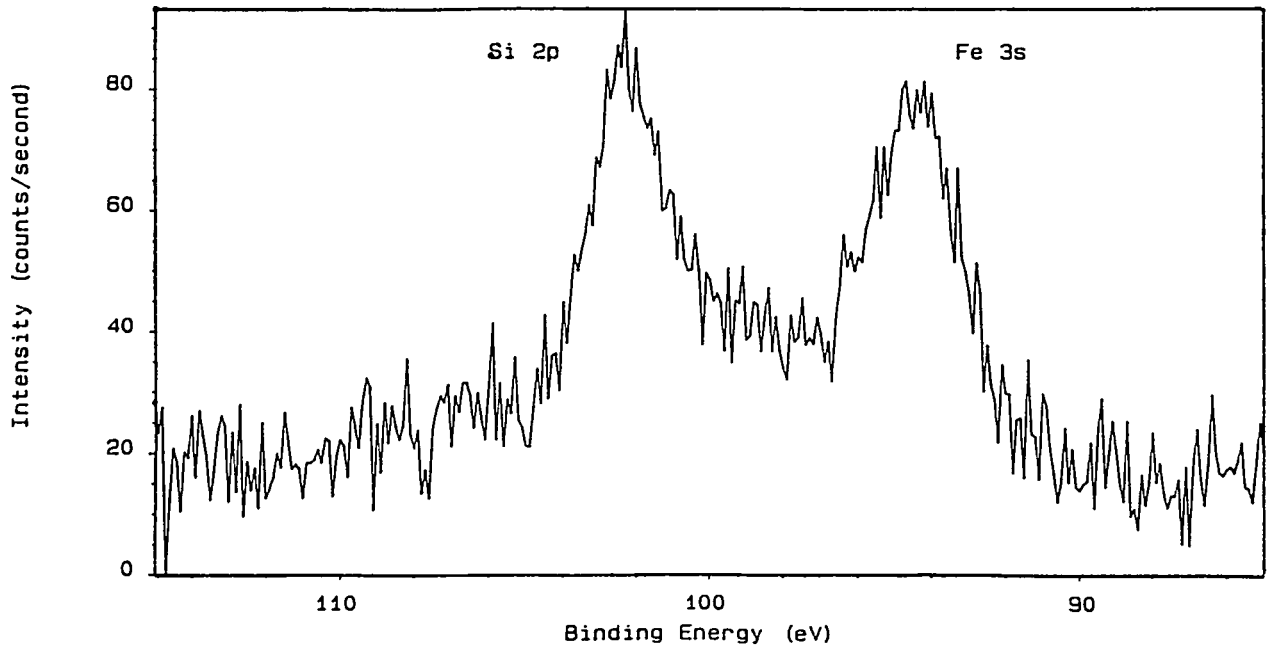

Figure 3 Si 2p XPS narrow scan spectra for the Si modified FHYD

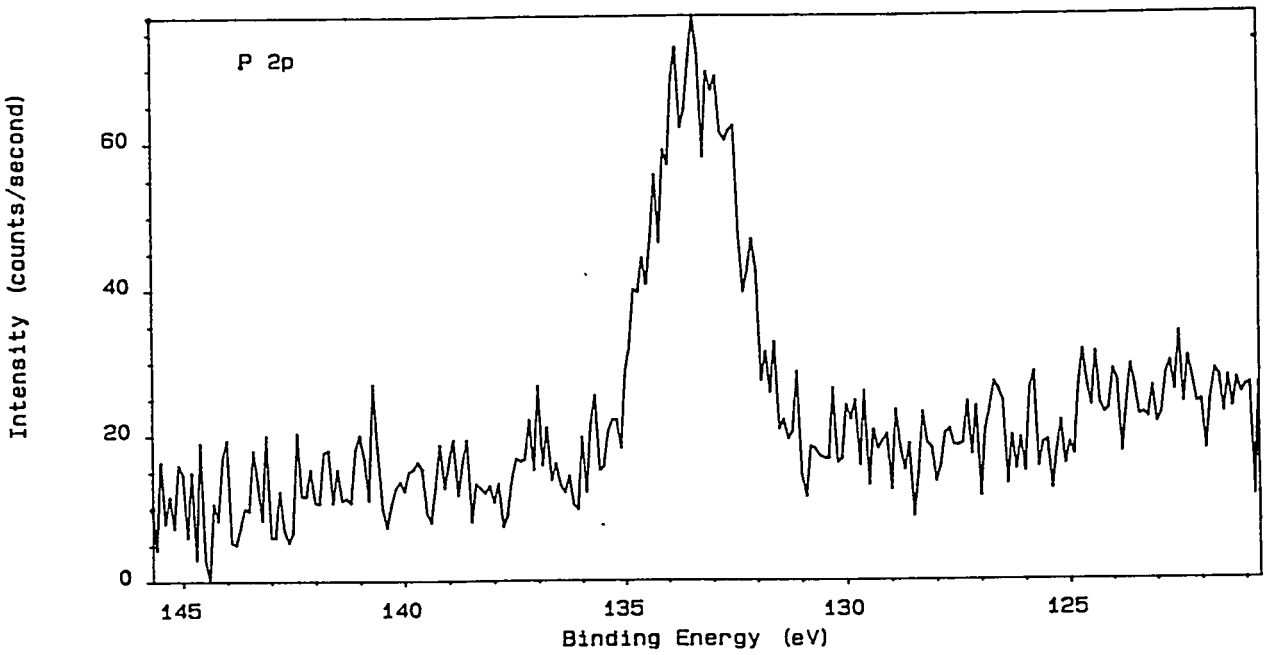

Figure 4 P 2p XPS narrow scan spectra for the P modified FHYD

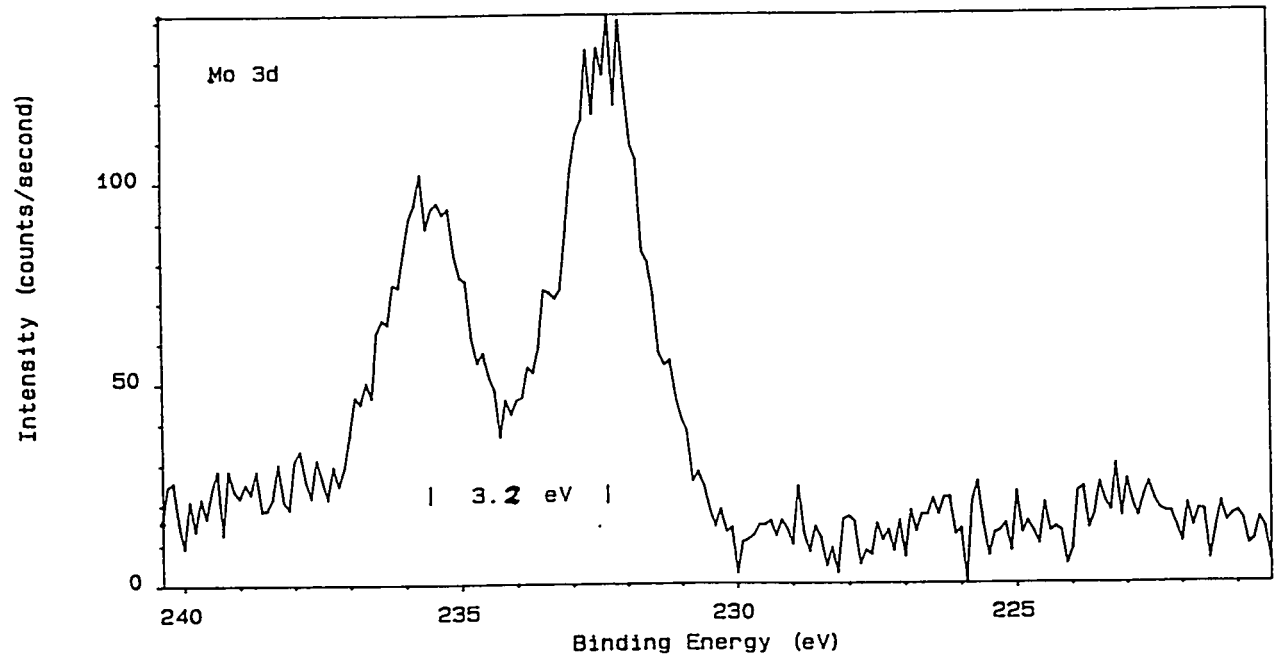

Figure 5 Mo 3d XPS narrow scan spectra for the Mo modified FHYD

TASK III

Project III.6

BIOPROCESSING OF COAL

D. Bhattacharyya, M.I.H. Aleem, R.I. Kermode,
M.V.S. Murty, D. Schieche
University of Kentucky

SUMMARY

This year, the effect of bacterial concentration and pressure on the biological hydrogenation of fumaric acid to succinic acid using H2 has been studied. A suitable method to analyze succinic acid using HPLC or enzymatic techniques is being developed. In order to investigate the hydrogen limitation, high pressure (500 psig) hydrogen gas was applied in a multipurpose bioreactor which was constructed in our laboratory. A preliminary study with *D. desulfuricans* under (normal and high pressure) hydrogen showed complete reduction of fumarate within 24 hours. An experiment was then repeated twice and results indicate that increasing hydrogen pressure does indeed enhance the biohyrogenation of fumarate. A mass-transfer based model describing the biological hydrogenation of organics has been developed. The model parameters will be evaluated using reaction rate data and statistical analysis software. New organic model compounds such as ferulic and cinnamic acid have been identified for the biohydrogenation study.

During the current year, new approaches have been initiated to reduce the time required for the reprecipitation of iron released from pyrite in the presence of *Acidianus brierleyi*. The time required for iron reprecipitation on the surface of coal was decreased to 11 days (from 21) when the pH of the medium (2.5) increased to 2.8. Increase of microbial adsorption on polymer and coal surfaces for even dispersion of reprecipitated ultra-fine iron catalyst (FeOOH) on the surfaces of polymer and coal may enhance direct liquefaction and quality of oil. Therefore, a preliminary bioprocessing study has been conducted on a mixture of polyethylene and coal.

Mossbauer data showed that all the biotreated coals containing different high pyrite, high sulfur Illinois coals (IBC #102,105), and pyrite free DECS coal with added pyrite, (with initial pH 2.5) completely (i.e., below the detection limit) removed pyrite in 21 days. The biotreated DECS #17 coal with added pyrite showed FeOOH formation with less than 120 A° particle size. It also showed an increase of the liquefaction conversion of 14% over the control which did not contain *A. brierleyi*. An extensive literature survey was also done for the possibility of partial degradation of polymers in the presence of coal.

Ia. Biohydrogenation of Fumarate - Effect of Cell Concentration

The use of *Desulfovibrio desulfuricans* (ATCC #7757) to biologically hydrogenate organics has been continued. An experiment was conducted to gain insight into the connection

between the concentration of bacteria and the hydrogenation reaction rate of fumaric acid to succinic acid under anaerobic conditions utilizing hydrogen gas.

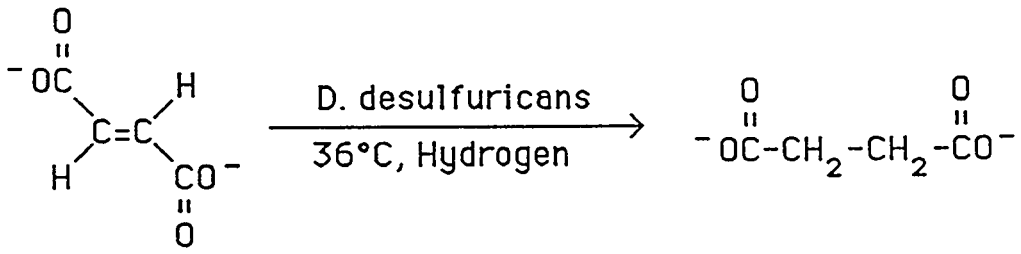

Specifically, this experiment explored the effect that doubling the cell concentration would have on the reaction rate.

The solution medium (1, 2) contained the following compounds in amounts scaled to grams per 1 liter of solution: 2.322 fumaric acid; 0.5 K2HPO4; 1.0 NH4Cl; and 0.02 CaCl2.2H2O. After mixing up the chemical medium, the pH was adjusted to 7.4. Then the medium was sterilized and nitrogen was sparged through the system to attain sterile anaerobic conditions. The substrate concentration was 20 mmol fumarate.

Five 100 ml flasks were placed in a constant temperature water bath at 36°C and filled with 100 ml of media. One flask served as a control, and the remaining four were inoculated with bacteria. Two of the flasks were inoculated with 0.20 g of bacteria and the other two were inoculated with 0.10 g of bacteria (dry cell weight). Hydrogen gas was sparged through each flask to promote mixing and maintain anaerobic conditions, as well as to provide a hydrogen source for the bacteria. Every twelve hours, 2 ml samples were removed from the flasks and filtered through 0.45 ≠ m membranes to remove the bacteria. The samples were then frozen. The experiment was continued for eight days.

The samples are being analyzed using a HPLC equipped with an organic acids column (Supelco Supelcogel C-610H HPLC) or an enzymatic method. The system can measure the concentration of fumarate and succinate in each sample.

Ib. Biohydrogenation of Fumarate - Effect of Hydrogen Pressure

We conducted several experiments on the biohydrogenation of coal and model compounds in the presence of microorganisms (3). The development of a high pressure bioreactor was given in last year's annual report (May 1,1992 - April 30,1993). Work on the use of sulfate reducing bacteria to hydrogenate organic compounds has been continued. We decided to use *D. desulfuricans* in experiments to investigate the hydrogenation of soluble organics under low and high pressure hydrogen gas.

A preliminary experiment indicated that hydrogenation occurred at high pressure (500 psig) without killing the bacteria. We conducted two experiments using the same medium mixture (20 mmolar fumarate) that was made for the cell concentration study above. The pressures for the low and high pressure reactors would be atmospheric and 500 psig, respectively. Each reactor volume was set at 300 ml, leaving approximately 50 ml of headspace. The bacterial cultures were equally suspended in both high and low pressure reactors. Temperatures were maintained at 36°C and each reactor was stirred to attain perfectly mixed, batch conditions. The flowrate of hydrogen gas through both reactors was set at 45 liters per day. Each reactor had its own hydrogen feed line because the reactor system was modified with a second flow valve that put the reactors in a parallel arrangement.

Samples were taken every three hours. These samples were filtered through a 0.45 ⫩ m membrane to separate out the bacteria. Fumarate concentration was measured using ultraviolet spectroscopy at a wavelength of 210 nm. The samples were then frozen. Figure 1 and Figure 2 show the concentration of fumarate over the duration of the two experiments. It is important to notice that the reaction occurred faster in the high pressure reactor than in the low pressure reactor for both experiments.

The experimental results are being fit to a mathematical model we developed for biological hydrogenation. A description of that model is given in the next section.

Ic. A Model of Biological Hydrogenation

It is important to employ mathematical modelling to experimental results in order to gain further insight into biohydrogenation. Several investigators have fit mathematical models based on Monod growth kinetics to sulfate reduction data (4-6). For the biohydrogenation of organics, there is insignificant bacterial growth during the reaction. A kinetic mass-transfer model is purposed where diffusion into the periplasmic layer of the cell is coupled with enzymatic reaction.

Figure 3 illustrates a schematic for a bacterial cell. Transport of the organic substrate is assumed to be in a direction perpendicular to the cell wall. The diffusion coefficient is assumed to be independent of concentration and position. Most sulfate reducing bacteria do not grow unless sulfate is present, so the cell concentration will be assumed constant. The transient mass transfer equation for diffusion with chemical reaction is then

$$D \_2S/\_x2 - rs = \_S/\_t \qquad (1)$$

where S = Organic substrate, mol/L
x = Dimensionless cell membrane thickness
t = time, seconds
D = Diffusion coefficient, m2/s
rs = Reaction rate, mol/(L-s).

The boundary conditions are

$$t = 0,\ S = 0,\ 0 < x < 1. \qquad (2)$$

$$t > 0,\quad D \_S/\_x = a(S\_-Ss),\ x = 1 \qquad (3)$$

where a = Constant, cm/s

S_{∞} = Equilibrium surface concentration at infinite time, mol/L

Ss = Surface concentration at the wall, mol/L

The reaction rate data can be can be can be fit to different models depending on the assumptions made. For instance, the reaction rate rs, might be fitted to a simple kinetic model, or the bacteria might also act as an enzyme catalyst. Then it would be logical to fit the data to Michaelis-Menton kinetics. Equations can also be added to account for changes in cell concentration if they are needed.

Transient data on substrate concentration and cell growth can be used to determine the model constants by nonlinear regression. A computer package such as Statistical Analysis System (SAS) can be used. The derivatives in equation (1) can be approximated using finite difference formulas.

Id. Hydrogenation of Other Soluble Organics

Since the pressure of hydrogen gas is important to the biological hydrogenation of fumarate, it is desired to see if other organic compounds can similarly be hydrogenated. One such compound is trans-cinnamic acid. The proposed reaction is

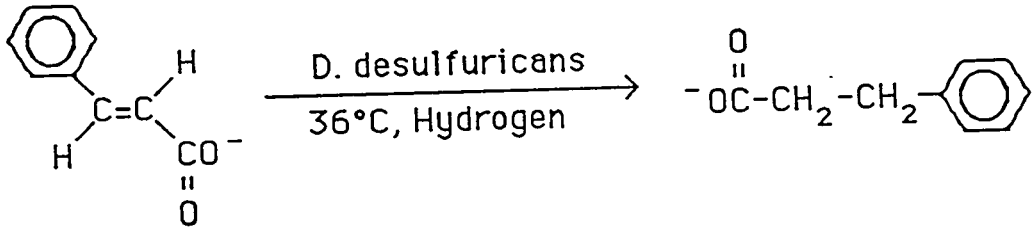

Another potential compound for biohydrogenation is trans-ferulic acid. The reaction for this chemical is

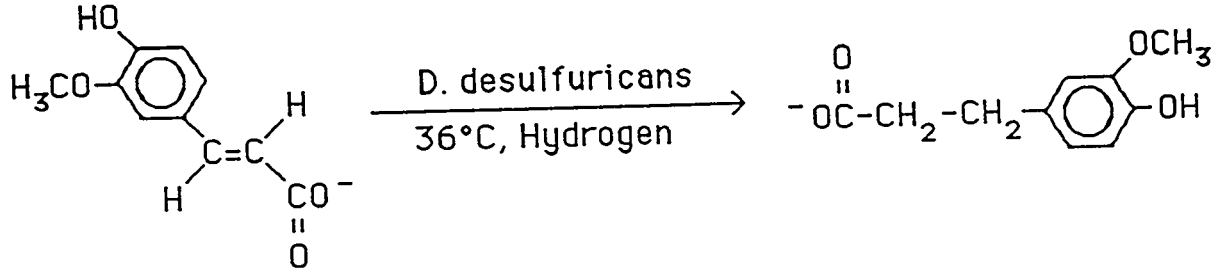

A shake flask experiment to investigate the hydrogenation of these compounds is under way. Results from this experiment will be reported at the annual meeting of the CFFLS.

IIa. Reprecipitation of active Iron Catalysts on coal and Polymeric Materials in the presence of Microorganisms

This part of report deals with the improvement on the formation of ultra-fine active iron particles and even distribution of the fine FeOOH crystals on the surface of coal and waste polymers by using aerobic thermophiles. An interesting metabolic activity of some of these bacteria is that they can control micro-fine crystal size (e. g., FeOOH). This is due to the lipid membrane and other excreted biopolymer coatings, which prevent further growth of the crystals (7- 9). An added advantage of the bacteria is that they tend to adhere to the coal, thus increasing the probability of forming and sticking these crystals on the surface of coal or other solid substrates.

We have already reported that *A. brierleyi* can change the iron forms of biotreated coals (7, 10, 11) with enhanced liquefaction due to the FeOOH particles formation on the surface of coal. However, this process of biotreatment requires longer period (over 20 days) of incubation for the reprecipitation of liquid phase iron. During the bioprocessing of coal by *A. brierleyi*, the pH of the medium decreased due to the production of acid unless the pH of the medium was controlled by the addition of alkali. In all the previous experiments the pH of the medium was either left uncontrolled or kept controlled at a constant pH (e.g. 2.5) till the completion of the bioprocessing of coal. However, in our recent experiment the initial pH was maintained at 2.4 (constant) for the rapid release of iron. For the maximum release of liquid phase iron concentration required approximately 10 days. At the end of 10th day the pH of the medium was shifted from 2.4 to 2.8 by the addition of 0.05 M NaOH. This shift in pH resulted in rapid precipitation of liquid phase iron with in a day of further incubation (Figure 4). The liquefaction yield of the biotreated coal sample obtained at the end of 11th day, was increased by 12% over the control sample. The samples obtained after 11th day of treatment did not show any further increase in liquefaction. The coal obtained from the bioprocessing is to be further analyzed for iron phases.

We are also in the process of verifying the formation of microcrystals of iron based catalysts on the coal, polymers, and rubber surfaces by changing various physical and chemical parameters (pH, temperature, and CO2 concentration, different polymers, and rubber) of the bio-reaction system. In a preliminary experiment, polyethylene (low density, 2.5 W%) and IBC coal #105 (2.5 W%) was treated with *A. brierleyi* at 68°C with a pH of 2.4 and incubated on a shaker. The pH of the medium was maintained at 2.4 for 9 days. At the end of 10th day, pH of the medium was raised to 2.8 for rapid precipitation of liquid phase iron. Coal + polymer mixture was collected at the end of 10th day by filtration and dried it overnight at 85°C. These coal samples will be subjected to subsequent direct liquefaction.

IIb. FeOOH formation on Bioprocessed IBC and DECS Coals in the presence of *Acidianus brierleyi*

Different coal samples (IBC #101 and #105 equivalent to Argon premium coal and DECS

#17), with varying amounts of iron and sulfur, were used for the catalyst formation. IBC #101 and #103, which have very high pyrite (1.2 to 2.4 % dry basis) and total sulfur (3.4 to 4.4% dry basis) were subjected to biotreatment with *A. brierleyi* at pH 2.5 and 65°C under aerobic conditions. DECS #17 which has a negligible quantity of pyritic and non-pyritic iron, was mixed with pyrite (2500 ppm). This mixture was then subjected to biotreatment with A. brierleyi at pH 2.5 and 68°C. The biotreated coals were analyzed using Mossbauer spectroscopy (by Dr. Huffman's group) to further elucidate the effect of biotreatment particularly to determine the forms of iron (Figure 5 and 6). However, the liquefaction conversion went up by 14% only in the case of DECS coal treated with *A. brierleyi* (Table 1). It is also interesting to note that FeSO4 was utilized in the presence of *A. brierleyi* (Figure 5). The implication of this property is yet to be determined (12).

The amount of sulfate released by the biotreated coals into the aqueous phase was measured by the gravimetric method. Biotreated IBC #105 showed complete utilization of the pyritic sulfur (2.4% dry basis) as sulfate in the aqueous phase (Figure 7). Of the three biotreated coals studied, IBC #105 (with 2.4% pyrite dry basis) showed significant release of iron (220 ppm, at the end of 15 days) into the aqueous phase and then started to decrease the liquid phase iron concentration. Whereas the control showed only increase of liquid phase iron (148 ppm, at the end of 21 days) (Figure 8) (12).

IIc. Review of Literature on Catalyst formation and Partial Degradation of Polymers by Microorganisms in the Presence of Coal

Extensive literature survey was done to find out the possibility of using polymers for the coprocessing of coal in the presence of microorganisms. In spite of several advances in the bioprocessing of coal (13), no information is available on the effect on the bioprocessing of coal in the presence of polymeric materials. In the past few years, many of the plastics and polymers [e.g. polyurethane, polyethylene, poly (hydroxyalkanoates), and nylon 2,6] have been reported to be amenable to biodegradation (14-21). Another major source of waste is paper and cellulosics, which are highly biodegradable. Coprocessing (by direct liquefaction) of cellulosic waste and coal has already been studied (22). Therefore, biological coprocessing of coal with waste materials such as polyesters, rubber tires, and cellulosics can achieve the dual purpose of reusing the waste materials by co-liquefaction with coal. The biological pretreatment should also result in upgrading quality of the coal-liquids with simultaneous reduction of sulfur content. In view of the latest developments on the necessity of reusing recalcitrant waste materials and partial biodegradation of polymers (to lower molecular weights) the following research has to be pursued: studies on in-situ formation of ultra-fine iron based metal catalysts on coal and polymers surface and effect of partial biodeterioration of polymers in the presence of coal (aqueous or in the presence of recycling liquids/solvents).

In our research on biocatalysis, biotreated coal showed dramatic improvement in liquefaction yield (25%) over control (11). Further increase in the liquefaction yield and improvement of quality of oils may be accomplished by means of microbial coprocessing of coal with polymers /and or rubber. We assume that the uniform distribution of iron catalyst on the surface of solid waste materials may facilitate improvement in subsequent direct liquefaction yield and quality. Some thermophilic microorganisms e.g. *Acidianus brierleyi*, can also

effectively desulfurize coal simultaneously. Biodesulfurization of coal (up to 5% sulfur) and rubber [1% sulfur (1, 2)] will unequivocally enhance the quality of oil. Therefore, as mentioned in the section I, initial experiment was conducted for catalyst formation on polymer (PE) in the presence of coal by the influence of *A. brierleyi.*

References

1. Murty, M.V.S., personnel communication (1992).
2. Postgate, J.R., The Sulphate-Reducing Bacteria, 2nd edition, Cambridge University Press, Cambridge, 1984.
3. Murty, M.V.S., Aleem, M.I.H., Kermode, R.I., and Bhattacharyya, D., J. Chem. Tech. Biotech., (1994) (in press).
4. Herrera, L., Hernandez, J., Ruiz, P., and Gantenbein, S., Environmental Toxicology and Water Quality, 6:225-237 (1991).
5. Okabe, S., Characklis, W.G., Biotech. Bioeng., 39:1031-1042 (1992).
6. Okabe, S., Nielsen, P.H., and Characklis, W.G., Biotech. Bioeng., 40:725-734 (1992).
7. Bhattacharyya, D., M. Hsieh, Francis, H., Kermode, R.I., , Khalid, A.M., and Aleem, M.I.H. Resour., Conserv. Recycl., 3, 81 (1990).
8. Piccolini, R.J., Japan Chem. Week, 31, 5 (1990).
9. Sakaguchi, T., Burgess, and Matsunga, J. Nature. 365, 47 (1993).
10. Aleem, M.I.H., Bhattacharyya, D., Kermode, R.I., Huffman, G.P., Murty, M.V.S., Ashraf, M., Harish, V. ACS Div. of Fuel Chem., Preprints, 36, 53 (1991).
11. Kermode, R.I., Madhu, V., Murty, M.V.S., Bhattacharyya, D., and Aleem, M.I.H. Chem. Eng. Commun. (1993) (Communicated).
12. Murty, M.V.S., Aleem, M.I.H., Kermode, R.I., and Baattacharyya, D. Generation of iron-based catalysts on high and low pyrite coals in the presence of Acidianus brierleyi. Energy & Fuels (1994) (Manuscript under preparation).
13. Murty, M.V.S., Bhattacharyya, D., and Aleem, M.I.H. In " Biological Degradation and Bioremediation of Toxic Chemicals" G. R. Chaudhry (ed.), Dioscorides Press, Portland, OR (1993) (in press).
14. Mukai, K, Yamada, K., Doi, Y., Polymer Degradation and Stability, 41, 85 (1993).
15. Nakamura, S., Doi, Y., Scandola, M., Macromolecules, 25, 4237 (1992).
16. Yoshiharu, K. and Doi, Y., J. Environ. Polymer Degradation, 1, 81 (1993).
17. Gonsalves, K.E., Chen, X., Cameron, J.A. Macromolecules, 25, 3309 (1992).
18. Nishida, H. and Yutaka, T., J. Appl. Polymer Science, 46, 1476 (1992).
19. Koestler, R.J. (Ed.), Intern. Biodeter., 28, Elsevier Sci. Publ. Ltd, Barking, Engl. (1991).
20. Jesudason, J.J., et al., J. Environ. Polymer Degradation, 1, 89(1993).
21. Chiellini, E. and Solaro, R., CHEMTECH (July), 29 (1993).
22. Jung, H., Tierney, J.W., Wender, I., ACS Div. of Fuel Chem., Preprints, 38, 880 (1993).

Table 1. Composition and Phases of Iron Determined by Mossbauer Analysis of IBC and DECS Coals (5%) Incubated with and without *A.brierleyi* at 68°C, pH 2.5 (initial), and Agitated for 21 Days

	% Fe			
Coal type	Pyrite	FeOOH[a]	Jarosite	$FeSO_4$
IBC #101T	nd	36	64	-
IBC #101C	11	nd	89	-
IBC #105T	nd	22	78	0
IBC #105C	12	nd	85	3
DECS #17[b]T	nd	12	88	-
DECS #17[b]C	80	nd	14	5

T - Test or coal was treated with *A. brierleyi*

C - Control or coal was treated without *A. brierleyi*

- - Below detection limit

a - The IS value for FeOOH is .37 ± 0.02 mm/sec

b - Pyrite (2500 ppm) was added to the DECS coal

Figure 1. Fumarate Treated With D. desulfuricans and Hydrogen Gas at 36°C, pH 7.4

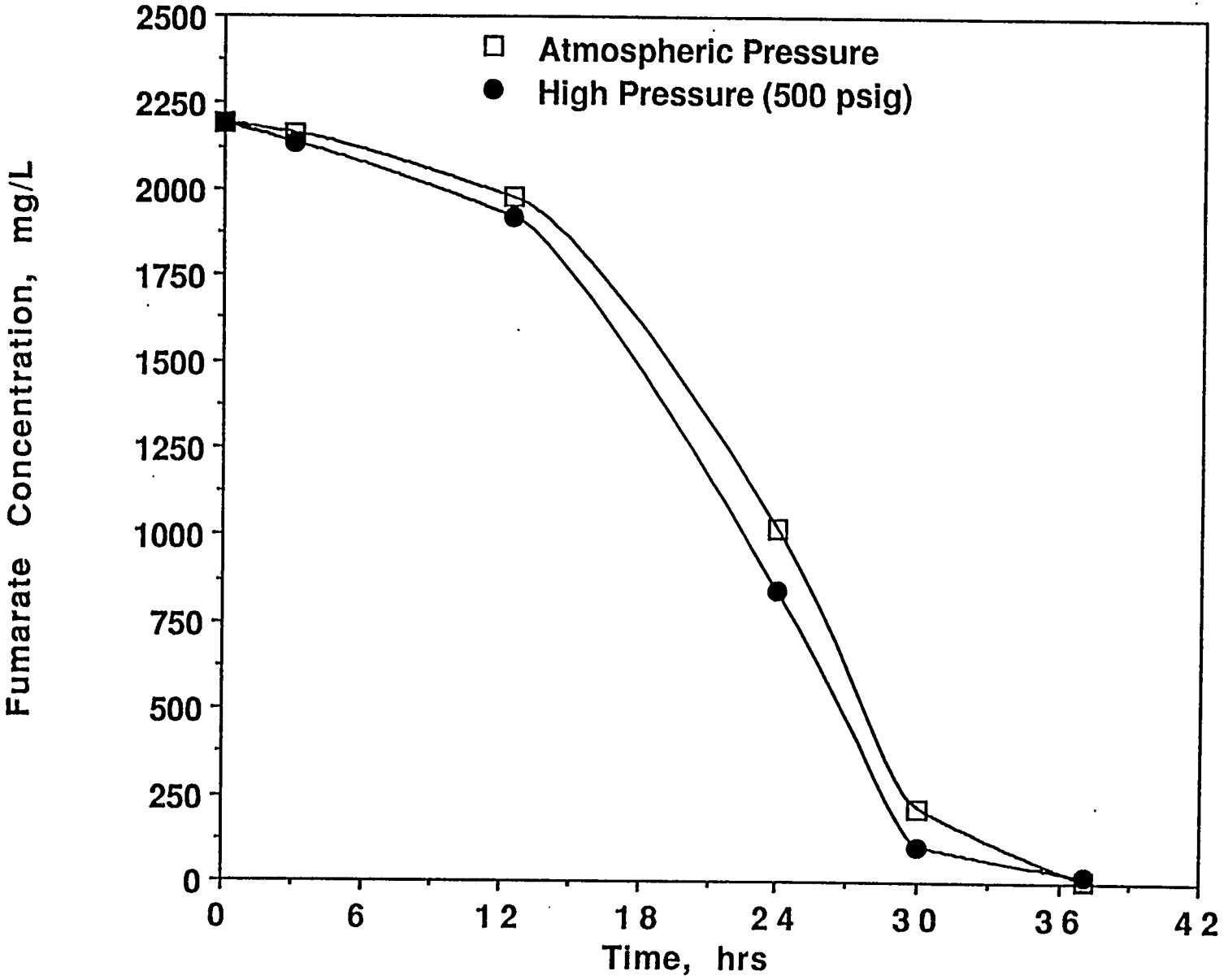

Figure 2. Fumarate Treated With D. desulfuricans and Hydrogen Gas at 36°C, pH 7.4

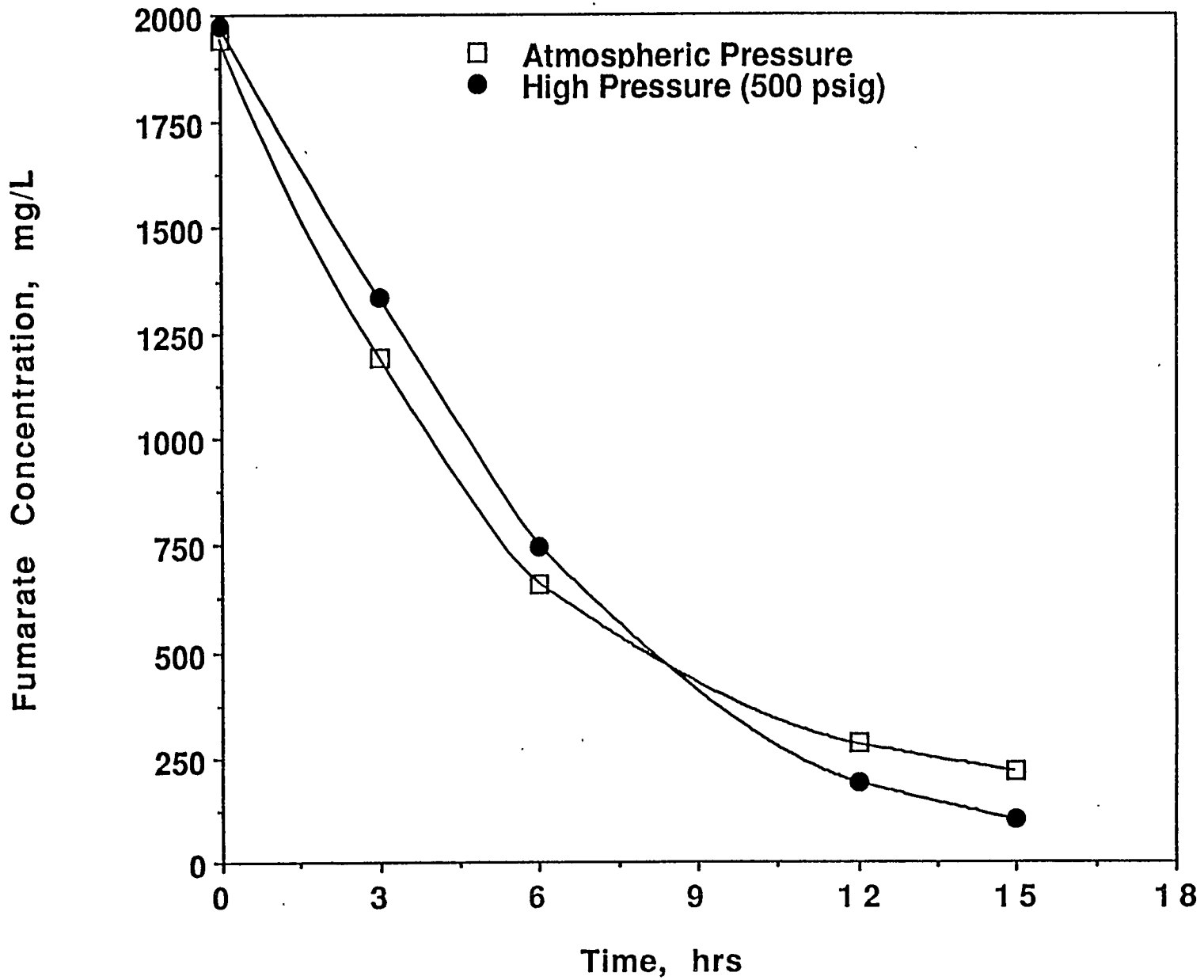

482

Figure 3. Mathematical Model of a Bacterial Cell

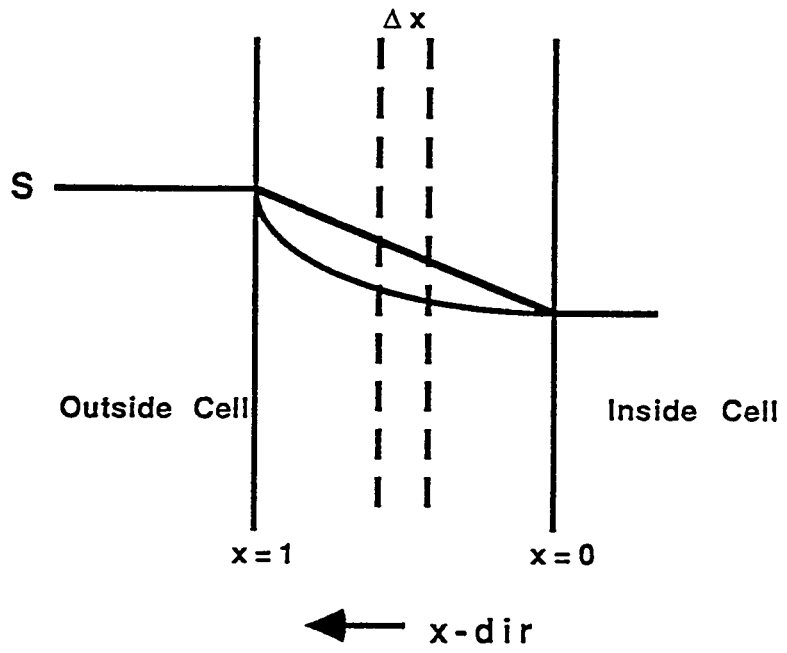

Figure 4. Rapid precipitation of liquid phase iron on coal IBC #105 when treated with A.brierleyi

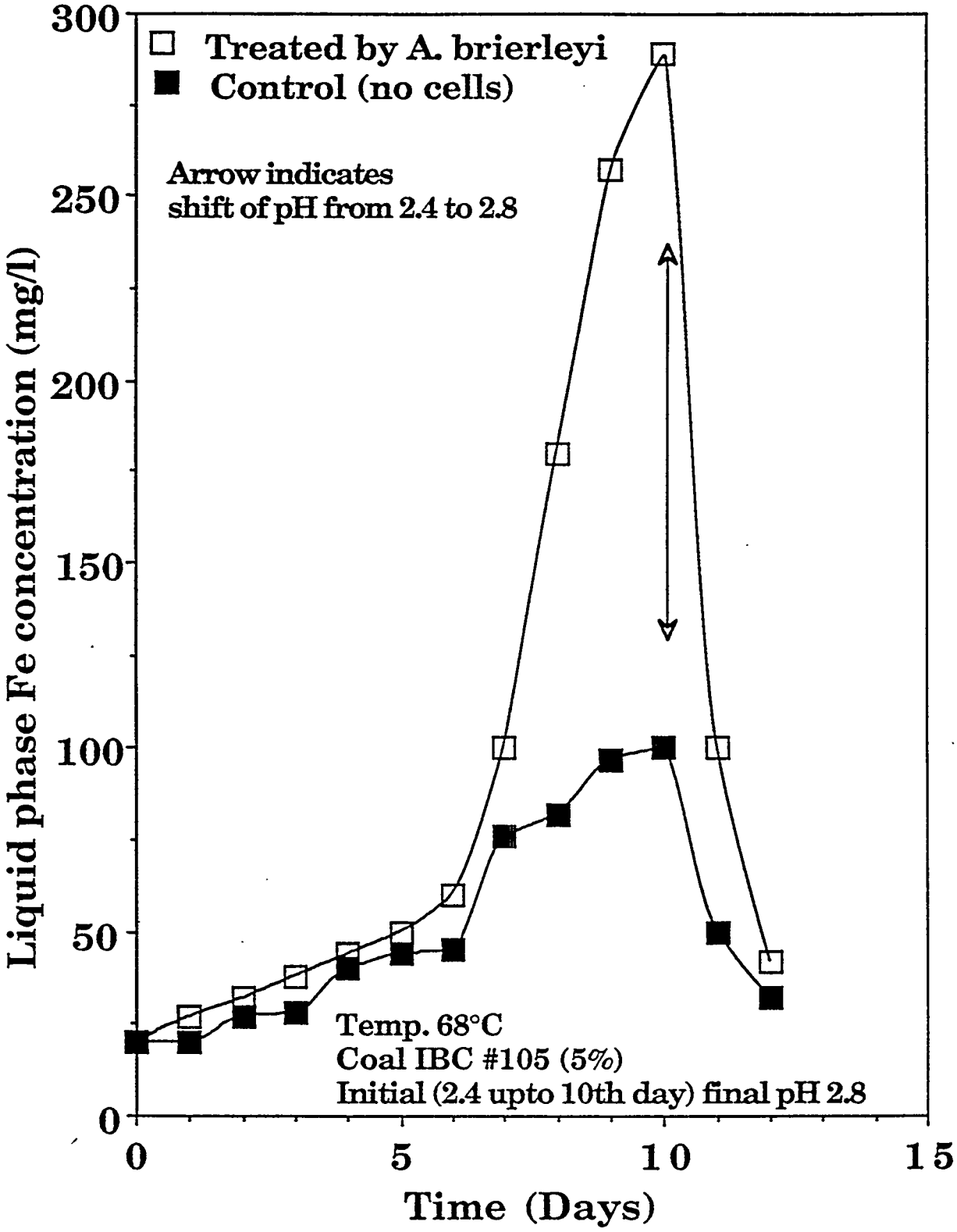

Figure 5. Mössbauer spectrum of the DECS #17 coal with added pyrite after treatment with A.brierleyi at 68°C and pH 2.5

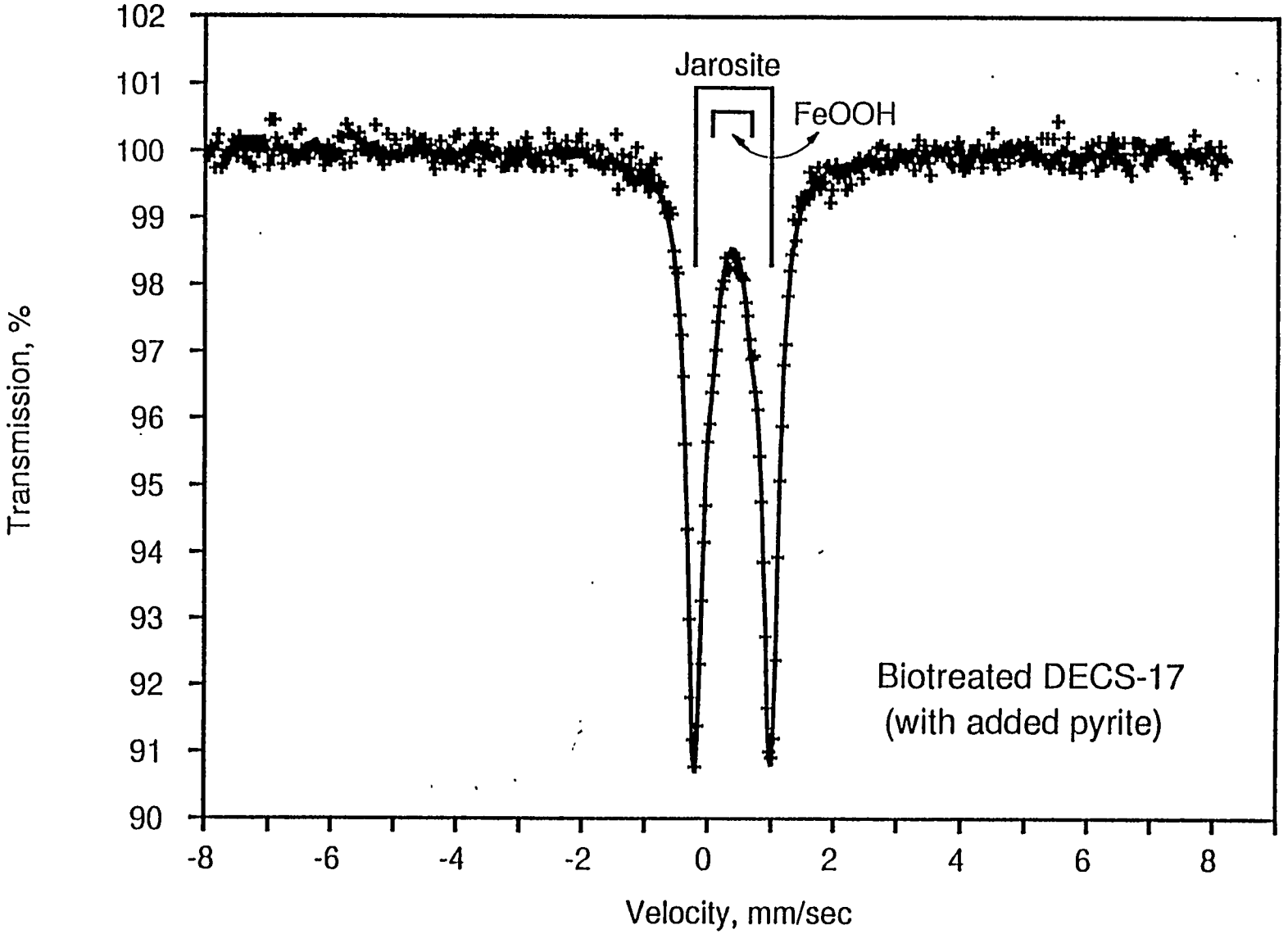

Figure 6. Mössbauer spectrum of the DECS #17 coal with added pyrite after treatment without A.brierleyi at 68°C and pH 2.5

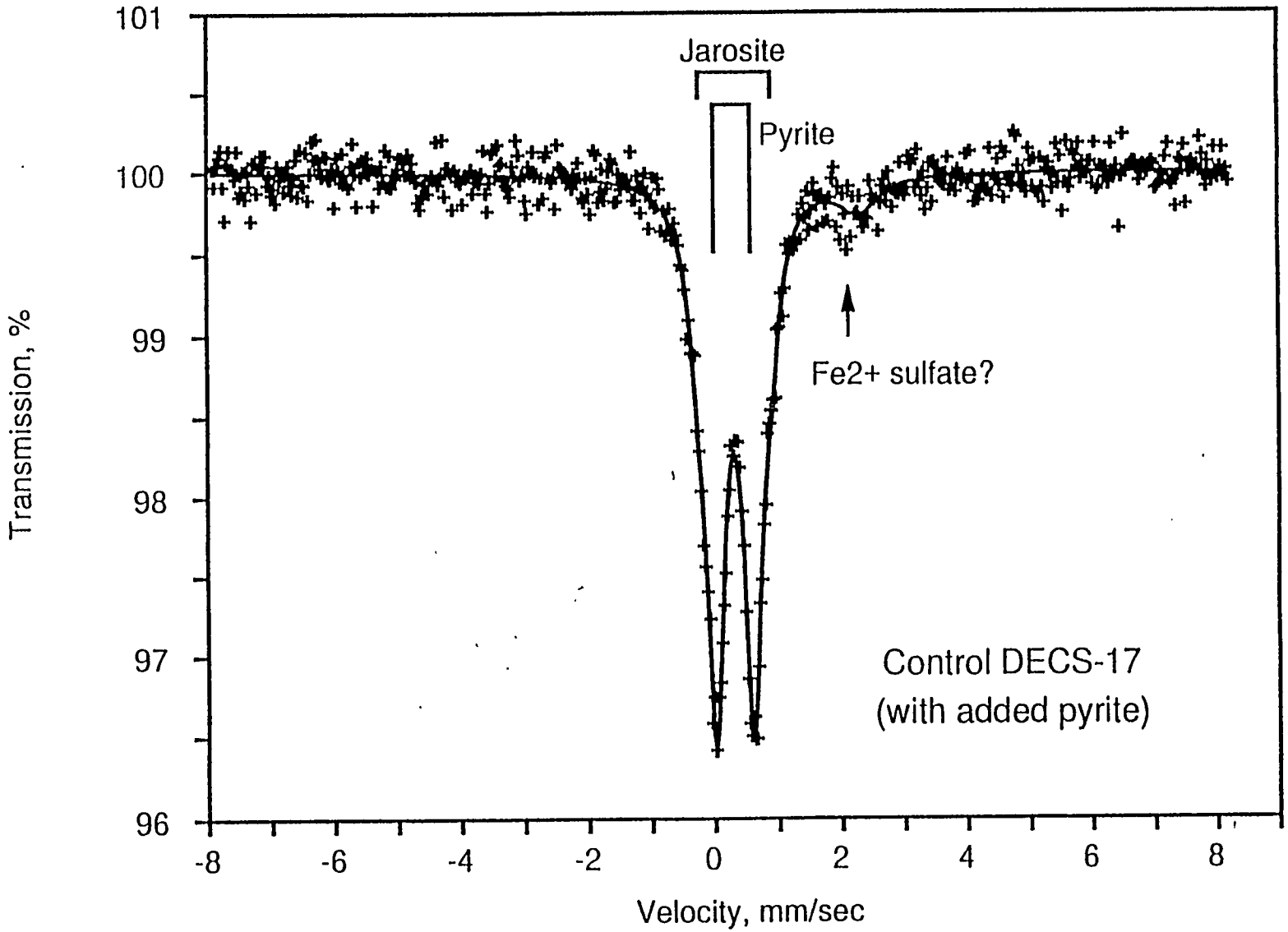

Figure 7. Sulfate released from IBC #105 when incubated with A. brierleyi at 68°C and pH 2.5

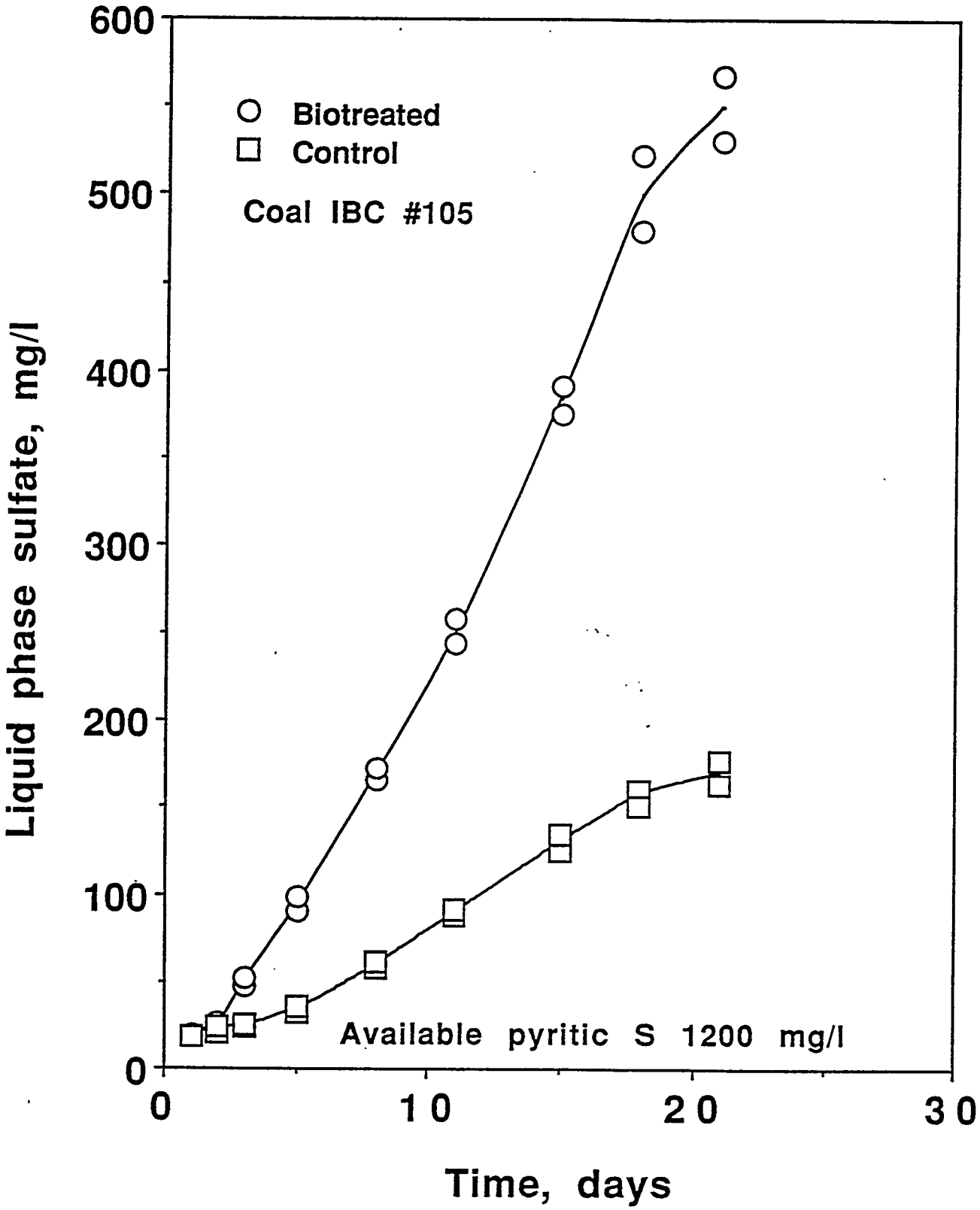

Figure 8. Variation of liquid phase iron released from IBC #105 when incubated with A. brierleyi

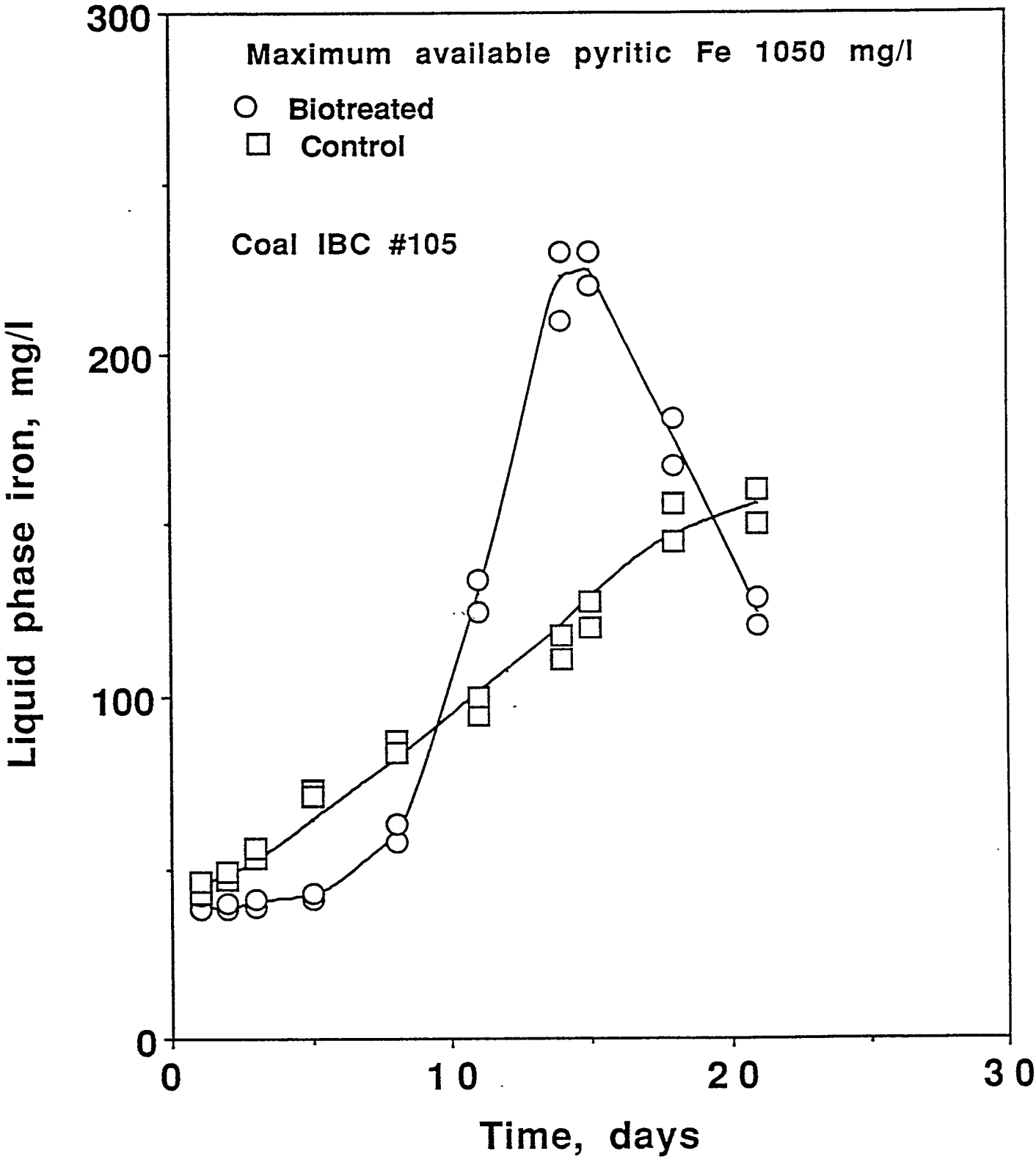

TASK III

Project III.7

CATALYTIC DEHYDROGENATION OF MODEL COMPOUNDS AND COAL IN RELATION TO COAL LIQUEFACTION

Irving Wender, John W. Tierney and G.D. Holder
University of Pittsburgh

Introduction

The catalytic dehydrogenation of model compounds has been carried out to gain information of the nature of donor hydrogen in heavy materials such as coal, direct coal liquefaction recycle oils (resids) and heavy oils derived from petroleum. An attempt was made to gain information on the ease with which donor hydrogen is added to a hydrogen acceptor such as stilbene. Most of this work was carried out with polycyclic hydroaromatic compounds. However, it was ascertained by ^{1}H-NMR that cyclolefinic structures such as those found in cholesterol may play a role in hydrogen transfer. Phenolic structures also evolve hydrogen in the presence of a dehydrogenation catalyst. Attempts have been made to ascertain the manner in which hydroaromatics, cyclic olefins and phenols influence each other in hydrogen transfer reactions. Catalytic dehydrogenation experiments were also carried out on eight recycle oils obtained from a continuous coal liquefaction facility. Evidence of their hydrogen donor abilities were obtained and related to the coal liquefaction process. Results demonstrate that catalytic dehydrogenation could be a valuable technique to assess the amount and the nature of transferable hydrogen in coal, resids and heavy petroleum residues.

We expect that hydroaromatic, phenolic and cyclolefinic structures can transfer hydrogen at different rates and interactions between these structures during catalytic dehydrogenation have been studied.

Results and Conclusions

Effect of Phenolic Groups on Catalytic Removal of Hydroaromatic Hydrogen

The model compound, 9-phenanthrol, released molecular hydrogen when catalytically dehydrogenated with Pd as the catalyst and phenanthridine as the vehicle. It was found by GC-MS that the evolution of H_2 was due to a reaction between phenanthrol molecules to form ethers. This must occur by reaction of the phenolic -OH groups with aromatic hydrogen in phenanthrol

since no H_2 would be evolved if two hydroxyl groups in 9-phenanthrol condensed with the formation of water. The dehydrogenation of a mixture of 9,10-dihydroanthracene (9,10-DHA) and 9-phenanthrol gave off less molecular hydrogen than the sum expected from the dehydrogenation of the individual compounds. It seems likely that interaction between the hydroaromatic structures in 9,10-DHA and the phenolic group in 9-phenanthrol has taken place. This type of interactions was studied by dehydrogenation of different ratios of mixtures of 9-phenanthrol and 9,10-DHA. It was found that the interaction between these two type of molecules becomes significant with an increase of the phenolic -OH concentration in the mixture. The dehydrogenation residue was analyzed by ^{1}H-NMR; a peak at 5.4 ppm indicated that the reaction between the phenolic -OH and hydroaromatic structures did occur during catalytic dehydrogenation. It may be that interactions between phenolic -OH groups and hydroaromatic structures take place and this has implication for the hydrogen donor ability of recycle solvents in direct coal liquefaction.

We had the opportunity of examining the hydrogen donor ability by catalytic dehydrogenation of eight well-documented recycle oils (resids) obtained from different coal liquefaction facilities; the samples were provided by CONSOL Inc. The description and analysis of these samples are summarized in Table 1. One coal liquefaction resid (sample 6 in Table 1), which is rich in -OH groups based on FT-IR analysis, was chosen to study the effect of phenolic structures on catalytic removal of hydroaromatic hydrogen. We were able to replace the hydrogen in the phenolic group by formation of trimethylsilyl ethers. FT-IR analysis shows a large decrease in peak intensity at -3300 cm^{-1} after blocking. This was ascribed to the -OH binding vibration and to a large peak at 1000 cm^{-1}, ascribed to Si-O stretching vibration.

We found that silylation of the phenolic hydrogen reduced the amount of total donatable hydrogen on catalytic dehydrogenation. The difference in hydrogen evolution between the original resid and the silylated resid was only apparent after 60 minutes of reaction. It is believed that the hydrogen in the phenolic groups is released after hydroaromatic hydrogen is removed. This difference in the amount of hydrogen released from the silylated sample and unsilylated sample represents the concentration of phenolic hydrogen in the resid. We expected that hydroaromatic hydrogens would be better hydrogen donors than phenolic hydrogens.

Determination of Hydrogen Donor Ability of Recycle Oils in Relation to DCL

We define total donatable hydrogen content as the cumulative amount of H_2 evolved from the recycle solvents at 150 min in a phenanthridine vehicle at 350°C with $Pd/CaCO_3$ as catalyst. It measures the hydrogen that can be evolved on catalytic dehydrogenation. We also define hydrogen donor ability as the cumulative amount of hydrogen transferred to a hydrogen acceptor (stilbene) at a lower temperature (248°C). We found that, at 248°C with quinaldine as vehicle, the total amount of hydrogen removed as H_2 gas from resids derived from Black Thunder coal were highest, but the amount of hydrogen transferred to the hydrogen acceptor was less, indicating that these resids may not be effective in hydrogen utilization for DCL. The amount of hydrogen transferred from resids derived from Illinois No. 6 coal to the hydrogen acceptor (stilbene) is significantly higher, although the total amount of hydrogen removed from them is less. These resids probably have higher hydroaromatic content and may be good donor solvents in DCL.

Attempts were made to interpret the date obtained in catalytic dehydrogenation of these resids in light of the DCL process. We found that the hydrogen donor ability of resids derived from Illinois No. 6 coal was higher than those derived from Pittsburgh seam coal (Table 1). It seems that the predispersion of hydrated iron oxide catalyst in DCL improves the quality of the resids.

Black Thunder coal was used in both the Wilsonville and HRI coal liquefaction systems. It appears that resids produced from the particular HRI liquefaction run would be better recycle oils than those from the Wilsonville run.

This study demonstrates that catalytic dehydrogenation is a useful technique in determination of donatable hydrogen content and hydrogen donor ability of DCL resids. The hydrogen transfer ability of the resids is probably related to their performance in coal liquefaction.

Correlation Between Catalytic Dehydrogenation and ^{1}H-NMR Analysis

An AMOCO heavy oil ($1000°F^+$) was catalytic dehydrogenated at 350°C with phenanthridine as the vehicle. The amount of donatable hydrogen content measured as the amount of H_2 evolved is 12.1 atoms/100 atoms carbon of the heavy oil. The dehydrogenation residues were washed with HCl(aq) and then analyzed by ^{1}H-NMR. We found that the peaks within 1.8-4.0 ppm ascribed to hydroaromatic and cyclic olefinic hydrogen disappeared after

dehydrogenation. Quantitative analysis shows that these types of hydrogen account for 9.0 wt% of total hydrogen the heavy oil. On the basis of elemental analysis, the donatable hydrogen content as determined by ^{1}H-NMR is 13.1 atoms/100 atoms carbon of the heavy oil, in keeping with the catalytic dehydrogenation measurements.

Future Work

The phenolic -OH derivation techniques will be improved. The effect of phenolics on the catalytic removal of hydroaromatic hydrogen as well as other structures will be studied. Model compounds such as 2-naphthalenol and 9-phenanthrol will be silylated and catalytically dehydrogenated with coal or coal liquefaction resids.

Structures resembling heavy petroleum bottoms, such as cholesterol, will be dehydrogenated. The fate of hydroxyl hydrogen and cyclolefinic hydrogen as well as hydroaromatic structures formed during catalytic dehydrogenation of cholesterol will be determined.

Batch microreactor studies will be conducted using partially dehydrogenated hydroaromatics, phenolics and other hydrogen donor as solvents to provide information for coal liquefaction process.

Table 1. Comparison of Hydrogen Donor Ability of Coal Liquefaction Resids (provided by CONSOL Inc.)

Sample Number	Sample Description: Run, Coal, ashy or THF-soluble, wt% H, as det. basis	Total Donatable H_2[a] (Absolute Basis), cc H_2/g sample	Total Donatable H_2 as percent of Resid H_2 Content[b], %	Hydrogen Donor Ability[c] (Absolute Basis) cc H_2/g sample	Hydrogen Donor Ability as percent of Resid[d] H_2 Content, %
1	Wilsonville 257, Illinois No.6, ashy, 7.33	236	28.6	67.7	8.3
2	Wilsonville 257, Illinois No. 6, THF-soluble, 8.15	286	31.3	74.3	8.2
3	Wilsonville 259, Pittsburgh seam, ashy, 5.95	215	32.3	68.9	10.3
4	Wilsonville 259, Pittsburgh seam, THF-soluble, 6.74	246	32.5	70.0	9.3
5	Wilsonville 262 B, Wyodak and Anderson, ashy, 6.58	175	23.7	49.3	6.7
6	Wilsonville 262 B, Wyodak and Anderson, THF-soluble 8.19	248	27.0	61.7	6.7
7	HRI CC-2, P2, Wyodak and Anderson, THF-soluble, 8.16	194	21.2	48.7	5.4
8	HRI CC-15, P9, Wyodak and Anderson, THF-soluble, 7.46	260	31.1	71.3	8.5

a. H_2 evolved in 150 min at 350°C
b. Total donatable hydrogen calculated as percent of total hydrogen content
c. Maximum amount of hydrogen transferred to hydrogen acceptor in 300 min at 248°C
d. Hydrogen donor ability calculated as the percent of total hydrogen content

TASK III

Project III.8

CHARACTERIZATION OF INITIAL STEPS IN HYDROGENATION OF COAL MODEL COMPOUNDS BY COAL LIQUEFACTION CATALYSTS

S.D. Worley and W.C. Neely
Department of Chemistry
Auburn University

The Interaction of Dihydrogen with Iron Catalysts

Using a high-pressure infrared cell reactor, and techniques utilized previously in these laboratories for investigating the FTIR of surface hydride species on transition metals, [1,2] the interaction of dihydrogen with Fe_2O_3 and Fe_3O_4 films was studied. The purpose of these experiments was to use the integrated areas of the iron hydride infrared bands to measure the thermodynamic parameters ΔH and ΔS for Fe-H or Fe-H_2 adsorption, so that information concerning the binding strength of these species to the coal catalysts could be obtained. Unfortunately, the current high-pressure infrared cell reactor utilized here can only be heated to about 250°C which apparently is not sufficient to cause reduction of the Fe species. Thus the initial experiments failed to reveal infrared data for the species of interest. Currently a new high-pressure infrared cell reactor is under construction (see Figure 1) which should allow reduction at temperature up to 600°C; these higher temperatures should be sufficient to reduce the Fe species properly. The high-pressure dihydrogen experiments will be repeated during the coming year with the new cell reactor.

Comparison of Reaction Products from Catalytic Hydrogenation of Model Compounds with Those Formed by Direct Reaction with Atomic Hydrogen

A microwave discharge powered source for atomic hydrogen was fabricated. However, it became evident that despite the apparent efficiency of such a reactor, from the viewpoint of generation of high concentrations of atomic hydrogen, that it was very difficult to use for collection of gaseous and low-boiling reaction products. Accordingly, the apparatus was revised to include a metod for heterogeneous reaction of condensed-phase substrates with gas-phase

active molecules which had been used in previous research.[3] In this latter work, a microwave system was used to generate a stream of gas-phase excited oxygen molecules, O2(1 g). The stream of excited oxygen was then passed over a bed of glass beads which had been coated with the compound to be reacted with the excited oxygen. After the desired exposure time, the beads were removed, and the reaction products were collected for analysis by washing the beads with a suitable solvent.

An alternative approach for hydrogen atom generation is the use of a system which employs the silent discharge plasma approach used by Guesser, et al.[4] While these workers operated their apparatus at ca. 0.1 millitorr, we would expect to operate it at atmospheric pressure, thus reducing the loss of volatile materials.

A design combining the Guesser generator with our glass support bead method is shown in Figure 2. The individual parts are: (1) outer electrode; (2) outer insulator; (3) teflon bushing; (4) viton O-ring; (5) discharge reactor volume; (6) glass support beads; (7) inner electrode; (8) outer electrode; (9) gas inlet; (10) dismounting joint for adding and removing beads.

In operation, ca. 4-12 kV are applied to the two electrodes. Characteristic microdischarges between the opposite dielectric surfaces occur and generate electron bursts whose energy distribution centers on 5 eV. Thus, they possess an ample energy for dissociation of the H-H bond to produce atomic hydrogen. It has been estimated that using a low pressure silent discharge reactor, the atomic hydrogen generated is about 1-3% of the molecular hydrogen present.[4] This compares well with the estimated concentration of atomic oxygen in such a system operated with oxygen at atmospheric pressure. It is to be emphasized that this system does not generate a stream of atomic hydrogen, but rather microbursts of H-atoms. Calculations on the rate of wall collisions versus gas phase collisions using the known rate constant for H-atom recombination[5] show that wall collision, and hence reaction with material coated on the beads, can compete favorably with loss of atomic hydrogen by recombination.

When this approach was tried for hydrogenation, it was found that, unfortunately, an undesirable amount of direct decomposition (as opposed to hydrogenation) of the model compound occurred. This was caused, apparently, by direct electron impact on the test substrates.

In view of this difficulty, the system will again be modified. A new design will provide a silent discharge at sufficiently low pressure to ensure a mean free path of H-atoms on the order

of 1-2 cm. The sample will be located below the discharge so that the atomic hydrogen flux passes across the sample surface, but the sample is not exposed to the direct impact of electrons.

References

1. Wey, J.P., Neely, W.C., and Worley, S.D., J. Phys. Chem., 95, 8881 (1991).
2. Fang, T.H., Wey, J.P., Neely, W.C., and Worley, S.D., J. Phys. Chem., 97, 5128 (1993).
3. Neely, W.C., Martin, J.M., and Barker, S.A., Photochem. and Photobiol., 48, 423 (1988).
4. Guesser, H.D. and Czubryt, J.J., Fuel, 67, 375 (1988).
5. Baulch, D.L., Cobos, C.J., Cox, R.A., Esser, C., Frank, P., Just, T., Kerr, J.A., Pilling, M.J., Troe, J., Walker, R.W., and Warnatz, J., J. Phys. Chem. Ref. Data, 21, 411 1992).

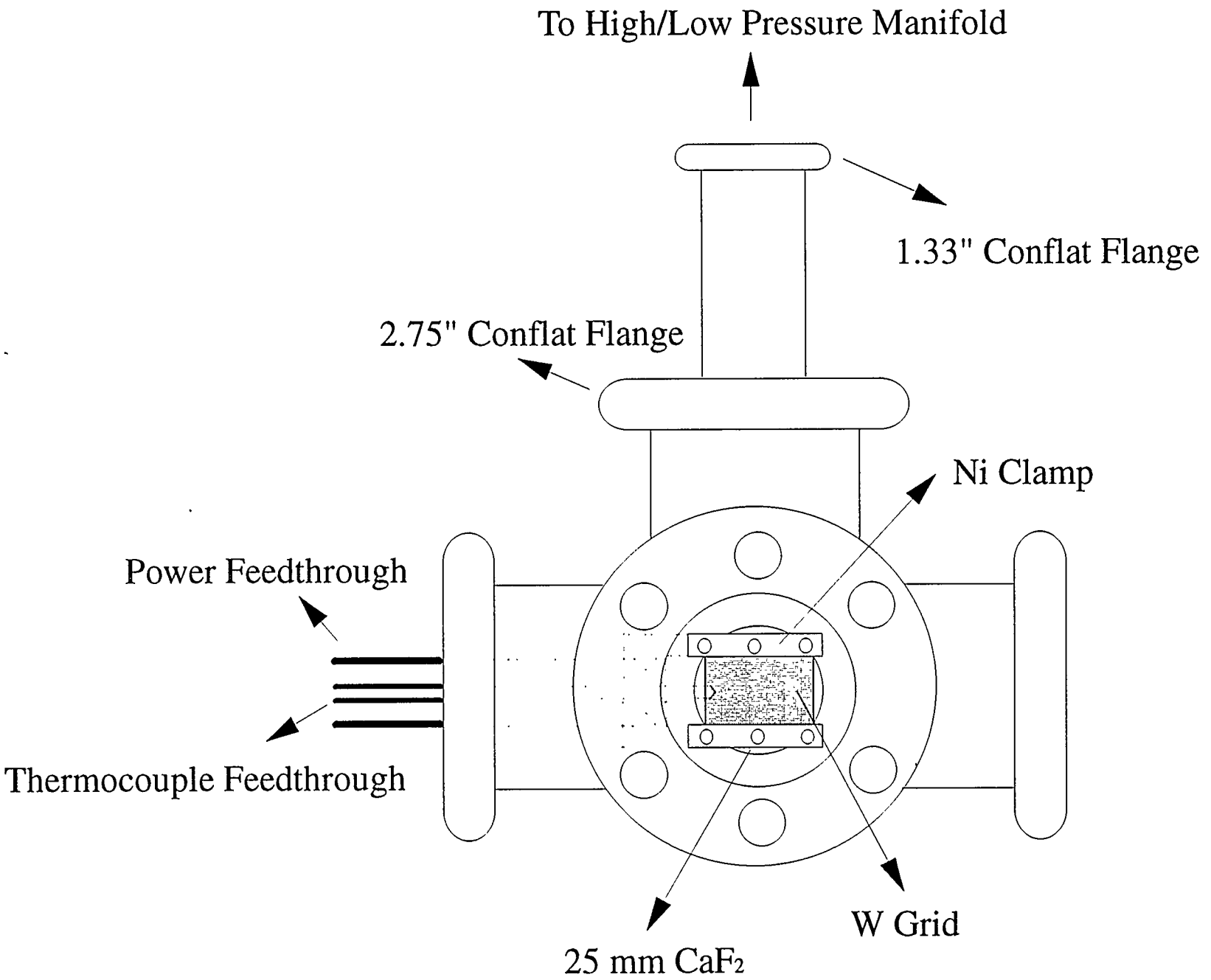

Figure 1. 5-Way Cross Infrared Cell

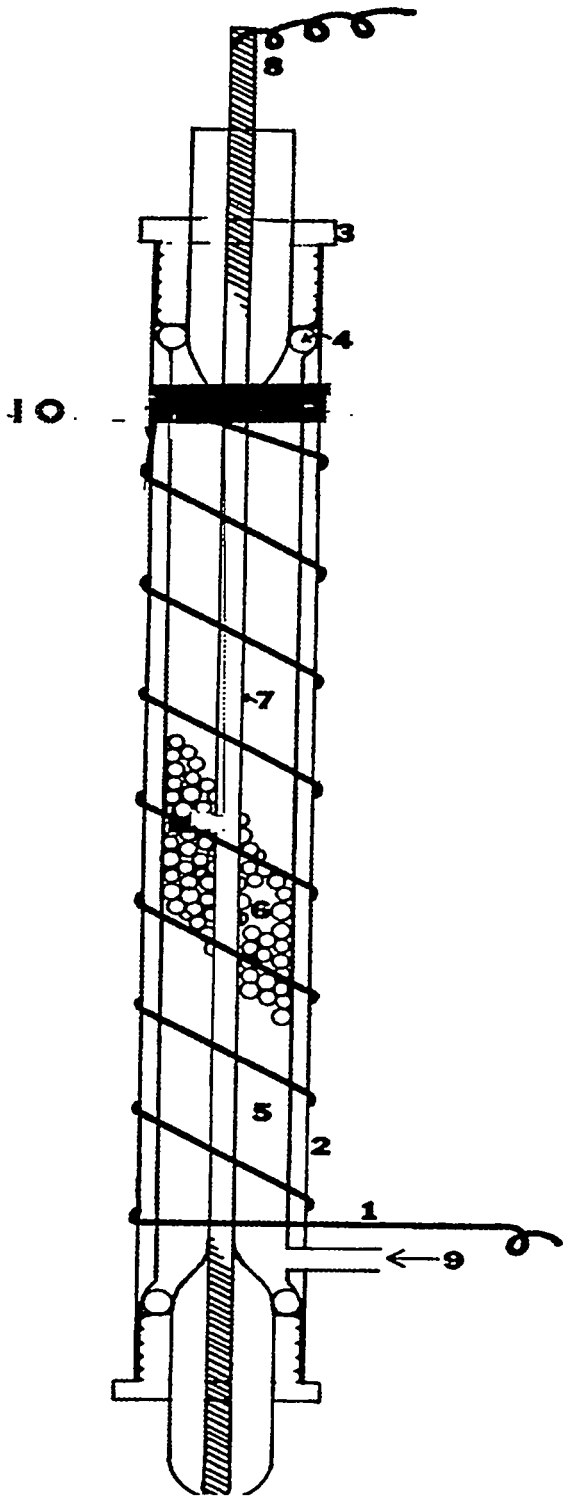

Figure 2

TASK IV

IN SITU ANALYTICAL TECHNIQUES FOR COAL LIQUEFACTION AND COAL LIQUEFACTION CATALYSTS

Coordinators: Mohindar Seehra and
Henk Meuzelaar

TASK IV

Project IV.1

HIGH PRESSURE/HIGH TEMPERATURE ESR SPECTROSCOPY OF FREE RADICALS IN COAL LIQUEFACTION AND COPROCESSING, AND CATALYST TESTING AND CHARACTERIZATION

M. S. Seehra and M. M. Ibrahim
Physics Department
West Virginia University

OBJECTIVES

The objectives of this research project for the 1993-1994 year were as follows: (i) Test various Fe-based catalysts prepared by other CFFLS researchers for direct coal liquefaction (DCL) experiments using in-situ electron spin resonance (ESR) spectroscopy of free radicals and compare the findings with the results of DCL experiments; (ii) Characterize Fe-based catalysts by x-ray diffraction (XRD) and magnetometry; and (iii) Initiate in-situ ESR experiments of coprocessing of coal with waste polymers. Our accomplishments in these tasks are presented below followed by a list of publications and conference presentations based on these studies.

SUMMARY OF RESULTS

(i) Objective 1:

Under this objective, two major accomplishments are noteworthy: First, our ESR measurements with nine Fe-based catalysts mixed with Blind Canyon coal showed that the free radical enhancement due to the catalysts at 400°C is linearly proportional to the % oil yield obtained in the standard DCL experiments of Pradhan et al[1] and second, using new experimental approaches, we have monitored, in-situ and in real time, the effects of catalysts and additives on the free radicals of a coal maintained at high temperatures. These results, detailed in recent papers,[2,3] are summarized below.

In this work, nine Fe-based catalysts viz. $Fe_2O_3/SO_4(1)$, $Fe_2O_3/SO_4(2)$, $Mo/Fe_2O_3/SO_4$, $Fe_2O_3/SnO_2/SO_4$, Fe_2O_3/MoO_4, Fe_2O_3/WO_4, $FeOOH/SO_4$, $Mo/FeOOH/SO_4$ and Fe_7S_8, prepared

by Prof. Wender, were tested for their hydrocracking abilities of Blind Canyon coal using in-situ high temperature ESR spectroscopy of coal free radicals. The catalysts were characterized for chemical phase and for their particle size by x-ray diffraction. The intensities N_s of the free radicals were measured from room temperature to 500°C in flowing H_2 gas, without and with the catalyst plus elemental sulfur loadings, in the ratios Fe/coal ~ 1% and Fe/S = 1/2. It was found that above about 350°C, the catalyst loaded samples yield higher N_s. A free radical density ratio $R = N_s(\text{catalyst})/N_s(\text{coal})$ at 400°C was defined to measure the hydrocracking abilities of the catalysts. The experimental R values vary from a high of 2.45 for Fe_2O_3/WO_4 to a low of 1.10 for $Mo/FeOOH/SO_4$. A plot of R vs % oil yield from the DCL experiments of Pradhan et al[1] (Fig.1) shows that % oil yield increases linearly with R demonstrating the usefulness of the ESR technique for testing catalysts. This plot also shows that Mo substituted catalysts give higher oil yield for the same R, presumably due to the hydrogenation effect of Mo. These results have demonstrated that the hydrocracking abilities of the Fe-based catalysts for DCL can be quantified by ESR and that suitable ESR experiments can provide useful information on the activity of a DCL catalyst.

The procedures and experimental details of our high temperature/high pressure (500°C/700 psi) ESR cavity system for the in-situ monitoring of free radicals have been described in earlier publications[2-4]. In the new approach adopted for the results reported here, we have modified the standard ESR tube by attaching to it a side tubing through which a catalyst can be added any time, while the coal sample is being held at a high temperature (inset of Fig. 2). This is then followed by monitoring the free radical concentration, N_s as a function of time to investigate the effect of the added catalyst. All our experiments were carried out on the Blind Canyon Coal since, of the ten Argonne Premium coals, it has the least amount of ash. This is important since Silbernagel et al[5] have shown that paramagnetic impurities mask the free radicals. For the Blind Canyon coal, this masking effect is only about 2%.[4]

In Fig. 2, we show the effect of two additives to the coal on the N_s as a function of time. The coal alone was first maintained at 400°C and the N_s was measured with time. After about 75 minutes, the additive, the catalyst $Fe_2O_3/SnO_2/SO_4$, which in earlier experiments showed considerable hydrocracking ability[2], was added to the coal through the side tube. The catalyst was added in the ratio Fe/coal ~ 0.01 along with elemental S in the ratio Fe/S~0.5 to

simulate the actual DCL experiments.[1] N_s becomes constant after a few minutes for the coal alone, and when the catalyst was added (indicated by the arrow) about 25% increase in N_s is observed. N_s then becomes constant with time, suggesting that reaction is complete.

A piece of waste tire tread was the second additive used in a similar experiment, also shown in Fig. 2. For our ESR experiments we have used shredded pieces (~1mm size) of a waste-tire (Goodyear Vector) material. The tire pieces were added 1:1 by weight to coal maintained at 480°C for about 53 minutes (Fig.2). Here we see that after adding the tire, a significant decrease in the free radical density with time is observed, the effect of which is not yet saturated even after about 50 minutes of reaction time. This decrease in N_s is indicative of a definite reaction of tire material with coal. Note that the additives by themselves do not give an ESR signal at the temperatures investigated, as verified in separate experiments.

To verify the above results in more traditional steady-state experiments, we show in Fig. 3, N_s versus temperature for the cases of Fig. 1 viz. coal alone, coal + sulfur + catalyst ($Fe_2O_3/SnO_2/SO_4$), and coal + Goodyear tread and also for coal + Michelin tread. For the catalyst, the N_s values compared to coal alone are larger at all elevated temperatures, the effect becoming more pronounced at temperatures above 300°C. This confirms the hydrocracking effect of the catalyst (the experiments are carried out in flowing H_2 gas). On the other hand, both tire treads shift the cracking temperature of the coal from about 320°C to about 240°C and considerably lower the free radical density of the coal above about 400°C. We note that lowering of the free radical concentration can result from hydrogenation, as e.g. seen from in-situ high pressure (hydrogen) experiments on the Blind Canyon coal, (Fig. 4). Tire is rich in hydrogen and organic material since the typical constituents of tire are about 44% butadiene rubber, 20% aromatic oil, 33% carbon black and about 1% each of ZnO and S[6]. Earlier studies on pyrolysis of scrap tires has shown that a high yield of oil and gas could be obtained comparable to fossil fuels[7], and catalytic pyrolysis with molten salts can improve the efficient conversion of hydrogen in the scrap tires[8]. The co-liquefaction experiments of coal with waste tires by Farcasiu et al have shown that tire indeed facilitates more hydrogenated, heptane soluble products[6]. Based on these studies, we infer that the decrease in free radical concentration with tire above 400°C is probably due to hydrogenation of coal

facilitated by the tire material.

The results presented above on a nearly ash-free, Blind Canyon coal have demonstrated that the free radicals observed by in-situ ESR experiments do provide excellent probes for monitoring the effects of catalysts and hydrogenation. It is likely that these free radicals are normally very reactive but that their life-time has been increased because of the low-diffusion in the nearly solid or viscous states of the coal and coal products. These new approaches should allow more extensive applications of the ESR technique in investigating the effects of catalysts to coal as well as coprocessing of coal with waste tires.

(ii) Objective 2:

Objective #2 deals with the characterization of the catalysts by XRD and magnetometry. Results of the XRD experiments such as the chemical phase of the nine Wender catalysts, as well as their average particle size are reported in the recent paper[2]. All these catalysts have also been investigated by magnetometry. Only few of the catalysts show superparamagnetism whereas the remaining catalysts show more complicated magnetic properties. These results are undergoing thorough analysis, results of which will be reported in future reports.

For one of the catalysts viz. FeOOH based 'nanocat' sample of average size 30Å, we have carried out detailed ESR, magnetization, XRD and Mossbauer studies (in collaboration with Huffman et al) and the results were reported at a conference and published in a recent paper[9]. XRD showed that the 'nanocat' is neither α-Fe_2O_3 nor α-FeOOH based but that it converts to Fe_3O_4 (α-Fe_2O_3) on heating to 800°K in vacuum (air). Temperature-dependent studies show that this material is a superparamagnet with a blocking temperature ~100°K and dramatic changes observed near 50°K are all related to the thermal motion of the superparamagnetic particles. The observation of the ESR signal is believed to be due to the uncompensated surface spins of Fe^{3+}. Similar studies have now been extended to four surface modified ferrihydride catalysts (cat5, cat10, 0.02Si/FHD and 0.1Si/FHD) obtained from Huffman et al. XRD studies show particle size ~20Å but only cat5 and 0.02Si/FHD show ESR signals. Presumably stronger surface coating by Si has eliminated the uncompensated Fe^{3+} surface spins in 0.1Si/FHD. All these four catalysts are superparamagnetic with narrower particle size distribution as compared to the 'nanocat' sample. These results are being

prepared for a publication.

(iii) Objective 3:

ESR experiments of coprocessing of Blind Canyon coal with waste-tire rubber from Goodyear Vector tire and with polystyrene and polyethylene have been completed and they were reported at the ACS meeting in Chicago[10]. We have also completed our investigations on the coprocessing of Blind Canyon coal with a tire material (Michelin) and all the constituents of the tire such as butadiene rubber, aromatic oil, and carbon black, obtained from Dr. Farcasiu.

Thermogravimetric (TG) measurements of coal with the tread and its components show that the total mass loss at 500°C is few percent (about 0.5 to 12%) larger than the projected mass loss assuming no interaction, suggesting some interaction of the coal with tread and tread components. This indicates that there are some additional volatiles evolved during coprocessing of coal with tread or its components. While there is only a small difference in evolution of volatiles for coal coprocessed with tread or its components from TG, ESR measurements show more definite reactions in coprocessing. The variation of free radical density with temperature, in hydrogen flow for coal and coal added with tread (1:1 by weight) was shown in Fig. 3. A preliminary run on each of the components and tread showed no detectable ESR signal. So, the free radicals seen here are all associated with coal only. Since TG experiments showed only minor additional mass loss in coprocessing of coal with any of the components/tread, the free radical densities are corrected for mass loss due to coal alone using the equation: $N_s = N_T\ (T/RT)/m_c$ where N_T is the free radical density at any temperature T (in Kelvin), RT is the room temperature (298°K) and m_c is the mass of coal at that temperature.

From the plot (Fig. 3) we immediately see two important results in coprocessing of coal with tread: (i) the major cracking of coal occurs at lower temperatures (~240°C) compared to the thermal cracking of coal which occurs around 320°C. (ii) Unlike the thermal cracking of coal, where the N_s keeps increasing with temperature beyond 320°C, for coal with tire the N_s peak near 400°C followed by a decrease at higher temperatures, due to hydrogenation of coal in the presence of tread. For comparison, in Fig. 3 we also show the variation of N for coal with another waste tire, a highway run Goodyear (vector) which shows

results similar to the Michelin tire. This result is supportive of the results of Farcasiu and Smith[6] which indicated improved yield and more hydrogenated products in coprocessing of coal with tread.

Tread is made up of 33% carbon, 20% aromatic oil and 44% of butadiene rubber beside sulfur (1%) and zinc oxide (1%). Of these, carbon is well known for its good catalytic activity in cracking model compounds and sulfur and zinc oxide are also good catalysts. In order to understand the effect and role of these components of tread in hydrogenation of coal, similar ESR experiments were conducted mixing the components separately with coal. In Fig. 5 a plot of variation of N_s with temperature for selected mixtures is shown. None of the components mixed separately with coal reproduce the effect of tread. On the other hand, all the components seem to promote cracking of coal, the styrene butadiene rubber and zinc oxide showing the largest increase in free radical concentration. To bring out the effect of the coprocessing on free radical density, we define a ratio $R=N_c/N_{coal}$, where N_c is the free radical density for coal with the component/tread and N_{coal} is for coal at the same temperature. A bar diagram of R at 350°, 400° and 480°C is shown in Fig. 6 (R will be 1 if there is no effect on N_s due to coprocessing). Fig. 6 shows that all the components promote cracking of coal, which increases N_s with temperature more compared to thermal cracking of coal. Only tread with coal shows a decreasing R with temperature indicating strong cracking beginning at lower temperatures followed by increasing hydrogenation at higher temperatures.

To understand the effect of combination of the tread components we did two experiments: First, using the modified sample tube, we monitored the variation of N_s with time by heating the coal to 420°C and adding carbon and styrene butadiene successively at about 60 and 120 min. respectively. Here we saw a moderate increase in N_s due to the addition of these components, signifying their cracking capabilities. In another experiment, all the components were taken in the proper ratio to simulate the tread, and mixed with coal (coal: styrene rubber: cis rubber: carbon: oil: S: ZnO = 100: 35: 8.5: 33: 20: 1: 1), and for this sample, the variation of N_s with temperature shows no difference from thermal cracking of coal. This is an unexpected result showing that the effect of the sum total of components does not equal the effect of whole tread.

In summary, results of the free radical monitoring of the coprocessing of Blind

Canyon coal with tire-treads show a definite lowering of the cracking temperature of the coal and possibly enhanced hydrogenation above 400°C. Both of these results suggest improved liquefaction of the coal with tread. On the other hand, the individual tread components only show enhanced cracking effect without lowering the cracking temperature and without increased hydrogenation at higher temperatures observed with the tire tread.

Finally we carried out some initial kinetic studies on the degradation of polymers and commingled plastics obtained from University of Utah. ESR experiments at 380°C showed that the thermal degradation of commingled plastics is strongly time-dependent since the free radicals were observed only after heating for four hours, and additional heating lowered the N_s. TG experiments on plastics at different heating rates are underway to determine the activation energy for degradation. These studies are expected to give quantitative information on the kinetics, with and without catalysts.

REFERENCES

1. Pradhan, V. R., Hu, J.,Tierney, J. W., & Wender, I. Energy Fuels 1993 7, 446-454.

2. Ibrahim, M. M. & Seehra, M. S. Energy Fuels, 1994 8, 48-52.

3.Ibrahim, M. M. & Seehra, M. S., Energy Fuels (submitted for publication)

4. Seehra, M. S. & Ghosh, B. J. Anal. Appl. Pyrol. 1988 13, 209-220; Seehra et al Fuel 1986 65, 1315-1316; Ibrahim, M. M. & Seehra, M. S. ACS Fuel Chem. Preprints 1992 37, 1131-1140.

5. Silbernagel, B. G. Gebhard, L. A. Flowers II, R. A. & Larsen, J. W. Energy Fuels 1991 5, 561-568.

6. Farcasiu, M. Chemtech, January 1993, 22-24

7. Williams, P.T., Besler S. & Taylor, D.T. Fuel 1990 69, 1474-1482.

8. Chambers, C., Larsen, J.W., Li, W., & Wlesen, B. Ind. Eng. Chem. Process. Des. Dev. 1984 23, 648-654.

9. Ibrahim, M. M. Edwards, G. Seehra, M. S. Ganguly, B. & Huffman, G. (to be published in J. Appl. Phys. (April 94 issue)

10. Ibrahim, M. M. & Seehra, M. S. ACS Fuel Chem. Preprints, 1993 38, 841-847.

PUBLICATIONS/PRESENTATIONS

1. Testing of Fe-based catalysts for direct coal liquefaction using in-situ Electron spin resonance spectroscopy, M. M. Ibrahim and M. S. Seehra, Energy Fuels, 1994 8, 48-52. Talk presented at the ACS meeting, Denver, April, 1993.

2. Magnetism and spin dynamics of nanoscale FeOOH particles, M. M. Ibrahim, G. Edwards, M. S. Seehra, B. Ganguly and G. P. Huffman, to be published in J. Appl. Phys,. Talk presented at the Inter. conference on Magnetism and Magnetic Materials, Minneapolis, October 1993.

3. Thermogravimetric and free radical evidence for improved liquefaction of coal with waste tires, M. M. Ibrahim and M. S. Seehra, ACS Div. Fuel Chem. Preprints, 38, 841-847 (1993); talk presented at the ACS meeting, Chicago, August, 93.

4. Presented an invited talk entitled "High temperature/High pressure ESR spectroscopy of free radicals in coal liquefaction, coprocessing and catalyst testing" at the Contractors Review Meeting hosted by the Pittsburgh Energy Technology Center, September 1993.

5. Magnetic properties of ferrihydrite nanocrystallites, M. M. Ibrahim, M. S. Seehra, Z. Feng, J. Zhao & G. P. Huffman, presented at the APS meeting, Pittsburgh, March 1994.

6. Coprocessing of coal with waste tires and polymers: in-situ electron spin resonance investigations, submitted as a chapter for the ACS symposium series on "Utilization of wastes and renewable resources".

7. New approaches to in-situ Electron Spin Resonance investigations of coal conversion processes, M. M. Ibrahim & M. S. Seehra, submitted to Energy Fuel.

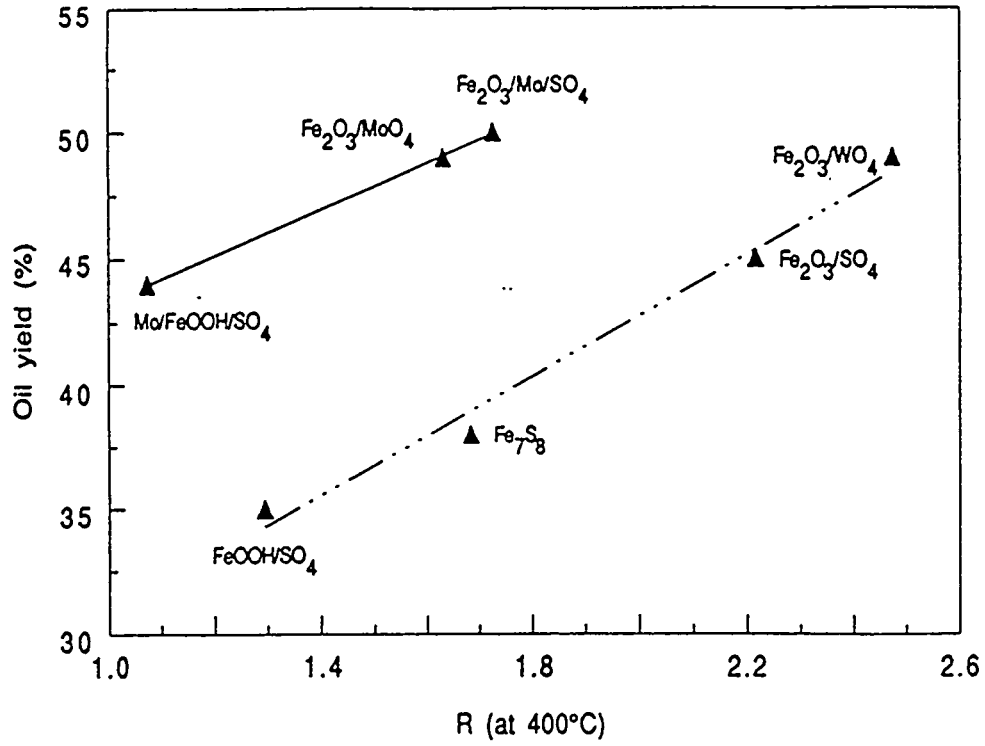

Fig. 1. Variation of % oil yield from liquefaction experiments[1] with ratio R from our work. Lines are linear fits with correlation factor 0.99.

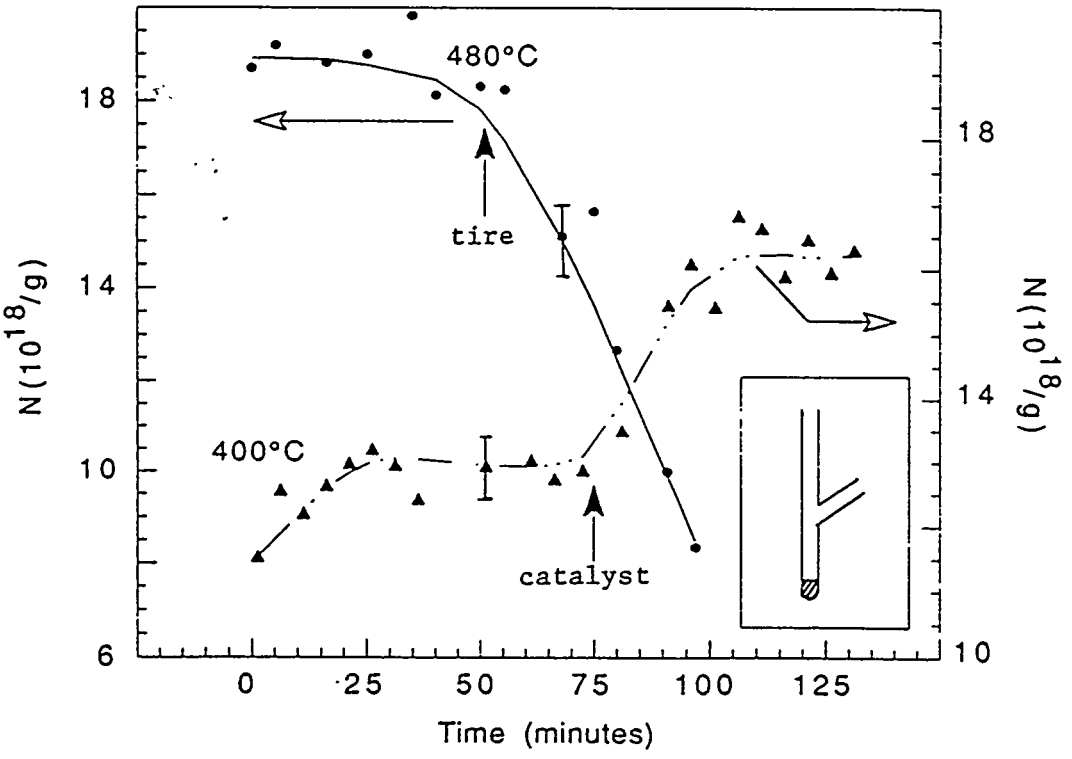

Fig. 2. Variation of N_S with time before and after adding the catalyst/waste tire to coal. The arrow indicates the time when the additive is added. The modified sample tube for ESR measurements is shown in the inset.

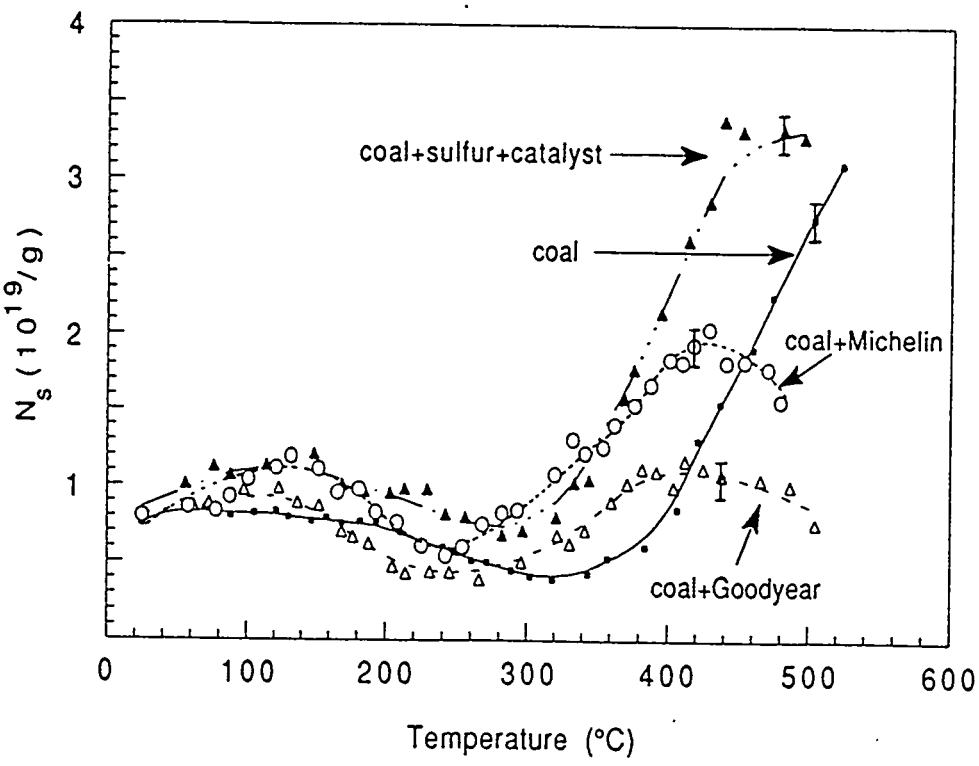

Fig. 3. Variation of N_s with time for the four cases discussed in the text. Measurements were under flowing H_2.

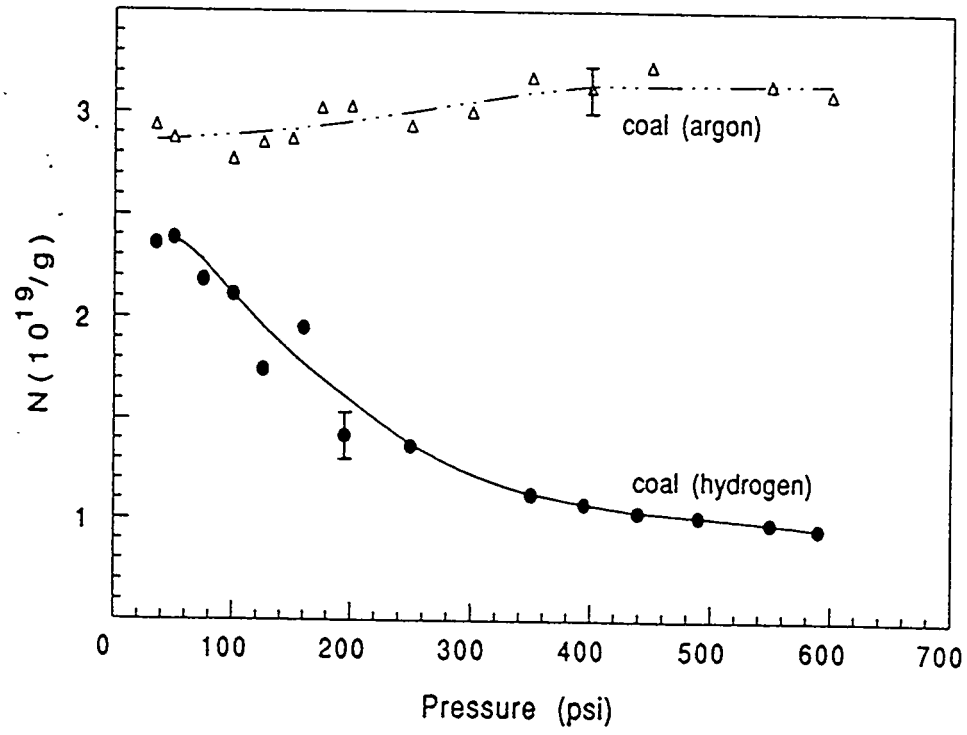

Fig. 4. Variation of N_s of coal with H_2 and Ar pressures at 440°C. Lines are drawn through the points for visual aid.

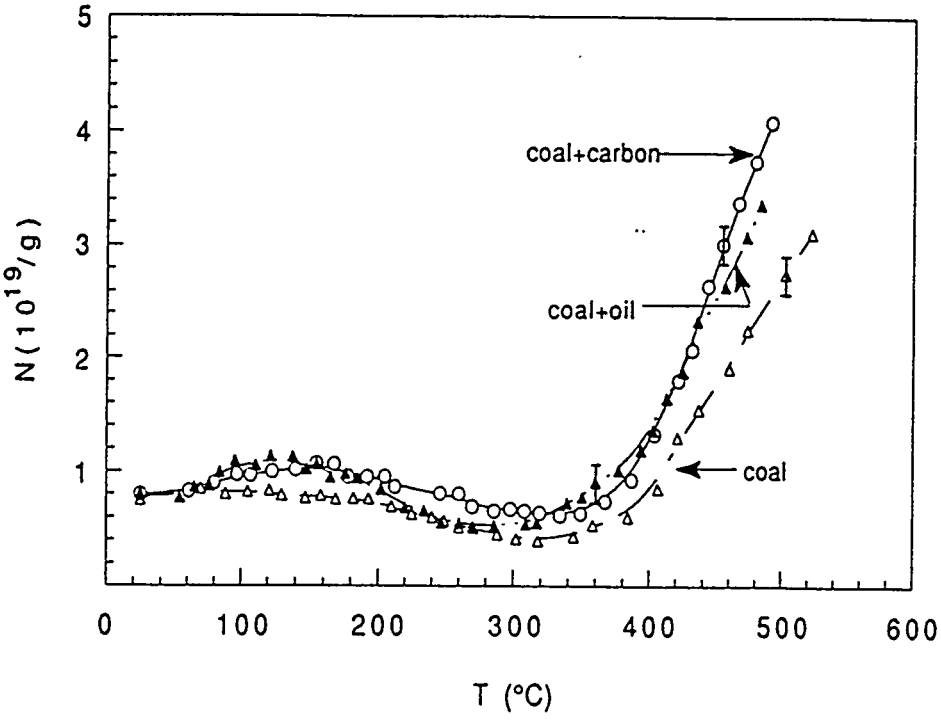

Fig. 5. Variation of N_s with temperature for coal mixed with two of the components of tread viz. carbon (2:1) and aromatic oil (4:1).

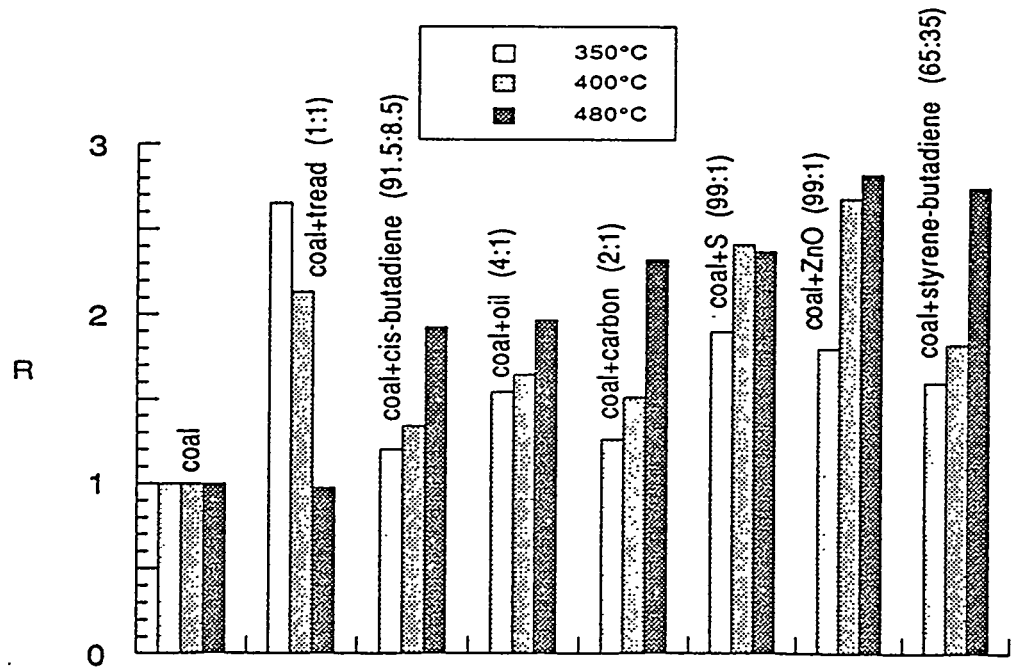

Fig. 6. Plot of R at selected temperatures for coal mixed with tread and all its components in the ratios indicated.

TASK IV

Project IV.2

MICROSCALE SIMULATION OF HIGH PRESSURE THERMAL AND CATALYTIC CONVERSION PROCESSES IN COAL AND WASTE POLYMERS WITH ON-LINE GC/MS

Henk L.C. Meuzelaar, Kui Liu, Emma Jakab
University of Utah

The main research activities during the last fiscal year were as follows:

- Fundamental studies on co-processing of coal with polymers such as waste rubber tire, commingled waste plastic, polystyrene and polyethylene using a specially developed high pressure TG/GC/MS system.
- Thermal and catalytic reactions of styrene butadiene rubber (SBR) in the high pressure TG/GC/MS system.
- Studies on the decomposition of wood and its components (cellulose, lignin) in a two stage microreactor using methanol and water as a solvent medium.

1. Fundamental Studies on Co-Processing of Coal with Polymers

Experiments on decomposition of polymers such as waste rubber tire, commingled waste plastic, polystyrene, polyethylene and coal were performed in the high pressure TG/GC/MS system [1] under a hydrogen pressure of 900 psig. The TG profiles (weight loss vs. reaction temperature) are shown in Figure IV.2.1 and their different shapes suggest implications for co-processing. The waste plastic (mainly polyethylene) weight loss curve is well represented by polyethylene standard materials. Since polyethylene type plastic decomposes at higher temperatures than the maximum pyrolysis rate temperature (Tmax) of coal but melts at lower temperatures (e.g., 150 C or less), the molten plastic should has the potential to promote contact between the coal and the solid catalyst. The rubber tire samples have approximately 30% carbon black left while the organic components appear to have been

completely devolatilized. The volatile products of individual polymer decomposition experiments were monitored by means of GC/MS but will not be discussed here.

Co-processing runs of coal with waste rubber tire, commingled waste plastic, polyethylene and polystyrene (coal to plastic ratio 1:1) were performed at a constant heating rate at 10 C/min under 900 psi hydrogen pressure. The experimental results of the mixtures of coal with the polymers studied all show approximately additive behavior when applying a 10 C/min heating rate. Because of the continuous temperature rise the rate of thermal reactions increase so fast that the total weight loss is controlled by the thermal decomposition of the individual components. However, when a mixture of coal with polystyrene was subjected to a different temperature program using a constant heating rate of 10 C/min up to 370 C, isothermal hold for one hour and final heating up to 600 C at 10 C/min both the TG and GC/MS profiles indicated a strong interaction between the coal and polystyrene (Figure IV.2.2). The weight loss of the mixture is increased compared to a predicted value based on the linear sum of the individual components at the temperature of 370 C. The result is confirmed by the total product evolution profile. The coal lost about 18% weight by the end of isothermal period at 370 C, but the volatile products were not detected by MS due to their low intensity, so the total ion chromatogram of coal is not shown in the figure. The total abundance of the volatile products of polystyrene detected at 370 C can be seen in the total ion chromatogram (TIC) (Figure IV.2.2b). Since the polystyrene is not completely degraded in 60 mins at 370 C, further reaction occurs when the temperature is increased, resulting in additional product evolution at temperatures above 400 C. The total ion chromatogram of the mixture (Figure IV.2.3c) shows that the products are formed mostly during the isothermal period. The strong interaction between coal and polystyrene could be due to the mineral matter in coal acting as a catalyst and accelerating the decomposition of the polystyrene.

A similar behavior is observed when the SBR polymer sample is studied in combination with the solid superacid ZrO_2/SO_4^{2-} catalyst. At a constant heating rate of 10 C/min, the 10% ZrO_2/SO_4^{2-} catalyst added has little influence upon the rate of decomposition of SBR polymer. However, when the same sample is subjected to a different temperature

program using a heating rate of 10 C/min up to 370 C and then kept under isothermal conditions for one hour before being heated up to 500 C at 10 C/min, the effect of the catalyst on the rate of decomposition of SBR polymer is clearly observed [2]. Careful selection of the reaction temperatures and temperature histories of the polymer/catalyst and polymer/coal mixtures was found to be crucial in demonstrating catalytic effects and blending effects as opposed to primarily thermal processes.

2. Fundamental Studies on Thermal and Catalytic Reactions of Styrene Butadiene Rubber (SBR) in the High Pressure TG/GC/MS System.

The effect of the superacid catalyst (ZrO_2/SO_4^{2-}), as a potential coal liquefaction catalyst [3], on the decomposition of SBR, polystyrene and PDVB was studied. The catalyst was prepared by Prof. J.S. Shabtai's group, with which a close collaboration exists. First of all, the thermal and catalytic reactions of SBR were investigated. In order to compensate for the poor contact between the powdered, insoluble catalyst and SBR, as much as 10% of each catalyst ($ZrO_2/SO_4^{=}$, carbon black and $(NH_4)_2MoS_4$) was added to the individual polymer samples. Comparison of the thermogravimetric curves (Figure IV.2.3) shows that the $ZrO_2/SO_4^{=}$ catalyst increases the weight loss by about 17% at 370 C whereas carbon black and $(NH_4)_2MoS_4$ have no measurable effect on the overall rate of SBR decomposition.

Several main product evolution profiles of SBR with various catalysts are shown in Figure IV.2.4. The production of benzene (Figure IV.2.4a) is significantly promoted by the $ZrO_2/SO_4^{=}$ catalyst indicating that the solid superacid catalyst has very strong hydrogenolysis activity for α-alkyl-arene bond cleavage. The catalyst contains both the Bronsted acid and the Lewis acid sites [4]. The Bronsted acid sites protonate the aromatic ring and the subsequent α-cleavage results in the formation of benzene and aliphatic compounds. These findings are in agreement with the observation of Shabtai et al. [3] that the $ZrO_2/SO_4^{=}$ catalyst is very effective in the hydrogenolytic α-cleavage of 1,2-dinaphthylethane. The presence of Bronsted acid sites also promotes transalkylation reactions between alkylbenzenes and styrene as evidence by the increased evolution of isomeric methylstyrenes (Figure IV.2.4b) and

benzene. The increased yield of styrene (Figure IV.2.4c) and α-methylstyrene (Figure IV.2.4b) can be explained by the parallel Lewis acid functionality character of the catalyst. When the Lewis acid sites abstract hydride ions from the benzylic carbons, benzylic carbonium ions are formed. Subsequently, styrene and α-methylstyrene are formed by β-scission of the benzylic carbonium ion. The yields of saturated products such as ethylbenzene (Figure IV.2.4d) and isopropylbenzene were increased. The reasons are not quite clear due to the lack of information of polybutadiene decomposition with the ZrO_2/SO_4^{2-} catalyst. Further experiments will be done with the polybutadiene polymer.

Although the $(NH_4)_2MoS_4$ catalysts does not affect the overall rate of decomposition significantly, some changes in the product composition are observed. The $(NH_4)_2MoS_4$ catalyst behaves as a bifunctional catalyst, showing both ring hydrogenation (more ethylbenzene (Figure IV.2.4d) and isopropyl benzene) and hydrogenolysis (more styrene (Figure IV.2.4c) and α-methylstyrene (Figure IV.2.4b)) activity. Carbon black does not produce a measurable effect at 370 C, but at temperatures above 400 C it has some ring hydrogenation activity as indicated by the higher yield of saturated (e.g., ethylbenzene (Figure IV.2.4d) and isoproprylbenzene).

3. Studies on the Decomposition of Wood in a Two Stage Microreactor with On-line GC/MS

The shortcoming of the high pressure TG/GC/MS system is that only solvent-free conversion reactions can be studied. In order to investigate the processes in the presence of donor solvent, a two-stage tubing reactor with on-line GC/MS was developed in our laboratory. Thermochemical processes have the potential for producing valuable chemicals and liquid fuels from lignocellulosic materials. In addition to pyrolysis and hydropyrolysis, biomass thermolysis in various solvent environments has been studied extensively. The application of solvent can minimize the condensation of intermediate components, resulting in higher liquid yield and decreased char formation. The two stage microreactor used for lignocellusic materials is shown in Figure IV.2.5.

Thermal conversion of white birch wood and wood components was studied using water-methanol mixture as a solvent. The samples were heated at 20 C/min up to 400 C under 300 psi pressure. The pyrolysis and solvent vapors were introduced into the GC/MS at 1.3 minute intervals through a heated fused silica capillary transfer line. The total ion chromatogram of white birch (Figure IV.2.6a) illustrates that several compounds were separated within the short sampling interval at 120 C GC column temperature. The highest rate of product evolution occurs at significantly lower temperature (about 320 C) using 5% water in methanol as a solvent than in hydrogen atmosphere (370 C in TG experiments) apparently due to the stabilizing effect of solvent on initial products. Figure IV.2.6b shows the average mass spectrum in which the low molecular mass products (e.g., CO_2, CH_3COOH, $HOCH_2CHO$) are primarily released from hemicellulose and cellulose, whereas the most abundant higher molecular mass products represent lignin monomers (e.g., alkyl syringols). The evolution profiles of the individual products show pronounced differences as seen in Figure IV.2.7. The characteristic hemicellulose products (e.g., m/z 60, hydroxyacetaldehyde and acetic acid; m/z 114, 3-hydroxyl-1,5-pentenolactone) are evolved at the lowest temperature followed by cellulose (e.g., m/z 126, methylhydroxypyranone) and lignin (e.g., m/z 124, guaiacol; m/z 154, syringol) products. TG/GC/MS results (not shown here) also clearly reveal the different thermal stability of wood components.

Wood components such as cellulose and lignin were studied separately in order to understand the fundamental reactions of wood conversion. By changing the water/methanol ratio it was concluded that water enhances the decomposition significantly, whereas methanol plays a key role in the catalytic upgrading reactions. The pyrolysis vapors produced in the reactor were upgraded in the second stage with different catalysts e.g., $SiO_2Al_2O_3$ and $NiMo/Al_2O_3$. By using various catalysts pyrolysis vapors can be transformed into different products such as aromatic hydrocarbons and phenolic compounds. These results will be discussed at the upcoming CFFLS annual meeting July 1994.

REFERENCES

1. Liu, K., Jakab, E., McClennen, W.H., Meuzelaar, H.L.C., *ACS Preprint, Div. of Fuel Chem.*, 38 (1993), 823.

2. Liu, K., Jakab, E., Zmierczak, W., Shabtai, J., and Meuzelaar, H.L.C., *ACS Preprint, Div. of Fuel Chem.*, 39 (1994), 576.

3. Zmierczak, W., Xiao, X., Shabtai, J., *J. Energy & Fuels*, 1994, in press.

4. Arata, K., *Advances in Catalysis*, 37, 1990, 163.

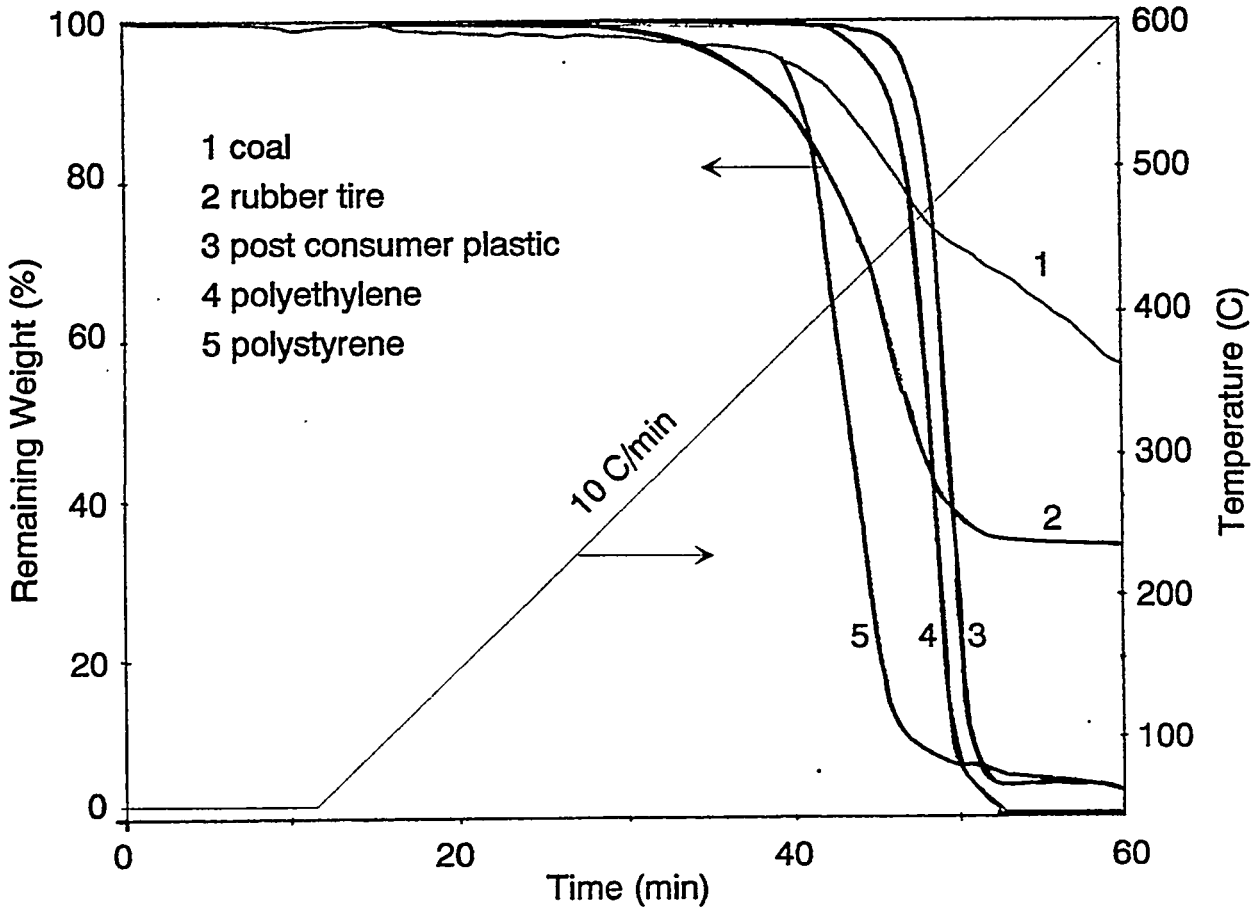

Figure IV.2.1. Hydropyrolysis TG curves of synthetic polymers and coal at 900 psi (H_2).

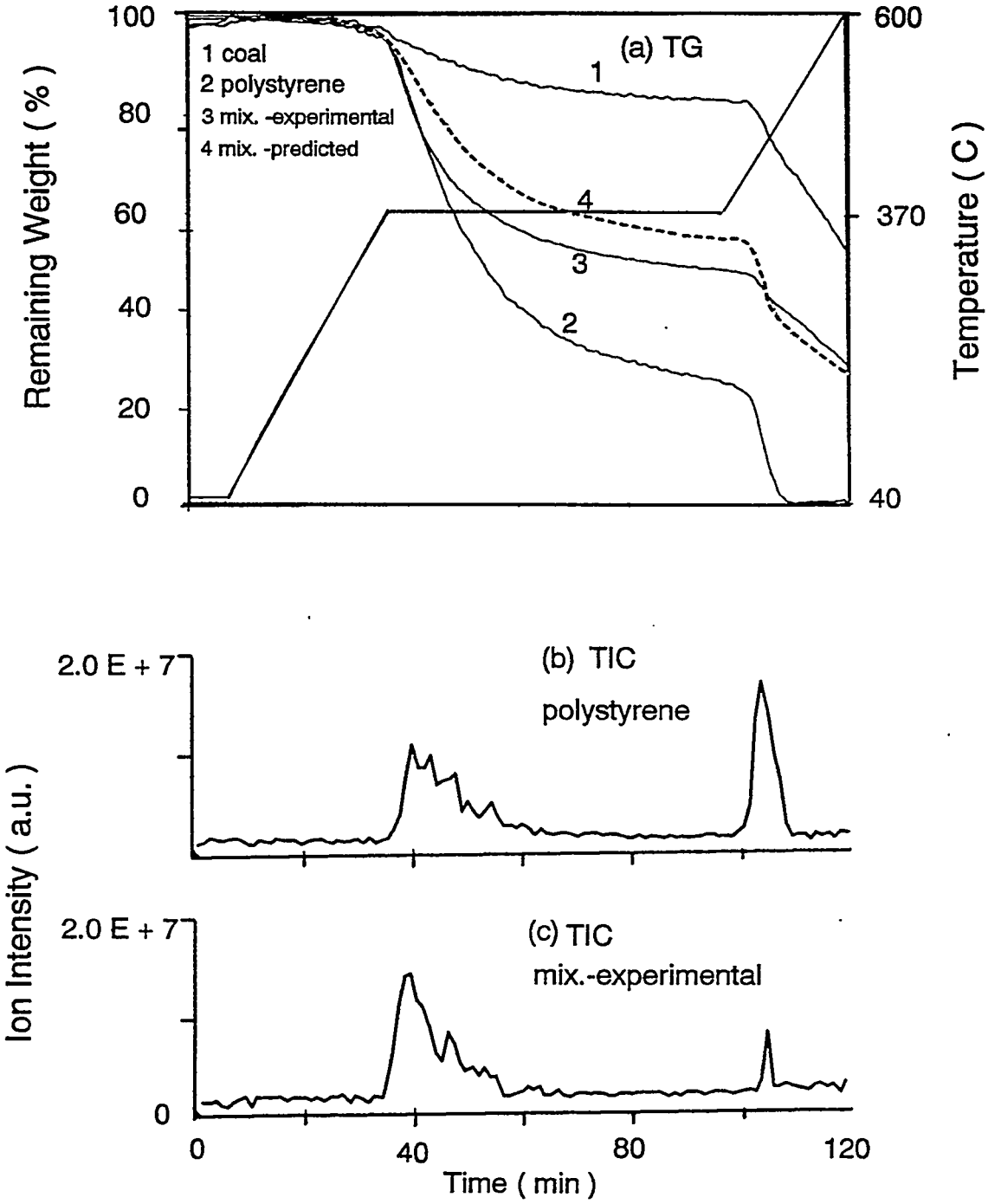

Figure IV.2.2. a) Hydropyrolysis TG curves of coal and polystyrene at 370 C isothermal temperature at 900 psi (H_2); b) total ion intensity profile of polystyrene hydropyrolysis at 900 psi (H_2), and c) total ion intensity profile of coal and polystyrene hydropyrolysis at 900 psi (H_2).

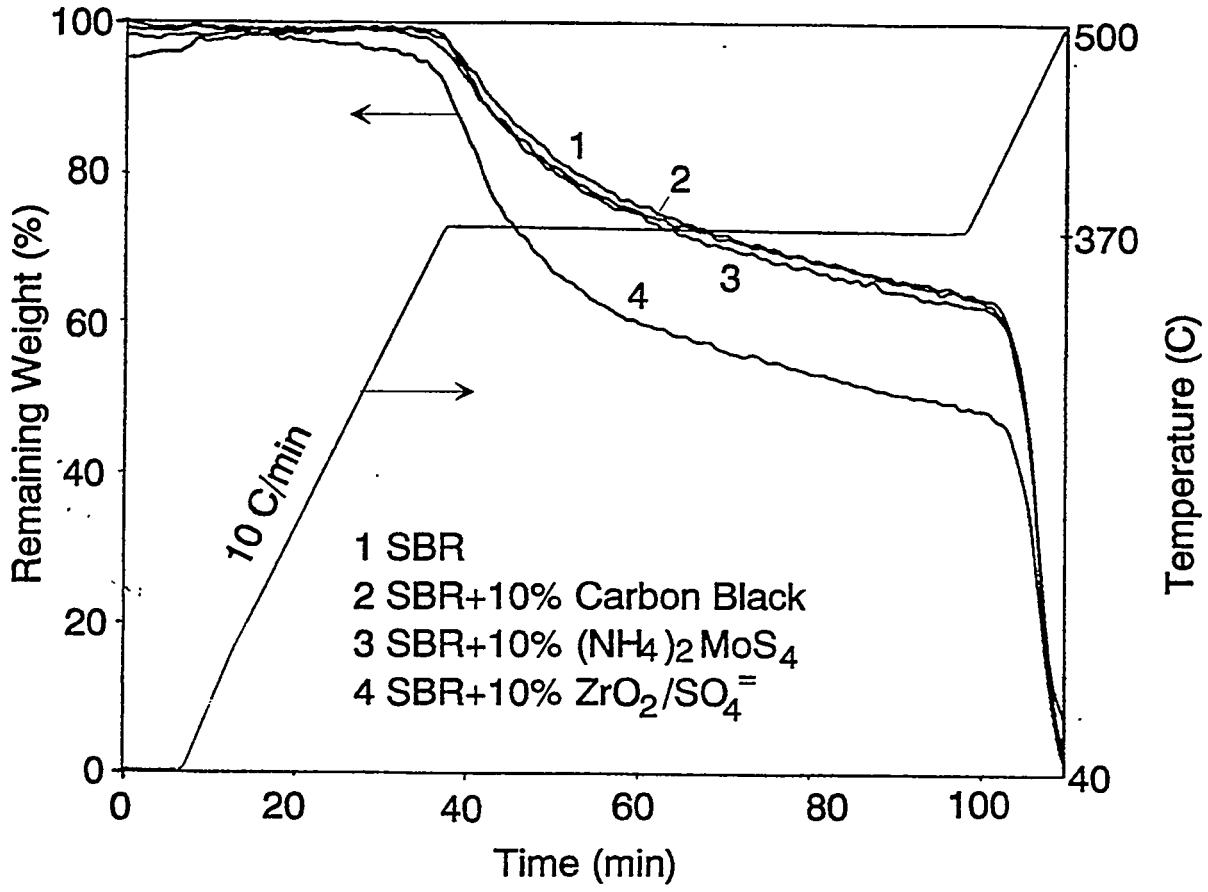

Figure IV.2.3. TG curves of SBR polymer with various catalysts at 900 psig (H_2).

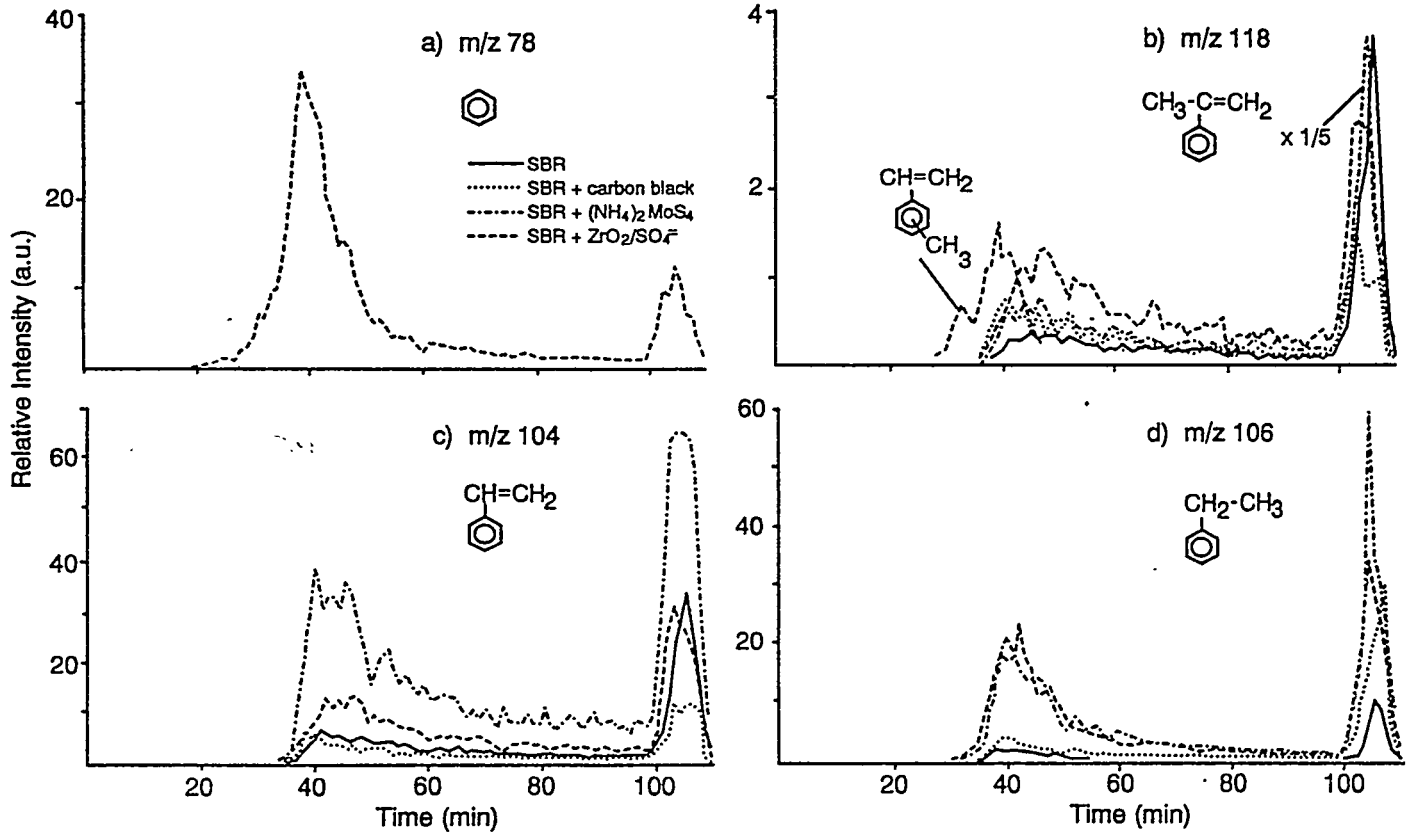

Figure IV.2.4. Effect of catalysts on evolution profile of SBR polymer decomposition products. a) m/z 78, benzene; b) m/z 118, methylstyrene; c) m/z 104, styrene; and d) m/z 106, ethylbenzene.

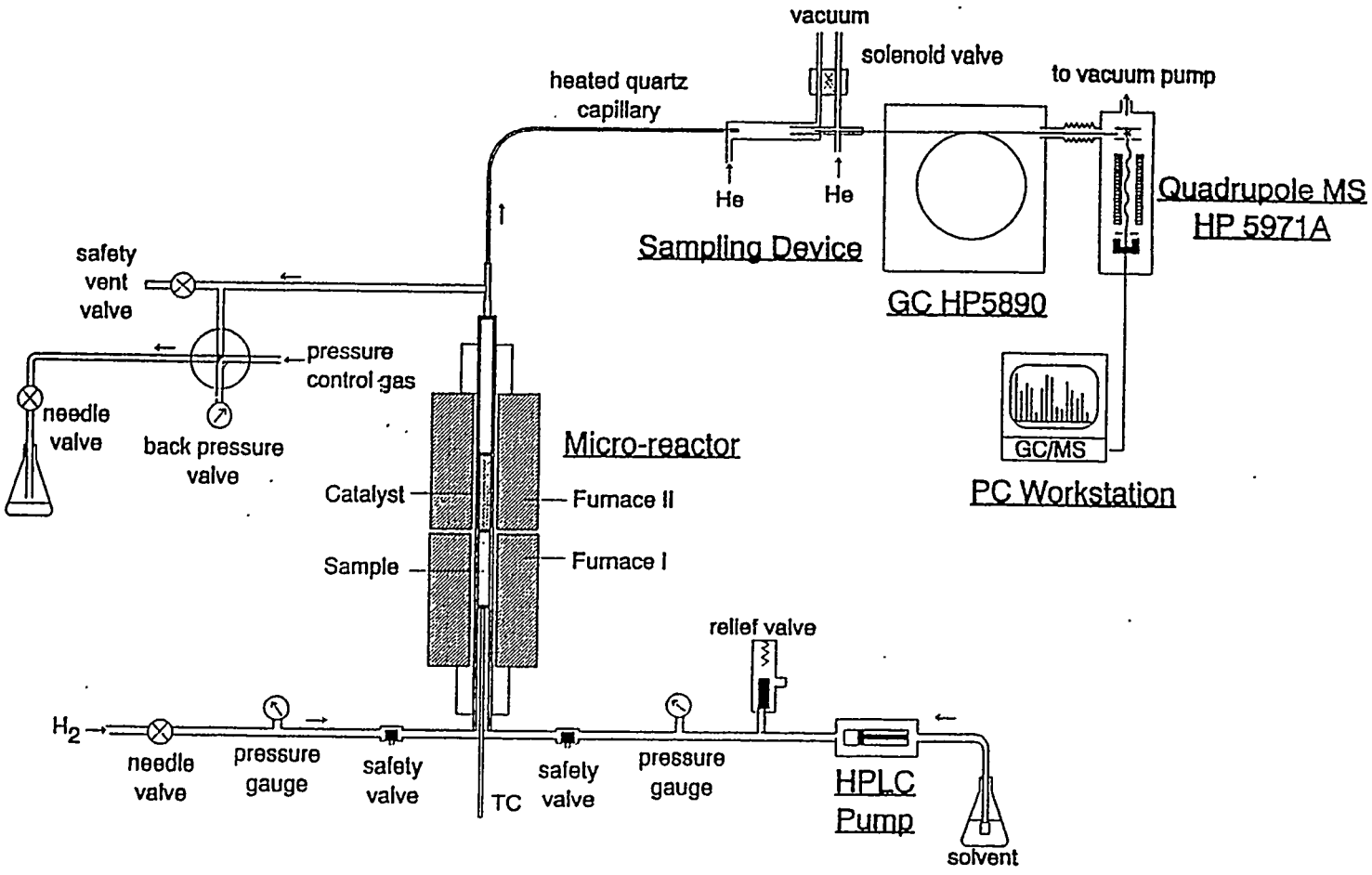

Figure IV.2.5. Schematic of the two stage micro reactor with on-line GC/MS.

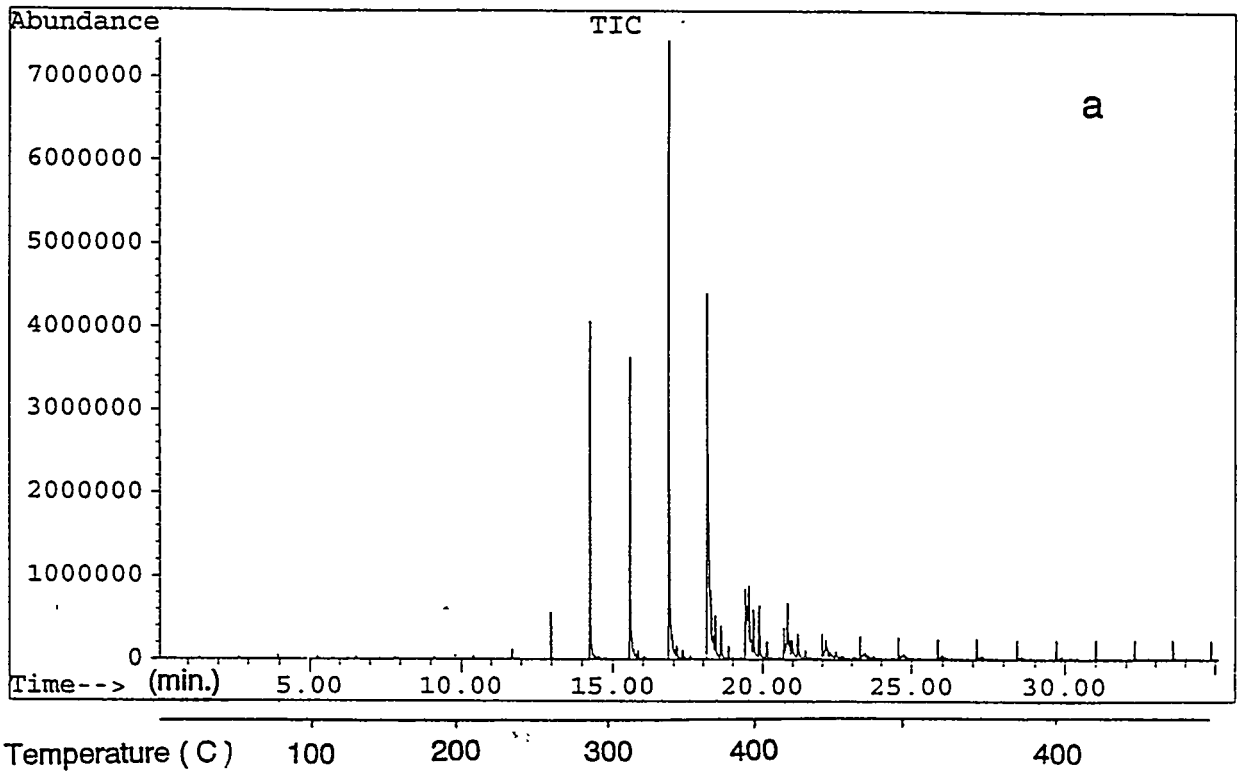

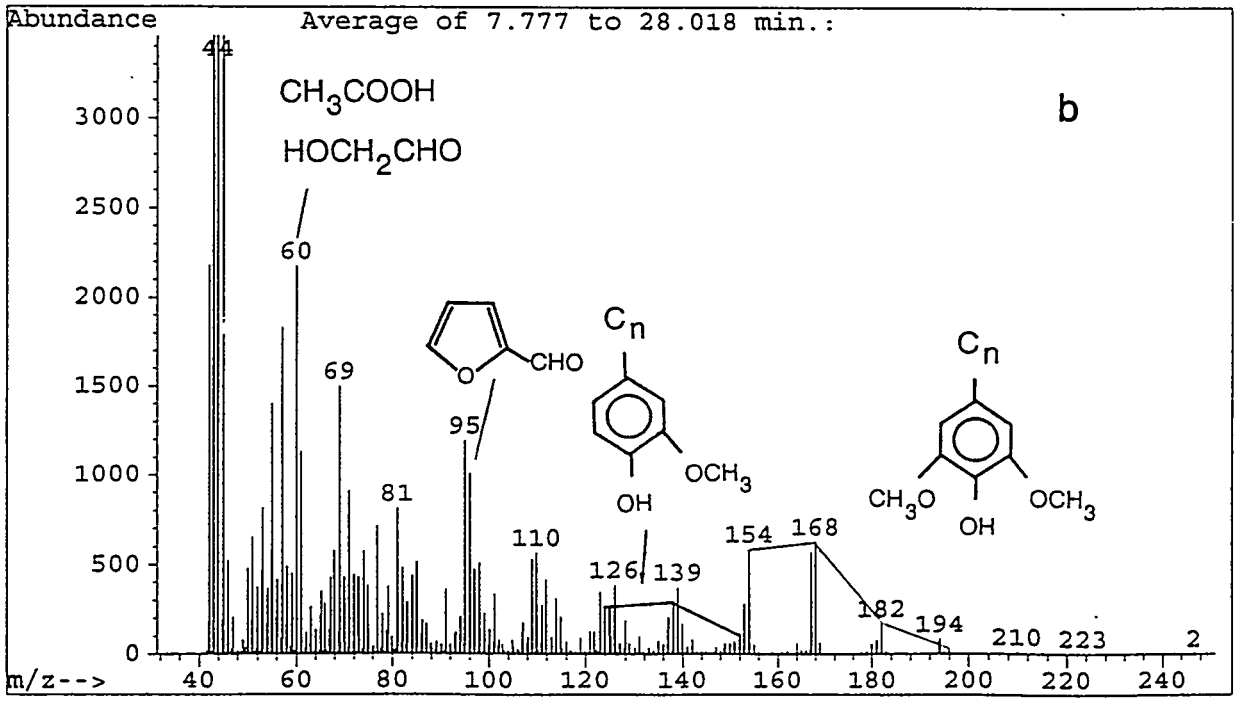

Figure IV.2.6. a) Total ion chromatogram of liquefaction products from wood; b) average mass spectrum of liquefaction products from wood.

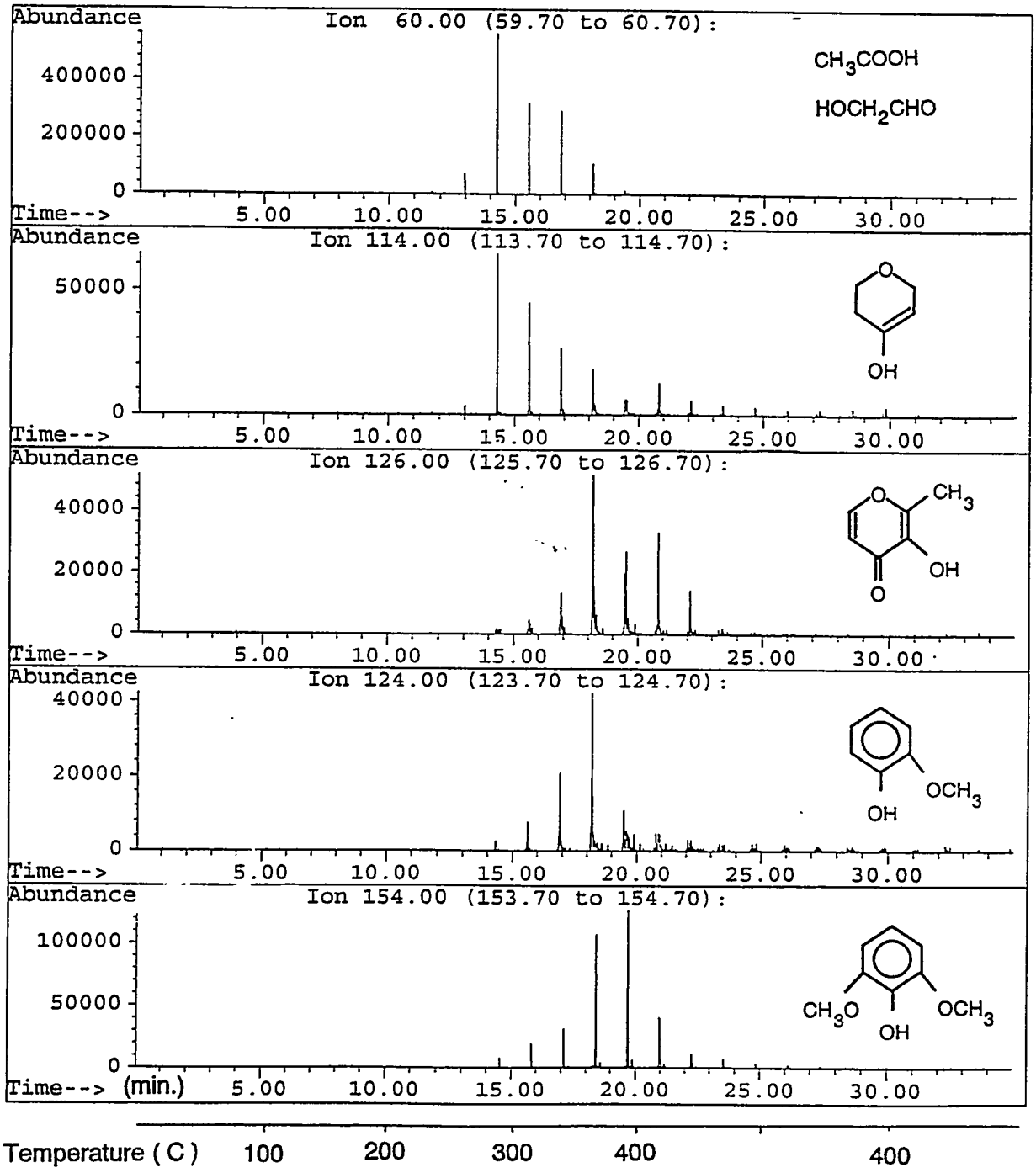

Figure IV.2.7. Evolution profiles of selective liquefaction products from wood.

TASK IV

Project IV.3

IN SITU XAFS AND MOSSBAUER SPECTROSCOPIC STUDIES OF DCL CATALYSTS

N. Shah, J. Zhao, Z. Feng, M.M. Taghiei,
K.R.P.M. Rao, F.E. Huggins, G.P. Huffman
University of Kentucky

Introduction:

We have modified Neils and Burlitch design to build an *in-situ* cell for XAFS investigation of direct coal liquefaction (DCL) catalysts. This design of cell can reproduce elevated temperature and hydrogen pressure employed in the micro autoclave (tubing bomb) reactors while letting a seven KeV synchrotron generated x-ray beam through. Here we present iron K-edge *in-situ* XAFS data on several catalysts used for direct coal liquefaction.

Modifications of the *in-situ* cell:

Figure 1 is a schematic of the modified *in-situ* cell. Two x-ray transparent graphite windows (capable of withstanding 1800 psi hydrostatic pressures) are sandwiched between water cooled flanges while the center flange and the coal/catalyst sample within the reactor are heated to reaction temperatures with cartridge heaters. Unlike Neils and Burlitch design, here the window assemblies are kept at room temperature and therefore the graphite windows do not delaminate from the copper gaskets at higher temperatures to produce gas leaks.

Sample Preparation:

A thin 13 mm. dia. pellet of the sample was made by pressing about 150 mg. of coal with about 5% Fe loading catalyst and enough elemental sulfur to convert all Fe into FeS stoichiometry, at 10 ton pressure with a hydraulic press. Several catalyst systems were tested during this run: (1) Black thunder coal was ion-exchanged using iron acetate solution to get 3.78 wt.% Fe loading and (2) 5 wt.% of binary ferrihydrite catalyst (with 5 wt.% SiO_2) in Blind Canyon (DECS-17) coal and (3) 5 wt.% of citric acid treated ferrihydrite catalyst in Blind Canyon (DECS-17) coal.

Reaction Conditions:

The cell was charged up to 1000 psig (cold) hydrogen and the entire assembly was placed in the XAFS experimental hutch. Because of the proximity of the heating and cooling regions, temperature controller had trouble maintaining the temperature close to the set point and large (25C) over and undershooting fluctuations of the temperature from the set point were observed. The hydrogen pressure and reaction conditions in this *in-situ* cell are the same as those employed in tubing bomb micro autoclave reactors. The only difference is the absence of a liquid hydrogen donor solvent and a shaking mechanism to improve mass

transfer. Since the intention of the experiment is to study the transformations of the catalyst phase and not the reaction yields, the mass transfer limitations of the present setup are not critical.

Results:

Figures 2 and 3 show a series of Fe K-edge XANES and radial structure functions for ferrihydrite/citric acid and Fe ion exchanged catalyst systems. Both catalyst systems show transformation of the iron oxyhydroxide phase to the pyrrhotite phase. The transformation temperatures appear to be different for different systems. This transformation occurs over a range of temperature conditions. This lack of a sharp transition can be due to either (1) a nonhomogeneous transition within the sample matrix, i.e., some (smaller?) catalyst particles transform at lower temperature and some at little higher temperature, or, (2) there are more than one transformation. It is well known that pyrrhotite exhibits several phases depending on the vacancy in $Fe_{1-x}S$ matrix. Vacancy rearrangement over a range of temperatures can lead to changes in the XAFS results over a wider range of temperatures. Further analysis of these results is under progress.

Reference:

T.L. Neils, J.M. Burlitch, J. Catal., **118**, (1989), 79-94.

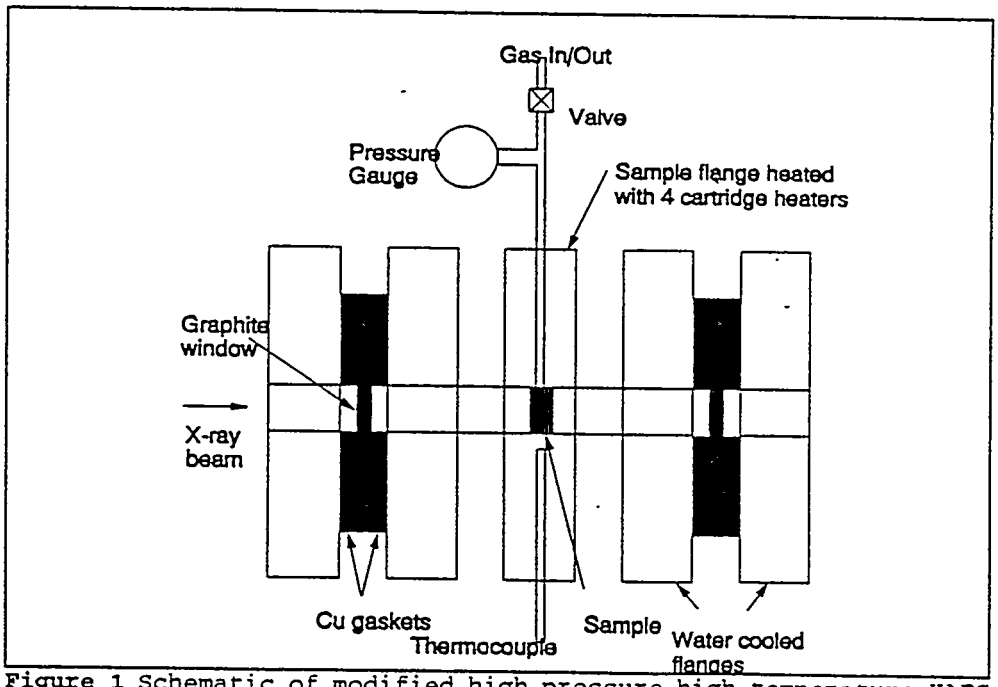

Figure 1 Schematic of modified high pressure high temperature XAFS cell for *in-situ* characterization of DCL catalysts.

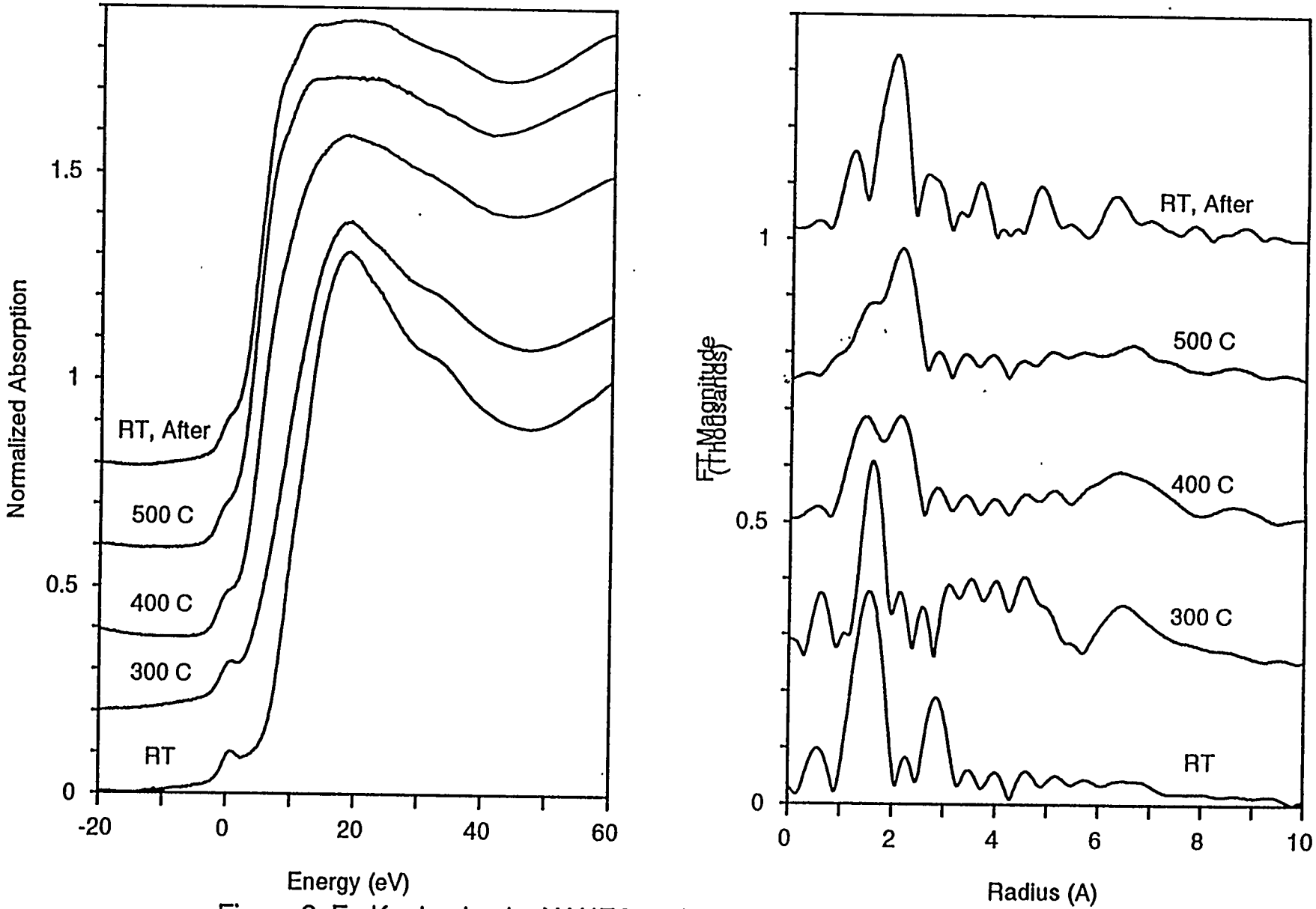

Figure 2. Fe K edge in-situ XANES and RSF of FeOOH/citric acid catalyst in Blind Canyon (DECS-17) coal. 950 psi (cold) hydrogen pressure.